

seismicity in the Banning-San Gorgonio area. Like the Tejon Pass bend in the 1857 rupture zone, the San Gorgonio bend spawns a major left-lateral fault (the Pinto Mountain fault) conjugate to the San Andreas system. Unlike the situation at Tejon Pass, however, the San Andreas fault at San Gorgonio splays into a complex pattern of branching and intersecting fault segments. South of San Gorgonio, the San Andreas fault reconverges into a single strand and bends again to the more southeasterly trend that characterizes the southern section of the fault system.

This section of the fault system south of the Transverse Ranges is transitional from oblique spreading along the axis of the Gulf of California to the obliquely convergent strike-slip displacement that dominates deformation along the continental section of the San Andreas transform boundary to the north. Several major strike-slip faults run west of and subparallel to the main strand of the San Andreas fault south of the Transverse Ranges. These faults, which are considered part of the San Andreas system and include the Imperial, San Jacinto, and Elsinore faults, accommodate a significant proportion of the plate-boundary motion. The Imperial and San Jacinto faults, in particular, have produced more moderate earthquakes than any other segment within the fault system (see chap. 6; Hanks and others, 1975).

#### SOUTHERN BRANCH OF THE SAN ANDREAS FAULT

The most intense seismicity along the main trace of the southern section of the San Andreas fault is associated with the San Gorgonio bend and is concentrated between the two principal branches of the San Andreas fault: (1) the Mission Creek fault, or northern branch of the San Andreas; and (2) the Banning fault, which runs nearly due west from the south end of the Mission Creek fault toward an ambiguous junction with the San Jacinto fault just south of San Bernardino (see fig. 5.3A and maps at front of book). Neither strand forms a continuous structure through the bend. This San Gorgonio seismicity cluster produced numerous  $M=5.0-6.5$  earthquakes in the 1930's and 1940's, and in 1986 it produced the  $M_L=5.6$  North Palm Springs earthquake, which involved dextral strike-slip displacement on the north-dipping Banning fault (Jones and others, 1986). The background seismicity in this area is the highest in southern California, but it is distributed throughout a volume and cannot be clearly associated with any fault. To the west, seismicity associated with the Banning cluster abuts the dense lineation of epicenters coincident with the northernmost segment of the San Jacinto fault. Nicholson and others (1986) suggested that much of the seismicity within the upper 10 km of the crust in this cluster involves left-lateral slip on a series of northeast-striking faults; however, Jones

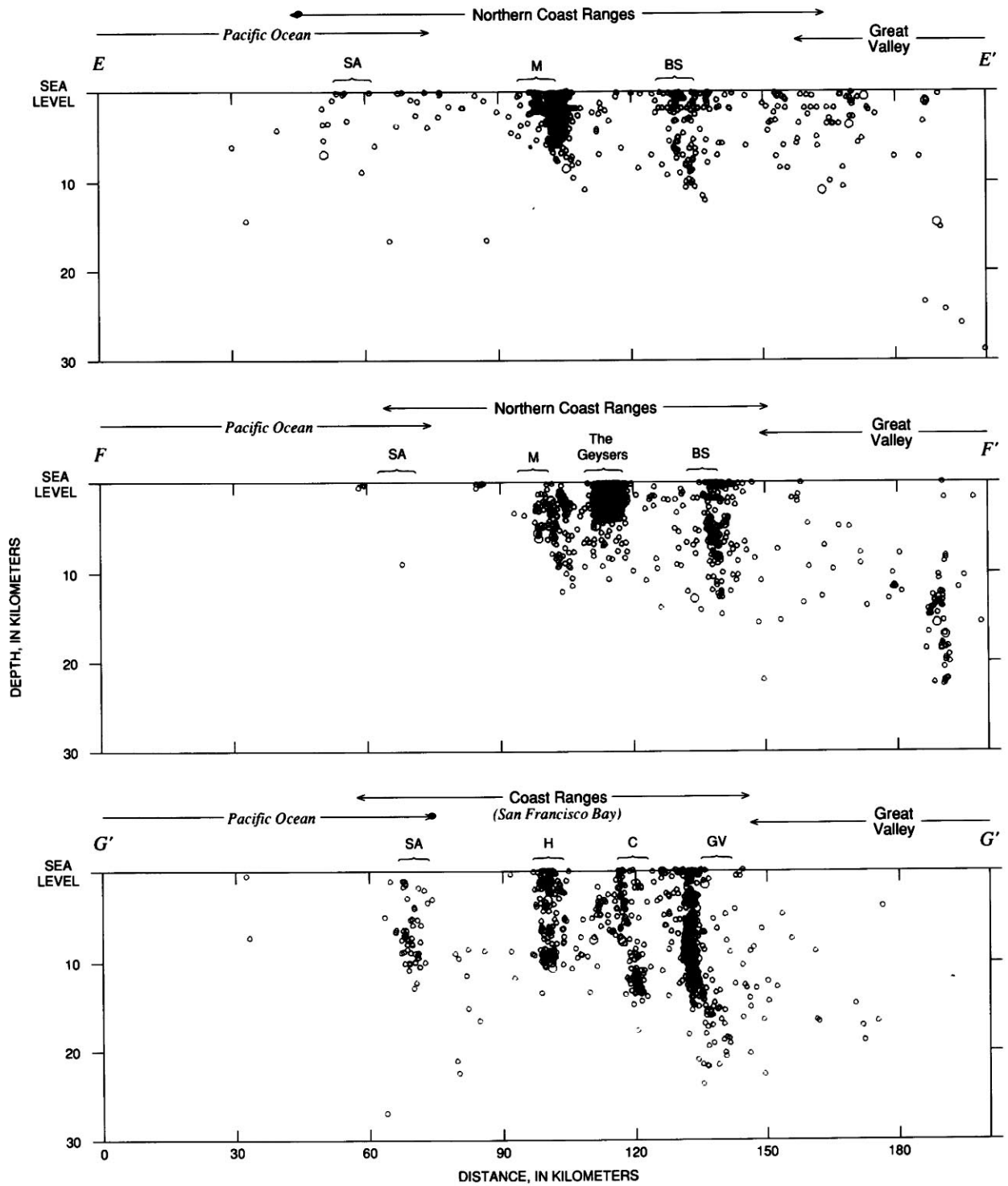
(1988) pointed out that the evidence for northeast-trending lineations of epicenters within the Banning cluster is less than clear.

Diffuse seismicity extends northward from the Banning cluster into the San Bernardino Mountains and eastward into the Pinto Mountains, with no clear lineations along the sinistral Pinto Mountain fault. Indeed, a diffuse, north-south-trending lineation of epicenters seems to cut directly across the Pinto Mountain fault from the west-central Pinto Mountains. Two  $M=5.2$  earthquakes (see events 75, 76, fig. 5.11A) with right-lateral strike-slip planes parallel to this trend occurred at the north end of this zone in 1975 and 1979. Somewhat farther south, however, a broad, east-west-trending lineation appears to coincide with the Blue Cut fault. Even farther south, a second broad lineation extends eastward from near the junction of the Banning and Mission Creek branches, although this lineation does not coincide with a mapped fault.

The southernmost section of the San Andreas fault, the Indio segment, which extends from the junction of the Banning and Mission Creek branches southward to the end of the San Andreas at the Salton Sea, has been almost completely aseismic in historical time. At the north end of this segment, periodic swarms of small ( $M \leq 4$ ) earthquakes a few kilometers east of the San Andreas appear to occur on small northeast-trending structures (for example, Norris and others, 1986; Jones, 1988). The sparse background seismicity is also offset a few kilometers to the east from the surface trace of the San Andreas. Although the possibility of systematic offsets related to  $P$ -wave-velocity contrasts across the fault has not been investigated in detail, the observed offset seems too large to be explained entirely by lateral velocity contrasts.

Although it has not ruptured with a major earthquake in historical time, the aseismic Indio segment of the San Andreas fault seems to have much in common with the 1857 and 1906 rupture zones. Sieh (1986) presented geologic evidence for at least four major ruptures along the Indio segment since A.D. 1000; the last occurred approximately 300 yr ago. Unlike the two major locked sections, however, the south end of the Indio segment adjacent to the Salton Sea shows minor aseismic creep (Louie and others, 1985) and has shown episodes of sympathetic slip accompanying  $M \approx 6$  earthquakes on the Imperial fault and the southern section of the San Jacinto fault (Sieh, 1982). Not only is the Indio segment aseismic, but also the entire Coachella block extending from the San Andreas fault on the northeast to the crest of the San Jacinto Mountains on the southwest.

A cross section of hypocenters along the southern branch of the San Andreas fault ( $M-M'$ , fig. 5.9B) shows that the earthquakes associated with the bend at San



A

FIGURE 5.8.—Transverse depth sections across the San Andreas fault system in the northern (A) and central (B) Coast Ranges. See figure 5.6 for locations of sections and explanation of symbols, which are scaled with enlargement of cross sections. Faults: BS, Bartlett

Springs; C, Calaveras; GV, Greenville; H, Hayward; M, Maacama; R, Rinconada; SA, San Andreas; SG, San Gregorio; SNA, Sur-Nacimiento. BV, Bear Valley on cross section J-J'. FRT, Franciscan terrane.



THE SAN ANDREAS FAULT SYSTEM, CALIFORNIA

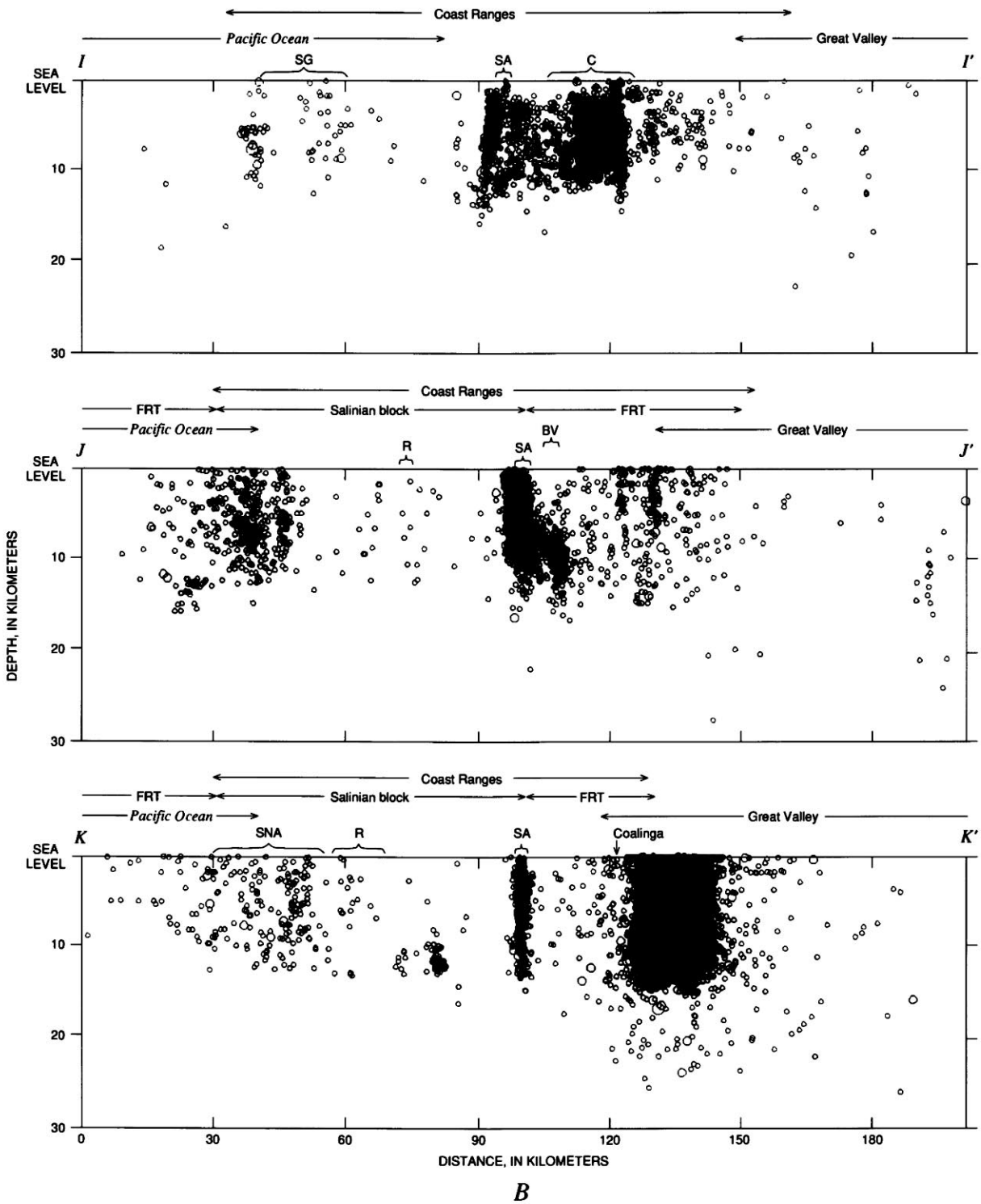


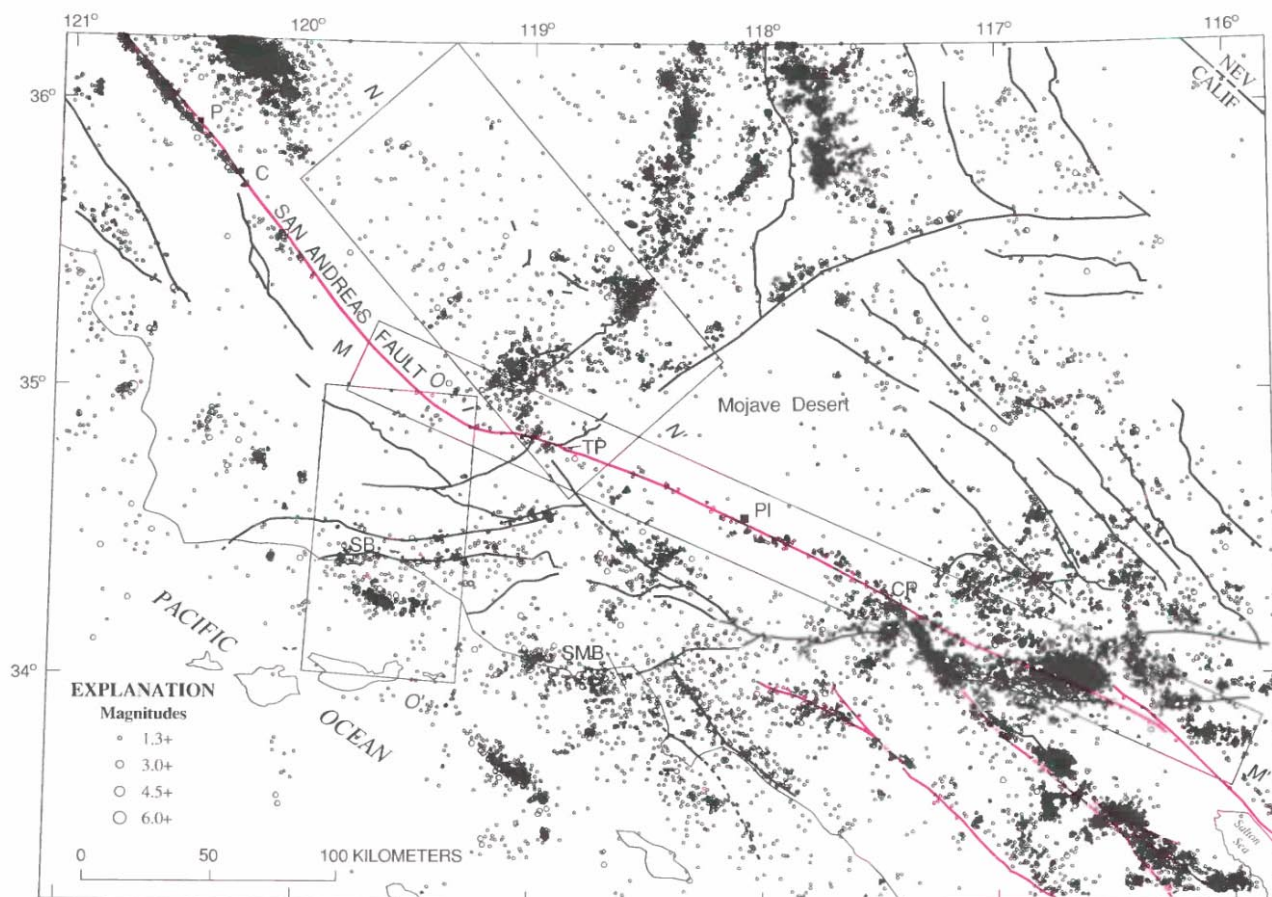
FIGURE 5.8. — Continued.

Gorgonio are among the deepest in southern California, with maximum focal depths approaching 25 km. The maximum focal depths deepen southward along the San Andreas fault from about 12 km beneath the Mojave segment to 25 km beneath the San Gorgonio fault. At the south end of the San Gorgonio area, however, maximum focal depths abruptly decrease to 10 km. This shallowing of seismicity is associated with a shift in the most concentrated seismicity from between the two segments (Mission Creek and Banning) of the San Andreas to east of the Mission Creek fault. The sparse seismicity of the Indio segment is limited to depths of 5 km or less.

#### ASSOCIATED FAULTS

Although the southernmost section of the San Andreas fault is almost completely aseismic, associated subparal-

lel faults are extremely active. These faults are marked by the three bold north-south- to northwest-trending alignments of epicenters that dominate the seismicity pattern within the San Andreas fault system south of the Transverse Ranges (fig. 5.10A), from east to west: (1) the Brawley seismic zone (Johnson, 1979), defined by a dense, spindle-shaped cluster of epicenters connecting the north end of the Imperial fault and the south end of the Indio segment of the San Andreas fault; (2) the northwestward alignment of densely clustered epicenters along the San Jacinto fault zone, which appears to branch from the northern section of the Imperial fault; and (3) the northwestward alignment of more diffusely clustered epicenters along the Elsinore fault, which appears to branch from somewhere near the south end of the Imperial fault.



A

FIGURE 5.9.—Seismicity in the southern Coast Ranges and Transverse Ranges. A, Earthquake locations, showing major branches of the San Andreas fault system in red; faults dotted where concealed. Magnitude symbols shown in explanation are scaled with enlargement of cross sections. C, Cholame; CP, Cajon Pass; P, Parkfield; PI,

Palmdale; SB, Santa Barbara; SMB, Santa Monica Bay; TP, Tejon Pass. B, Depth sections outlined in figure 5.9A. Faults: B, Banning; G, Garlock; MC, Mission Creek; N.Br.SA, northern branch of the San Andreas; PM, Pinto Mountain; SA, San Andreas; SJ, San Jacinto; WW, White Wolf.



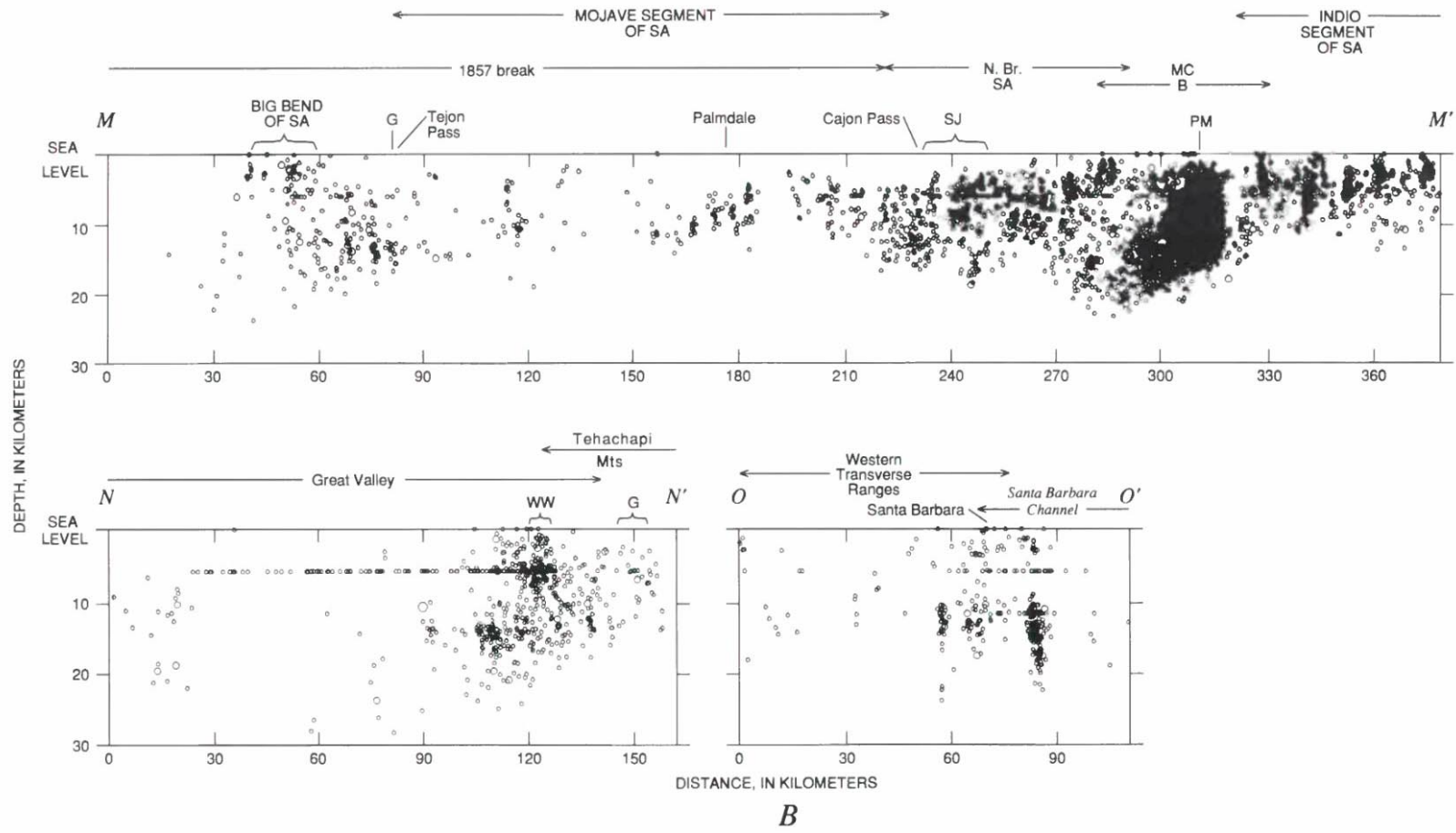


FIGURE 5.9. — Continued.

The Brawley seismic zone and the cluster of epicenters at the south end of the Imperial fault (coincident with the Cerro Prieto volcanic-geothermal field in Mexico) represent the two northernmost in the series of small spreading centers offset by right-lateral transform faults that characterize oblique spreading in the Gulf of California (Lomnitz and others, 1970; Johnson and Hill, 1982). The Imperial fault itself, which is marked by a scattered alignment of epicenters, serves as the transform fault between these two small spreading centers. The  $M=7.1$  El Centro earthquake ruptured the entire length of the Imperial fault in 1940, and the  $M=6.6$  Imperial Valley earthquake of 1979 ruptured the north two-thirds of the fault; intensity data suggest that moderate earthquakes ( $5.5 < M < 6.3$ ) in 1906, 1915, 1917, and 1927 may also have been located on the Imperial fault (Johnson and Hill, 1982). Most of the aftershocks associated with the 1979 Imperial Valley earthquake were concentrated in the south half of the Brawley seismic zone, which was first recognized because of the many earthquake swarms it produced from 1973 through mid-1979 (Hill and others, 1975; Johnson 1979; Johnson and Hutton, 1982). Many of the individual swarm sequences, as well as individual clusters of events in the aftershock sequence, defined lineations transverse to the strike of the Imperial fault and the long axis of the Brawley seismic zone. Most earthquakes within the Brawley seismic zone have strike-slip focal mechanisms; thus, kinematically, these transverse lineations represent conjugate structures to the dominant north-northwestward trend of the Imperial-Brawley fault system.

Irregular clusters of epicenters mark the San Jacinto fault zone, which runs along the southwest base of the Santa Rosa and San Jacinto Mountains. These clusters tend to be concentrated near bends and junctions within the complex set of multiple fault strands that form the surface expression of this fault zone. In several places, particularly within the southern and northern sections of the fault zone, epicenters define linear concentrations that tend to be closely aligned with mapped fault traces. The San Jacinto fault zone has produced at least 10 earthquakes of  $M=6.0-6.6$  since 1890, the most recent of which were the  $M=6.2$  earthquake of 1954, the  $M=6.6$  Borrego Mountain earthquake of 1968, and the  $M=6.6$  Superstition Hills earthquake of 1987. Thatcher and others (1975) pointed out that this series of historical  $M > 6$  earthquakes along the San Jacinto fault zone has left two seismic gaps: one along the northern 40 km of the fault, and the other along a 20-km-long stretch of the central section of the fault zone (the Anza gap). The Anza gap shows up in figure 5.10A as a relatively quiescent stretch of the fault zone between two dense clusters, with a third cluster located off the fault zone some 20 km

southwest of the gap (see Fletcher and others, 1987; Sanders and Kanamori, 1984).

The Elsinore fault zone is defined not so much by a coincident alignment of epicenters as by the loci of western end points for clusters of epicenters elongate northeastward between the Elsinore and San Jacinto fault zones. This pattern is most pronounced along the southeast half of the fault; the northwest half, which defines the northeast scarp of the Elsinore Mountains, is marked by scattered clusters of epicenters. As the Elsinore fault enters the Los Angeles Basin to the north, it splays into the Whittier and Chino faults. Historical seismicity levels are considerably lower along the Elsinore fault than either the San Jacinto fault zone or the Imperial fault/Brawley seismic zone. The largest historical earthquake on the Elsinore fault was an  $M=6$  event in 1910 in the central section. The Whittier Narrows earthquake ( $M_L=5.9$ ) of 1987, which caused over \$300 million in damage, was located at the north end of the Elsinore-Whittier fault. Because its mechanism was thrust faulting on an east-west-striking plane with a shallow dip, however, it does not appear to be simply related to the Elsinore system.

Seismicity in the relatively quiescent southwestern corner of California between the Elsinore fault and the coast shows up in figure 5.10A as small, sparsely scattered clusters of epicenters. Activity picks up again, however, in the vicinity of the major northwest-striking faults along the coast (the Rose Canyon fault through San Diego and the Newport-Inglewood and Palos Verdes faults along the western margin of the Los Angeles Basin). Except for weak alignments along the Newport-Inglewood fault, which ruptured with an  $M=6.3$  earthquake in 1933 (Richter, 1958), the seismicity patterns associated with these faults show little tendency to align along mapped fault traces.

The cross sections in figure 5.10B emphasize that, except in the immediate vicinity of the Salton Sea, maximum focal depths associated with earthquakes aligned along the principal branches of the southern section of the San Andreas fault system are systematically deeper than those aligned along its central and northern sections. Maximum focal depths, for example, decrease from 15 to 18 km beneath the central section of the Imperial fault near the United States-Mexican border to less than 10 km beneath the north end of the Brawley seismic zone at the southeast tip of the Salton Sea (cross sec.  $Q-Q'$ , fig. 5.10B). The focal depths associated with earthquakes along the Coyote Creek, Superstition Hills, and Superstition Mountain faults forming the southwestern section of the San Jacinto fault zone adjacent to the Salton Sea are concentrated in the upper 10 km of the crust (cross sec.  $P-P'$ , fig. 5.10B).



Those segments of the San Andreas fault system in southern California with maximum focal depths shallower than 12 to 15 km are also those that show evidence of aseismic creep (see Louie and others, 1985). Indeed, actively creeping segments of the San Andreas fault system throughout California seem to be confined to those along which microearthquakes are concentrated in the shallow crust (focal depths of less than 12–15 km).

Moving northwestward along the San Jacinto fault zone, the base of the seismogenic crust deepens systematically to a maximum of 20 km beneath the stretch adjacent to San Jacinto Mountain (which at 3,293 m, is the second highest point in southern California) midway along the fault zone (cross sec.  $P-P'$ , fig. 5.10B). The base of the seismogenic crust maintains this 20-km depth farther northwestward along the fault zone to its junction with the Banning fault just south of San Bernardino (fig. 5.10A), beyond which it begins to shallow again. Note, in particular, that earthquakes tend to be concentrated between 10- and 20-km depth beneath the San Jacinto fault zone, leaving the upper 10 km of the crust relatively quiescent along the middle stretch of the fault zone. The dense knot of hypocenters in the upper 5 km of the crust midway along cross section  $P-P'$  corresponds to the cluster of epicenters 15 km southwest of the fault zone near the Anza gap (fig. 5.10A). The Anza gap itself shows up between  $\Delta=120$  and 140 km in cross section  $P-P'$  as a quiescent zone below and southeast of the shallow cluster of hypocenters (Fletcher and others, 1987; Sanders, 1987). The distribution of hypocenters beneath the Elsinore fault zone (cross sec.  $R-R'$ , fig. 5.10B) is in many ways similar to that beneath the San Jacinto fault zone. Maximum focal depths increase northwestward from 12–15 km at the southeast end of the fault near the United States-Mexican border to about 20 km midway along the fault zone (generally coincident with the highest topography in this section of the Peninsular Ranges) and then gradually decrease farther northwestward toward the Los Angeles Basin. Maximum focal depths show evidence of increasing again at the northwest end of the fault as it approaches the Transverse Ranges and branches into the Whittier and Chino faults. The hypocenters along the south half of the Elsinore fault also tend to concentrate in the lower 10 km of the seismogenic crust, although this pattern is not as well defined in the diffuse seismicity of the Elsinore fault zone as in the dense clustering along the San Jacinto fault zone.

#### FOCAL MECHANISMS AND TRANSFORM-BOUNDARY KINEMATICS

Focal mechanisms of selected earthquakes recorded in California from 1933 through 1988 are shown in figure 5.11A, and the corresponding source parameters are

listed in tables 5.2 and 5.3. Primary considerations in the selection of these events were (1) size—larger events were chosen where available, because they represent large-scale processes along major boundaries; (2) date of occurrence—the quality of data for focal-mechanism determinations improved significantly during the mid-1970's; and (3) location—some larger events were omitted because they were redundant in terms of mechanism and location, and some smaller events were included because they occurred in regions of significant seismicity where no larger events were available. Most focal mechanisms were determined from first arrivals at stations in the northern and southern California seismic networks. The evolving capability of these networks for such studies is reflected in the number of stations in the networks, summarized in table 5.1. Fault-plane solutions for the few large earthquakes on the list before the mid-1970's were supported by observations from stations outside the California networks.

Since the mid-1970's, focal mechanisms have been determined for only a fraction of the events for which adequate local first-motion data were available. Therefore, in addition to the three considerations listed above, there was a fourth, the interests of the investigators who analyzed the data. These interests included topical studies of large earthquakes and aftershock sequences, analyses of regional traveltimes on the basis of  $M \geq 4$  earthquakes, and a special study of the focal mechanisms of earthquakes on or near the San Andreas fault in southern California (Jones, 1988).

Focal mechanisms discussed in the first two subsections below are for earthquakes in the contiguous Coast Ranges-Transverse/Peninsular Ranges-Mojave Desert region associated with the principal seismic expression of the San Andreas fault system, where the seismic networks are best developed. Outside that region, except for the Cape Mendocino area and the vicinity of Long Valley caldera, the few well-determined focal mechanisms that are available provide only limited information on tectonic processes.

#### STRIKE-SLIP KINEMATICS OF THE SAN ANDREAS FAULT SYSTEM

Most moderate and large ( $M \geq 3$ ) earthquakes along the San Andreas fault and its major branches produce nearly pure right-lateral displacements along near-vertical planes that closely follow the surface traces of the respective fault segments. This relatively simple kinematic pattern holds for the great earthquakes that rupture "locked" sections of the fault every few hundred years (Sieh, 1981), as well as for nearly all the moderate earthquakes that rupture limited patches along persistently active segments of the fault system (Ellsworth and others, 1982; Jones, 1988). Displacements associated with

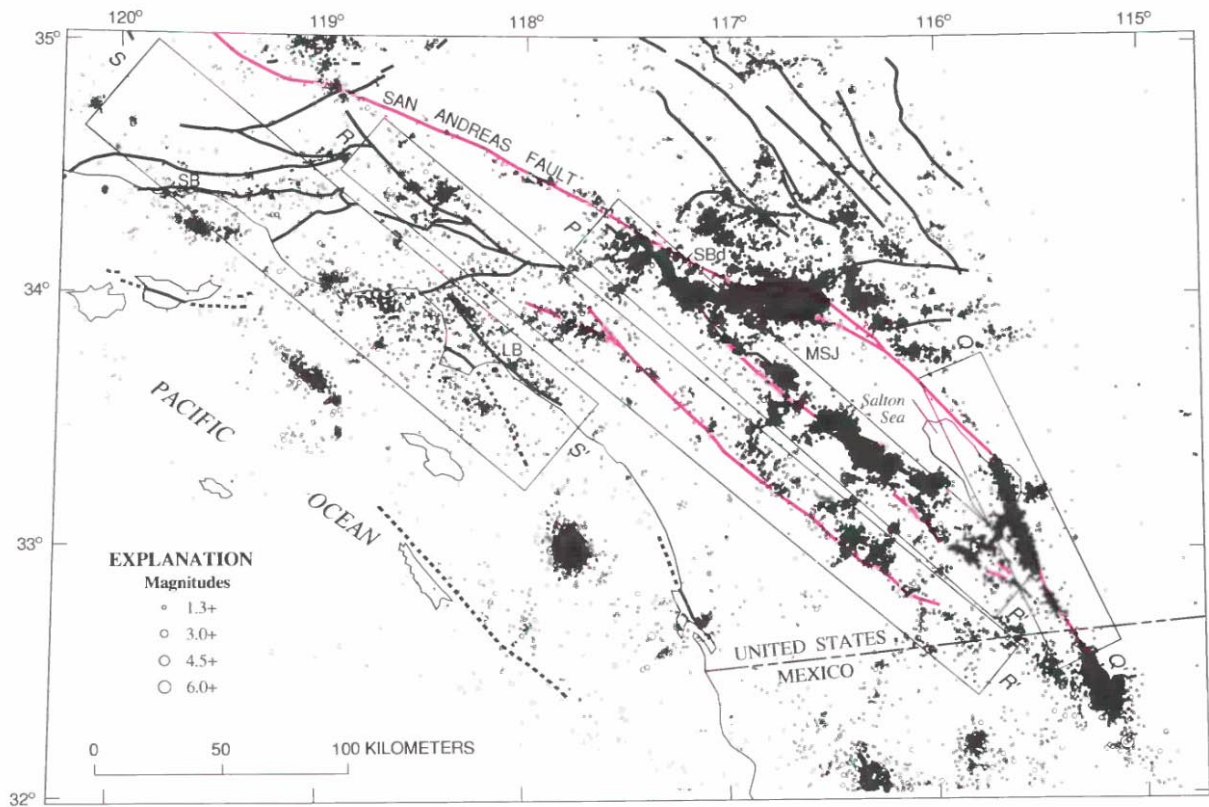


these earthquakes dominate the kinematic pattern along the transform boundary in California. DeMets and others (1987) and Minster and Jordan (1987), for example, argued that the cumulative displacement from earthquakes along the faults in the San Andreas system, together with the contribution from aseismic slip along its creeping segments, accounts for 60 to 70 percent of the total displacement between the Pacific and North American plates.

The fault-parallel strike-slip displacements typical of San Andreas earthquakes are illustrated in figure 5.11A by focal mechanisms along the San Andreas fault and its major branches from the United States-Mexican border to north of Clear Lake. In central California, such mechanisms mark the San Andreas fault itself from San Francisco to Cholame (events 26, 36, 38, 45, 46), the Calaveras-Greenville fault (events 23, 28-34) and the Hayward fault (event 27). Farther north, such mecha-

nisms occur along the Green Valley-Bartlett Springs fault (event 15) and the Rodgers Creek-Healdsburg-Maacama faults (events 16, 17, 19, 20). In southern California, such mechanisms mark the San Jacinto fault (events 78, 82-85) and the Imperial fault (event 89). Along the coast west of the San Andreas fault, similar focal mechanisms occur along the San Gregorio-Palo Colorado fault (events 39, 40) in northern California and along the Newport-Inglewood fault zone (events 62, 71), the Rose Canyon fault (event 73), and the San Clemente fault (event 70) in southern California.

Exceptions to this simple pattern for moderate ( $M \geq 4$ ) events along the San Andreas fault and its major branches appear to be limited to regions of unusual complexity, such as the major bends in the San Andreas near Cajon Pass (event 69) and San Geronio Pass (event 80). Jones and others (1986) attributed the July 8, 1986, earthquake (event 80) to right-lateral slip on the Banning



A

FIGURE 5.10.—Seismicity along the southern section of the San Andreas fault system. A, Earthquake locations, showing major branches of the San Andreas fault system in red; faults dotted where concealed. Magnitude symbols shown in explanation are scaled with enlargement of cross sections. BZ, Brawley seismic

zone; LB, Long Beach; MSJ, Mount San Jacinto; SB, Santa Barbara, SBd, San Bernardino. B, Depth sections outlined in 5.10A. Faults: CU, Cucamonga; NI, Newport-Inglewood; W, Whittier.



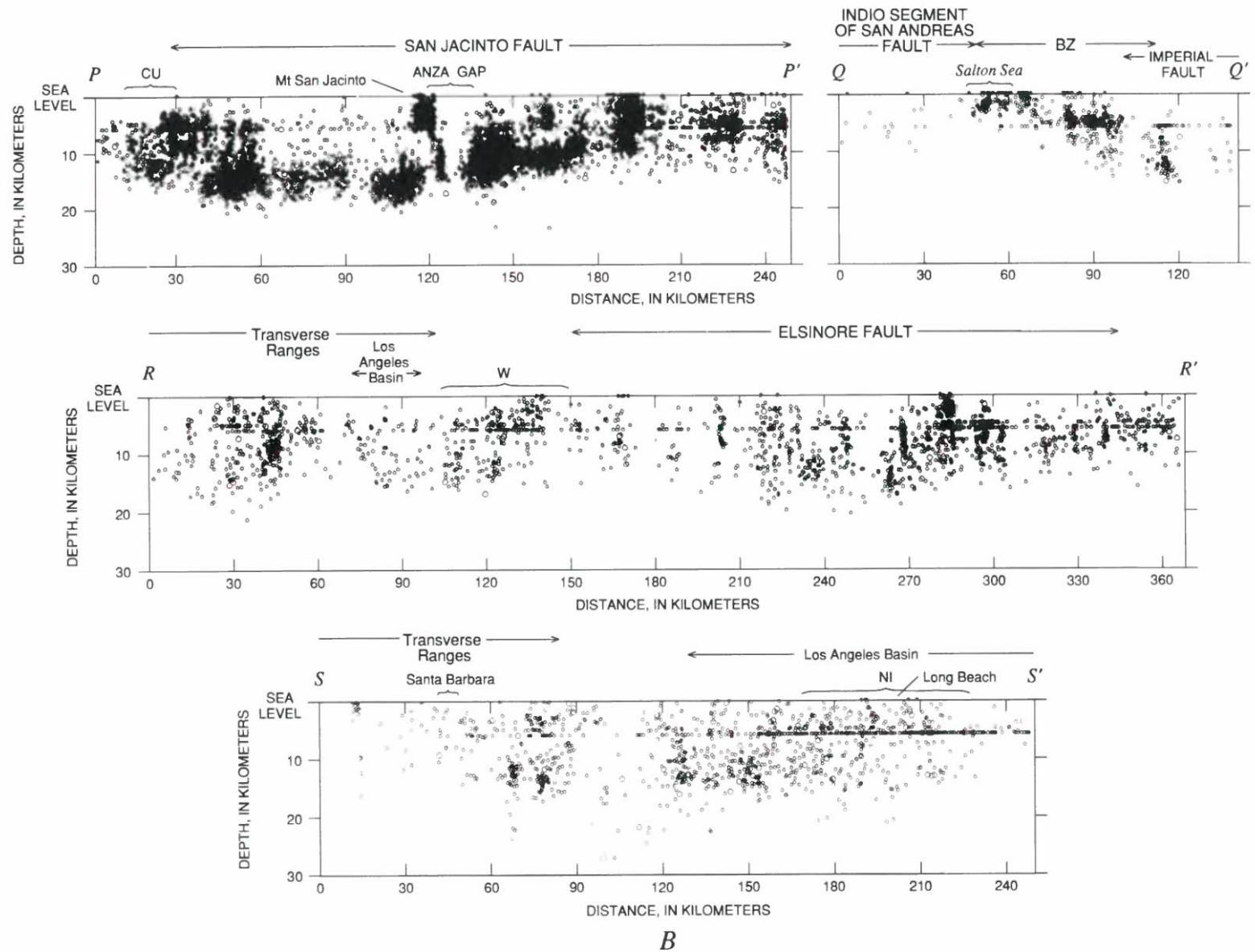


FIGURE 5.10. —Continued.

segment of the San Andreas fault where it dips 45° N. beneath the San Bernardino Mountains. The October 17, 1989,  $M=7.1$  Loma Prieta earthquake involved nearly equal amounts of right and reverse slip along a section of the San Andreas fault that takes a slight westerly bend

through the Santa Cruz Mountains and dips 70° SW. (see chap. 6). Smaller ( $M < 4$ ) events near, but probably not on, the fault show a great variety of focal mechanisms that reflect varying conditions along the fault; these mechanisms range from reverse or reverse-oblique slip

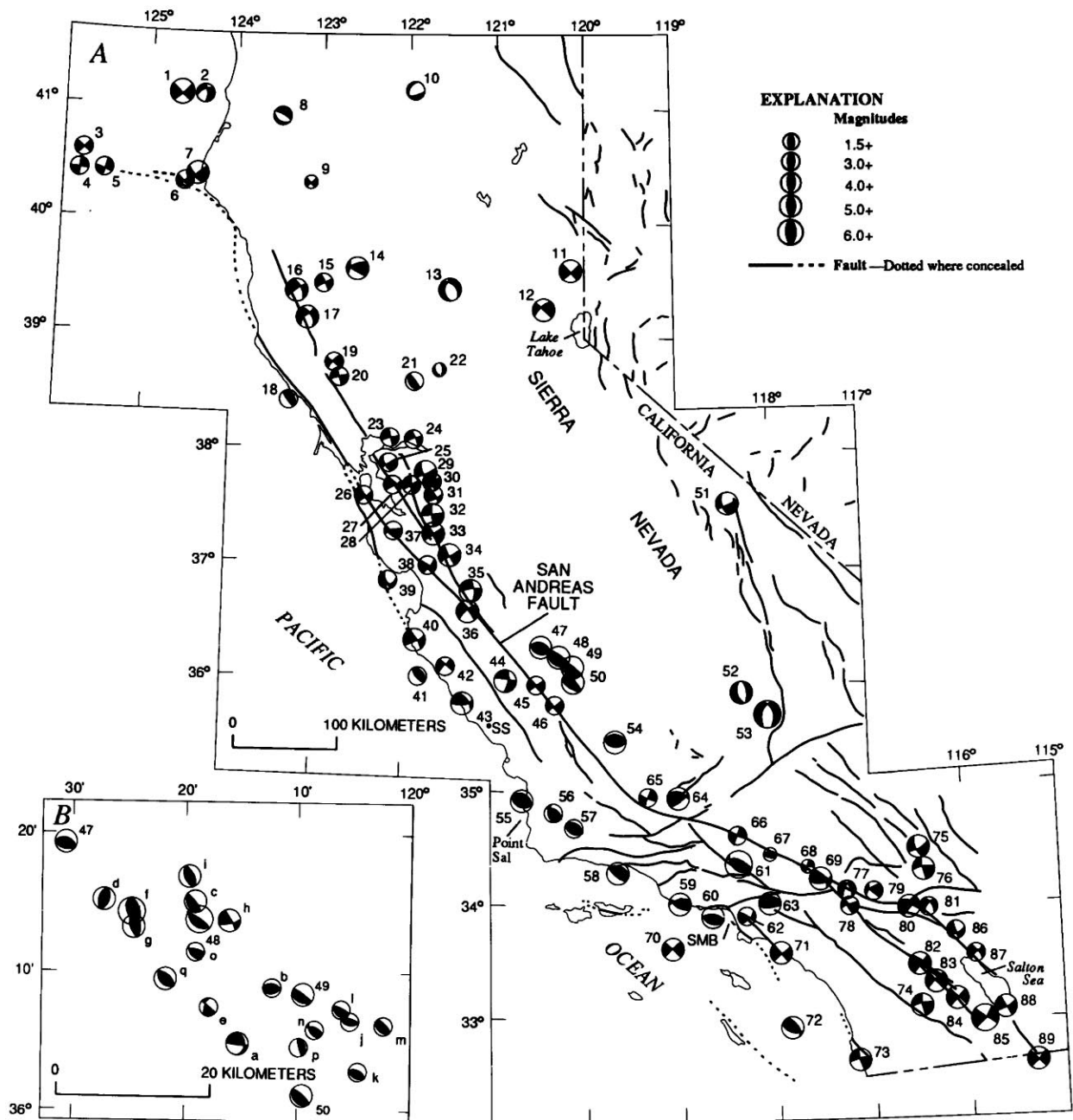


FIGURE 5.11.—Focal mechanisms for larger earthquakes. A, California. SMB, Santa Monica Bay; SS, San Simeon. Numbers refer to table 5.2. B, Coalinga-Kettleman Hills region (events 47-50, fig. 5.11A). Letters and numbers refer to table 5.3. Circle size increases with magnitude from 3.5 to 6.7.



TABLE 5.2.—Locations and focal-mechanism parameters for selected earthquakes in California

[ $M_L$ , estimated local magnitude. For  $M_L < 3$ , estimate is based on coda magnitude (see Lee and Stewart, 1981); for  $M_L > 3$ , estimate is based on peak amplitude and associated period (see Eaton and others, 1970). Focal-mechanism parameters: DA, dip angle; DD, dip azimuth]

Event	Date (yr/mo/d)	Time (G.m.t.)	Lat N.	Long W.	Depth (km)	$M_L$	Focal-mechanism parameters		
							DD (°)	DA (°)	Rake (°)
1	801108	1027:32.5	41°06.96'	124°39.87'	6.0	7	138	82	-8
2	801110	0624:07.3	41°06.79'	124°24.06'	7.5	4	337	52	-391
3	801109	0409:07.5	40°35.62'	125°46.45'	15	5.4	134	90	0
4	801108	1125:34.6	40°25.22'	125°48.83'	15	4	5	90	180
5	831220	1041:05.2	40°25.44'	125°31.35'	15	5.7	21	90	180
6	810916	1241:14.7	40°20.38'	124°35.64'	28.9	4.8	319	80	0
7	870731	2356:58.0	40°25.33'	124°26.61'	16.4	5.8	146	90	-20
8	870409	2034:09.0	40°56.32'	123°29.14'	26.2	4.1	27	68	-93
9	820912	0651:31.9	40°21.57'	123°08.52'	50.7	3	52	78	-170
10	820621	0643:37.6	41°10.66'	121°56.64'	7.3	4.3	168	64	-59
11	660912	1641:02.6	39°36.23'	120°09.61'	10	6	134	80	0
12	801128	1821:12.2	39°16.32'	120°27.74'	21.8	5.5	314	60	0
13	750801	2020:12.8	39°26.33'	121°31.71'	5.5	5.7	270	65	-70
14	820903	1858:24.1	39°36.92'	122°34.96'	14.6	4.2	214	74	127
15	781112	1307:57.0	39°29.46'	122°57.09'	10.2	4.3	60	80	180
16	771122	2115:52.2	39°25.10'	123°16.19'	6.6	5.1	65	44	-166
17	780326	0027:03.8	39°11.82'	123°08.49'	6.0	4.7	55	54	-169
18	780331	0103:26.8	38°28.92'	123°20.04'	6.4	3.6	56	20	90
19	820529	1302:23.9	38°47.87'	122°49.35'	4.8	4.3	39	90	-167
20	770911	2346:11.5	38°39.96'	122°45.61'	7.0	3.7	76	90	-167
21	780908	1659:47.6	38°37.86'	121°54.59'	8.1	4.3	239	20	90
22	870103	1354:18.0	38°44.89'	121°37.90'	11.4	1.8	90	56	-68
23	770905	1745:28.0	38°09.68'	122°10.44'	7.5	3.7	76	90	180
24	770604	2057:07.8	38°09.42'	121°54.51'	18.3	3.6	70	80	180
25	770108	0938:07.0	37°54.94'	122°11.58'	10.4	4.5	240	66	180
26	790428	0044:44.7	37°37.32'	122°27.68'	11.6	4.2	49	70	169
27	840327	0336:35.3	37°43.48'	122°08.41'	3.3	4.5	55	56	173
28	770814	1425:34.4	37°43.42'	121°56.40'	6.5	3.5	60	84	180
29	800124	1900:09.1	37°50.20'	121°46.88'	11.9	5.9	247	75	-170
30	800127	0233:35.8	37°45.12'	121°42.54'	12.4	5.3	232	78	180
31	770621	0243:06.7	37°37.83'	121°40.55'	10.3	4.6	59	80	157
32	860331	1155:39.9	37°28.05'	121°41.63'	8.3	5.8	262	80	180
33	840424	2115:18.8	37°18.56'	121°40.68'	8.4	6.2	236	82	180
34	790806	1705:22.3	37°06.70'	121°30.03'	9.6	5.9	240	84	180
35	860126	1920:51.2	36°48.53'	121°16.10'	4.8	5.8	87	70	-170
36	820811	0746:43.0	36°37.60'	121°18.02'	9.2	4.5	53	85	-166
37	770727	2151:17.2	37°19.06'	122°07.24'	6.8	3.5	212	48	124
38	820818	0843:49.5	37°01.34'	121°44.66'	11.8	4.3	38	80	166
39	780702	1157:56.7	36°53.40'	122°10.86'	6.2	4	249	78	-147
40	840123	0540:19.9	36°22.13'	121°52.74'	7.7	5.2	60	78	173
41	860708	0040:23.0	36°03.81'	121°50.17'	11.9	4.4	60	34	90
42	830721	0123:33.0	36°09.17'	121°32.64'	5.2	3.9	41	90	-175
43	830829	1010:30.9	35°50.17'	121°20.70'	6.6	5.4	51	55	139
44	851124	1921:38.6	36°01.16'	120°53.12'	11.3	4.4	102	70	-170
54	820625	0358:23.0	35°57.43'	120°33.11'	9.1	4.2	51	80	180
46	660702	1216:15	35°47.3-	120°20.6-	9.1	3.5	231	78	180
47	821025	2226:03.7	36°19.31'	120°30.44'	11.0	5.5	198	28	90
48	830502	2342:38.1	36°13.96'	120°18.57'	10.0	6.7	217	23	90
49	850804	1201:55.8	36°08.59'	120°09.44'	11.4	5.7	217	14	90
50	850807	0016:03.41	36°01.13'	120°09.46'	14.9	4.6	216	20	82
51	860721	1442:26.1	37°31.91'	118°26.67'	9.1	6.5	245	58	180
52	831021	2244:00	35°54.9-	118°19.9-	4.4	4.5	83	46	-85
53	460315	1349:35.9	35°43.50'	118°03.27'	22	6.3	76	45	-117
54	880222	0743:12.8	35°29.84'	119°42.13'	19.1	4.2	182	44	90
55	800529	0338:47.5	34°58.65'	120°42.37'	9.2	5.1	28	34	98
56	820923	2042:50.6	34°52.19'	120°21.76'	4.8	4	36	56	63
57	841025	1036:02.4	34°44.21'	120°08.85'	6	4.5	211	43	90
58	780813	2254:53.4	34°20.82'	119°41.75'	12.1	5.1	10	26	57
59	730221	1445:57.3	34°03.89'	119°02.10'	8	5.9	350	36	55
60	790101	2314:38.9	33°56.65'	118°40.88'	11.1	5	10	60	85
61	710209	1400:41.8	34°24.67'	118°24.03'	8.1	6.4	20	54	76

TABLE 5.2.—Locations and focal-mechanism parameters for selected earthquakes in California—Continued

Event	Date (yr/mo/d)	Time (G.m.t.)	Lat N.	Long W.	Depth (km)	$M_L$	Focal-mechanism parameters		
							DD (°)	DA (°)	Rake (°)
62	790227	1540:58.9	33°56.7'	118°19.5'	9.7	3	135	60	20
63	871001	1442:19.8	34°03.11'	118°04.56'	14.7	6.1	175	65	90
64	520721	1152:14	35°00.—'	119°01.—'	0	7.7	140	63	49
65	820421	2119:30.2	35°00.48'	119°20.94'	15.0	3.2	201	76	170
66	781107	0028:45.6	34°39.93'	118°24.27'	13.4	2.6	200	85	176
67	840414	0227:02.6	34°29.51'	118°04.01'	11.9	2.9	357	56	80
68	850719	1617:01.7	34°23.20'	117°39.79'	8.1	2.8	196	80	169
69	700912	1430:53.0	34°16.18'	117°32.40'	8	5.4	55	60	140
70	810904	1550:50.3	33°40.26'	119°06.67'	5	5.3	315	80	0
71	330311	0154:07.8	33°36.99'	117°58.00'	0	6.3	320	90	0
72	860713	1347:08.2	32°58.24'	117°52.19'	6	5.3	50	50	110
73	850618	0428:14.8	32°40.22'	117°10.33'	12.1	4	255	85	175
74	841010	2122:58.9	33°08.26'	116°30.06'	11.6	4.5	260	80	191
75	750601	0138:49.2	34°30.94'	116°29.72'	4.1	5.2	247	70	-165
76	790315	2107:16.5	34°19.63'	116°26.68'	2.1	5.2	258	81	167
77	810912	2123:07.3	34°09.90'	117°15.93'	4.2	3.8	294	63	-52
78	851002	2344:12.4	34°01.40'	117°14.71'	15.2	4.8	242	75	165
79	781120	0655:09.1	34°09.07'	116°58.52'	12.9	4.3	227	75	145
80	860708	0920:44.5	33°59.91'	116°36.38'	11.1	5.6	30	45	170
81	850119	0030:13.0	33°59.64'	116°23.83'	2.9	3.9	310	63	-40
82	800225	1047:38.5	33°30.05'	116°30.79'	13.9	5.5	38	68	191
83	690428	2320:42.9	33°20.60'	116°20.78'	20	5.8	230	80	191
84	680409	0228:59.1	33°11.39'	116°07.72'	11	6.4	42	90	180
85	871124	1315:56.4	33°00.69'	115°51.31'	1.7	6.2	125	80	0
86	831227	2134:37.7	33°46.79'	116°07.32'	2.7	3.1	251	82	-148
87	791204	0828:17.6	33°34.55'	115°54.75'	5.1	2.7	51	71	-165
88	810426	1209:28.4	33°05.90'	115°37.90'	3.0	5.7	150	80	0
89	791015	2316:53.4	32°36.81'	115°19.09'	12.1	6.6	42	90	180

on easterly-striking planes (events 37, 67), through right-lateral strike slip on planes parallel to the San Andreas fault (events 65, 66, 68, 87), to normal or normal-oblique slip on northerly-striking planes (events 77, 81).

Moderate earthquakes with strike-slip focal-mechanisms that are not located on major faults of the San Andreas system but yet are broadly associated with it commonly have right-slip planes, with strikes ranging from northwestward (event 42) to north-southward (events 35, 44, 74, 75, 76, 86). In most cases, these right-slip planes agree in strike with local mapped faults or with alignments of epicenters that strongly suggest active faults (events 75, 76).

#### CRUSTAL CONVERGENCE ADJACENT TO THE SAN ANDREAS FAULT SYSTEM

One of the more important results to emerge from high-resolution focal-mechanism studies in recent years is that earthquakes occurring even a short distance off faults of the San Andreas system can involve displacements that diverge sharply from local San Andreas strike-slip displacements. This pattern is particularly

pronounced in the strong component of reverse slip at large angles (more than 60°) to the local strike of the San Andreas fault on both sides of the San Andreas fault system in both the Transverse and Coast Ranges.

North-south convergence within the Transverse Ranges is dominated by reverse slip on easterly-striking planes. The  $M=7.7$  Kern County earthquake of 1952 (event 64), which occurred on the south-dipping White Wolf fault along the north flank of the Transverse Ranges about 25 km north of the junction of the San Andreas and Garlock faults, and the  $M=6.6$  San Fernando earthquake of 1971 (event 71), which ruptured a 20-km-long stretch of the northeast-dipping San Gabriel-San Fernando thrust faults (Whitcomb, 1971; Heaton, 1982), are two striking examples of this deformation. So, also, is the alignment of  $M=5-6$  reverse-slip earthquakes (events 59, 60, 63) along the southern margin of the Transverse Ranges. The reverse slip on east-west-striking planes associated with these earthquakes suggests that the north-dipping Santa Monica-Cucamonga fault serves as an important convergent boundary between the Peninsular and Transverse Ranges.

Figure 5.11A also shows that the east-west-trending zone of convergence associated with these earthquakes



TABLE 5.3.—Locations and focal-mechanism parameters for earthquakes in the Coalinga-Kettleman Hills region

[Same symbols as in table 5.2]

Event	Date (yr/mo/d)	Time (G.m.t.)	Lat N.	Long W.	Depth (km)	$M_L$	Focal-mechanism parameters		
							DD (°)	DA (°)	Rake (°)
a	760114	2143:59.5	36°04.88'	120°15.09'	9.0	4.7	85	42	168
47	821025	2226:03.7	36°19.31'	120°30.44'	10.9	5.5	198	23	90
48	830502	2342:38.1	36°13.96'	120°18.57'	10.0	6.7	217	23	90
b	830522	0839:21.7	36°09.03'	120°12.09'	10.5	4.2	164	40	73
c	830524	0902:17.7	36°15.24'	120°19.00'	8.9	4.7	256	18	111
d	830611	0309:52.2	36°15.33'	120°27.01'	2.4	5.2	107	50	90
e	830612	0131:27.5	36°07.55'	120°17.71'	14.5	4.0	296	44	168
f	830722	0239:54.1	36°14.44'	120°24.53'	7.3	6.0	85	38	102
g	830722	0343:01.0	36°13.31'	120°24.37'	7.9	5.0	72	30	85
h	830909	0916:13.5	36°13.91'	120°15.90'	6.7	5.3	64	75	161
i	840219	0943:09.4	36°17.10'	120°19.47'	10.7	4.5	66	52	90
49	850804	1201:55.8	36°08.59'	120°09.44'	11.4	5.7	217	14	90
j	850804	1208:41.3	36°06.67'	120°05.23'	10.9	4.3	188	44	85
k	850804	1515:39.3	36°02.85'	120°04.57'	11.1	4.4	203	26	90
l	850805	1445:37.8	36°07.48'	120°05.99'	7.5	4.4	229	20	105
50	850807	0016:03.4	36°01.13'	120°09.46'	14.9	4.6	216	20	82
m	850809	0847:09.7	36°06.36'	120°02.32'	9.9	3.6	218	30	82
n	850809	1242:18.8	36°05.94'	120°08.39'	6.1	3.8	233	38	113
o	850914	0302:44.6	36°11.57'	120°18.89'	9.4	3.6	225	44	112
p	850915	0909:46.8	36°04.72'	120°09.68'	13.1	3.5	77	16	90
q	870214	0726:50.3	36°09.56'	120°21.53'	14.6	5.2	238	48	98

curves northward near Santa Monica Bay and continues northwestward along the coast at least as far as Point Sal and probably as far as San Simeon. Focal mechanisms of earthquakes along this zone from Point Sal to Whittier (events 55–60, 63) are predominantly reverse slip, with slip directions nearly normal to the local trend of the zone. The focal mechanism of event 43 near San Simeon, which indicates right-oblique reverse slip on a northeast-dipping plane parallel to the coast, is intermediate between those of event 40 at Point Sur and event 55 at Point Sal.

Reverse-slip focal mechanisms for offshore events 18 and 41 in central California and for event 72 in southern California suggest that the offshore crust is undergoing compression normal to the coastline throughout the length of the San Andreas fault system. The Coalinga-Kettleman Hills earthquake sequence of 1982–85 (events 47–50, fig. 5.11A) emphasizes the important role of crustal convergence along the southern Coast Ranges-Great Valley boundary in central California. The principal events in this sequence (event 48, Coalinga, and event 49, Kettleman Hills, fig. 5.11A) involved reverse slip on subparallel planes at depths of 10 to 12 km that dip gently (approx 20°) southwest. Much of the aftershock activity, however, occurred at shallower depths and involved high-angle reverse slip on planes dipping steeply (45°–70°) northeast (events f, g, i, o, q, fig. 5.11B). Displacements associated with these earthquakes, which are nearly perpendicular to the San Andreas fault, represent

a convergent process in which Franciscan melange on the west is being wedged between crystalline basement and the overlying Great Valley sedimentary sequence on the east (Wentworth and others, 1983; Eaton, 1990).

The boundary between the Coast Ranges and Great Valley is marked by reverse-slip earthquakes throughout much of its length: event 54 southeast of the Kettleman Hills, the Coalinga-Kettleman Hills sequence, event 21 near Winters east of Lake Berryessa, and event 14 west of Oroville. The similarity in focal mechanism of event 21 near Winters to the Coalinga and Kettleman Hills main shocks suggests that the convergent process acting in the southern Coast Ranges is common to the entire eastern margin of the Coast Ranges. Indeed, the strong earthquakes that shook the Winters-Vacaville-Dixon area in 1892, just south of event 21, resemble the Coalinga-Kettleman Hills sequence in both setting and intensity distribution. Focal mechanisms of smaller earthquakes along the Coast Ranges-Great Valley boundary in central California studied by Wong and others (1988) also suggest convergence across that boundary.

Convergence normal to the strike of the San Andreas fault is not limited to the coast and the Coast Ranges-Great Valley boundary described above. In a detailed examination of the focal mechanisms of aftershocks of the 1984 Morgan Hill earthquake, Oppenheimer and others (1988) concluded that the direction of maximum compression immediately adjacent to the Calaveras branch of the San Andreas fault is at an angle of about 80° to the N. 10°



W. strike of the fault. Along the entire stretch of the San Andreas fault from Parkfield to the Salton Sea, Jones (1988) found a constant angle of  $65^\circ$  between the strike of the fault and the maximum-principal-stress direction for earthquakes occurring off the fault.

This evidence from earthquake focal mechanisms and other stress indicators (such as borehole breakouts and fold axes) that the maximum principal compressive stress may be oriented at a high angle to the local strike of the San Andreas fault seems to contradict long-accepted ideas for brittle failure in the crust based on laboratory experiments in rock mechanics. Zoback and others (1987) and Oppenheimer and others (1988) suggested that these relations can be explained by an exceptionally low average shear strength for the San Andreas fault system. As pointed out by Lachenbruch and McGarr in chapter 10, however, the strength and state of stress along the San Andreas fault are still matters for discussion.

#### EAST-WEST EXTENSION IN THE SIERRA NEVADA

The three moderate-earthquake focal mechanisms for the Sierra Nevada and its western foothills shown in figure 5.11A all indicate normal faulting on northerly-striking planes and suggest pervasive east-west extension throughout the Sierra Nevada. Event 52 is in a dense north-south-trending band of epicenters about 15 km east of the Kern River canyon, and event 53 is in a north-south-trending band of earthquakes about 10 km west of the Sierra frontal fault near Walker Pass. These relations suggest that the east-west spreading and associated normal faulting on northerly-striking faults of the Great Basin are encroaching into the southeast corner of the Sierra Nevada block (Jones and Dollar, 1986).

Event 13 is the main shock ( $M=5.7$ ) of an earthquake sequence on a north-south-striking, west-dipping normal fault near the Oroville Dam that occurred in 1975. The uplift of the Sierra Nevada relative to the Great Valley to the west indicated by the focal mechanism of this event is also visible in the Chico monocline, which marks the Sierra Nevada-Great Valley boundary northwest of Oroville.

#### CONJUGATE FAULTING IN THE SIERRA NEVADA-GREAT BASIN BOUNDARY ZONE

The Sierra Nevada-Great Basin boundary zone is represented in figure 5.11A by three focal mechanisms. Events 11 and 12 lie northwest of Lake Tahoe along the edge of a minor gap in the band of seismicity along the east edge of the Sierra Nevada. Both events appear to have resulted from left-lateral slip along steeply dipping, northeast-striking faults; both events had aftershock regions that were elongate northeast-southwest. About

250 km southeast, the  $M=6.4$  July 21, 1986, Chalfant Valley earthquake (event 51) resulted from right-lateral strike-slip displacement on a north-northwest-striking surface dipping  $60^\circ$  SW. An  $M=5.7$  foreshock on July 20 resulted from left-lateral strike slip on a northeast-striking, northwest-dipping surface. These two conjugate slip surfaces merge at their north ends (Cockerham and Corbett, 1987; Smith and Priestly, 1988).

The zone of intense seismicity in the vicinity of Long Valley caldera and the Sierra Nevada block to the south produced 11  $M \geq 5.5$  earthquakes from 1978 through 1984 (Savage and Cockerham, 1987), as well as many thousands of smaller events and numerous earthquake swarms. Most of the larger events occurred in the Sierra Nevada block south of Long Valley caldera, involving left-lateral slip along near-vertical, north-south- to north-northeast-striking faults. One of four  $M \approx 6$  events that occurred on May 25-27, 1980, however, was located within the south moat of the caldera along the west-northwest-striking fault zone that produced most of the earthquake swarms (see Hill and others, 1985a, b).

#### FRAGMENTATION OF THE SOUTHEAST CORNER OF THE GORDA PLATE

The 1980 Eureka  $M=7.2$  earthquake occurred along a fault break that extended from the continental slope 40 km west of the coastline at lat  $41^\circ$  N. for a distance of 140 km southwestward to the MFZ, virtually cutting off the southeast corner of the Gorda plate. Focal mechanisms of the main shock and largest aftershock (events 1, 3, fig. 5.11A) both indicate left-lateral strike-slip displacement along a vertical fault that coincides with the line of aftershocks. Some early aftershocks, including event 4 and other moderate events farther east along the MFZ, have focal mechanisms that indicate right-lateral slip along the MFZ. Although the main shock occurred beneath the Continental Shelf, it seems clear that the 1980 earthquake primarily involved the Gorda plate because the fault broke well beyond the base of the continental slope and the edge of the North American plate. Moreover, left-lateral slip along the 1980 break stimulated right-lateral slip along the adjacent part of the MFZ. Ongoing right-lateral displacement along the MFZ is also indicated by event 5 (Dec. 1983).

Two moderate earthquakes near Cape Mendocino in 1981 and 1987 (events 6 and 7, respectively) had focal mechanisms similar to that of the 1980 Eureka earthquake, indicating left-lateral strike-slip displacement on steeply dipping, northeast-striking planes. Aftershocks of the 1987  $M=5.8$  event outlined a narrow, steeply dipping, northeast-trending, 20-km-long zone between about 15- and 25-km depth that extended southwestward from the shoreline just north of Cape Mendocino to the



MFZ. This aftershock zone appears to cut off the southeasternmost corner of the Gorda plate just north of the abrupt eastward termination of intense seismicity along the MFZ, at a point that might be taken as the Mendocino triple junction from the viewpoint of seismicity.

Relative horizontal extension at seismogenic depths is suggested by events 2 and 8. Event 2 (Nov. 10, 1980; 7 km deep) was the largest in a detached cluster of shallow aftershocks 20 km east of the 1980 main shock, and event 8 (Apr. 9, 1987; 26 km deep) occurred about 100 km east of the 1980 main shock in the zone of seismicity associated with the subducting Gorda plate.

### DISCUSSION

The Pacific plate moved northwestward with respect to the North American plate by 300 to 400 mm during the 7-yr interval 1980–86. Earthquakes occurring along the San Andreas fault system during the same interval, however, accommodated only a small fraction of this relative plate motion. Only four earthquakes of  $M > 5$  occurred along branches of the San Andreas fault system during 1980–86: the pair of  $M = 5.9$ – $5.3$  Livermore earthquakes (events 29, 30, fig. 5.10A) on the Greenville fault (Jan. 24–27, 1980), the  $M = 6.2$  Morgan Hill earthquake (event 33) on the Calaveras fault (Apr. 24, 1984), and the  $M = 5.6$  North Palm Springs earthquake (event 80) on the Banning segment of the San Andreas fault (July 8, 1986). Each of these moderate San Andreas earthquakes ruptured fault segments limited to 20 to 30 km in length, with average displacements over the respective rupture surfaces of 100 to 200 mm (see Hartzell and Heaton, 1986). As is typical of earthquakes along the San Andreas fault system, each of these events involved nearly pure right-lateral strike-slip displacement coincident with the local strike of the fault. As is also typical of San Andreas earthquakes, slip on the first three events occurred on near-vertical fault planes with a northwestward to north-northwestward strike. The North Palm Springs earthquake, which ruptured a section of the east-west-striking Banning fault in the structurally complex San Geronio bend in the fault system at the southern margin of the Transverse Ranges, represents an important deviation from typical San Andreas earthquakes. Although its displacement was dominantly right-lateral strike slip, it occurred along a plane that dips  $45^\circ$  N. (Jones and others, 1986) and included a small but significant component of reverse slip (Mendoza and Hartzell, 1988). With the arguable exception of the North Palm Springs earthquake (arguable because of the complex section of the fault system in which it occurred), however, none of these  $M > 5$  earthquakes ruptured the main trace of the San Andreas fault. Indeed, the two most recent  $M > 5$  earth-

quakes to clearly do so were the  $M = 6$  Parkfield earthquake of 1966 (Bakun and McEvilly, 1984) and the  $M = 7.1$  Loma Prieta earthquake of 1989 (see chap. 6).

Thus, aside from the displacement accommodated by steady aseismic slip at a rate of 32 to 37 mm/yr along the creeping section of the fault in central California, most relative plate motion across the San Andreas transform boundary during this 7-yr interval accumulated as elastic shear strain. Accordingly, the earthquakes plotted in figures 5.3 through 5.9 are symptomatic of accumulating strain along the San Andreas fault system rather than of effective strain release. The latter requires rupture with a major earthquake along one of the locked stretches of the San Andreas fault.

### SEISMICITY PATTERNS AND THE EARTHQUAKE CYCLE

What changes in spatial-temporal patterns of earthquake occurrence might we expect to see as the next great earthquake on the San Andreas fault approaches? Both historical and instrumental seismicity records indicate that the spatial distribution of earthquakes in California changes only slowly over periods of decades to centuries, although the intensity of activity within this distribution fluctuates year to year (Ellsworth and others, 1981; Hill and others, in press; Hutton and others, in press). Temporal fluctuations in activity during the interval 1980–86, for example, were dominated by a short-lived aftershock sequence following the 1980 Eureka  $M = 7.2$  earthquake and by the long-lived aftershock sequence following the 1983 Coalinga  $M = 6.7$  earthquake. The overall spatial distribution of earthquakes in California, however, remained nearly stationary throughout this 7-yr interval. Furthermore, the spatial pattern defined by 1980–86 seismicity is much the same as that outlined by the record of  $M \geq 5$  earthquakes that extends back nearly 200 yr (see chap. 6).

Variations in the historical rate of moderate to large ( $M > 5$ ) earthquakes in central California before and after the 1906 San Francisco earthquake appear to mimic those described by Fedotov (1965) and Mogi (1968) for the earthquake cycle associated with great, subduction-zone earthquakes in Japan, Kamchatka, and the Kurile Islands (see chap. 6; Ellsworth and others, 1981). The history of instrumentally recorded  $M < 5$  earthquakes in California is too short, however, to indicate whether we might expect to see distinctive changes in the seismicity pattern a short time (months to years) before the next great earthquake on the San Andreas fault. We have yet to see, for example, whether the quiescent (locked) segments of the San Andreas fault remain aseismic except for the rupture of a great earthquake, or whether these segments become active with small to moderate earthquakes as foreshock activity to great earthquakes.



#### DISTRIBUTED SEISMICITY AND DEFORMATION OF THE PLATE MARGINS

The two largest earthquakes in California during the interval 1980-86 occurred off the faults of the San Andreas system, and their occurrence emphasizes the importance of deformation within the plate margins along the San Andreas transform boundary. The  $M=7.2$  Eureka event (Nov. 8, 1980), for example, involved deformation internal to the Gorda plate; and the  $M=6.7$  Coalinga event (May 2, 1983) involved crustal shortening with reverse slip perpendicular to the San Andreas fault. These two earthquakes and the many smaller, "off fault" events (fig. 5.4A) reflect local deviations from the simple rigid-plate approximation of plate tectonics.

#### DEFORMATION OF THE GORDA PLATE

As the small, youthful Gorda plate is subducted obliquely northeastward beneath the North American plate, it is being subjected to north-south compression in response to a component of convergence between the larger, older Juan de Fuca plate to the north and the Pacific plate to the south (Jachens and Griscom, 1983; Wilson, 1986). Distorted marine magnetic anomalies within the Gorda plate indicate that it has undergone progressive internal deformation over the past 5 Ma in response to this compression (Silver, 1971), and current seismicity within the plate (fig. 5.4) indicates that this deformation continues to the present.

The 1980 Eureka  $M=7.2$  earthquake emphasizes that part of this deformation occurs with left-lateral slip on northeast-striking faults within the plate. The seismicity map and cross sections (fig. 5.4) demonstrate that deformation associated with the Gorda plate terminates abruptly against the Pacific plate in a steeply north-dipping zone of interaction along the MFZ, which can be followed on shore beneath the North American plate as a gently east-dipping, subhorizontal zone of widely scattered small to moderate earthquakes. Thus, convergence between the Gorda and Pacific plates across the MFZ apparently occurs by crushing and thickening of the southern margin of the Gorda plate as it is jammed against the anvil-like mass formed by the thicker and colder Pacific plate. Diminished east-west stress in the Gorda plate resulting from the subducting limb of the plate farther east serves to increase the difference between the maximum (north-south) and minimum (east-west) compressive stresses within the plate, leading to left-lateral strike-slip displacements along northeast-striking faults, as in the  $M=7.2$  Eureka earthquake. This process accommodates the convergent component of Gorda-Pacific plate motion along the east end of the MFZ

at the expense of fragmentation and eastward expansion of the Gorda plate north of the MFZ.

#### THE SAN ANDREAS DISCREPANCY

Much of the seismicity adjacent to the San Andreas fault system is attributable to differences between the long-term slip rate and direction (slip vector) along the San Andreas fault system and that predicted for relative motion between the Pacific and North American plates along the San Andreas transform boundary on the basis of global models of plate motion. Minster and Jordan (1978, 1987) predicted that the direction of dextral slip between the Pacific and North American plates along the San Andreas transform boundary in central California is  $N. 35^{\circ} W.$  The main trace of the San Andreas system, however, strikes  $N. 41^{\circ} W.$  through central and northern California and  $N. 65^{\circ}-70^{\circ} W.$  through the Transverse Ranges in southern California. DeMets and others (1987) concluded that the marine magnetic anomalies at the mouth of the Gulf of California constrain the slip rate to an average of 49 mm/yr over the past 3 to 4 Ma. Both long-term geologic offset data and geodetic data measured over the past several decades, however, indicate that the average slip rate along the San Andreas fault system is only about 35 mm/yr. The contribution to deformation of the western margin of the North American plate from spreading across the Basin and Range province is about 10 mm/yr in a  $N. 56^{\circ} W.$  direction (Minster and Jordan, 1987). Ellsworth (see chap. 6) suggests that most of the San Andreas discrepancy can be explained if the component of dextral slip associated with historical Basin and Range earthquakes reflects a long-term trend superimposed on the  $N. 56^{\circ} W.$  spreading direction. If so, then the residual component of Basin and Range extension perpendicular to the San Andreas fault system is approximately balanced by convergence across the Coast Ranges and continental margin.

#### CONVERGENCE NORMAL TO THE SAN ANDREAS FAULT SYSTEM

Focal mechanisms of earthquakes occurring off the San Andreas fault system suggest that the component of the San Andreas discrepancy normal to the fault system may, indeed, be accommodated by distributed brittle deformation on either side of the fault system. These mechanisms range from dextral strike slip on planes subparallel to the San Andreas fault, through oblique-reverse slip, to nearly pure reverse slip with a slip direction perpendicular to the San Andreas fault.

The Coalinga-North Kettleman Hills earthquake sequence provides clear evidence for crustal convergence perpendicular to the San Andreas fault system in the



Coast Ranges. The several smaller events with similar mechanisms to the north along both the eastern and western (coastal) margins of the Coast Ranges (fig. 5.11) suggest that the convergence responsible for the Coalinga earthquake may be active the length of the Coast Ranges (Wong and others, 1988; Eaton and Rymer,

1990). The subparallelism of fold axes within the Coast Ranges with the San Andreas fault indicates that fault-normal convergence has been important for the past 3 Ma in central California (fig. 5.12; Page and Engebretson, 1984). Namson and Davis (1988) proposed that the entire system of Coast Range folds may be genetically related to

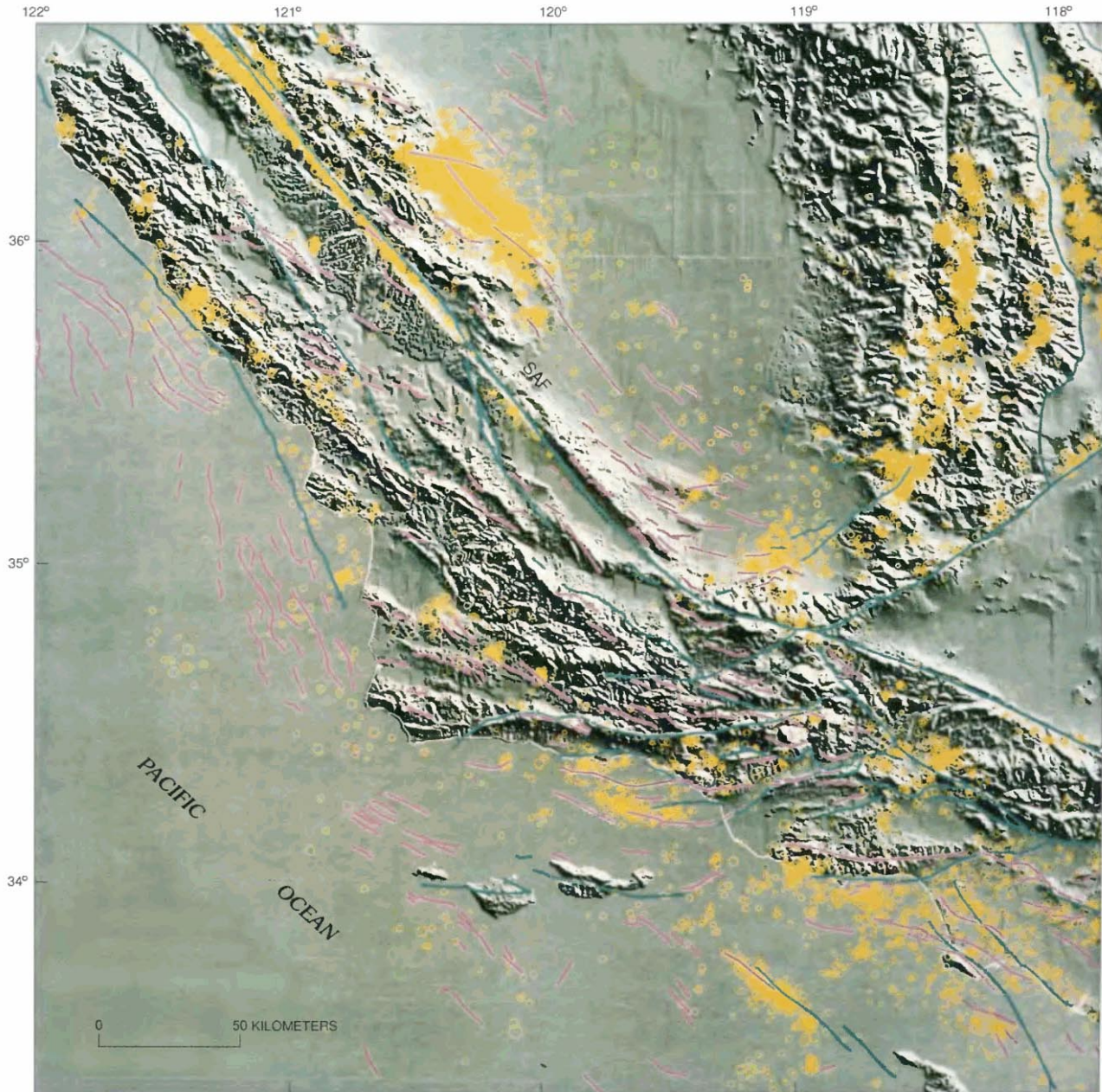


FIGURE 5.12.—Seismicity from 1980 to 1986 superimposed on digital shaded-relief image of central California, showing faults (blue) and fold axes (red). Size of symbol for epicenters (yellow) increases with magnitude from 1 to 6. Shaded relief by Raymond Batson, U.S. Geological Survey (illumination from north at 30°); overlays from Ross Stein (unpub. data, 1989). SAF, San Andreas fault.



Coalinga-like earthquake sequences and low-angle (blind) thrust faults that are rooted in a decollement near the base of the seismogenic crust. The reverse focal mechanisms for earthquakes associated with offshore faults along the western margin of the Coast Ranges suggest that, here, convergence involves westward thrusting of the Coast Ranges over oceanic crust of the Pacific plate.

The pronounced discrepancy in the strike of the San Andreas fault through the Transverse Ranges with respect to the Pacific-North American plate slip direction provides an obvious source of local crustal convergence (Hill and Dibblee, 1953; Atwater, 1970), and the associated structural complexities serve to distribute brittle deformation (seismicity) much more widely about the San Andreas fault system in southern California than about the relatively straight sections of the fault system in central and northern California. The largest earthquake in California since the great 1906 San Francisco earthquake occurred near the northern margin of this convergent regime; this  $M=7.7$  Kern County earthquake ruptured some 35 km of the southeast-dipping White Wolf fault with left-oblique reverse slip on July 21, 1952.

The focal mechanisms of larger Transverse Range earthquakes, together with the mapped attitudes of major faults with Holocene offsets, show that much of this convergence occurs with slip on north-dipping thrust faults within and along the southern margin of the central Transverse Ranges (fig. 5.11A). For earthquakes in the western Transverse Ranges, the direction of reverse slip is more southwestward, consistent with thrusting of the western Transverse Ranges over the Pacific plate similar to that in the Coast Ranges to the north.

#### EXTENSIONAL DEFORMATION AND THE SOUTHERN SECTION OF THE SAN ANDREAS FAULT SYSTEM

The fault-normal convergence that dominates deformation adjacent to the San Andreas fault system through both the Coast Ranges and Transverse Ranges gives way rather abruptly to the extensional regime of the Salton Trough near the southern margin of the intensely active San Geronio bend in the fault. Focal mechanisms of earthquakes occurring on secondary structures adjacent to the seismically quiescent Indio segment of the San Andreas fault, for example, show a mix of strike- and dip-slip mechanisms. As is the case farther north, however,  $P$ -axes for these earthquakes tend to be oriented at a high angle ( $60^{\circ}$ - $65^{\circ}$ ) to the fault, suggesting that the Indio segment of the fault may also be relatively weak (Jones, 1988).

One particularly noteworthy aspect of seismicity south of the Transverse Ranges is the tendency for earthquakes to occur along conjugate strike-slip structures. Recall that the Sierra Nevada-Great Basin boundary

zone also shows this tendency and that both regions are subject to extensional deformation, earthquake swarms, and late Quaternary volcanism. Earthquake sequences within the southern section of the San Andreas fault system commonly produce epicenter lineations that intersect at nearly a  $90^{\circ}$  angle with the northwest-striking right-slip plane and the northeast-striking left-slip plane. Earthquake-swarm sequences in the Brawley seismic zone, for example, typically occur along northeast-striking lineations normal to the trace of the adjacent Imperial fault (Johnson, 1979), and the  $M=5.7$  Westmorland earthquake of 1981 involved left-lateral slip along several subparallel, northeast-striking planes (Johnson and Hutton, 1982). The diffuse lineations of epicenters spanning the area of the Peninsular Ranges between the San Jacinto and Elsinore faults also tend to be orthogonal to these two branches of the San Andreas fault system (fig. 5.10A). An impressive recent example of this orthogonal conjugate pattern is the  $M=6.2$  and  $6.6$  Superstition Hills earthquakes of November 24, 1987 (Magistrale and others, 1988).

The kinematics of these conjugate structures remains a matter of conjecture. Dextral slip along throughgoing faults of the San Andreas system must certainly dominate deformation, and the shorter, northeast-striking structures must play only a secondary role. Nicholson and others (1986) proposed that the northeast-striking lineations represent the boundaries between blocks rotating clockwise much like roller bearings, between subparallel pairs of dextral strike-slip faults. Hill (1977) and Weaver and Hill (1978/79) suggested that within local spreading centers, such as the Brawley seismic zone, conjugate strike-slip structures form miniature triple junctions with a dike or normal fault that subtends the acute angle between the conjugate strike-slip faults.

#### MAXIMUM FOCAL DEPTHS AND THICKNESS OF THE SEISMOGENIC CRUST

Maximum focal depths of earthquakes beneath the San Andreas transform boundary range from less than 5 km beneath the Geysers geothermal field in the northern Coast Ranges to more than 20 km beneath the Transverse Ranges, the eastern margin of the Coast Ranges, and the San Jacinto and Elsinore faults in southernmost California. Beneath relatively straight segments of the San Andreas fault system through central California, maximum focal depths range from 12 to 15 km (figs. 5.7, 5.8). Sibson (1983) pointed out that these variations in maximum focal depth along the San Andreas fault system are inversely correlated with surficial heat flow, and he argued that the maximum depth of earthquakes coincides with the temperature-dependent transition from brittle failure in the upper crust to aseismic, quasi-plastic flow in



the lower crust and upper mantle. For quartz-bearing rocks typical of the upper crust and deformation rates typical of the San Andreas fault system ( $1 \times 10^{-14}$  to  $1 \times 10^{-13} \text{ s}^{-1}$ ), this brittle/ductile transition occurs at about 300 °C (Sibson, 1983). By this interpretation, the thin seismogenic crust beneath both the Geysers and Brawley geothermal fields in northern and southern California, respectively, reflects elevated temperatures in the shallow crust, whereas the relatively thick seismogenic crust beneath the Transverse Ranges and the eastern margin of the Coast Ranges reflects depressed temperatures in the midcrust associated with crustal convergence. Although temperature may dominantly influence the thickness of the seismogenic crust, local variations in rock composition (particularly the presence or absence of modal quartz and structural water) and in strain rate can also be important. These variations, for example, may help explain isolated clusters of deep earthquakes, such as the 20- to 24-km-deep events north of San Pablo Bay in central California (see cross secs. *F-F'*, *G-G'*, fig. 5.8*B*).

In any case, the thickness of the seismogenic crust beneath the San Andreas transform boundary seems to be much more strongly related to temperatures in the crust than to the structural thickness of crust defined by the depth to the Moho (see chap. 8). This relation is strikingly illustrated by the twofold increase in thickness of the seismogenic crust beneath the rootless Transverse Ranges.

#### DECOLLEMENT AT THE BASE OF THE SEISMOGENIC CRUST?

A theme common to models of crustal convergence along the San Andreas fault system involves low-angle reverse slip on decollement surfaces near the base of the seismogenic crust (Wentworth and others, 1983; Webb and Kanamori, 1985; Namson and Davis, 1988; Eaton and Rymer, 1990). A natural extension of this theme leads to a view of the seismogenic crust as a conglomeration of relatively rigid blocks interacting by frictional slip along weak preexisting faults (block boundaries) in response to regional stresses transmitted through both the brittle crust and quasi-plastic deformation in the underlying lithosphere (Hill, 1982). However, the nature of a decollement surface at the base of the brittle crust and the relation of the seismogenic San Andreas fault system to the aseismic transform boundary in the underlying lithosphere remain speculative. It is not yet clear, for example, whether the San Andreas fault continues below the seismogenic crust as a narrow, near-vertical boundary (possibly offset a substantial distance from the seismogenic fault by slip on the horizontal decollement surface) that slips by quasi-plastic, mylonitic deformation

or whether it broadens rapidly with depth into a wide shear zone spanning, say, the entire width of the Coast Ranges (see chap. 7; Sibson, 1983).

#### CONCLUSIONS

The spatial-temporal pattern of earthquake occurrence within the seismogenic crust along the San Andreas fault system is the brittle manifestation of distributed deformation of the lithosphere between the Pacific and North American plates along the San Andreas transform boundary. As we develop a more complete model of the long-term behavior of the seismogenic crust, including relations between great, plate-boundary earthquakes that periodically rupture the principal strand of the San Andreas fault system and the persistent background of small to moderate earthquakes on adjacent structures, our image of the deeper deformation will improve. Together will come a more complete understanding of the processes controlling deformation along the transform boundary and of the earthquake cycle.

#### REFERENCES CITED

- Allen, C.R., 1968, The tectonic environments of seismically active and inactive areas along the San Andreas fault system, *in* Dickinson, W.R., and Grantz, Arthur, eds., *Proceedings of conference on geologic problems of San Andreas fault system*: Stanford, Calif., Stanford University Publications in the Geological Sciences, v. 11, p. 70-82.
- 1981, The modern San Andreas fault, *in* Ernst, W.G., ed., *The geotectonic development of California* (Ruby volume 1): Englewood Cliffs, N.J., Prentice-Hall, p. 511-534.
- Astiz, Luciana, and Allen, C.R., 1983, Seismicity of the Garlock fault, California: *Seismological Society of America Bulletin*, v. 73, no. 6, pt. A, p. 1721-1734.
- Atwater, Tanya, 1970, Implications of plate tectonics for the Cenozoic evolution of western North America: *Geological Society of America Bulletin*, v. 81, no. 12, p. 3513-3535.
- Bakun, W.H., Clark, M.M., Cockerham, R.S., Ellsworth, W.L., Lindh, A.G., Prescott, W.H., Shakal, A.F., and Spudich, Paul, 1984, The 1984 Morgan Hill, California, earthquake: *Science*, v. 225, no. 4659, p. 288-291.
- Bakun, W.H., and Lindh, A.G., 1985, The Parkfield, California, earthquake prediction experiment: *Science*, v. 229, no. 4714, p. 619-623.
- Bakun, W.H., and McEvilly, T.V., 1984, Recurrence models and Parkfield, California earthquakes: *Journal of Geophysical Research*, v. 89, no. B5, p. 3051-3058.
- Bolt, B.A., McEvilly, T.V., and Uhrhammer, R.A., 1981, The Livermore Valley, California, sequence of January 1980: *Seismological Society of America Bulletin*, v. 71, no. 2, p. 451-463.
- Bolt, B.A., and Miller, R.D., 1975, Catalogue of earthquakes in northern California and adjoining areas 1 January 1910-31 December 1972: Berkeley, University of California, Seismographic Station, 567 p.
- Boore, D.M., 1977, Strong-motion recordings of the California earthquake of April 18, 1906: *Seismological Society of America Bulletin*, v. 67, no. 3, p. 561-577.



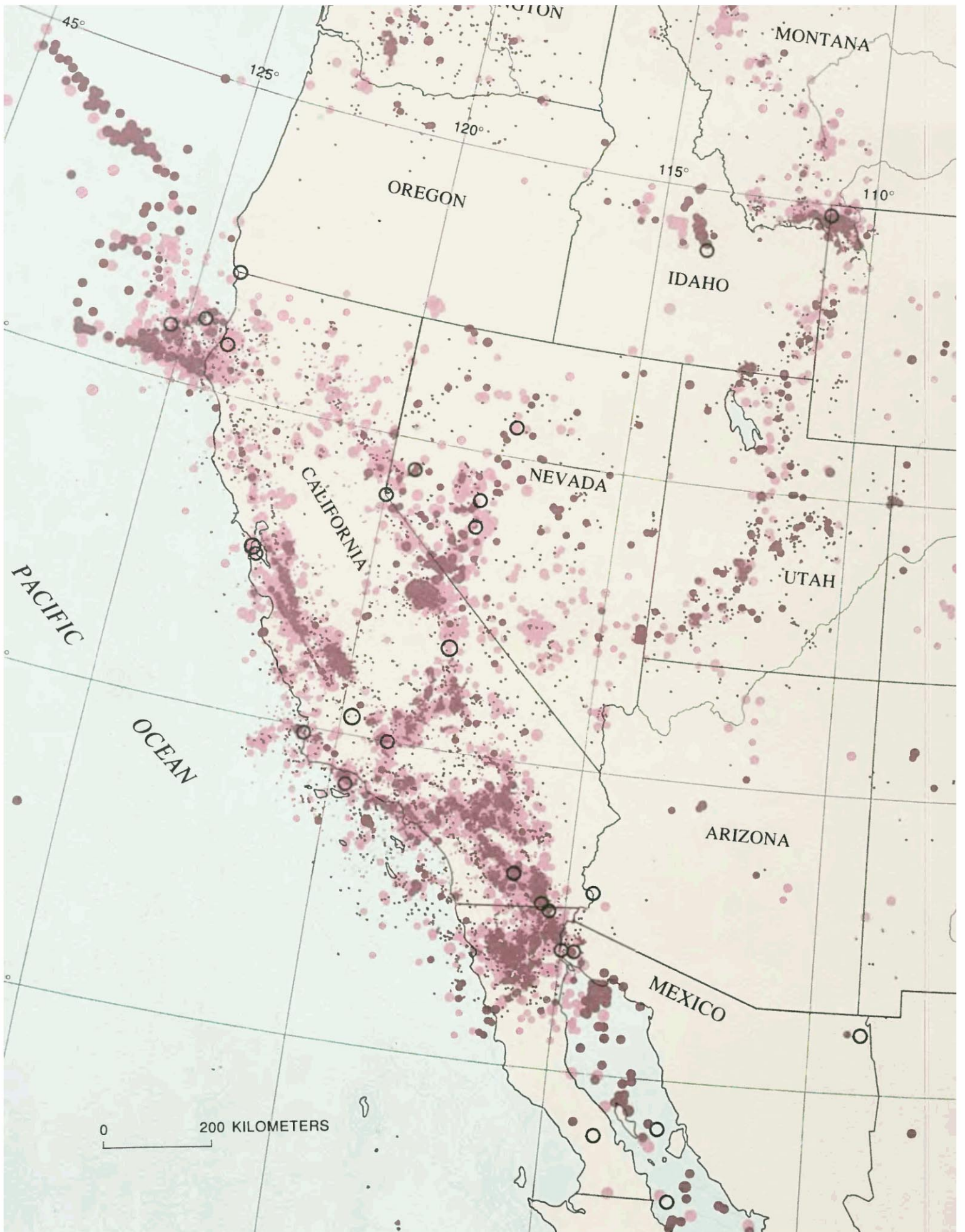
- Cockerham, R.S., 1984, Evidence for a 180-km-long subducted slab beneath northern California: *Seismological Society of America Bulletin*, v. 74, no. 2, p. 569-576.
- Cockerham, R.S., and Corbett, E.J., 1987, The 1986 Chalfant Valley, California, earthquake sequence: Preliminary results: *Seismological Society of America Bulletin*, v. 77, no. 1, p. 280-289.
- Dehlinger, Peter, and Bolt, B.A., 1984, Seismic parameters along the Bartlett Springs fault zone in the Coast Ranges of northern California: *Seismological Society of America Bulletin*, v. 74, no. 5, p. 1785-1798.
- DeMets, Charles, Gordon, R.G., Stein, Seth, and Argus, D.F., 1987, A revised estimate of the Pacific-North America motion and implications for western North America plate boundary zone tectonics: *Geophysical Research Letters*, v. 14, no. 9, p. 911-914.
- Dickinson, W.R., 1981, Plate tectonics and the continental margin of California, in Ernst, G.W. ed., *The geotectonic development of California* (Ruby volume 1): Englewood Cliffs, N.J., Prentice-Hall, p. 2-28.
- Donnelly-Nolan, J.M., Hearn, B.C., Jr., Curtis, G.H., and Drake, R.E., 1981, Geochronology and evolution of the Clear Lake Volcanics, in McLaughlin, R.J., and Donnelly-Nolan, J.M., eds., *Research in the Geysers-Clear Lake geothermal area, northern California*: U.S. Geological Survey Professional Paper 1141, p. 47-60.
- Eaton, J.P., 1989, Dense microearthquake network study of northern California earthquakes, chap. 13 of Litehiser, J.J., ed., *Observatory seismology, a centennial symposium for the Berkeley Seismographic Stations*: Berkeley, University of California Press, p. 199-224.
- 1990, The earthquake and its aftershocks from May 2 through September 30, 1983, chap. 8 of Rymer, M.J., and Ellsworth, W.E., eds., *The Coalinga, California, earthquake of May 2, 1983*: U.S. Geological Survey Professional Paper 1487, p. 113-170.
- Eaton, J.P., Lee, W.H.K., and Pakiser, L.C., 1970a, Use of micro-earthquakes in the study of the mechanics of earthquake generation along the San Andreas fault in central California: *Tectonophysics*, v. 9, no. 2-3, p. 259-282.
- Eaton, J.P., O'Neill, M.E., and Murdock, J.N., 1970b, Aftershocks of the 1966 Parkfield-Cholame, California, earthquake: A detailed study: *Seismological Society of America Bulletin*, v. 60, no. 4, p. 1151-1197.
- Eaton, J.P., and Rymer, M.J., 1990, Regional seismotectonic model for the southern Coast Ranges, chap. 7, of *The Coalinga, California, earthquake of May 2, 1983*: U.S. Geological Survey Professional Paper 1487, p. 97-111.
- Eberhart-Phillips, Donna, and Oppenheimer, D.H., 1984, Induced seismicity in the Geysers geothermal area, California: *Journal of Geophysical Research*, v. 89, no. B2, p. 1191-1207.
- Ellsworth, W.L., 1975, Bear Valley, California, earthquake sequence of February-March 1972: *Seismological Society of America Bulletin*, v. 65, no. 2, p. 483-506.
- Ellsworth, W.L., Lindh, A.G., Prescott, W.H., and Herd, D.G., 1981, The 1906 San Francisco earthquake and the seismic cycle, in Simpson, D.W., and Richards, P.G., eds., *Earthquake prediction: An international review* (Maurice Ewing Series 4): Washington, American Geophysical Union, p. 126-140.
- Ellsworth, W.L., Olson, J.A., Shijo, L.N., and Marks, S.M., 1982, Seismicity and active faults in the eastern San Francisco Bay region, in Hart, E.W., Hirschfeld, S.E., and Schulz, S.S., eds., *Conference on Earthquake Hazards in the Eastern San Francisco Bay Area, Hayward, Calif., 1982*, Proceedings: California Division of Mines and Geology Special Publication 62, p. 83-91.
- Fletcher, J.B., Haar, L.C., Hanks, T.C., Baker, L.M., Vernon, F.L., Berger, Jon, and Brune, J.N., 1987, The digital array at Anza California: Processing and initial interpretation of source parameters: *Journal of Geophysical Research*, v. 92, no. B1, p. 369-382.
- Fedotov, S.A., 1965, Regularities in the distribution of strong earthquakes in Kamchatka, the Kuril Islands and northeastern Japan: *Akademia Nauk SSSR, Institut Fiziki Zemli Trudy*, v. 36, p. 66-93.
- Hanks, T.C., Hileman, J.A., and Thatcher, Wayne, 1975, Seismic moments of the larger earthquakes of the southern California region: *Geological Society of America Bulletin*, v. 86, no. 8, p. 1131-1139.
- Hartzell, S.H., and Heaton, T.H., 1986, Rupture history of the 1984 Morgan Hill, California, earthquake from the inversion of strong motion records: *Seismological Society of America Bulletin*, v. 76, no. 3, p. 649-674.
- Heaton, T.H., 1982, The 1971 San Fernando, [California], earthquake: A double event?: *Seismological Society of America Bulletin*, v. 72, no. 6, p. 2037-2062.
- Hileman, J.A., Allen, C.R., and Nordquist, J.M., 1973, Seismicity of the southern California region 1 January 1932 to 31 December 1972: Pasadena, California Institute of Technology, Seismological Laboratory, 487 p.
- Hill, D.P., 1977, A model for earthquake swarms: *Journal of Geophysical Research*, v. 82, no. 8, p. 1347-1352.
- 1982, Contemporary block tectonics: California and Nevada: *Journal of Geophysical Research*, v. 87, no. B7, p. 5433-5450.
- Hill, D.P., Bailey, R.A., and Ryall, A.S., 1985a, Active tectonic and magmatic processes beneath Long Valley caldera, eastern California: An overview: *Journal of Geophysical Research*, v. 90, no. B13, p. 11111-11120.
- Hill, D.P., Eaton, J.E., Ellsworth, W.L., Cockerham, R.S., Lester, F.W., and Corbett, E.J., in press, The Seismotectonic fabric of central California, in Slemmons, D.B., Engdahl, E.R., Blackwell, D.D., Schwartz, D.P., and Zoback, M.D., eds., *Neotectonics of North America* (DNAG Associated Volume GSMV-1): Boulder Colo., Geological Society of America.
- Hill, D.P., Mowinkel, Penelope, and Peake, L.G., 1975, Earthquakes, active faults, and geothermal areas in the Imperial Valley, California: *Science*, v. 188, no. 4195, p. 1306-1308.
- Hill, D.P., Wallace, R.E., and Cockerham, R.S., 1985b, Review of evidence on the potential for major earthquakes and volcanism in the Long Valley-Mono Craters-White Mountains regions of eastern California: *Earthquake Prediction Research*, v. 3, no. 3-4, p. 571-594.
- Hill, M.L., and Dibblee, T.W., 1953, San Andreas, Garlock, and Big Pine faults—a study of the character, history, and tectonic significance of their displacements: *Geological Society of America Bulletin*, v. 64, no. 4, p. 435-438.
- Hutton, L.K., Jones, L.M., Hauksson, Egill, and Given, D.D., in press, Seismotectonics of southern California, in Slemmons, D.B., Engdahl, E.R., Blackwell, D.D., Schwartz, D.P., and Zoback, M.D., eds., *Neotectonics of North America* (DNAG Associated Volume GSMV-1): Boulder, Colo., Geological Society of America.
- Jachens, R.C., and Griscom, Andrew, 1983, Three-dimensional geometry of the Gorda plate beneath northern California: *Journal of Geophysical Research*, v. 88, no. B11, p. 9375-9392.
- Johnson, C.E., 1979, I, CEDAR—an approach to the computer automation of short-period local seismic networks; seismotectonics of the Imperial Valley of southern California: Pasadena, California Institute of Technology, Ph.D. thesis, 343 p.
- Johnson, C.E., and Hill, D.P., 1982, Seismicity of the Imperial Valley, in *The Imperial Valley, California, earthquake of October 15, 1979*: U.S. Geological Survey Professional Paper 1254, p. 59-76.
- Johnson, C.E., and Hutton, L.K., 1982, Aftershocks and pre-earthquake seismicity, in *The Imperial Valley, California, earthquake of October 15, 1979*: U.S. Geological Survey Professional Paper 1254, p. 15-24.



- Jones, L.M., 1988, Focal mechanisms and the state of stress on the San Andreas fault in southern California: *Journal of Geophysical Research*, v. 93, no. B8, p. 8869-8891.
- Jones, L.M., and Dollar, R.S., 1986, Evidence for basin-and-range extensional tectonics in the Sierra Nevada: The Durwood Meadows swarm, Tulare County, California (1983-1984): *Seismological Society of America Bulletin*, v. 76, no. 2, p. 439-462.
- Jones, L.M., Hutton, L.K., Given, D.D., and Allen, C.R., 1986, The North Palm Springs, California, earthquake sequence of July 1986: *Seismological Society of America Bulletin*, v. 76, no. 6, p. 1830-1837.
- LaForge, R., and Lee, W.H.K., 1982, Seismicity and tectonics of the Ortigalita fault and southeast Diablo Range, California, in Hart, E.W., Hirschfeld, S.E., and Schulz, S.S., eds., Conference on Earthquake Hazards in the Eastern San Francisco Bay Area, Hayward Calif., 1982, Proceedings: California Division of Mines and Geology Special Publication 62, p. 93-101.
- Lee, W.H.K., Eaton, M.S., and Brabb, E.E., 1971, The earthquake sequence near Danville, California, 1970: *Seismological Society of America Bulletin*, v. 61, no. 6, p. 1771-1794.
- Lee, W.H.K., and Stewart, S.W., 1981, Principles and applications of microearthquake networks: New York, Academic Press, 293 p.
- Lomnitz, Cinna, Mosser, Federico, Allen, C.R., Brune, J.N., and Thatcher, Wayne, 1970, Seismicity and tectonics of the northern Gulf of California region, Mexico. Preliminary results: *Geofisica Internacional*, v. 10, no. 2, p. 27-48.
- Louie, J.N., Allen, C.R., Johnson, D.C., Haase, P.C., and Cohn, S.N., 1985, Fault slip in southern California: *Seismological Society of America Bulletin*, v. 75, no. 3, p. 811-833.
- Magistrale, Harold, Jones, L.M., and Kanamori, Hiroo, 1988, The Superstition Hills, California, earthquakes of 24 November 1987: *Seismological Society of America Bulletin*, v. 79, no. 2, p. 239-251.
- Mayer-Rosa, Dieter, 1973, Travel-time anomalies and distribution of earthquakes along the Calaveras fault zone, California: *Seismological Society of America Bulletin*, v. 63, no. 2, p. 713-729.
- Mendoza, Carlos, and Hartzell, S.H., 1988, Inversion for slip distribution using teleseismic *P* waveforms: North Palm Springs, Borah Peak, and Michoacan earthquakes: *Seismological Society of America Bulletin*, v. 78, no. 3, p. 1092-1111.
- Minster, J.B., and Jordan, T.H., 1978, Present-day plate motions: *Journal of Geophysical Research*, v. 83, no. B11, p. 5331-5354.
- Minster, J.B., and Jordan, T.H., 1987, Vector constraints on western U.S. deformation from space geodesy, neotectonics, and plate motions: *Journal of Geophysical Research*, v. 92, no. B6, p. 4798-4804.
- Mogi, Kiyoo, 1968, Some features of recent seismic activity in and near Japan (1): University of Tokyo, Earthquake Research Institute Bulletin, v. 46, pt. 6, sec. A, p. 1225-1235.
- Morton, D.M., and Matti, J.C., 1987, The Cucamonga fault zone: geologic setting and Quaternary history, chap. 12 of *Recent reverse faulting in the Transverse Ranges, California*: U.S. Geological Survey Professional Paper 1339, p. 179-203.
- Namson, J.S., and Davis, T.L., 1988, Seismically active fold and thrust belt in the San Joaquin Valley, central California: *Geological Society of America Bulletin*, v. 100, no. 2, p. 257-273.
- Nicholson, Craig, Seeber, Leonardo, Williams, Patrick, and Sykes, L.R., 1986, Seismicity and fault kinematics through the eastern Transverse Ranges, California: Block rotation, strike-slip faulting and low-angle thrusts: *Journal of Geophysical Research*, v. 91, no. B5, p. 4891-4908.
- Norris, Robert, Jones, L.M., and Hutton, K.L., 1986, The Southern California Network Bulletin, July 01 through December 31, 1985: U.S. Geological Survey Open-File Report 86-337, 15 p.
- Oppenheimer, D.H., 1986, Extensional tectonics at The Geysers geothermal area, California: *Journal of Geophysical Research*, v. 91, no. B11, p. 11463-11476.
- Oppenheimer, D.H., Reasenberg, P.A., and Simpson, R.W., 1988, Fault-plane solutions for the 1984 Morgan Hill, California, earthquake sequence: Evidence for the state of stress on the Calaveras fault: *Journal of Geophysical Research*, v. 93, no. B8, p. 9007-9026.
- Page, B.M., and Engebretson, D.C., 1984, Correlation between the geologic record and computed plate motions for central California: *Tectonics*, v. 3, no. 2, p. 133-155.
- Pavoni, Nazario, 1973, A structural model for the San Andreas fault zone along the northeast side of the Gabilan Range, in Kovach, R.L., and Nur, Amos, eds., Proceedings of the conference on tectonic problems of the San Andreas fault system: Stanford, Calif., Stanford University Publications in the Geological Sciences, v. 13, p. 259-267.
- Poley, C.M., 1988, The San Ardo, California, earthquake of 24 November 1985: *Seismological Society of America Bulletin*, v. 78, no. 3, p. 1360-1366.
- Reasenberg, P.A., and Ellsworth, W.L., 1982, Aftershocks of the Coyote Lake, California, earthquake of August 6, 1979: A detailed study: *Journal of Geophysical Research*, v. 87, no. B13, p. 10637-10655.
- Richter, C.F., 1958, Elementary seismology: San Francisco, W.H. Freeman, 768 p.
- Rogers, A.M., Harmsen, S.C., Corbett, E.J., Priestley, K.F., and DePolo, D.M., in press, The seismicity of Nevada and some adjacent areas of the Great Basin, in Slemmons, D.B., Engdahl, E.R., Blackwell, D.D., Schwartz, D.P., and Zoback, M.D., eds., Neotectonics of North America (DNAG Associated Volume GSMV-1): Boulder, Colo., Geological Society of America.
- Sanders, C.O., and Kanamori, Hiroo, 1984, A seismotectonic analysis of the Anza seismic gap, San Jacinto fault zone, southern California: *Journal of Geophysical Research*, v. 89, no. B7, p. 5873-5890.
- Sauber, Jeanne, McNally, K.C., Pechmann, J.C., and Kanamori, Hiroo, 1983, Seismicity near Palmdale, California, and its relation to strain changes: *Journal of Geophysical Research*, v. 88, no. B3, p. 2213-2219.
- Savage, J.C., and Cockerham, R.S., 1987, Quasi-periodic occurrence of earthquakes in the 1978-1986 Bishop-Mammoth Lakes sequence, eastern California: *Seismological Society of America Bulletin*, v. 77, no. 4, p. 1347-1358.
- Schulz, S.S., Mavko, G.M., Burford, R.O., and Stuart, W.D., 1982, Long-term fault creep observations in central California: *Journal of Geophysical Research*, v. 87, no. B8, p. 6977-6982.
- Sibson, R.H., 1983, Continental fault structure and the shallow earthquake source: *Geological Society of London Journal*, v. 140, no. 5, p. 741-767.
- Sieh, K.E., 1978, Slip along the San Andreas fault associated with the great 1857 earthquake: *Seismological Society of America Bulletin*, v. 68, no. 5, p. 1421-1448.
- 1981, A review of geological evidence for recurrence times of large earthquakes, in Simpson, D.W., and Richards, P.G., eds., Earthquake prediction: An international review (Maurice Ewing Series 4): Washington, American Geophysical Union, p. 181-207.
- 1986, Slip rate across the San Andreas fault and prehistoric earthquakes at Indio, California [abs.]: *Eos (American Geophysical Union Transactions)*, v. 67, no. 44, p. 1200.
- Sieh, K.E., and Jahns, R.H., 1984, Holocene activity of the San Andreas fault at Wallace Creek, California: *Geological Society of America Bulletin*, v. 95, no. 8, p. 883-896.
- Silver, E.A., 1971, Tectonics of the Mendocino triple junction: *Geological Society of America Bulletin*, v. 82, no. 11, p. 9265-2878.

- Smith, K.D., and Priestly K.F., 1988, The foreshock sequence of the 1986 Chalfant, California, earthquake: *Seismological Society of America Bulletin*, v. 78, no. 1, p. 172-187.
- Spieth, M.A., 1981, Two detailed seismic studies in central California. Part I: Earthquake clustering and crustal structure studies of the San Andreas fault near San Juan Bautista. Part II: Seismic velocity structure along the Sierra foothills near Oroville, California: Stanford, Calif., Stanford University, Ph.D. thesis, 174 p.
- Stein, R.S., and King, G.C.P., 1984, Seismic potential revealed by surface folding: 1983 Coalinga, California, earthquake: *Science*, v. 224, no. 4651, p. 869-871.
- Stein, R.S., and Thatcher, Wayne, 1981, Seismic and aseismic deformation associated with the 1952 Kern County, California, earthquake and relationship to the Quaternary history of the White Wolf fault: *Journal of Geophysical Research*, v. 86, no. B6, p. 4913-4928.
- Sykes, L.R., and Seeber, Leonardo, 1985, Great earthquakes and great asperities, San Andreas fault, southern California: *Geology*, v. 13, no. 12, p. 835-838.
- Thatcher, Wayne, Hileman, J.A., and Hanks, T.C., 1975, Seismic slip distribution along the San Jacinto fault zone, southern California, and its implications: *Geological Society of America Bulletin*, v. 86, no. 8, p. 1140-1146.
- Thatcher, Wayne, and Lisowski, Michael, 1987, Long-term seismic potential of the San Andreas fault southeast of San Francisco, California: *Journal of Geophysical Research*, v. 92, no. B6, p. 4771-4784.
- Van Wormer, J.D., and Ryall, A.S., 1980, Sierra Nevada-Great Basin boundary zone: Earthquake hazards related to structure, active tectonic processes, and anomalous patterns of earthquake occurrence: *Seismological Society of America Bulletin*, v. 70, no. 5, p. 1557-1572.
- Walter, S.R., 1986, Intermediate-focus earthquakes associated with Gorda plate subduction in northern California: *Seismological Society of America Bulletin*, v. 76, no. 2, p. 583-588.
- Ward, S.N., 1988, North America-Pacific plate boundary, an elastic-plastic megashear: evidence from very long baseline interferometry: *Journal of Geophysical Research*, v. 93, no. B7, p. 7716-7728.
- Weaver, C.S., and Hill, D.P., 1978/79, Earthquake swarms and local crustal spreading along major strike-slip faults in California: *Pure and Applied Geophysics*, v. 117, no. 1-2, p. 51-64.
- Webb, T.H., and Kanamori, Hiroo, 1985, Earthquake focal mechanisms in the eastern Transverse Ranges and San Emigdio Mountains, southern California and evidence for a regional decollement: *Seismological Society of America Bulletin*, v. 75, no. 3, p. 737-757.
- Wentworth, C.M., Walter, A.W., Bartow, J.A., and Zoback, M.D., 1983, Evidence on the tectonic setting of the 1983 Coalinga earthquakes from deep reflection and refraction profiles across the southeastern end of Kettleman Hills, *in* Bennett, J.H., and Sherburne, R.W., eds., *The 1983 Coalinga, California earthquakes*: California Division of Mines and Geology Special Publication 66, p. 113-126.
- Wesson, R.L., Burford, R.O., and Ellsworth, W.L., 1973, Relationship between seismicity, fault creep, and crustal loading along the central San Andreas fault, *in* Kovach, R.L., and Nur, Amos, eds., *Proceedings of the conference on tectonic problems of the San Andreas fault system*: Stanford, Calif., Stanford University Publications in the Geological Sciences, v. 13, p. 303-321.
- Whitcomb, J.H., 1971, Fault-plane solutions of the February 9, 1971, San Fernando earthquake and some aftershocks, *in* *The San Fernando, California, earthquake of February 9, 1971*: U.S. Geological Survey Professional Paper 733, p. 30-33.
- Wilson, D.S., 1986, A kinematic model for the Gorda deformation zone as a diffuse southern boundary of the Juan de Fuca plate: *Journal of Geophysical Research*, v. 91, no. B10, p. 10259-10269.
- Wong, I.G., Ely, R.W., and Kollmann, A.C., 1988, Contemporary seismicity and tectonics of the northern and central Coast Ranges-Sierran Block boundary zone, California: *Journal of Geophysical Research*, v. 93, no. B7, p. 7813-7833.
- Zoback, M.D., Zoback, M.L., Mount, V.S., Suppe, John, Eaton, J.P., Healy, J.H., Oppenheimer, D.H., Reasenber, P.A., Jones, L.M., Raleigh, C.B., Wong, I.G., Scotti, Oona, and Wentworth, C.M., 1987, New evidence on the state of stress of the San Andreas fault system: *Science*, v. 238, no. 4830, p. 1105-1111.





*Motion between the North American and Pacific plates at the latitude of the San Andreas fault produces a broad zone of large-magnitude earthquake activity extending more than 500 km into the continental interior. The San Andreas fault system defines the western limits of plate interaction and dominates the overall pattern of seismic strain release. Few of the  $M \geq 6$  earthquakes that have occurred in the past 2 centuries were located on the San Andreas fault proper, an observation emphasizing the importance of secondary faults for both seismic-hazard assessment and tectonic processes.*

## 6. EARTHQUAKE HISTORY, 1769–1989

By WILLIAM L. ELLSWORTH

### CONTENTS

	Page		Page
Introduction-----	154	Seismicity of the western Basin and Range province—Continued	
Earthquake history of the San Andreas fault system-----	155	Principal earthquakes—Continued	
Principal earthquakes-----	156	December 21, 1932 ( $M=7.2$ )-----	167
July 28, 1769 ( $M=6$ )-----	156	July 6, 1954 ( $M=6.6$ ) and August 24, 1954 ( $M=6.8$ ) ---	167
December 8, 1812 ( $M=7$ )-----	157	December 16, 1954 ( $M=7.1$ and 6.8)-----	168
December 21, 1812 ( $M=7$ )-----	157	July 21, 1986 ( $M=6.2$ )-----	168
June 10, 1836 ( $M=6\frac{3}{4}$ )-----	158	Seismicity of the Mendocino triple junction and the Gorda plate -	169
June 1838 ( $M=7$ )-----	158	Principal earthquakes-----	169
January 9, 1857 ( $M=8\frac{1}{4}$ )-----	158	November 23, 1873 ( $M=6\frac{3}{4}$ )-----	169
October 21, 1868 ( $M=7$ )-----	159	April 16, 1899 ( $M=7$ )-----	169
February 24, 1892 ( $M=7$ )-----	159	January 31, 1922 ( $M=7.3$ )-----	169
April 19 and 21, 1892 ( $M=6\frac{1}{2}$ and $6\frac{1}{4}$ )-----	159	January 22, 1923 ( $M=7.2$ )-----	169
December 25, 1899 ( $M=6.4$ )-----	159	December 21, 1954 ( $M=6.6$ )-----	169
April 18, 1906 ( $M=8\frac{1}{4}$ )-----	159	November 8, 1980 ( $M=7.2$ )-----	169
November 21, 1915 ( $M=7.1$ )-----	161	Discussion-----	169
April 21, 1918 ( $M=6.9$ )-----	162	Rate of seismicity-----	171
November 4, 1927 ( $M=7.3$ )-----	162	Paradox of the missing plate motion-----	171
March 11, 1933 ( $M=6.3$ )-----	162	Earthquake recurrence and characteristic earthquakes-----	172
December 30 and 31, 1934 ( $M= 6.5$ and $7.0$ )-----	162	The seismic cycle-----	173
May 19, 1940 ( $M=7.1$ )-----	163	Future uses of earthquake history-----	174
July 21, 1952 ( $M=7.7$ )-----	163	Catalog of major earthquakes, 1769–1989-----	175
February 9, 1956 ( $M=6.8$ )-----	164	Catalog compilation-----	175
April 9, 1968 ( $M=6.5$ )-----	164	Quantification of earthquakes and magnitude scales-----	176
February 9, 1971 ( $M=6.5$ )-----	164	The Richter scale ( $M_L$ )-----	177
October 15, 1979 ( $M=6.5$ )-----	164	Surface-wave magnitude ( $M_S$ ) and body-wave	
May 2, 1983 ( $M=6.5$ )-----	164	magnitude ( $m_b$ )-----	177
November 24, 1987 ( $M=6.6$ )-----	164	Seismic intensity and earthquake magnitude ( $M_I$ )-----	177
October 18, 1989 ( $M=7.1$ )-----	165	Seismic moment ( $M_0$ ), radiated energy, and moment	
Seismicity of the western Basin and Range province-----	166	magnitude ( $M$ )-----	178
Principal earthquakes-----	166	Summary magnitude ( $M$ )-----	178
March 26, 1872 ( $M=7.6$ )-----	166	References cited-----	178
October 3, 1915 ( $M=7.3$ )-----	167		

◀ FIGURE 6.1.—Seismicity highlights broad and complex zones of active tectonism in the western United States. Dots, earthquakes scaled by magnitude in unit-magnitude steps, smallest for  $M < 4$ ; circles, earthquakes of  $M > 7$ ; red dots, recent events, generally since 1975; pink symbols, historical events. From Engdahl and Rinehart (1988).



## INTRODUCTION

Between Punta Gorda on the northern California coast and the head of the Gulf of California, 1,350 km to the southeast, lies the active transform boundary that forms the modern San Andreas fault system (fig. 6.1). Dextral motion between the North American and Pacific plates along this system is accommodated within an elongate zone, broadening from about 100 km at its north end to about 300 km in southern California. The San Andreas fault proper hugs the east side of this zone at its south terminus and gradually migrates across the zone, lying on the west edge of the zone at its north terminus. The

San Andreas fault system transmits about three-fourths of the relative motion across the plate boundary, as shown by various geologic and geodetic evidence. Much of this motion is stored elastically in the upper crust along the major faults in the system, ultimately to be released in large plate-boundary earthquakes. These large earthquakes and their implications for the mechanics of North American-Pacific plate interactions are the subject of this chapter.

Earthquake activity in California and Nevada at the latitude of the San Andreas fault extends well beyond the confines of the San Andreas system (fig. 6.2). In the past century alone, only about half of the  $M \geq 6$  activity has

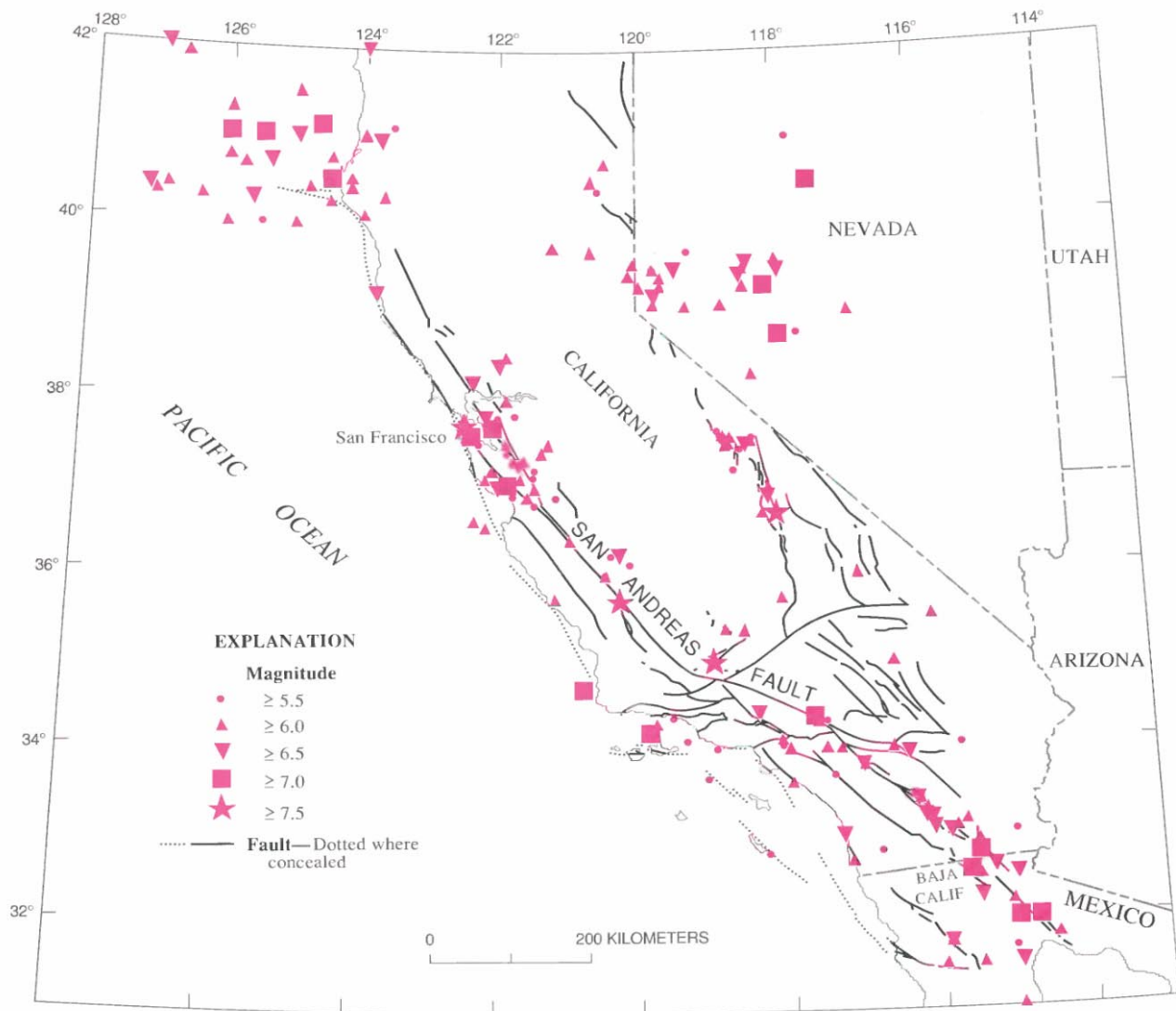


FIGURE 6.2.—Seismicity of California, Nevada, and northern Baja California, 1769–1989. Earthquakes are listed in table 6.1 and plotted by magnitude class.

fallen within the San Andreas system; of the rest, half is associated with the western Basin and Range province, and the other half with the Mendocino triple junction and the Gorda plate. Although activity in the latter region reflects the tectonics of the triple junction and the collision of the Gorda plate with the North American plate, seismicity east of the San Andreas system along the east flank of the Sierra Nevada and in the Basin and Range province reflects the incomplete accommodation of plate motion along the San Andreas fault system. A significant proportion of this "missing" motion occurs in the Basin and Range, the seismicity of which plays an integral role in the tectonics of the plate boundary.

### EARTHQUAKE HISTORY OF THE SAN ANDREAS FAULT SYSTEM

The historical record of major earthquakes affecting California, western Nevada, and northernmost Baja California (table 6.1) includes basic seismologic data on 206 of the largest earthquakes occurring between 1769 and 1989. This catalog lists all known events of  $M \geq 6$  and includes new and updated information on their locations.

The record of seismicity within the San Andreas fault system and surrounding regions is both geographically and temporally uneven and incomplete before the introduction of practical seismographic instrumentation around the turn of the 20th century. In general, the density and distribution of people who left written accounts of their experiences determines the reliability of the catalog during the preinstrumental period. From the establishment of the Franciscan missions beginning in 1769 until their secularization in the 1830's, detailed accounts of events that damaged the missions are available, and these accounts form the primary source material for earthquakes occurring during this period. Life in California was a constant struggle for survival at that time; posting to a mission evidently was considered a hardship assignment, and so essentially nothing was recorded about events that were only felt, even when they were destructive at nearby missions. After secularization and before the gold rush, the quality of the record degrades with the cessation of the annual reports of the missions. Other sources of records also are notably weak during the Mexican period, from the early 1830's until 1846.

The discovery of gold in 1848 transformed the written record of earthquakes with the advent of newspapers throughout the gold fields in the Sierran foothills and in the San Francisco Bay region. Printed accounts of earthquakes have been extensively used, notably by Topozada and others (1988), to quantify the seismicity of California from 1850 onward. They estimated that their historical catalog is probably complete for the San

Francisco Bay region and central Sierra Nevada from 1850 on for earthquakes of  $M \approx 6$ . The same level of completeness is not achieved, however, for the San Andreas fault system in southern California until the 1890's. Statewide, the catalog of earthquakes is substantially complete for earthquakes of  $M \approx 7$  after about 1850 (see Agnew, 1985). The quality of the catalog for central Nevada, where much significant 20th century seismicity has occurred, is less complete. Questions remain today about purported events as late as 1903 in this region (Slemmons and others, 1959).

Reports of the local effects of earthquakes continue to play a major role in determining the locations and sizes of earthquakes well into the 20th century. The earliest seismographs capable of systematically detecting California and Nevada earthquakes were installed throughout the world by John Milne beginning in 1896. Seismograms from these instruments and their successors provide useful instrumental magnitudes from 1898 onward. However, not until the development of the Wood-Anderson seismograph and its deployment throughout California beginning in 1926 do instrumental measurements fully supplant noninstrumental magnitudes and epicentral locations.

The objective in assembling a single catalog from these many sources, spanning many different types and qualities of information, has been to achieve uniform spatial coverage without sacrificing any events of historical significance.  $M=6$  was chosen as the threshold magnitude because probably all events of this magnitude are known from the instrumental period beginning in 1898, and the preinstrumental record is reasonably complete at this level in some areas for an additional half-century. All earthquakes with at least one reported magnitude of at least 6.0 have been included in the catalog. Because magnitude is an estimated quantity and has some inherent uncertainty, events with reported magnitudes within a few tenths of a unit of 6.0 are also included. In addition to those earthquakes with cataloged magnitudes, original documents for others with reported high intensities or of particular historical significance have been reexamined in an attempt to refine their locations and magnitudes.

A word of introduction should be added about earthquake locations and magnitude scales and their use in this chapter. Earthquakes are complex physical processes generated by sudden slip on faults, and as such they can only be grossly characterized by simple concepts. Two seismologic conventions are in common use for assigning a single geographic coordinate to an earthquake: One measures the center of energy release, frequently as estimated from the intensity distribution for preinstrumental events; the other measures the location of the initial point of rupture, or hypocenter, as determined from seismic traveltime measurements. Either point on



the Earth's surface above the hypocenter or the center of the intensity distribution is sometimes referred to as the epicenter, and each type of location appears in table 6.1, with preference given to instrumental epicenters. Fortunately, the geographic differences between these distinct physical measures become significant only for the largest events,  $M \approx 7$ , when viewed at the scale of the entire San Andreas fault system.

Magnitude, as commonly used to compare the sizes of different earthquakes, also represents an extreme simplification of the earthquake process and by itself cannot fully characterize the size of any event. Traditionally, seismologists have developed a suite of magnitude scales, each with its own purpose and range of validity to measure an earthquake. Because no single magnitude scale can be systematically applied to the entire historical record, a summary magnitude,  $M$ , is introduced here to facilitate comparisons between events. As described below in the subsection entitled "Quantification of Earthquakes and Magnitude Scales,"  $M$  is taken as the surface-wave magnitude ( $M_S$ ), when available, and as a modified intensity magnitude ( $M_I$ ) during the preinstrumental era. Generally speaking,  $M$  provides a better relative measure of the static, geologic increment of fault slip in the earthquake than it does of the severity of shaking.

The earthquake history of California, western Nevada, and northern Baja California presented here has apparent limitations and can doubtlessly be improved through further research. Nevertheless, it provides a firm observational basis for assessing the tectonic implications of the 2-century-long seismic history, as well as of the prospects for future earthquake activity.

#### PRINCIPAL EARTHQUAKES

In this section, we briefly discuss some events of particular historical, social, or scientific significance. Although each of the 117 San Andreas fault system events in table 6.1 merits discussion, this task is far beyond the scope of this review, and so the reader is referred to the reports by Richter (1958), Coffman and others (1982), and Townley and Allen (1939) for an introduction to many of these events. Table 6.1 also omits several historically significant events with magnitudes well below the nominal threshold of  $M=6$  adopted here, and so it something less than a complete reference on San Andreas seismicity.

My major effort in constructing this catalog has gone into identifying and validating all reported events of  $M \geq 6$ . Two conspicuous omissions from table 6.1, events that are commonly mentioned in the literature but that could not be substantiated upon further inspection, should be noted. The first is the 1852 earthquake alleged

to have ruptured the Big Pine fault (for example, Jennings, 1975). Topozada and others (1981) failed to find any evidence supporting the occurrence of a major earthquake at that time in the region. Geologic inspection of the surface trace of the fault by M.M. Clark (oral commun., 1988) similarly failed to provide evidence of any historical activity. The other deleted event appears on the seismicity map by Guter (1988) at lat  $35^\circ$  N., long  $125^\circ$  W., with an epicenter from the catalog of Abe and Noguchi (1983). Although a large ( $M_S=6.8$ ) earthquake certainly took place on March 22, 1902, no evidence has been uncovered to support a location anywhere on shore in California or, for that matter, in the Western United States. The original location determined by Milne in 1903 placed the event well off the California-Oregon coast at lat  $42^\circ$  N., long  $130^\circ$  W.

JULY 28, 1769 ( $M=6$ )

The earthquake history of California serendipitously begins with the first overland expedition through the State in 1769. In response to the perceived threat posed by Russian expansion into the northern Pacific and growing British presence in the northwestern Pacific, Spain embarked on the colonization of present-day California through the establishment of a series of Franciscan missions, supported by military garrisons at San Diego and Monterey. In the summer of 1769, Gaspar de Portolá led the first expedition from San Diego to establish a land route to Monterey.

On July 28, while camped along the Santa Ana River, about 50 km southeast of Los Angeles, a sharp earthquake was felt that " \* \* \* lasted about half as long as an Ave Maria" (fig. 6.3). From the diaries of three members of the expedition, we know that earthquakes were felt on nearly a daily basis through August 3, as the party traveled northwestward to near San Gabriel and then westward across Los Angeles to the Pacific. The diary of Fray Juan Crespi (Bolton, 1927) mentions no fewer than a dozen aftershocks, some described as violent. After August 4, no further earthquakes were mentioned as the expedition traveled into the San Fernando Valley and exited to the north.

These sketchy reports suggest that the explorers traveled near or through the epicentral area of a moderate earthquake (Richter, 1973; Topozada and others, 1981). Comparisons between the accounts of the aftershocks and more recent events suggest an event of similar size and location to the 1933 Long Beach, 1971 San Fernando, or 1987 Whittier Narrows earthquake. If significance is placed on the absence of aftershocks while crossing the source region of the 1971 San Fernando earthquake, the evidence would seem to favor a source in the Los Angeles Basin. An event on either the San



Andreas or San Jacinto faults, some 50 km to the northeast, could conceivably have been the source of the 1769 earthquake. The description of the duration of strong shaking, however, suggests a magnitude more of 5–6 than of 7–8.

A more distant source would make the long, felt aftershock sequence even more remarkable because it would be well removed from the expedition route.

DECEMBER 8, 1812 ( $M=7$ )

The first of two significant earthquakes to occur in southern California in 1812 occurred on December 8 and destroyed the church at Mission San Juan Capistrano, killing 40 neophytes (fig. 6.4); damage was also sustained

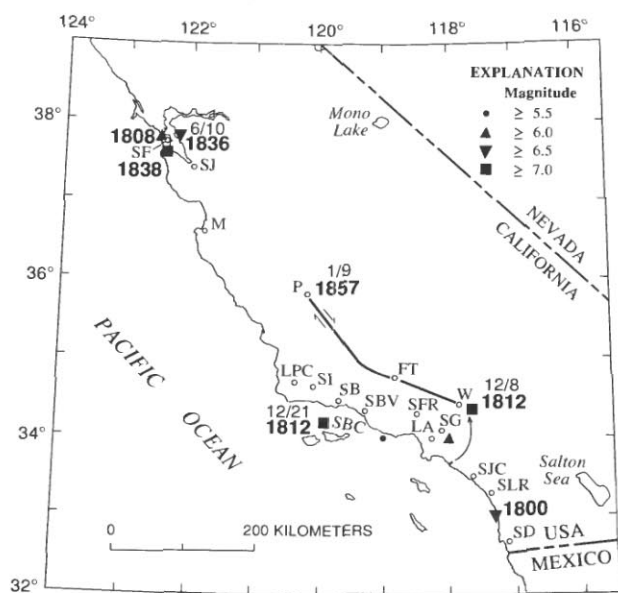


FIGURE 6.3.—Early accounts of significant earthquakes reflect the sparse settlement of California in a narrow coastal corridor before the population explosion accompanying the gold rush in 1849. Accounts of the few well-documented events (dates shown) principally derive from mission records at San Diego (SD), San Luis Rey (SLR), San Juan Capistrano (SJC), San Gabriel (SG), San Fernando Rey (SFR), San Buenaventura (SBV), Santa Barbara (SB), Santa Inez (SI), and La Purisima Concepción (LPC), and from the towns of Los Angeles (LA) and Fort Tejon (FT) in southern California. Accounts from the Spanish capital Monterey (M), San Francisco (SF), and San Jose (SJ), as well as mission sources, detail events in north half of the State. Uncertainties in the interpretation of every event before the great earthquake of 1857 (rupture shown; arrows indicate direction of relative movement) are well illustrated by newly uncovered evidence suggesting a San Andreas origin for the December 8, 1812, shock near Wrightwood (head of connecting arrow), well inland of traditional location along the coastal Newport-Inglewood fault (tail of arrow). Earthquake of December 21, 1812, locates in the Santa Barbara Channel (SBC). Foreshocks of the great earthquake of 1857 locate near Parkfield (P), suggesting unilateral rupture propagation to the southeast.

at San Gabriel. The accounts of this earthquake and the later one on December 21 cannot be readily disentangled at San Fernando Rey and at San Buenaventura, considerably complicating the interpretation of this event.

Analyses of these scanty data by Topozada and others (1981) and Evernden and Thompson (1985) place the epicenter along the south half of the Newport-Inglewood fault zone (fig. 6.3). This location is somewhat constrained by the interpretation of no damage at Buenaventura during the event. The Los Angeles Star of January 10, 1857, however, stated that the December 8 event severely damaged the church tower (Agnew and Sieh, 1978). The same story attributed the collapse of the stone arch roof of the church at San Juan Capistrano to poor construction, a possibility made credible by the death of the master mason before completion of the church (fig. 6.3; Duncan Agnew, oral commun., 1988).

Recently, Jacoby and others (1988) proposed that this event ruptured the San Andreas fault at Wrightwood (fig. 6.3), on the basis of dendrochronologic dating of distress to trees growing on the fault trace. Sieh and others (1989) argued that this rupture extended at least 25 km northwestward into the peat bog at Pallet Creek. The fault rupture in this event preserved at Pallet Creek is comparable in size to the rupture formed in the 1857 earthquake.

The preferred location of the December 8, 1812, earthquake on the San Andreas fault as proposed by Jacoby and others appears in table 6.1. A magnitude of about 7 is consistent with the inferred extent of damage. The lateral extent of rupture is unconstrained to the southeast and may well have extended into the San Bernardino Valley. However, the accounts of the earthquake from Indians living in the San Bernardino Valley that were thought to place some constraint on the rupture are now believed to be fictitious (Harley, 1988), leaving Mission San Gabriel, some 40 km from the rupture, as the nearest point of observation.

DECEMBER 21, 1812 ( $M=7$ )

The second major episode of earthquake activity in 1812 damaged the missions along the Santa Barbara Channel and western Transverse Ranges just 13 days later, on December 21 (fig. 6.3). All investigators place this event in the Santa Barbara Channel and assign a magnitude of about 7 (see Topozada and others, 1981, and Evernden and Thompson, 1985, for two recent analyses). This sequence appears to have involved two events of comparable magnitude separated in time by about 15 minutes. A vigorous aftershock sequence accompanied the earthquakes and lasted until the end of the year at Mission Santa Barbara and Mission La Purisima Concepción. Reports of a tsunami appear to be exagger-



ated, although some kind of wave activity probably accompanied the earthquake (Topozada and others, 1981; McCulloch, 1985).

JUNE 10, 1836 ( $M=6\frac{3}{4}$ )

Little is known about the strong earthquake of June 10, 1836, that struck the then lightly populated San Francisco Bay region. An account of the event, published in the aftermath of the 1868 earthquake, provides the principal rationale for associating this event with the Hayward fault. Louderback (1947) systematically compared the two events and concluded that the 1836 earthquake probably ruptured the Hayward fault. Lindh (1983) proposed that the 1836 event ruptured the north half of the fault, whereas the 1868 event is known to have ruptured the south half, thereby avoiding the paradox of two large events on the same segment separated by a scant 32 years.

JUNE 1838 ( $M=7$ )

The pioneering historical work of Louderback (1947) reveals that a major earthquake with probable rupture of the San Andreas fault occurred in June 1838. Documentation of the event is so poor that its date cannot be fixed more precisely than "late June." Louderback concluded that the shock was comparable in magnitude to the 1906 earthquake. Current opinion suggests a smaller event involving only the 60+-km-long segment of the fault on the San Francisco peninsula (Working Group on Earthquake Probabilities, 1988).

JANUARY 9, 1857 ( $M=8\frac{1}{4}$ )

The great Fort Tejon earthquake of January 9, 1857, ruptured 300 km of the San Andreas fault from near Parkfield to Wrightwood and offset the fault by as much as 9½ m on the Carrizo Plain. The fault rupture and the effects of the earthquake have been extensively studied, notably by Agnew and Sieh (1978) and Sieh (1978b). The epicenter of this event appears to have been at the extreme northwest end of the fault rupture, as determined by the intensity patterns of two  $M=6$  foreshocks centered near Parkfield (Sieh, 1978a). Strong shaking lasted from 1 to 3 minutes, consistent with unilateral rupture propagation to the southeast (fig. 6.3).

The earthquake caused only two deaths in the sparsely settled southern California region. Damage was most severe along the fault zone; nearly every building sustained damage at Fort Tejon. In Los Angeles, then a city of about 4,000 people located approximately 60 km from the fault, some houses were cracked, but none were severely damaged (Agnew and Sieh, 1978). Modified Mercalli intensities (MMI's) of VII or more occurred in the San Fernando Valley, San Gabriel Valley, and Ventura region.

It is natural to compare the 1857 and 1906 earthquakes, the two greatest earthquakes of the San Andreas fault in historical time. The 1906 fault break was longer, whereas maximum and average surface offsets were larger in 1857. These differences approximately balance each other, and so the seismic moments of the two events are approximately equal. Moment magnitudes computed using comparable data are  $M=7.8$  for the 1857 earthquake

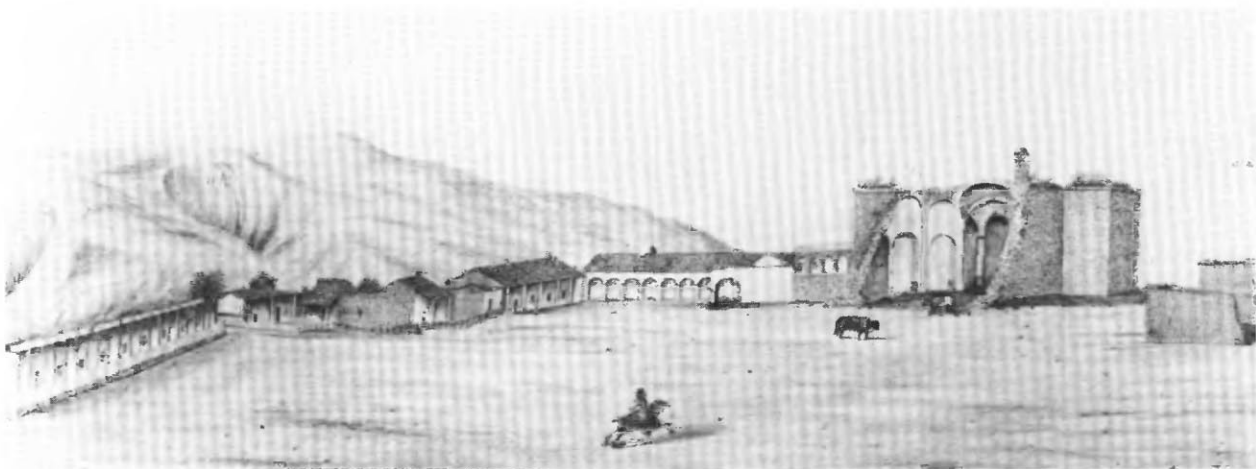


FIGURE 6.4.—Mission San Juan Capistrano as drawn by Henry Miller in 1856, 43 years after the December 8, 1812, earthquake. Vaulted stone church at right collapsed in that earthquake, killing 40 worshippers. Photograph courtesy of the Bancroft Library.

and  $M=7.7$  for the 1906 event. A summary magnitude of  $M=8\frac{1}{4}$  was assigned by analogy with the 1906 earthquake.

OCTOBER 21, 1868 ( $M=7$ )

Known as the "great San Francisco earthquake" until 1906, one of California's most destructive earthquakes occurred on October 12, 1868, resulting from slip on the Hayward fault. Heavy damage occurred in communities situated along the fault and in San Francisco and San Jose (fig. 6.5). Sadly, many of the engineering lessons learned from this earthquake and openly discussed at the time, such as the hazards of building on "made ground" reclaimed from the San Francisco Bay or the admonition to "build no more cornices," were long forgotten by the time of the 1906 earthquake.

FEBRUARY 24, 1892 ( $M=7$ )

The strong earthquake of February 24, 1892, located near the United States-Mexican border was assigned to the Agua Caliente fault north of the border by Topozada and others (1981) and to the Laguna Salada fault in Baja California by Strand (1980). The literature on earthquakes in Baja California contains numerous references to this earthquake as having originated near the Agua Blanca fault, about 100 km southwest of Strand's epicenter (for example, Richter, 1958). The two recent intensity maps clearly rule out this epicenter and place it on the southern section of the Elsinore fault system.

APRIL 19 AND 21, 1892 ( $M=6\frac{1}{2}$  AND  $6\frac{1}{4}$ )

A pair of strong earthquakes rocked the west side of the Sacramento Valley on April 19 and 21, 1892, heavily damaging the towns of Vacaville, Dixon, and Winters. The first shock was stronger and caused heavy damage at Vacaville; the aftershock was more severe at Winters. The earthquakes are reminiscent of the 1983 Coalinga, Calif., earthquake, in that both sequences were positioned along the western margin of the Central Valley. Focal mechanisms of small earthquakes located along this boundary zone show numerous examples of low-angle-thrust focal-mechanism solutions of similar orientation to the Coalinga earthquake, in addition to strike-slip mechanisms (see chap. 5; Wong and others, 1988), suggesting the possibility of a similar mechanism for these 1892 earthquakes.

DECEMBER 25, 1899 ( $M=6.4$ )

Heavy damage occurred in the towns of San Jacinto and Hemet, located along the San Jacinto fault, from an

earthquake on Christmas Day 1899. Six fatalities were attributed to the earthquake.

APRIL 18, 1906 ( $M=8\frac{1}{4}$ )

The California earthquake of April 18, 1906, ranks as one of the most significant earthquakes of all time. Today, its importance comes more from the wealth of scientific knowledge derived from it than from its sheer size. Rupturing the northernmost 430 km of the San Andreas fault from northwest of San Juan Bautista to the triple junction at Cape Mendocino (fig. 6.6), the earthquake confounded contemporary geologists with its large, horizontal displacements and great rupture length. Indeed, the significance of the fault and recognition of its large cumulative offset would not be fully appreciated until the advent of plate tectonics more than half a century later. Analysis of the 1906 displacements and strain in the surrounding crust led Reid (1910) to formulate his elastic-rebound theory of the earthquake source, which remains today the principal model of the earthquake cycle.

As a basic reference about the earthquake and the damage it caused, geologic observations of the fault rupture and shaking effects, and other consequences of the earthquake, Lawson's (1908) report remains the authoritative work, as well as arguably the most important study of a single earthquake. In the public's mind, this earthquake is perhaps remembered most for the fire it spawned in San Francisco, giving it the somewhat misleading appellation of the "San Francisco earthquake" (fig. 6.7). Shaking damage, however, was equally severe in many other places along the fault rupture. The frequently quoted value of 700 deaths caused by the earthquake and fire is now believed to underestimate the total loss of life by a factor of 3 or 4. Most of the fatalities occurred in San Francisco, and 189 were reported elsewhere.

At almost precisely 5:12 a.m. local time, a foreshock occurred with sufficient force to be felt widely throughout the San Francisco Bay area. The great earthquake broke loose some 20 to 25 s later, with an epicenter near San Francisco (Bolt, 1968; Boore, 1977). Violent shocks punctuated the strong shaking, which lasted some 45 to 60 s. The earthquake was felt from southern Oregon to south of Los Angeles and inland as far as central Nevada (fig. 6.6). The highest MMI's of VII to IX paralleled the length of the rupture, extending as far as 80 km inland from the fault trace. One important characteristic of the shaking intensity noted in Lawson's (1908) report was the clear correlation of intensity with underlying geologic conditions. Areas situated in sediment-filled valleys sustained stronger shaking than nearby bedrock sites, and the strongest shaking occurred in areas where ground



**Daily Morning Chronicle**  
 PUBLISHED BY  
**CHAS. DE YOUNG & CO.,**  
 No. 204 Montgomery street, between  
 Sacramento and Commercial.  
 PRINTED BY GEORGE W.  
 BAKER, CORNER FIFTH AND  
 MARKET STS.  
 THE ORIGINAL LIST OF LETTERS,  
 & LIST OF THE PARTISANS, IN PUBLISHED IN THE  
 CHRONICLE EVERY WEDNESDAY, IN CONNECTION  
 WITH THE WEEKLY NEWS.

THE DAILY  
**Morning Chronicle**  
 VOL. VIII. SAN FRANCISCO, WEDNESDAY, OCTOBER 28, 1868. NO. 90.

**Daily Morning Chronicle**  
 PUBLISHED BY  
**CHAS. DE YOUNG & CO.,**  
 No. 204 Montgomery street, between  
 Sacramento and Commercial.  
 PRINTED BY GEORGE W.  
 BAKER, CORNER FIFTH AND  
 MARKET STS.  
 THE ORIGINAL LIST OF LETTERS,  
 & LIST OF THE PARTISANS, IN PUBLISHED IN THE  
 CHRONICLE EVERY WEDNESDAY, IN CONNECTION  
 WITH THE WEEKLY NEWS.

**Earthquake**

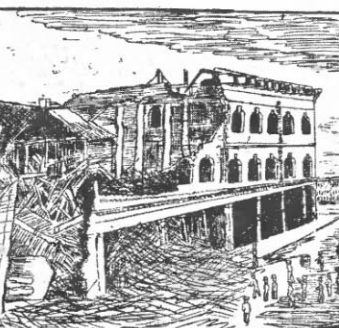
**THE GREAT EARTHQUAKE**

**OF OCTOBER 21st.**  
**The Severeest Ever Felt in San Francisco.**  
**FOR A FEW DAYS KILLED AND LAMED**  
**Nearly 10,000.**  
**Down Buildings, Destroyed and Damaged**  
**Property to the Value of Millions.**  
**A Massing of Houses Leap to**  
**be Remonstrated.**  
**THE GREATEST CALAMITY EVER**  
**BEFELL SAN FRANCISCO.**  
**Some Fatalities—The People Fright**  
**and Horror.**  
**How the Buildings Were Destroyed.**  
**THE ILLUMINATING POINT IN**  
**ALASKA'S HISTORY.**  
**Some Illustrations of Property in**  
**San Francisco and Hayward.**  
**THE "EARTHQUAKE" IN THE**  
**WEST.**

**ILLUSTRATED EARTHQUAKE EDITION.**



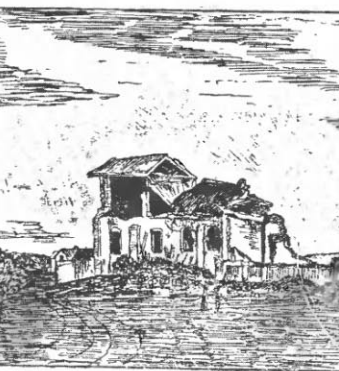
The One Works.



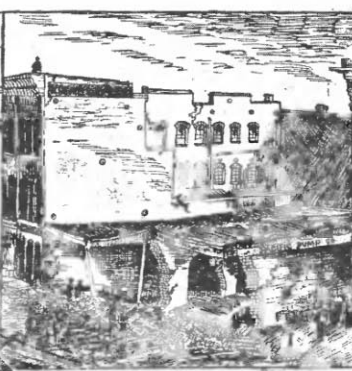
Coffey & Biscoe's Building.



Railroad House and Rosenbann's Tobacco Warehouse.



San Loure Court-house.



California Street, below Sanson.

The 21st of October, one of the most disastrous days in our history, was witnessed by the city of San Francisco. At 11 o'clock, a severe earthquake was felt, which was followed by a series of aftershocks. The earthquake was the most severe ever felt in San Francisco, and it caused the death of nearly 10,000 people. The damage to property was estimated at \$100,000,000. The earthquake was caused by the Hayward fault, which is a branch of the San Andreas fault system. The earthquake was felt throughout the city, and it caused the collapse of many buildings. The most severely damaged buildings were the Coffey & Biscoe Building, the Railroad House, and Rosenbann's Tobacco Warehouse. The San Loure Court-house was almost completely destroyed. The earthquake was a great calamity for the city, and it caused a great deal of suffering and loss.

The earthquake of October 21st, 1868, was a great calamity for the city of San Francisco. It caused the death of nearly 10,000 people and the destruction of property worth \$100,000,000. The earthquake was caused by the Hayward fault, which is a branch of the San Andreas fault system. The earthquake was felt throughout the city, and it caused the collapse of many buildings. The most severely damaged buildings were the Coffey & Biscoe Building, the Railroad House, and Rosenbann's Tobacco Warehouse. The San Loure Court-house was almost completely destroyed. The earthquake was a great calamity for the city, and it caused a great deal of suffering and loss.

FIGURE 6.5.—San Francisco *Morning Chronicle* of October 28, 1868, richly illustrates severe damage sustained by buildings of poor design or located on filled land during earthquake on the Hayward fault. Reduction of this figure from its original publication size has made some type illegible; it is not needed to convey information intended by this illustration. Photograph courtesy of the Bancroft Library.



reclaimed from San Francisco Bay failed in the earthquake. Modern seismic-zonation practice accounts for the differences in seismic hazard posed by varying geologic conditions (see Borchardt, 1975, and Ziony, 1985, for analyses of the San Francisco Bay and Los Angeles regions, respectively).

The characteristics and amount of surface fault slip in this earthquake varied to a remarkable degree along the length of the rupture. Peak displacements of 6 m were measured near Olema on the Point Reyes peninsula, where the surface trace of the rupture formed a sharp, well-defined break (fig. 6.8). In contrast, the fault break was extremely difficult to recognize along its southernmost 90 km, where the surface offset averaged only about 1½ m or less (see chap. 7).

The magnitude of 8.3 commonly quoted for the 1906 earthquake comes from Richter (1958) and, within the precision of reporting, is identical to the 8¼ listed by Gutenberg and Richter (1954). Table 6.1 also lists other magnitudes for this earthquake, derived from recent analyses of both the same data used by Gutenberg and Richter and new data. Strictly speaking, a "Richter magnitude" ( $M_L$ ) for the earthquake cannot be determined because no appropriate seismographs were in

operation at the time. Jennings and Kanamori (1979) used related measurements extracted from simple pendulums at Yountville, Calif., and Carson City, Nev., to derive  $M_L=6.9$ , substantially smaller than the traditionally quoted value.  $M_L$ , which is based on the single largest peak on a seismogram at approximately 1-s period and takes into account neither the duration of the event nor longer period motions, is saturated for this event.

Geller and Kanamori (1977) used the unpublished worksheets of Gutenberg and Richter to compute a body-wave magnitude of  $m_b=7.4$ , using the procedure of Gutenberg and Richter (1956). Because long-period (14 s)  $P$ -waves were used in this calculation, it cannot be directly compared to the short-period  $m_b$  values routinely reported today.

Other workers since Gutenberg and Richter have studied the long-period surface waves of the 1906 earthquake and computed  $M_S$  values. Bolt (1968) confirmed an  $M_S$  of about 8¼, whereas Lienkaemper (1984) found  $M_S=8.3$  from an analysis of all the records collected by Reid (1910). Lienkaemper's magnitude combined data from both damped and undamped instruments, correcting each for magnification at the appropriate period of motion. Abe (1988), who analyzed only the undamped Milne seismograms, obtained  $M_S=7.8$ , using slightly different procedures and a systematic set of station-magnitude corrections. Also, the four damped seismometers (all in Europe) give  $M_S=8.1$ . Longer period (50-100 s) surface waves analyzed by Thatcher (1975) indicate a seismic moment of  $4 \times 10^{27}$  dyne-cm, equivalent to  $M=7.7$ , in agreement with the seismic moment of  $5 \times 10^{27}$  dyne-cm obtained from geodetic data, thus giving  $M=7.8$  (Thatcher and Lisowski, 1987). Finally, Topozada and Parke (1982) assigned an intensity magnitude ( $M_I$ ) of 7.8 on the basis of the total area (48,000 km<sup>2</sup>) undergoing shaking of MMI VII or higher.

The "traditional" magnitude of 8¼ is retained here, except where seismic moment is used for quantitative purposes.

NOVEMBER 21, 1915 ( $M=7.1$ )

The major earthquake of November 21, 1915, triggered a spectacular steam eruption of a mud volcano, creating a 100+-m crater in Volcano Lake, Baja California, near the north terminus of the Cerro Prieto fault. Extensive cracking of the levee around the lake was noted at the time of the shock, but no tectonic ground displacements were found (Seismological Society of America Bulletin, 1916). This event may well be related to the November 29, 1852, earthquake ( $M=6\frac{1}{2} \pm$ ), which also triggered a mud-volcano eruption at Volcano Lake that was observed at Fort Yuma, Ariz. Each of these events was probably associated with the Cerro Prieto fault.

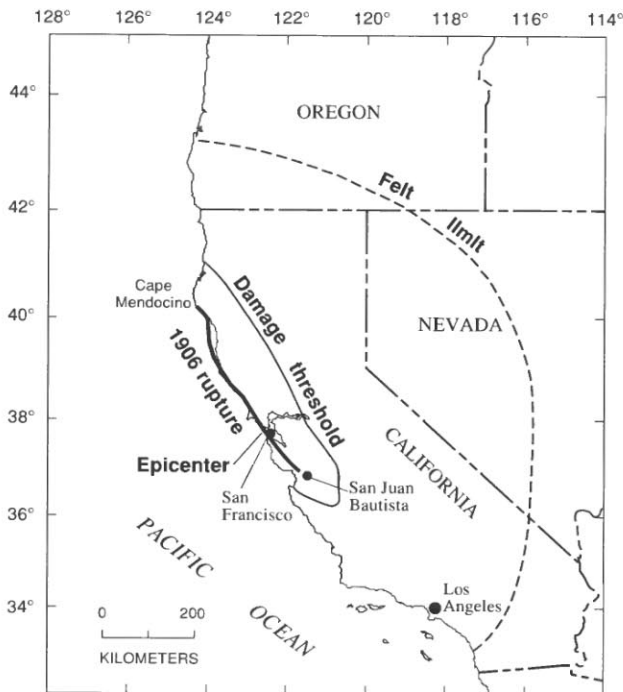


FIGURE 6.6.—California earthquake of 1906 showing extent of fault rupture along the San Andreas fault, location of epicenter near San Francisco, maximum extent of structural damage, and limits of perception of shock. Modified from Lawson (1908) and Topozada and Parke (1982).



APRIL 21, 1918 ( $M=6.9$ )

The communities of Hemet and San Jacinto were severely damaged for the second time in 19 years by the large earthquake of April 21, 1918, on the San Jacinto fault. Both the 1899 and 1918 earthquakes produced similar intensity patterns throughout the southern California region, and these two events have been compared to each other. However, surface waves on Milne seismograms at common stations (Victoria, British Columbia, and Toronto, Ontario, Canada; San Fernando, Spain) average 3 times larger for the 1918 earthquake, corresponding to a difference in  $M_S$  of  $\frac{1}{2}$  unit. As with the 1836 and 1868 earthquakes on the Hayward fault, the relation between the rupture zones in these two events is unclear. Surprisingly, no surface rupture was found for an event of this size, despite a specific search for it.

NOVEMBER 4, 1927 ( $M=7.3$ )

The Lompoc earthquake of November 4, 1927, is the largest known event in the San Andreas system west of

the San Andreas fault proper. This event produced a tsunami with local runup heights of 1.5 to 1.8 m (McCulloch, 1985). The exact location of the earthquake and its association with any causative structure remain the subject of a spirited debate (Gawthrop, 1978, 1981; Hanks 1979, 1981).

MARCH 11, 1933 ( $M=6.3$ )

Rupture of the Newport-Inglewood fault on March 11, 1933, caused major damage and a loss of 115 lives in Long Beach and surrounding parts of the Los Angeles Basin. Structural damage to public schools was particularly serious, and had the event occurred when schools were in session, the calamity would have been far worse. The Field Act, mandating construction standards for schools in California, was enacted as a consequence of the earthquake.

DECEMBER 30 AND 31, 1934 ( $M=6.5$  AND  $7.0$ )

The major sequence that occurred along the Cerro Prieto fault on December 30 and 31, 1934, appears to



FIGURE 6.7.—San Francisco, Calif., on the morning of April 18, 1906. This famous photograph by Arnold Genthe shows Sacramento Street and approaching fire in the distance. Although some buildings sustained heavy damage in the earthquake, this and many other

photographs taken of the city before fire swept through show no visible evidence of damage in most structures. Photograph courtesy of the Fine Arts Museums of San Francisco, Achenbach Foundation for Graphic Arts.

have ruptured the surface trace of the fault near where it enters the Gulf of California. Aerial photographs of the fault crossing a tidal flat taken in 1935 show very fresh appearing fault morphology; subsequent photographs display a substantially subdued morphology (Kovach and others, 1962).



FIGURE 6.8.—Trace of 1906 earthquake rupture near point of maximum offset (6 m) near Olema on the Point Reyes peninsula north of San Francisco. Photograph by G.K. Gilbert. View northwestward.

MAY 19, 1940 ( $M=7.1$ )

The Imperial fault was discovered from its 60+-km-long rupture in the Imperial Valley earthquake of May 19, 1940. Faulting was predominantly right-lateral strike slip and attained a peak offset of more than 6 m at the United States-Mexican border (fig. 6.9). The first instrumental measurement of strong ground motion adjacent to a fault rupture was obtained from an accelerometer located about 7 km from the surface trace. This record, which provides clear evidence of irregular seismic-energy release during the course of the event (Trifunac and Brune, 1970), has played a major role in shaping building codes for earthquake-resistant design.

JULY 21, 1952 ( $M=7.7$ )

The Kern County or Arvin-Tehachapi earthquake of July 21, 1952, ruptured the White Wolf fault in the largest event to strike California since 1906. The earthquake led to 12 fatalities, and 2 more occurred during a large aftershock on August 22. Field studies of the earthquake (Oakeshott, 1955) describe the geologic, seismologic, and engineering aspects of the earthquake. From a tectonic standpoint, this event is notable for its conjugate relation to the San Andreas fault. Left-lateral slip with a significant reverse-slip component occurred on the northeast-striking, south-dipping fault plane.



FIGURE 6.9.—Surface faulting in 1940 Imperial Valley earthquake offset (6 m) regular rows of orange trees. Fault displacement along this section of the Imperial fault was confined to a narrow zone.



FEBRUARY 9, 1956 ( $M=6.8$ )

More than 19 km of the hitherto-unknown San Miguel fault in Baja California ruptured in the earthquake sequence of February 9, 1956. The fault offset was consistently right lateral and up to the northwest, and attained maximum horizontal and vertical separations of 78 and 91 cm, respectively (Shor and Roberts, 1958). The sequence contained numerous aftershocks, including three of  $M \geq 6$ . About 2 years earlier, a pair of  $M=6$  events that occurred to the south and west of the San Miguel fault may have been associated with the Agua Blanca fault.

APRIL 9, 1968 ( $M=6.5$ )

The Borrego Mountain earthquake of April 9, 1968, produced the first documented rupture of the San Jacinto fault system when right-lateral displacements of nearly 0.4 m occurred along a 30-km-long segment of the Coyote Creek fault. The U.S. Geological Survey (1972) published a detailed description of the event.

FEBRUARY 9, 1971 ( $M=6.5$ )

The San Fernando earthquake of February 9, 1971, ranks as one of the most serious California earthquakes in historical time. The event claimed 58 lives and caused more than half a billion dollars in property damage, including the destruction of two hospitals, a freeway interchange, and the Van Norman Dam. The earthquake ruptured north-dipping, high-angle reverse faults beneath the southern margin of the San Gabriel Mountains and broke the surface along a discontinuous, 15-km-long zone. Surface displacements averaged about 1 m. Seismograms of the earthquake reveal a steeply dipping deep fault and a more shallowly dipping near-surface fault (Langston, 1978; Heaton, 1982). Numerous publications report on detailed investigations of this event, including the summary report published by the U.S. Geological Survey (1971).

OCTOBER 15, 1979 ( $M=6.5$ )

The Imperial fault ruptured for the second time in less than 40 years in a major surface-faulting earthquake on October 15, 1979 (U.S. Geological Survey, 1982). The event broke the north 30 km of the fault, or approximately half the length of the 1940 fault break. However, it was clearly much smaller than the earlier event; maximum surface offsets were well under 1 m, in contrast to 6 m observed in 1940, and the seismic moment was smaller by nearly an order of magnitude. Within the zone of overlapping surface rupture, the two events display nearly

identical displacement profiles (Sharp, 1982), suggesting that the 1979 earthquake represents a characteristic rupture of this segment of the fault. Strong-ground-motion records for the 1979 earthquake form an unparalleled suite of near-field recordings and have stimulated numerous investigations into the dynamics of the source.

MAY 2, 1983 ( $M=6.5$ )

Our understanding of the nature of the earthquake hazard posed by active faults in the San Andreas fault system was fundamentally altered by the occurrence of the Coalinga earthquake of May 2, 1983, on a low-angle thrust fault deep beneath the western margin of the San Joaquin Valley (Rymer and Ellsworth, 1990). Before this event, it had been thought that the major, seismically active faults in California could be recognized on the basis of their surface exposures and record of late Quaternary activity. However, no surface expression exists for the fault system responsible for either this event or the  $M=5.9$  North Kettleman Hills earthquake of August 4, 1985, that adjoins it to the southeast. Instead of a surface fault, the buried deformation is expressed at the surface by active folds (the Coalinga anticline and the Kettleman Hills) that grew during the earthquakes (Stein and King, 1984).

The orientation of the fault and the style of movement on it present another major challenge to prevailing models of the San Andreas system, because this earthquake resulted from a release of compressive forces oriented nearly perpendicular to the trace of the San Andreas fault. Accumulating evidence on the orientation of the stress field astride the San Andreas fault suggests that only a small component of the total stress acts to accommodate the plate motion along the San Andreas fault itself (Mount and Suppe, 1987; Zoback and others, 1987).

NOVEMBER 24, 1987 ( $M=6.6$ )

The Superstition Hills fault ruptured in its entirety on November 24, 1987. The total amount of separation substantially increased by persistent afterslip in the months after the main shock; in fact, the rate of afterslip was so great on the south half of the surface break as to leave open the possibility that all of its displacement occurred as afterslip. The earthquake was preceded by a major foreshock ( $M=6.2$ ), on a conjugate, northeast-trending, left-lateral strike-slip fault that intersected the Superstition Hills fault at the main-shock epicenter. The surface-faulting pattern of the entire sequence was particularly remarkable for the occurrence of numerous breaks on other conjugate faults in the north quadrant around the main break (see Hanks and Allen, 1989).



OCTOBER 18, 1989 ( $M=7.1$ )

In the late afternoon of October 17, 1989, the San Andreas fault ruptured in its first major earthquake since 1906 at 5:04 p.m. P.d.t. (0004 G.m.t. on Oct. 18). Centered along a remote segment of the fault in the southern Santa Cruz Mountains, the Loma Prieta earthquake reruptured the southernmost 40 km of the 1906 fault break, producing the Nation's most costly natural disaster. The earthquake claimed 62 lives and injured an additional 3,757 people. It destroyed 963 homes and damaged more than 18,000 others, displacing 12,000 people from their residences. The combined dollar loss to the private and public sectors exceeded \$6 billion (Plafker and Galloway, 1989).

Damage in the epicentral region was most severe where the earthquake shaking was compounded by local ground failures, commonly involving landslide movement but also including some fractures of probable tectonic origin; the shaking clearly reactivated some fissures observed in 1906. Primary fault displacement, however, did not reach the surface. In the hard-hit communities of Santa Cruz, Watsonville, and Los Gatos, unreinforced-masonry buildings bore the brunt to the damage, and ground conditions played a significant role in the damage patterns.

The earthquake also caused grave damage and claimed the greatest number of lives far to the north, in San Francisco and Oakland, about 100 km from the epicenter. There, the earthquake selectively destroyed structures known to be at risk or located on poor ground (Plafker and Galloway, 1989). The root cause of the devastation in the Marina District of San Francisco (fig. 6.10), as well as at most other sites along the margin of the San Francisco Bay, was liquefaction-induced ground failure. All of these localities sit on land reclaimed from the bay and are underlain by young, water-saturated sedimentary deposits. As we know from the clear lessons of history, provided by the earthquakes of 1865, 1868, and 1906 (Lawson, 1908), such materials perform poorly even under modest levels of earthquake shaking. The collapse of the double-decked section of California Interstate Highway 880 in Oakland (fig. 6.10), where 41 people died, resulted principally from design defects. The section of the viaduct that collapsed was founded on soft estuarine sedimentary deposits that amplified the strong ground motion; the adjoining section, founded on alluvium, rode through the earthquake.

The earthquake broke the San Andreas fault where it makes a conspicuous leftward bend, connecting straighter subparallel segments to the north and south. The fault plane dips 70° SW., and movement in the earthquake involved comparable amounts of right-lateral strike slip and reverse slip, a kinematic response driven by the need

to remove material from this compressional fault bend as the Pacific plate moves to the northwest around it. The rupture nucleated at the base of the seismic zone, at 18-km depth, and spread unilaterally upward and bilaterally along strike, filling a conspicuous void in the preevent seismicity. Geodetic data collected immediately after the event suggest an average strike-slip displacement of 1.6 m and an average reverse-slip displacement of 1.2 m, rising from the hypocenter at 18 km to within 6 km of the surface.

The Loma Prieta earthquake fulfilled a long-term forecast for the rupture of this specific segment of the San Andreas fault (Lindh, 1983; Sykes and Nishenko,



FIGURE 6.10.—Damage in October 18, 1989, Loma Prieta earthquake occurred at distances as far as 100 km from the epicenter in areas underlain by water-saturated, unconsolidated material. *A*, Liquefaction-induced ground failure in the Marina district of San Francisco (top) was restricted to land reclaimed from the San Francisco Bay. *B*, In Oakland, the second deck of Interstate Highway 880 collapsed onto the first deck. Here, poor design was the principal culprit, although failed section sits atop estuarine sedimentary deposits that amplified the shaking.



1984; Working Group on California Earthquake Probabilities, 1988). The high earthquake potential assigned to this segment stemmed from its behavior in the 1906 earthquake, when the fault displacement, as measured at the surface, averaged about 1.5 m, far less than the average for the entire rupture. Estimates of the long-term slip rate along this segment of the San Andreas fault suggested that the strain released in the 1906 earthquake would be renewed in 75 to 136 years, implying that another earthquake was possible in the coming decades. With its occurrence, the Loma Prieta earthquake became the second event in 2 years to fill a recognized seismic gap along the San Andreas; the first was the 1987 Superstition Hills earthquake. The Loma Prieta earthquake also represents the third historical rupture of this segment of the San Andreas fault; the first was the October 8, 1865, earthquake, nominally assigned  $M=6\frac{1}{2}$ , which also caused liquefaction-induced ground failure in San Francisco.

#### SEISMICITY OF THE WESTERN BASIN AND RANGE PROVINCE

The advent of plate tectonics and its application to western North America by Atwater (1970) provided a unifying framework for the contemporary tectonics of the western Basin and Range and its interaction with the San Andreas fault system to the west. Deformation within the province reflects soft coupling of the San Andreas fault system to the North American craton and distribution of the relative plate motion—by mechanisms yet unknown—well over 500 km into the continental interior. The ubiquity of normal-fault-bounded ranges throughout the province tends to belie the underlying nature of present-day deformation within the region. Within historical time, this region has undergone nearly equal proportions of extension on normal faults and dextral shear on strike-slip faults.

The earthquake history of the western Basin and Range province is poorly known before the instrumental period, owing to sparse settlement of this high-desert region. The deficiencies of this record are illustrated by the uncertainties associated with fresh-appearing fault scarps discovered in 1911 near the north end of what would become the rupture zone of the 1954 Fairview Peak earthquake. Upon reviewing the scant historical evidence, Slemmons and others (1959) concluded that these scarps formed about 1903. The absence of an event of sufficient size in the instrumental record, however, suggests that the scarp forming event is older (or substantially smaller than  $M=6$ ). Current understanding of 19th-century seismicity includes an episode of activity along the California-Nevada State line, including a probable rupture of the Olinghouse fault on December 27,

1869 (Sanders and Slemmons, 1979), although this conclusion was questioned by Topozada and others (1981).

Surface faulting has accompanied numerous earthquakes in the region, the most significant of which are discussed below. Notable additional surface-faulting events include the  $M=6.3$  Excelsior Mountain, Nev., earthquake of 1934 and the  $M_L=5.6$  Fort Sage Mountain earthquake of December 14, 1950, located in northeastern California (Gianella, 1957). Ground rupture may have also accompanied the  $M=6$  earthquake of January 24, 1875 (see Gianella, 1957). If so, this observation would move the epicenter listed in table 6.1 to lat  $39\frac{3}{4}^\circ$  N., long  $120\frac{1}{2}^\circ$  W.

#### PRINCIPAL EARTHQUAKES

MARCH 26, 1872 ( $M=7.6$ )

The town of Lone Pine, Calif., was virtually leveled when the entire 100 to 110-km length of the Owens Valley fault ruptured on March 26, 1872, in one of the largest earthquakes in U.S. history. This fault, which lies in the middle of Owens Valley, is distinct from the normal faults bounding the front of the Sierra Nevada to the west. Considerable confusion has existed in the literature regarding the style of faulting in the 1872 earthquake, including interpretations of right-lateral, left-lateral, and normal-fault movement. A recent study of the earthquake offsets by Beanland and Clark (in press) unambiguously demonstrates that fault movement was predominately right-lateral strike slip, with an average horizontal displacement of 6 m (fig. 6.10). The vertical offsets were clearly smaller and averaged about 1 m down to the east. Beanland and Clark estimate a moment magnitude of  $M=7.5-7.7$ . Faulting in 1872 largely reactivated earlier Holocene scarps, as recognized by G.K. Gilbert when he visited the area in 1883.

The event was felt throughout most of California and Nevada, and as far east as Salt Lake City, Utah. Adobe and brick buildings in Owens Valley sustained the brunt of the damage. Minor damage also occurred in the San Joaquin and Sacramento Valleys on the opposite side of the Sierra Nevada, at distances of as far as 400 km. In Yosemite Valley, John Muir witnessed a spectacular rockfall triggered by the earthquake. As severe as the ground shaking must have been, it was noted in the Inyo, Calif., *Independent* of April 6, 1982, “\* \* \* that not a person would have been killed or hurt had their houses all been made of wood.” It is of some historical interest that the first long-term earthquake forecast, made by G.K. Gilbert in 1883 to the citizens of Salt Lake City, was based in part on his observations of the 1872 earthquake. In it, he noted that the rebuilding of Independence with wood-frame buildings was an extravagance, because this



great shock had relieved the accumulated strain, and so many generations would pass before conditions would permit another similar shock to occur (Gilbert, 1884):

The old maxim, "Lightning never strikes in the same spot twice" is unsound in theory and false in fact; but something similar might truly be said about earthquakes. The spot which is the focus of an earthquake (of the type here discussed [1872 Owens Valley]) is thereby exempted for a long time.

Many comparisons have been drawn between the Owens Valley earthquake and the great San Andreas earthquakes of 1857 and 1906. The size of the regions shaken in all three events are comparable, as are the maximum fault displacements. The two San Andreas events have significantly longer rupture lengths, and their seismic moments are larger by a factor of 2 to 3. Whether or not any or all of these earthquakes can be classified as "great" earthquakes becomes a question of semantics. All of them can be classified as great on the basis of their rupture lengths of 100 km or more (Kanamori, 1977), but they all have seismic moments more than 100 times smaller than the largest known earthquakes, such as the  $M=9.2$  Alaska earthquake of 1964. Practically speaking, these events are among the largest known strike-slip events, and they must be close to the size of the largest possible strike-slip events along the San Andreas fault system.

OCTOBER 3, 1915 ( $M=7.3$ )

The 1915 Pleasant Valley, Nev., earthquake of October 15, 1915, created a series of spectacular normal-fault scarps in the central Nevada seismic zone of the Basin and Range province (figs. 6.11, 6.12). Four major scarps formed during the earthquake, with an aggregate length of 59 km, and reruptured Holocene scarps at the base of the mountain blocks (Wallace, 1984). Fault movement in the earthquake appears to have been purely dip slip and averaged about 2 m on the steeply dipping fault plane. The earthquake was felt from western Utah to the Pacific coast and from northeastern Oregon to the United States-Mexican border. Instrumental measures of the magnitude range from 7.3 to  $7\frac{3}{4}$  and exceed the moment magnitude of 7.2 derived from field measurements ( $M_0=6.1 \times 10^{27}$  dyne-cm).

The Pleasant Valley earthquake lies at the north end of a 500-km-long belt of historical surface-faulting earthquakes within the central Nevada seismic zone and Owens Valley fault system. The four major earthquake sequences in this zone since 1872 leave two conspicuous seismic gaps that have been discussed as the potential loci of future major earthquake activity (fig. 6.11; Wallace, 1984).

DECEMBER 21, 1932 ( $M=7.2$ )

The second historical surface-faulting event in the central Nevada seismic zone on December 21, 1932, produced a discontinuous zone of surface faulting and fissures in the valleys west and north of Cedar Mountain (Gianella and Callaghan, 1934). Within the 60-km-long, north-northwest-trending zone where faulting was observed, most breaks struck east of north and showed clear evidence of right-lateral displacements (fig. 6.11).

JULY 6, 1954 ( $M=6.6$ ), AND AUGUST 24, 1954 ( $M=6.8$ )

The Rainbow Mountain earthquakes of July 6 and August 24, 1954, produced a zone of east-facing normal-fault scarps along the base of Rainbow Mountain, extend-

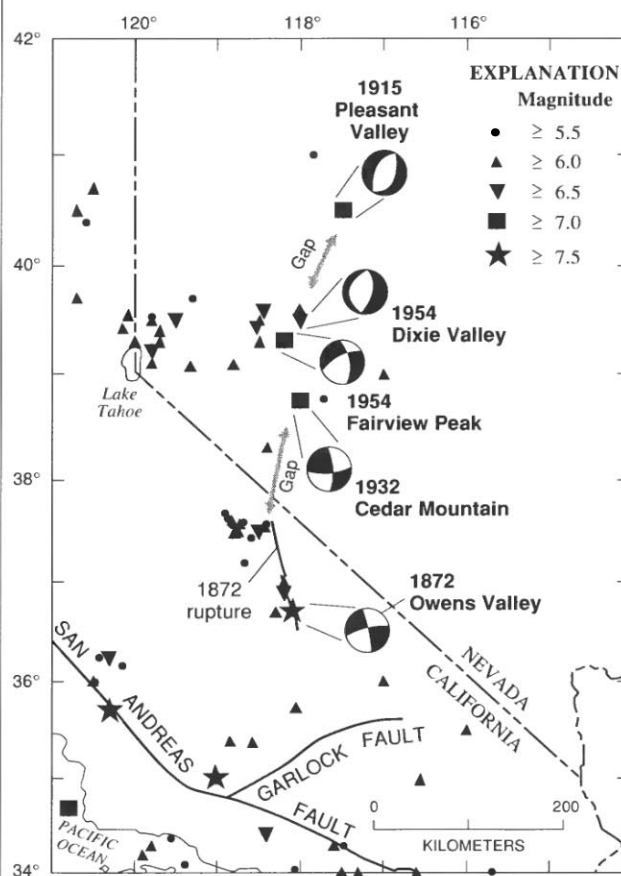


FIGURE 6.11.—California-Nevada region, showing locations of major historical earthquakes in the western Basin and Range province, 1857–1989. Focal mechanisms of five largest events in lower-hemisphere projection show compressional quadrant shaded and indicate significant shear as well as extensional strain in province. Seismic gaps (labeled) are potential loci of future major earthquake activity (Wallace, 1984).



ing northward into the Carson Sink. The July 6 event produced an 18-km-long surface rupture at the south end of this zone striking N. 15° E., with maximum displacements of about 30 cm. The August 24 shock extended the zone by 22 km in a N. 20° E. direction, with as much as 75 cm of normal-fault slip. Tocher (1956) noted that the displacement on the northern part of the July 6 break approximately doubled in amplitude between July 16 and September 9; the timing of the additional slip could not be determined.

DECEMBER 16, 1954 ( $M=7.1$  AND 6.8)

The Dixie Valley-Fairview Peak earthquakes of December 16, 1954, produced a 90-km-long zone of right-lateral oblique and normal faulting in the central Nevada seismic zone (fig. 6.11; Slemmons, 1957). The first shock, which occurred east of Fairview Peak, produced lateral displacements of more than 4 m and vertical displacements of as much as 3 m. Faulting along this 50-km-long zone was predominantly down to the east opposite Fairview Peak and changed polarity to the north. The second shock, which occurred 4 minutes later, had an epicenter on the east side of Dixie Valley in a left-stepping echelon arrangement with the earlier event. Normal-fault scarps formed along a 40-km-long zone at the base of the Stillwater Range some 20 km west of the

Rainbow Mountain faulting. Vertical displacements exceeded 2 m, and consistent strike-slip displacements were absent.

JULY 21, 1986 ( $M=6.2$ )

The Chalfant Valley earthquake of July 21, 1986, is the largest event to date in a series of 33 earthquakes of  $M_L \geq 5$  to occur since 1978 in the White Mountain seismic gap (Savage and Cockerham, 1987). Other principal events in this series include the May 25-27, 1980, Mammoth Lakes earthquakes ( $M=6.1, 5.9, 5.8, 6.0$ ) and the November 23, 1984, Round Valley earthquake ( $M=5.7$ ). The series of shocks is of interest not only because of its wide geographic distribution in the White Mountain seismic gap but also because of the contemporaneous uplift of Long Valley caldera (Hill and others, 1985). The Chalfant Valley earthquake created a 10+-km-long zone of fractures with as much as a few centimeters of dextral slip on the frontal-fault zone of the White Mountains (Lienkaemper and others, 1987). The earthquake focal mechanism and aftershock distribution show that the predominately dextral strike-slip displacement associated with this event occurred on a west-dipping fault plane that projects upward to meet the surface break.



FIGURE 6.12.—Fault trace of 1915 Pleasant Valley, Nev., earthquake remains clearly visible in this photograph by R.E. Wallace more than 60 years after event (Wallace, 1984).

### SEISMICITY OF THE MENDOCINO TRIPLE JUNCTION AND THE GORDA PLATE

The San Andreas fault terminates at its north end in a transform/transform/trench triple junction just seaward of Punta Gorda. Major earthquake activity lies along the Mendocino Fracture Zone, where it is an active transform fault, and to the north within the Gorda plate, which is undergoing intense internal deformation. The Wadati-Benioff zone is well defined to a depth of 30 km and can be traced eastward to a depth of more than 80 km (see fig. 5.5; Walter, 1986). Strong earthquakes within the Gorda plate locate off shore and span the position of the megathrust; these events appear to lie entirely within the oceanic lithosphere. The 1980 Eureka earthquake, for example, ruptured the Gorda plate from the landward to the seaward side of the megathrust. Despite the high level of seismicity, underthrusting events are rare.

#### PRINCIPAL EARTHQUAKES

NOVEMBER 23, 1873 ( $M=6\frac{3}{4}$ )

The severe earthquake of November 23, 1873, was felt from San Francisco to Portland, Oreg.; it inflicted the heaviest damage to Crescent City, Calif., and surrounding communities in the Klamath Mountains. The macroseismic epicenter near the California-Oregon State line and probably inland of the coastline is unique within both the historical and instrumental records.

APRIL 16, 1899 ( $M=7$ )

Little is known about the large earthquake of April 16, 1899, with an epicenter seaward of Eureka, where it was described as "one of the severest shocks of earthquake ever experienced." Topozada and others (1981) corrected the origin time of this event and assigned a nearshore epicenter and an  $M_I$  of 5.7. The earthquake was assigned an epicenter in the Gulf of Alaska by Milne (1901) on the basis of the traveltime of the maximum amplitude from the five reporting stations; however, a California location satisfies his data equally well. The absence of significant damage along the coast suggests an epicenter well out to sea. An instrumental magnitude ( $M_S$ ) of 7.0 is derived from the surface-wave amplitudes reported by Milne (see Abe and Noguchi, 1983).

JANUARY 31, 1922 ( $M=7.3$ )

The intensity pattern of the large earthquake of January 31, 1922, is generally similar to that of the 1899 event. This event was well recorded throughout the world.

JANUARY 22, 1923 ( $M=7.2$ )

The earthquake of January 22, 1923, strongly shook the Cape Mendocino region and toppled many chimneys in the area. This earthquake was probably associated with the Mendocino Fracture Zone.

DECEMBER 21, 1954 ( $M=6.6$ )

The strong earthquake of December 21, 1954, apparently was located in the crust of the North American plate above the descending Gorda plate. The relocation of this event by Smith and Knapp (1980) suggests a possible association with the active Mad River fault zone. One fatality is attributed to the earthquake.

NOVEMBER 8, 1980 ( $M=7.2$ )

The Eureka earthquake of November 8, 1980, resulted from 100-km-long, left-lateral strike-slip rupture of the Gorda plate along a northeast-striking fault (see fig. 5.5). Aftershocks of the earthquake extended from within 30 km of the coastline southwestward to the Mendocino Fracture Zone. The focal mechanism of the earthquake is thus conjugate to the San Andreas, with its tension axis aligned in the downdip direction. This event argues for high rates of internal deformation within the subducting oceanic lithosphere and against the extension of San Andreas-style faulting northward of the triple junction.

#### DISCUSSION

The spatial distribution of large earthquakes during the past 2 centuries defines the San Andreas fault system as a 100- to 300-km-wide zone containing numerous active faults in addition to the San Andreas fault proper (fig. 6.1). Except for the two largest events, the great 1857 and 1906 earthquakes that together ruptured two-thirds of the total length of the San Andreas fault, large earthquakes are conspicuously absent along the master fault itself. Although these two great earthquakes account for half of the seismic-strain release since 1769, most of the rest occurs on other, smaller elements of the fault system. Major historical events on these secondary faults, such as the 1927 Lompoc and 1952 Kern County earthquakes, serve to define the boundaries of the San Andreas system. Their mechanisms differ significantly from right-lateral strike slip parallel to the plate-motion vector and illustrate the diversity and complexity of seismic-strain release within the plate-boundary zone.

Over the timespan of the historical catalog, the most enduring characteristic of the earthquake distribution may be the spatial clustering of activity at specific localities along the plate boundary. Notable hotspots



include the Cerro Prieto, Imperial, San Jacinto, and Calaveras faults, all of which are major branches of the San Andreas fault, and the Parkfield segment of the San Andreas fault in the transition zone between the 1857 rupture and the 150-km-long central, creeping segment of the fault. In each of these areas, the seismic activity coincides with these high-slip-rate faults (1–3.5 cm/yr), and in some places it clearly represents recurrent rupture of the same segment of the fault. At greater distances from the San Andreas fault, the historical events (or sequences) tend to represent isolated occurrences on slower moving faults. Thus, although the overall seismicity spans the broad plate-boundary zone, seismic-strain release over the past 2 centuries correlates with the local rate of fault movement.

In general, the locations of historical earthquakes resemble the overall distribution of microearthquake activity, despite more than six orders of magnitude difference in average seismic moment (fig. 6.13; see chap. 5). One important difference between the distribution of large and small earthquakes is the virtual absence of smaller events along the San Andreas fault segments that ruptured in 1857 and 1906. Similarly, seismic activity is distinctly absent on the potentially dangerous segment between the 1857 break and the Imperial Valley. Except for the central, creeping segment, where numerous small events occur, the San Andreas fault is almost completely aseismic during the long intervals between its rupture in major earthquakes (see figs. 5.6, 5.9).

This inverse correlation between the source regions of large earthquakes and the distribution of smaller events can also be observed for smaller main shocks. Recent studies of the rupture dynamics of  $M=6$  events occurring within seismically active regions indicate that the rupture zones of these events are similarly aseismic, with smaller events occurring predominantly outside the slip surface, even during the aftershock sequence (Reasenber and Ellsworth, 1982; Hartzell and Heaton, 1986; Mendoza and Hartzell, 1988). Thus, the sites of future large earthquakes cannot be identified on the basis of minor seismicity alone.

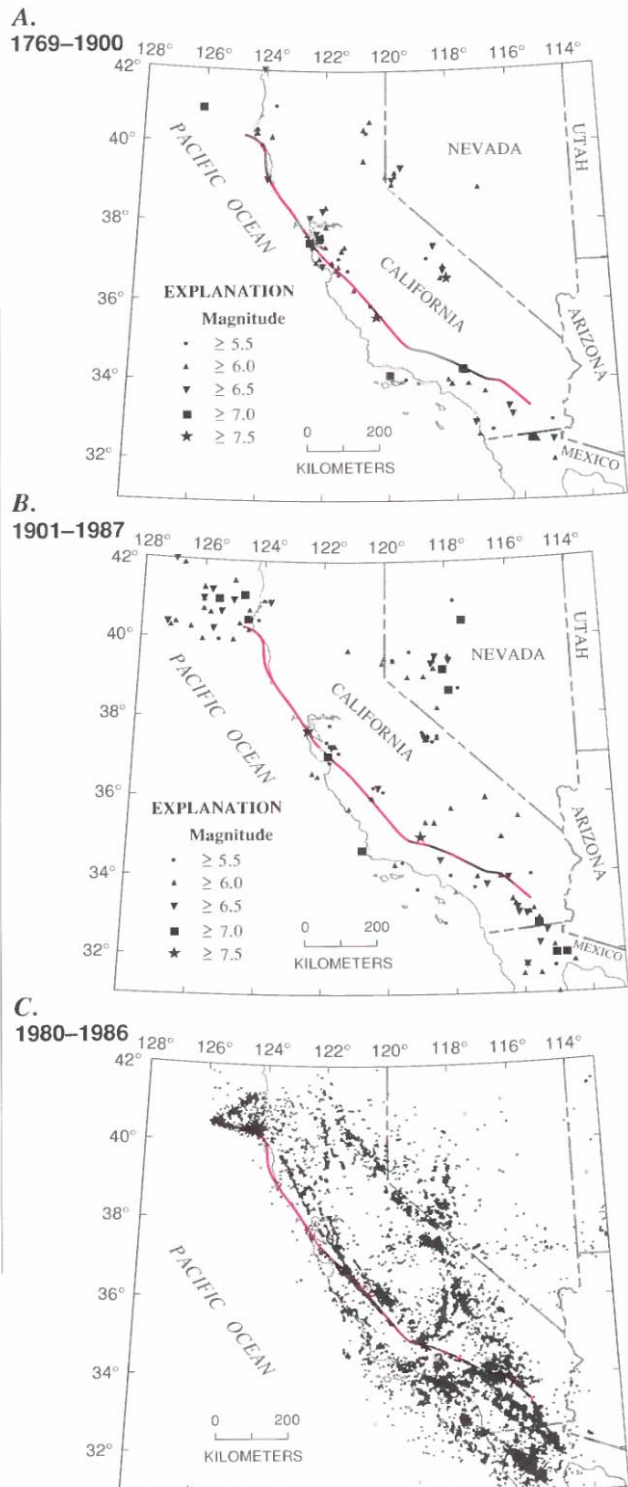


FIGURE 6.13.—Distribution of large and small earthquakes along the San Andreas fault system. In general, modern instrumental data (C; see chap. 5) portray same pattern of activity seen in large earthquakes from preinstrumental (A) and instrumental (B) eras. Some areas characterized by high levels of microearthquakes, such as well-defined faults east of northern section of the San Andreas fault (red line), have not produced significant earthquakes in historical time and so are considered probable sites of future activity.

## RATE OF SEISMICITY

The average rate of earthquake activity within the San Andreas system can be estimated from the Gutenberg-Richter frequency-magnitude relation  $\log N = a - bM$ , where  $N$  is the cumulative number of events of magnitude equal to or greater than  $M$  during a given time period. For the 77 events along the fault system with summary magnitudes  $M \geq 6$  since 1852, this relation well describes the population with  $a = 5.74$  and  $b = 1$  (fig. 6.14). Comparable results are obtained for subsets of  $M = 6$  events, such as the instrumental period (1898-1989).

It is useful to compare these results from the historical record with the frequency-magnitude relation determined from systematic microearthquake observations. If the historical rate of activity applies today and the frequency-magnitude relation for microearthquakes ( $M \geq 3$ ) is described by the same relation, then about 5,600  $M \geq 2$  events should be observed each year. This prediction exceeds the number of events observed during the interval 1980-87 by about a factor of 2 (see chap. 5) and suggests that a somewhat smaller value of  $b = 0.93$  may be more appropriate for the extended magnitude range.

For the catalog as a whole, the rate of earthquake occurrence is well described by a Poisson process, in which the probability of finding one or more events in any

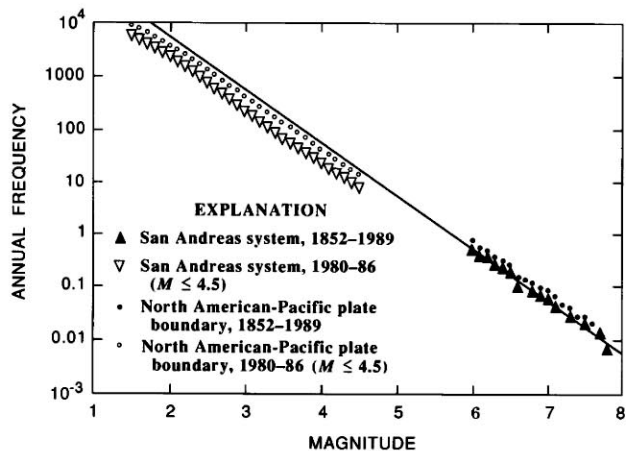


FIGURE 6.14.—Annual frequency of earthquakes of magnitude  $\geq M$  as derived from historical and modern instrumental catalogs. Gutenberg-Richter frequency-magnitude relation,  $\log N = a - bM$  with  $a = 5.74/\text{yr}$  and  $b = 1$ , describes observed distribution of earthquakes of  $M \geq 6$  within the San Andreas fault system during 138-yr interval from 1852 to 1989. Also shown are annual frequency of  $M \geq 6$  events from the broader Pacific-North American plate boundary, including the San Andreas fault system and the western Basin and Range province, and of  $M = 2-4.5$  events in both regions during 1980-86.

interval of  $t$  years is  $P = 1 - e^{-\lambda t}$ , where  $\lambda$  is the average rate of earthquake occurrence. It follows from the observed frequency-magnitude relation that the odds of having at least one  $M \geq 6$  event per year are 0.43. There is also an even chance of at least one  $M \geq 6$  event within any 15-month interval, one  $M \geq 7$  within any 12½-year interval, or one  $M \geq 8$  within any 125-year interval.

The rate of earthquake activity along the plate boundary can also be usefully compared with plate-motion estimates derived from plate-tectonic theory. Current estimates of the relative velocity across the North American-Pacific plate boundary, determined from the spreading rate in the Gulf of California of 5 cm/yr (DeMets and others, 1987), imply an annual seismic-moment rate of  $2 \times 10^{26}$  dyne-cm/yr for a 10-km-thick brittle crust, equivalent to a single  $M = 6.8$  earthquake. Earthquakes of this size occur far less often, and the principal seismic contribution to the plate motion comes from infrequent large events. The erroneous notion that the smaller events substantially contribute to the total is demonstrably false, as shown by summing the contributions of all the earthquakes below some magnitude. The innumerable events of  $M \leq 6$  occurring each year contribute less than 10 percent to the total seismic-strain release.

Within the San Andreas fault system, the total seismic-moment release since 1852 corresponds to 70 percent of the total North American-Pacific plate motion predicted by plate-tectonic models. This proportion is somewhat inflated because not all of the earthquakes act to transmit slip along the plate boundary; for example, the 1952 Kern County earthquake, the third largest in historic time, directly accommodated little plate-parallel motion. Although aseismic displacements account for some of the deficit, notably along the central, creeping section of the San Andreas fault, deformation occurring elsewhere, notably within the Basin and Range, contributes substantially to the relative motion between the North American and Pacific plates.

## PARADOX OF THE MISSING PLATE MOTION

The discrepancy between plate-tectonic estimates of relative motion across the North American-Pacific plate boundary and seismic estimates also holds for geologic and geodetic estimates of motion along the San Andreas fault system. The explanation of this apparent paradox is thought to include deformation within the Basin and Range province in western Nevada and eastern California (Atwater, 1970), which has been the locus of major seismic activity in historical time, including the third



largest event, in 1872, and 3 of the 11  $M \approx 7$  events in the 20th century.

It has long been recognized that the Basin and Range province has undergone substantial extension during the Cenozoic and is presently opening in a N. 60° W. direction (Zoback and Zoback, 1980). Historical seismicity partly agrees with this geologically derived pattern; however, it also indicates a significant component of dextral shear in nearly every well-studied historical event (Shawe, 1965; Doser, 1986). Because the geologic expression of strike-slip displacement is much more difficult to recognize and quantify than vertical slip, a major question is raised about the significance of the historic seismicity for the total strain within the western Basin and Range.

Since the 1872 earthquake, the net seismic strain within the Basin and Range province can be estimated by summing the contributions of individual events. The net shear strain thus determined indicates nearly equal components of extensional strain in a N. 60° W. direction and dextral shear trending N. 10° W. The resulting average-motion vector nearly coincides with the orientation of the San Andreas fault, and the lateral slip largely balances the coastward expansion of the province that results from extension alone. If both the rate and style of historical faulting accurately portray the long-term deformation within the region, they diminish the discrepancy between the predicted and observed rates of motion across the North American-Pacific plate boundary.

#### EARTHQUAKE RECURRENCE AND CHARACTERISTIC EARTHQUAKES

Over geologic time, the net displacement across a fault accumulates through the action of countless individual slip events. Measured over many displacement cycles, the average interval between events must equal the average event displacement divided by the remote slip rate. First principles, however, provide little guidance as to the properties of the recurrence, which might range from a totally random distribution of events in both space and time to identical earthquakes repeating at fixed intervals. If recurrence is essentially random, then long-term seismic hazard is described by the Poisson rate of activity, as discussed above. Greater regularities and systematics in recurrence imply that useful time-dependent forecasts of future activity can be derived from knowledge of the past behavior of the fault system.

Results for San Andreas earthquakes have played a central role in establishing the existence of broad regularities in the recurrence process. At Parkfield, the San Andreas fault has ruptured six times since 1857 in  $M \approx 6$  events with highly repeatable characteristics every  $22 \pm 6$  years. The latest three events, in 1922, 1934, and 1966, for which instrumental records exist, are virtually iden-

tical (fig. 6.15; Bakun and McEvilly, 1984). Amplitude data from Milne seismographs uncovered in the preparation of table 6.1 show that the 1901 and 1922 events produced the same surface-wave amplitudes on common stations, strengthening earlier speculations that all the 20th-century events are similar. Intensity data for the 1881 event (Toppozada and others, 1981) and for foreshocks to the great 1857 earthquake (Sieh, 1978b) place them along the Parkfield segment as well. These regularities in the size, location, and timing of all known events at Parkfield led Bakun and Lindh (1985) to propose a specific recurrence model for Parkfield earthquakes. On the basis of this model, the next in the series of characteristic events is anticipated before 1993, and its forecast represents the first formally endorsed earthquake prediction in the United States.

Geodetic analysis of the strain released in the 1966 earthquake and its subsequent reaccumulation led Segall and Harris (1987; see Harris and Segall, 1987) to identify the zone where strain accumulates and is released, the

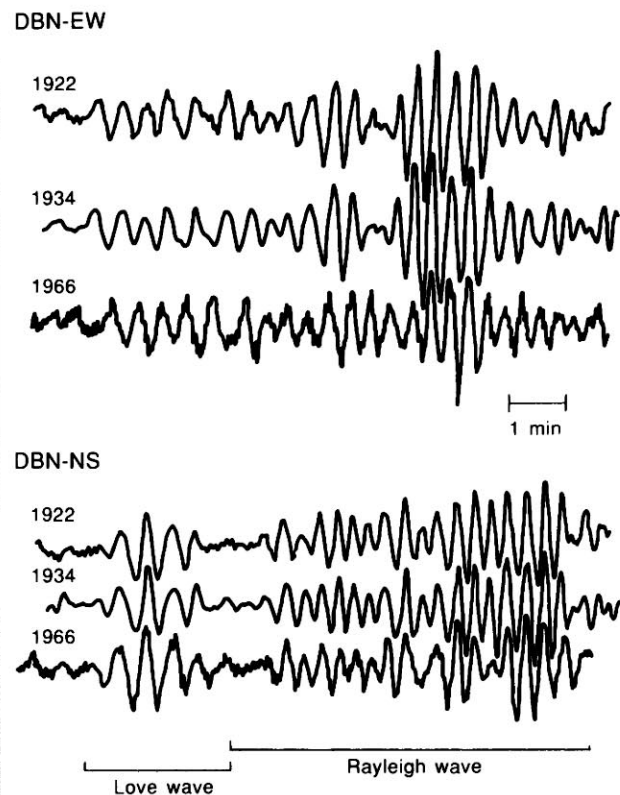


FIGURE 6.15.—Surface waves of 1922, 1934, and 1966 Parkfield, Calif., earthquakes as recorded on same seismograph in DeBilt, The Netherlands (DBN; EW, east-west; NS, north-south). These nearly identical waveforms and amplitudes led Bakun and McEvilly (1984) to propose recurrent rupture of same segment of the San Andreas fault as mechanism of Parkfield earthquakes.



"Parkfield asperity," as the center of the 1966 rupture zone. This zone of strain accumulation appears to be effectively locked during the interseismic period and corresponds to the center of the 1966 aftershock zone (Eaton and others, 1970) between about 4- and 10-km depth. The significantly fewer events in this part of the aftershock zone than in its periphery suggests that Parkfield earthquakes occur when this locked zone suddenly releases. Aftershocks appear to result from transfer of stress to the perimeter of the asperity.

This same pattern of concentrated coseismic slip occupying a quiet region within the overall aftershock distribution characterizes several recent, well-studied events (Mendoza and Hartzell, 1988), three of which, the Coyote Lake earthquake (Aug. 6, 1979), the Imperial Valley earthquake (Oct. 15, 1979), and the Morgan Hill earthquake (Apr. 24, 1984), all have probable antecedents within the historical record. Reasenber and Ellsworth (1982) identified the June 20, 1897, earthquake as a predecessor to the 1979 event and noted that the 82-year interval between events equaled the 1.2 m of coseismic slip determined by Liu and Helmberger (1983) divided by the long-term slip rate of 1.5 cm/yr for the Calaveras fault. Similarly, the 73-year interval between the July 11, 1911, event and the 1984 Morgan Hill earthquake (Bakun and others, 1984) well predicts the 0.8 to 1.0 m of maximum coseismic slip determined by Hartzell and Heaton (1986). The 1979 Imperial Valley earthquake is more complex because it reruptured only the northern 30 km of the May 19, 1940, fault break. Again, both the time interval between events and the fault-slip rate compare favorably with the fault slip at depth, as determined from seismograms (Hartzell and Heaton, 1983; Archuleta, 1984). Earlier ruptures of this or other segments of the Imperial fault may well be in the historical record, possibly including the April 19, 1906, event, which occurred the afternoon of the great 1906 earthquake in northern California.

Similar observations of recurrent faulting in events with characteristic magnitudes and locations from around the world (Nishenko and Buland, 1987) suggest a simple, first-order model for seismic potential. In this model, the future behavior of a specific segment of a fault can be forecast from knowledge of the size of past earthquakes, the timing and amount of slip in the latest event, and the long-term rate of fault movement (Lindh, 1983; Sykes and Nishenko, 1984). Accordingly, the probability of an event on a recently ruptured fault segment is low until the elastic strain rebuilds, which may be estimated from the geologic slip rate. As the strain rebuilds, the probability of another earthquake increases. Empirically, the time intervals between successive ruptures of a specific fault segment define a bell-shaped distribution that may be used to estimate the odds of the next event within

some future time interval, given that it has not yet occurred.

Probabilities for large earthquakes along the major branches of the San Andreas fault derived from this methodology differ markedly from Poisson estimates (Working Group on California Earthquake Probabilities, 1988). For example, the chance of a repetition of the great 1906 earthquake within the next 30 years (1988-2018) is less than 0.1. In contrast, the chance of an  $M=7\frac{1}{2}$ -8 earthquake on the southern section of the San Andreas fault is 0.6. When the Working Group's report was written, the southernmost part of the 1906 fault break was assigned the highest chance of failure of any segment of the north half of the San Andreas fault. Now that it has ruptured in the October 18, 1989, Loma Prieta earthquake, the probability of another rupture will be small for several decades. A clearer understanding of past seismicity can only help to improve and refine estimates of future seismicity.

#### THE SEISMIC CYCLE

An important implication of the characteristic-earthquake model is the existence of a repetitive cycle of strain accumulation and release (Fedotov, 1968). Mogi (1981) suggested the existence of definite stages in the cycle, including a low level of seismicity in the first part of the cycle once aftershock of the latest event subside, a rise in regional activity as strain accumulates, and ultimately the occurrence of another earthquake with its attendant foreshocks and aftershocks, which initiates the next cycle.

The long-term seismicity within the San Andreas fault system displays these characteristics along the rupture zone of the great 1906 earthquake (figs. 6.16, 6.17; Ellsworth and others, 1981). Activity was relatively high during the 19th century, as becomes particularly apparent after 1850, when the record is virtually complete. After the great 1906 earthquake, the level of seismicity changed drastically, and moderate events essentially ceased for 50 years. Since the mid-1950's, the activity level has increased and begun to approach the 19th-century level (Tocher, 1959). This change in activity associated with the 1906 earthquake has been noted many times (for example, Gutenberg and Richter, 1954), and it is an open question whether it represents a premonitory increase (Topozada and others, 1988) or whether the long quiescent period since 1906 is the essential feature (Ellsworth and others, 1981).

Comparable variations in seismicity appear to be present in southern California, although the historical record there is less reliable until about 1890. Along the rupture zone of the great 1857 earthquake, the available data suggest a similar period of low activity for several



decades after the event (fig. 6.17). Farther south, along the section of the fault that has not ruptured in 3 centuries, the activity level since at least the 1880's is reminiscent of the activity in the San Francisco Bay region before the 1906 earthquake (fig. 6.18). As a potential long-term indicator of high seismic potential, the seismicity surrounding the dormant southern section

of the San Andreas fault agrees with independent estimates of long-term potential derived from paleoseismology.

**FUTURE USES OF EARTHQUAKE HISTORY**

At this stage in our understanding of the San Andreas fault system, seismicity is still best described as a random

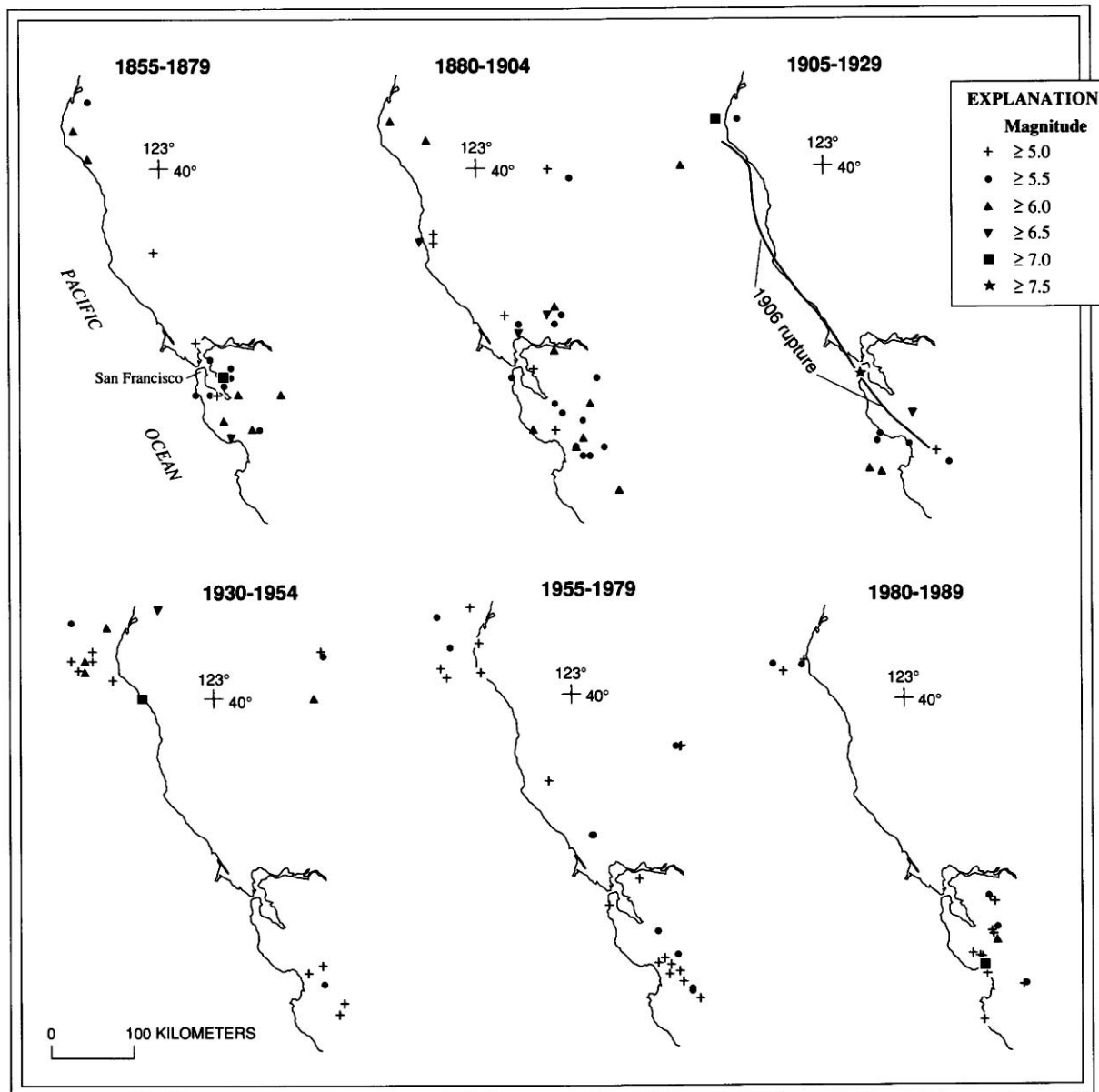


FIGURE 6.16.—Seismicity of the San Francisco Bay region in quarter-century epochs. Activity was high in the region during at least a half-century before 1906 earthquake and drastically declined afterward for the next half-century. Since the mid-1950's, activity has

begun to approach levels last seen in the 19th century. However, both geologic and geodetic evidence suggest that the next great earthquake will not occur for a century or more.

process over time, with a highly clustered spatial distribution. There are, however, tantalizing hints of underlying regularities, such as those in the characteristic earthquakes at Parkfield, or in the striking changes in seismicity associated with the 1906 earthquake. The next generation of refinements to this history will assuredly make comparable contributions by reducing the uncertainty in earthquake locations and magnitudes. Modern seismologic methods for extracting new information on the mechanisms of earthquakes have already proved practical for many events from the early instrumental period. Systematic treatment of the full instrumental catalog with these methods will provide a new basis for understanding the tectonics of the plate boundary and the mechanics of earthquakes.

### CATALOG OF MAJOR EARTHQUAKES, 1769–1989

#### CATALOG COMPILATION

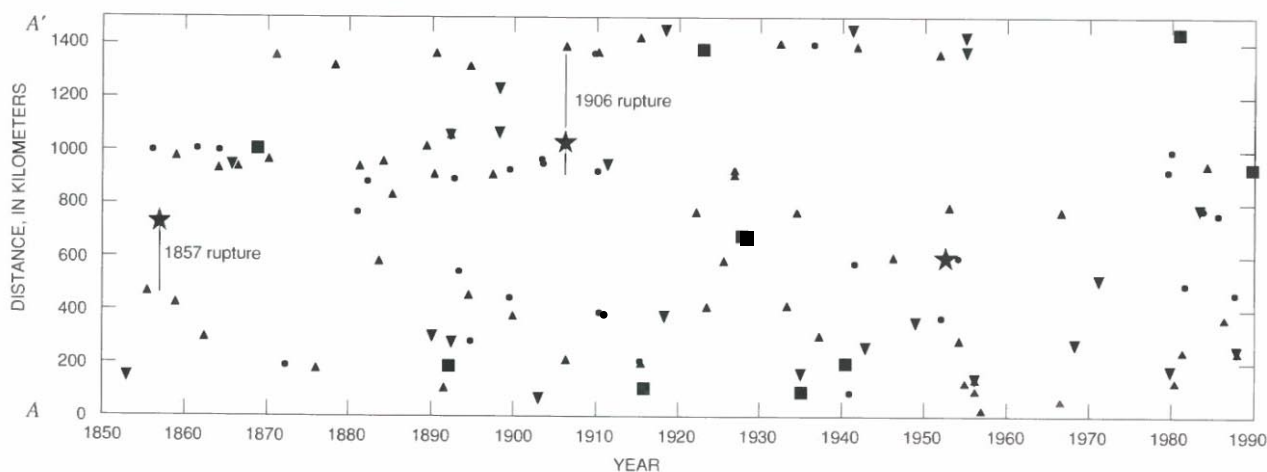
The publication of Edward S. Holden's catalog of Pacific coast earthquakes in 1898 represented the first systematic scientific inquiry into the seismic history of California and surrounding regions. This catalog, and its extension by McAdie (1907), formed the primary basis for the monumental catalog of Townley and Allen (1939) covering the years 1769–1928. These catalogs provide detailed descriptive accounts of virtually all the earth-

quakes that are now known from this period, and all subsequent analyses of seismicity up to the modern instrumental period build on these foundations.

Recent studies of preinstrumental seismicity have focused on quantification of the historical record. The catalog presented here relies heavily on the research of Tousson Topozada and his associates (Topozada and others, 1981; Topozada and Parke, 1982), who developed extensive new information on seismic intensities from newspaper accounts and other original sources, and determined locations and magnitudes from the resulting isoseismal maps. In addition, several special studies of important events by other workers have contributed to the catalog.

The development of practical seismographic instrumentation around the turn of the 20th century led to the rapid growth of seismologic data, particularly for those events large enough to register at teleseismic distances on the early instruments. The publication of the Circulars of the Seismological Committee of the British Association for the Advancement of Science (1899–1912) and their continuation as the International Seismological Summary from 1913 on indicate a detection threshold of about  $M \approx 6$  for the Western United States as early as 1898. Data from these and other sources enabled Gutenberg and Richter (1954) to systematically catalog seismicity from 1904 onward.

Modern seismographic instrumentation first installed in California in 1910 ushered in the era of earthquake



#### EXPLANATION

##### Magnitude

- $\geq 5.5$
- ▲  $\geq 6.0$
- ▼  $\geq 6.5$
- $\geq 7.0$
- ★  $\geq 7.5$

FIGURE 6.17.—Space-time diagram of seismicity since 1850 along the San Andreas fault system between head of the Gulf of California (A) and Punta Gorda (A'). Change in seismicity rate along northern section of the San Andreas fault associated with 1906 earthquake (fig. 6.13) may also be tentatively identified along 1857 earthquake rupture. Persistent activity characterizes south third of the plate boundary since 1890, spanning the entire interval of reliable earthquake reporting in this region.



observation at regional distances. The Bulletins of the Seismographic Stations of the University of California,

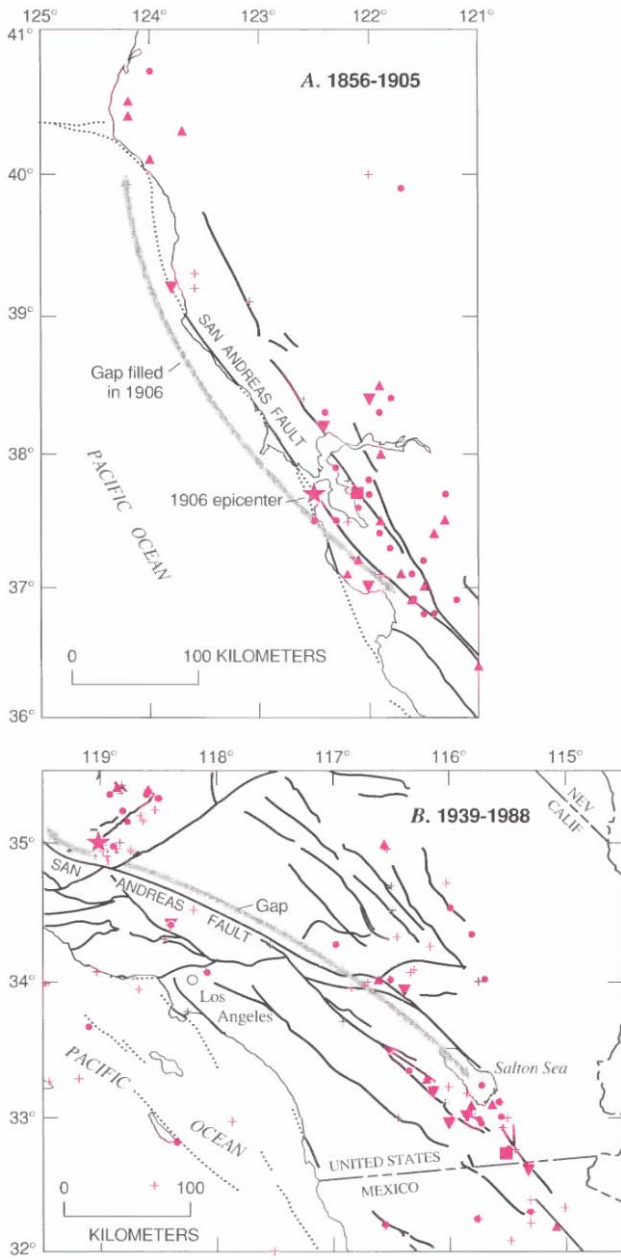
Berkeley, from 1910 to the present form the principal source for events in northern California and adjoining areas. Routine epicentral determinations and magnitude assignments for earthquakes in the southern California region date from 1932 and are taken from the catalog of the Seismological Laboratory of the California Institute of Technology, Pasadena. Additional instrumental results come from various other sources, chiefly the U.S. Geological Survey and the University of Nevada, Reno.

The resulting catalog of major earthquakes in California, western Nevada, and northernmost Baja California from 1769 to 1989 (table 6.1) contains 206 entries. This catalog omits several earthquakes listed in earlier catalogs where this or other recent studies have failed to corroborate previous interpretation as significant events or even, in some cases, their occurrence.

**QUANTIFICATION OF EARTHQUAKES AND MAGNITUDE SCALES**

Physical measures of the complex mechanical event producing the earthquake take many forms, including the dimensions of the faulted region, the amount of slip, and the strength of the radiated elastic waves. To relate the characteristics of one event to another, the observed quantities must generally be summarized through the use of either an empirical relation, such as magnitude, or a quantity derived from a physical model, such as seismic moment. Both procedures have their place, and the choice of one metric over another depends principally on the purposes of the comparison and the availability of common data.

Because no single procedure for determining magnitude can be applied to the entire historical record, the catalog must be quantified by using various magnitude scales. Each scale is briefly described below to define its origin and to clarify its relation to the other scales. I emphasize that each scale has a particular range of validity and that different magnitude scales will, in general, yield slightly different values for the same event. Such differences in magnitude seem to provide a never-ending source of interest and controversy for the news media, who commonly lump all scales together under the heading of "Richter scale." To the seismologist,



**EXPLANATION**

- |   |       |                        |
|---|-------|------------------------|
| + | ≥ 5.0 | — ····· Fault — Dotted |
| ● | ≥ 5.5 | where concealed        |
| ▲ | ≥ 6.0 |                        |
| ▼ | ≥ 6.5 |                        |
| ■ | ≥ 7.0 |                        |
| ★ | ≥ 7.5 |                        |

FIGURE 6.18.—Where will the next great earthquake strike along the San Andreas fault system? Numerous lines of evidence point to its long-dormant southernmost segment (B) as having the highest potential. Large earthquake activity in this region shares many similarities with activity in the San Francisco Bay region before 1906 earthquake (A). In both cases, absence of activity directly on the San Andreas fault is pronounced, and a high regional level of activity is concentrated along other major branches of the fault system.

such differences are neither surprising nor controversial and can, in fact, provide information on the underlying physical processes of the earthquake source.

I also emphasize that intensity scales characterize the effects of the earthquake at a particular location and are not magnitude scales. Strictly speaking, intensity values (or, for that matter, instrumentally measured values of ground-motion parameters) describe the vibratory motions that are the actual earthquake as observed at a particular location, whereas magnitude values describe the faulting event that generates the earthquake.

#### THE RICHTER SCALE ( $M_L$ )

The original magnitude scale of Richter (1935) was introduced for the purpose of providing an objective measure of the energy of each earthquake in the initial listing of earthquakes in the southern California region compiled by the Seismological Laboratory in Pasadena. Rather than attempting to measure the energy of the earthquake source directly, he chose to construct an empirical scale derived from a simple measure of the complex seismic waveform. Using only the maximum excursion of the seismogram as measured on a single type of instrument, the Wood-Anderson seismograph, he defined the local magnitude of an earthquake as

$$M_L = \log_{10} A - \log_{10} A_0(\Delta),$$

where the empirical function  $A_0$  depends only on the epicentral distance of the station,  $\Delta$ . The zero point was arbitrarily set by Richter to avoid negative magnitudes in the course of routine work. Use of common logarithms means that two earthquakes located at the same distance from a station and having peak amplitudes differing by a factor of 10 will differ by 1 magnitude unit. In practice, readings from all observing stations are averaged after adjustment with station-specific corrections to obtain the  $M_L$  value. Although Richter (1935) predicted that the local-magnitude scale "cannot hold to any high accuracy," history has proved it to be a powerful quantitative tool for ordering the relative sizes of earthquakes.

Several points about  $M_L$  should be emphasized. First, it is strictly defined only for the southern California region, although its applicability to coastal central and northern California has since been shown. Recent studies of the  $A_0$  curve suggest that it will require revision and regionalization. Second, because  $M_L$  has no actual physical units associated with it, other empirical magnitude scales may be freely adjusted to coincide with it. The local-magnitude scale has, in fact, been used as the basis for establishing essentially all other magnitude scales. Finally, because  $M_L$  is derived from measurements taken from a single, band-limited seismograph,  $M_L$  values

saturate once an earthquake becomes large enough. Thus, the "correct" Richter magnitude  $M_L=6.9$  for the great 1906 earthquake obtained by Jennings and Kanamori (1979) reflects the amplitude of seismic waves at periods near 1 s but not the total energy of this earthquake. Uniformly valid characterization of the "size" of an earthquake requires use of magnitude scales based on longer-period measures of the event.

#### SURFACE-WAVE MAGNITUDE ( $M_S$ ) AND BODY-WAVE MAGNITUDE ( $m_b$ )

The successful development of the local-magnitude scale encouraged Gutenberg and Richter to develop magnitude scales based on teleseismic observations of earthquakes. Two scales were developed, one based on surface waves,  $M_S$ , and one on body waves,  $m_b$ .

Surface waves with a period near 20 s generally produce the largest amplitudes on a standard long-period seismograph, and so the amplitude of these waves is used to determine  $M_S$ , using an equation similar to that used for  $M_L$ .

The body-wave magnitude,  $m_b$ , which was developed specifically to treat deep-focus earthquakes, presents yet another alternative scale for magnitude determination. Although it presently is the most commonly reported teleseismic magnitude, current practice in its determination differs from that employed by Gutenberg, and so it is omitted from table 6.1. As a short-period magnitude, modern  $m_b$  values measure the same part of the earthquake energy spectrum as  $M_L$ .

The magnitudes listed by Gutenberg and Richter (1954) that appear in table 6.1 as  $M_{G-R}$  are essentially  $M_S$  according to Geller and Kanamori (1977); magnitudes attributed to Richter (1958) are based on  $M_L$  or  $M_S$ .

Useful estimates of  $M_S$  can be obtained from many different types of long-period seismographs, including the undamped instruments deployed by Milne beginning in 1897. Abe and Noguchi (1983) constructed estimates of  $M_S$  from Milne seismograms to resolve a longstanding controversy concerning an apparent peak in global seismicity between 1904 and 1912. Abe (1988) later used the Milne data to determine magnitudes for smaller earthquakes in California between 1898 and 1912. His procedures have been used to compute  $M_S$  for additional California events occurring between 1898 and 1934, which are listed in table 6.1.

#### SEISMIC INTENSITY AND EARTHQUAKE MAGNITUDE ( $M_I$ )

Before the development of seismographs in the late 19th century, descriptions of the effects of earthquakes provided the only means for assessing earthquake size in all but the rare cases where surface faulting was well



described. A robust method for relating the area undergoing shaking of a given intensity or greater to  $M_L$  was developed by Topozada (1975) for California and western Nevada. Using these relations, Topozada and others (1981, 1982) successfully assigned an intensity magnitude,  $M_I$ , to many earthquakes. The isoseismal maps developed in the course of their research also generally provide our best estimates of epicentral locations. New  $M_I$  values have been determined for several events, using the same procedures as part of this study.

#### SEISMIC MOMENT ( $M_0$ ), RADIATED ENERGY, AND MOMENT MAGNITUDE ( $M$ )

Magnitude scales based on finite-bandwidth seismographs approach a maximum near which events of clearly different size or energy are indistinguishable. Saturation of  $M_L$  is apparent for both the 1906 and 1952 earthquakes listed in table 6.1. Recent work by Hutton and Boore (1987) suggests that the local-magnitude scale may begin to saturate at about  $M_L=6$ . Such saturation, which is understood to arise from the scaling law of the seismic spectrum (Aki, 1967), occurs when the peak of the energy spectrum lies below the frequency range of the Wood-Anderson seismograph.

By using the well-known properties of the seismic spectrum, magnitude scales can be constructed with uniform validity. One such scale,  $M_w$ , proposed by Kanamori (1977) is based on the seismic energy radiated in the form of elastic waves by the source. Another nearly equivalent magnitude scale,  $M$ , the moment magnitude, is based on the seismic moment,  $M_0=\mu Au$  (Aki, 1966), where  $A$  is the area of the earthquake rupture surface,  $u$  is the average fault displacement, and  $\mu$  is the shear modulus of the crustal volume containing the fault. Hanks and Kanamori (1979) took advantage of the nearly identical relations between  $M_0$  and both  $M_L$  and  $M_S$  to define  $M=\frac{2}{3}\log_{10} M_0-10.7$ , where  $M_0$  is measured in dyne-centimeters.

These two magnitude scales, though closely related, are not identical. Singh and Havskov (1980) showed that  $M_w=\frac{2}{3}(\log_{10} M_0+\log_{10} \Delta\sigma/\mu-12.1)$ , where  $\Delta\sigma$  is the stress drop. Earthquake stress drops generally fall in a narrow range over the entire magnitude spectrum, and so with  $\Delta\sigma/\mu\approx 10^{-4}$  (Kanamori, 1977),  $M_w=M$ . One advantage to  $M$  for the purpose at hand is its dependence on only the static fault offset and rupture area, which can be determined for the 1857 and 1872 earthquakes.

#### SUMMARY MAGNITUDE ( $M$ )

To construct a single, summary-magnitude scale,  $M$ , to characterize the relative size of all the events listed in table 6.1, I use each of the scales described above, being

careful to consider such factors as the historical period and event location, as well as the quality of individual determinations. Where choices between several magnitude estimates are possible, the summary magnitude,  $M$ , is weighted toward long-period estimates of magnitude. Specifically,  $M_S$  and  $M_{G-R}$  are selected when judged reliable (110 events). Many local magnitudes have thus been superseded by surface-wave magnitudes; this effect is most noticeable for the largest events, where saturation of  $M_L$  becomes important.  $M_L$  is the principal contributor to 20 summary magnitudes, half of which also have reported  $M$  values that agree well. For all but two events before 1898 (1857 and 1872) and for two 20th-century events,  $M$  is based on  $M_I$ . In effect, the summary magnitude is an intensity magnitude before 1898 and a teleseismic surface-wave magnitude thereafter.

If  $M$  is to be uniformly valid across the entire timespan of the catalog,  $M_I$  must be an unbiased estimator of  $M_S$  or  $M_{G-R}$ . To test this absence of bias, the correlation between  $M_I$  and the two surface-wave magnitudes has been examined for 23 events with reliable  $M_S$  or  $M_{G-R}$  estimates, and an  $M_I$  value determined from the isoseismal maps of Topozada and others (1981) and Topozada and Parke (1982). This comparison shows that although the two magnitude scales are well correlated,  $M_I$  systematically underestimates  $M_S$  and  $M_{G-R}$  by  $0.3\pm 0.3$  units. If the sample is restricted to  $M_S\leq 6.5$  ( $n=18$ ), the bias is  $0.2\pm 0.3$  units. To further investigate this apparent bias,  $M_L$  was compared with  $M_I$  for 10 common events, for which the bias was  $0.25\pm 0.2$  units. As a final check, the difference between  $M_S$  or  $M_{G-R}$  and  $M_I$  for the 12 events listed in table 6.1 also used by Topozada (1975) to develop  $M_I$  relations was found to be  $0.10\pm 0.19$  units.

On the basis of these results, the summary magnitudes from  $M_I$  values of Topozada and others (1981) have been adjusted upward by 0.15 units and then rounded to the nearest quarter magnitude unit. Thus, events of  $M_I=5.7$  become  $M=5\frac{3}{4}$ , and those of  $M_I=5.8$  become  $M=6$ . No magnitude adjustment exceeded a quarter unit.  $M_I$  values from other sources have simply been rounded to the nearest quarter unit, because they average 0.2 units higher than the values of Topozada and others (1981) and Topozada and Parke (1982), where comparisons can be made. Summary magnitudes for events before 1850 have not been adjusted upward, owing to the imprecision of the original estimates.

#### REFERENCES CITED

- Abe, Katsuyuki, 1988, Magnitudes and origin times from Milne seismograph data: Earthquakes in China and California, 1898-1912, in Lee, W.H.K., Meyers, Herbert, and Shimazaki, Kunihiko, eds., Historical seismograms and earthquakes of the



- world: San Diego, Calif., Academic Press, p. 37-50.
- Abe, Katsuyuki, and Noguchi, Shin'ichi, 1983, Revision of magnitudes of large shallow earthquakes, 1897-1912: *Physics of the Earth and Planetary Interiors*, v. 33, no. 1, p. 1-11.
- Agnew, D.C., 1985, Evidence on large Southern California earthquakes from historical records, in Shearer, C.F., *Minutes of the National Earthquake Prediction Evaluation Council, March 29-30, 1985*, Pasadena, California: U.S. Geological Survey Open-File Report 85-507, p. 77-90.
- Agnew, D.C., and Sieh, K.E., 1978, A documentary study of the felt effects of the great California earthquake of 1857: *Seismological Society of America Bulletin*, v. 68, no. 6, p. 1717-1729.
- Aki, Keiti, 1965, Maximum likelihood estimate of  $b$  in the formula  $\log N = a - bM$  and its confidence limits: *University of Tokyo, Earthquake Research Institute Bulletin*, v. 43, pt. 2, p. 237-239.
- 1966, Generation and propagation of  $G$  waves from the Niigata earthquake of June 16, 1964. Part 2. Estimation of earthquake moment, release of energy, and stress-strain drop from  $G$  wave spectrum: *University of Tokyo, Earthquake Research Institute Bulletin*, v. 44, pt. 1, p. 73-88.
- 1967, Scaling law of seismic spectrum: *Journal of Geophysical Research*, v. 72, no. 4, p. 1217-1231.
- Archuleta, R.J., 1984, A faulting model for the 1979 Imperial Valley earthquake: *Journal of Geophysical Research*, v. 89, no. B6, p. 4559-4585.
- Atwater, Tanya, 1970, Implications of plate tectonics for the Cenozoic tectonic evolution of western North America: *Geological Society of America Bulletin*, v. 81, no. 12, p. 3513-3535.
- Bakun, W.H., and McEvilly, T.V., 1984, Recurrence models and Parkfield, California, earthquakes: *Journal of Geophysical Research*, v. 89, no. B5, p. 3051-3058.
- Bakun, W.H., Clark, M.M., Cockerham, R.S., Ellsworth, W.L., Lindh, A.G., Prescott, W.H., Shakal, A.F., and Spudich, Paul, 1984, The 1984 Morgan Hill, California, earthquake: *Science*, v. 225, no. 4659, p. 288-291.
- Bakun, W.H., and Lindh, A.G., 1985, The Parkfield, California, earthquake prediction experiment: *Science*, v. 229, no. 4714, p. 619-624.
- Beanland, Sarah, and Clark, M.M., in press, The Owens Valley fault zone, eastern California, and surface rupture associated with the 1872 earthquake: *U.S. Geological Survey Bulletin*.
- Bolt, B.A., 1968, The focus of the 1906 California earthquake: *Seismological Society of America Bulletin*, v. 58, no. 1, p. 457-471.
- Bolton, H.E., 1927, *Fray Juan Crespi, missionary explorer on the Pacific coast, 1769-1774*: Berkeley, University of California Press, 402 p.
- Boore, D.M., 1977, Strong-motion recordings of the California earthquake of April 18, 1906: *Seismological Society of America Bulletin*, v. 67, no. 3, p. 561-577.
- Borcherdt, R.D., ed., 1975, *Studies for seismic zonation of the San Francisco Bay region*: U.S. Geological Survey Professional Paper 941-A, p. A1-A102.
- Coffman, J.L., von Hake, C.A., and Stover, C.W., eds., 1982, *Earthquake history of the United States*: Boulder, Colo., U.S. Department of Commerce, National Oceanic and Atmospheric Administration Publication 41-1, 208 p.
- DeMets, Charles, Gordon, R.G., Stein, Seth, and Argus, D.F., 1987, A revised estimate of Pacific-North America motion and implications for western North America plate boundary zone tectonics: *Geophysical Research Letters*, v. 14, no. 9, p. 911-914.
- Doser, D.I., 1986, Earthquake processes in the Rainbow Mountain-Fairview Peak-Dixie Valley, Nevada, region 1954-1959: *Journal of Geophysical Research*, v. 91, no. B12, p. 12572-12586.
- Eaton, J.P., O'Neill, M.E., and Murdock, J.N., 1970, Aftershocks of the 1966 Parkfield-Cholame, California, earthquake: A detailed study: *Seismological Society of America Bulletin*, v. 60, no. 4, p. 1151-1197.
- Ellsworth, W.L., Lindh, A.G., Prescott, W.H., and Herd, D.G., 1981, The 1906 San Francisco earthquake and the seismic cycle, in Simpson, D.W., and Richards, P.G., eds., *Earthquake prediction: An international review (Maurice Ewing Series 4)*: Washington, American Geophysical Union, p. 126-140.
- Engdahl, E.R., and Rinehart, W.A., 1988, *Seismicity map of North America*: Boulder, Geological Society of America.
- Evernden, J.F., and Thompson, J.M., 1985, Predicting seismic intensities, in Ziony, J.I., ed., *Evaluating earthquake hazards in the Los Angeles region—an earth-science perspective*: U.S. Geological Survey Professional Paper 1360, p. 151-202.
- Fedotov, S.A., 1968, The seismic cycle, quantitative seismic zoning, and long-term seismic forecasting, in Medvedev, S.V., ed., *Seismic zoning of the USSR: Jerusalem, Israel Program for Scientific Translations*, p. 133-164.
- Gawthrop, W.H., 1978, The 1927 Lompoc, California, earthquake: *Seismological Society of America Bulletin*, v. 68, no. 6, p. 1705-1716.
- 1981, Comments on "The Lompoc, California, earthquake (November 4, 1927,  $M=7.3$ ) and its aftershocks," by Thomas C. Hanks: *Seismological Society of America Bulletin*, v. 71, no. 2, p. 557-560.
- Geller, R.J. and Kanamori, Hiroo, 1977, Magnitudes of great shallow earthquakes from 1904 to 1952: *Seismological Society of America Bulletin*, v. 67, no. 3, p. 587-598.
- Gianella, V.P., 1957, Earthquake and faulting, Fort Sage Mountains, California, December, 1950: *Seismological Society of America Bulletin*, v. 47, no. 3, p. 173-177.
- Gianella, V.P., and Callaghan, Eugene, 1984, The Cedar Mountain, Nevada, earthquake of December 20, 1932: *Seismological Society of America Bulletin*, v. 24, no. 4, p. 345-384.
- Gilbert, G.K., 1884, A theory of the earthquakes of the Great Basin, with a practical application: *American Journal of Science*, ser. 3, v. 27, no. 157, p. 49-53.
- Goter, S.K., compiler, 1988, *Seismicity map of California*: U.S. Geological Survey Open-File Report 88-286, scale 1:1,000,000.
- Gutenberg, Beno, and Richter, C.F., 1954, *Seismicity of the earth and associated phenomena (2d ed.)*: Princeton, N.J., Princeton University Press, 310 p.
- 1956, Earthquake magnitude, intensity, energy and acceleration: *Seismological Society of America Bulletin*, v. 46, no. 2, p. 105-145.
- Hanks, T.C., 1979, The Lompoc, California, earthquake (November 4, 1927,  $M=7.3$ ) and its aftershocks: *Seismological Society of America Bulletin*, v. 69, no. 2, p. 451-462.
- 1981, Reply to W. Gawthrop's comments on "The Lompoc, California, earthquake (November 4, 1927,  $M=7.3$ ) and its aftershocks": *Seismological Society of America Bulletin*, v. 71, no. 2, p. 561-565.
- Hanks, T.C., and Kanamori, Hiroo, 1979, A moment magnitude scale: *Journal of Geophysical Research*, v. 84, no. B5, p. 2348-2350.
- Hanks, T.C., and Allen, C.R., 1989, The Elmore Ranch and Superstition Hills earthquakes of 24 November 1987: Introduction to the special issue: *Seismological Society of America Bulletin*, v. 79, no. 2, p. 231-238.
- Harley, R.B., 1988, Rev. Juan Caballeria: Historian or storyteller? Rethinking the 1810 Dumetz expedition: Redlands, Calif., San Bernardino County Museum Association Quarterly, v. 35, p. 42.
- Harris, R.A., and Segall, Paul, 1987, Detection of a locked zone at depth in the Parkfield, California, segment of the San Andreas fault: *Journal of Geophysical Research*, v. 92, no. B8, p. 7945-7962.
- Hartzell, S.H., and Heaton, T.H., 1983, Inversion of strong ground motion and teleseismic waveform data for the fault rupture history of the 1979 Imperial Valley, California, earthquake: *Seismological*



- Society of America Bulletin, v. 73, no. 6, pt. A, p. 1553-1583.
- 1986, Rupture history of the 1984 Morgan Hill, California earthquake from the inversion of strong motion records: *Seismological Society of America Bulletin*, v. 76, no. 3, p. 649-674.
- Heaton, T.H., 1982, The 1971 San Fernando earthquake: A double event?: *Seismological Society of America Bulletin*, v. 72, no. 6, p. 2037-2062.
- Hill, D.P., Wallace, R.E., and Cockerham, R.S., 1985, Review of evidence on the potential for major earthquakes and volcanism in the Long Valley-Mono Craters-White Mountains regions of eastern California: *Earthquake Prediction Research*, v. 3, no. 3-4, p. 571-594.
- Hutton, K.L., and Boore, D.M., 1987, The  $M_L$  scale in southern California: *Seismological Society of America Bulletin*, v. 77, no. 6, p. 2074-2094.
- Jacoby, G.C., Sheppard, P.R., and Sieh, K.E., 1988, Irregular recurrence of large earthquakes along the San Andreas fault: Evidence from trees: *Science*, v. 241, no. 4862, p. 196-199.
- Jennings, C.W., compiler, 1975, Fault map of California with locations of volcanoes, thermal springs, and thermal wells: California Division of Mines and Geology Geologic Data Map 1, scale 1:750,000.
- Jennings, P.C., and Kanamori, Hiroo, 1979, Determination of local magnitude  $M_L$ , from seismoscope records: *Seismological Society of America Bulletin*, v. 69, no. 4, p. 1267-1288.
- Kanamori, Hiroo, 1977, The energy release in great earthquakes: *Journal of Geophysical Research*, v. 82, no. 20, p. 2981-2987.
- Kovach, R.L., Allen, C.R., and Press, Frank, 1962, Geophysical investigations in the Colorado Delta region: *Journal of Geophysical Research*, v. 67, no. 7, p. 2845-2871.
- Langston, C.A., 1978, The February 9, 1971 San Fernando earthquake: A study of source finiteness in teleseismic body waves: *Seismological Society of America*, v. 68, no. 1, p. 1-29.
- Lawson, A.C., chairman, 1908, The California Earthquake of April 18, 1906: Report of the State Earthquake Investigation Commission: Carnegie Institution of Washington Publication 87, 2 v.
- Lienkaemper, J.J., 1984, Comparison of two surface-wave magnitude scales:  $M$  of Gutenberg and Richter (1954) and  $M_S$  of "Preliminary Determination of Epicenters": *Seismological Society of America Bulletin*, v. 74, no. 6, p. 2357-2378.
- Lienkaemper, J.J., Pezzopane, S.K., Clark, M.M., and Rymer, M.J., 1987, Fault fractures formed in association with the 1986 Chalfant Valley, California, earthquake sequence: Preliminary report: *Seismological Society of America Bulletin*, v. 77, no. 1, p. 297-305.
- Lindh, A.G., 1983, Preliminary assessment of long-term probabilities for large earthquakes along selected fault segments of the San Andreas fault system in California: U.S. Geological Survey Open-File Report 83-63, 14 p.
- Liu, H.-L., and Helmlinger, D.V., 1983, The near-source ground motion of the 6 August 1979 Coyote Lake, California, earthquake: *Seismological Society of America Bulletin*, v. 73, no. 1, p. 201-218.
- Louderback, G.D., 1947, Central California earthquakes of the 1830's: *Seismological Society of America Bulletin*, v. 37, no. 1, p. 33-74.
- McAdie, A.G., 1907, Catalogue of earthquakes on the Pacific coast, 1897-1906: Smithsonian Institution of Washington Miscellaneous Collections, v. 49, art. 5, 64 p.
- McCulloch, D.S., 1985, Evaluating tsunami potential, in Ziony, J.I., ed., *Evaluating earthquake hazards in the Los Angeles region—an earth-science perspective*: U.S. Geological Survey Professional Paper 1360, p. 375-413.
- Mendoza, Carlos, and Hartzell, S.H., 1988, Aftershock patterns and main shock faulting: *Seismological Society of America Bulletin*, v. 78, no. 4, p. 1438-1449.
- Milne, John, 1901, Analyses of large earthquakes recorded in 1899: British Association for the Advancement of Science Meeting, 70th, Dover, 1900, Report, p. 60-104.
- Mogi, Kiyoo, 1981, Seismicity in western Japan and long-term earthquake forecasting: in Simpson, D.W., and Richards, P.G., eds., *Earthquake prediction: An international review (Maurice Ewing Series 4)*: Washington, American Geophysical Union, p. 43-51.
- Mount, V.S., and Suppe, John, 1987, State of stress near the San Andreas fault: Implications for wrench tectonics: *Geology*, v. 15, no. 12, p. 1143-1146.
- Nishenko, S.P., and Buland, Ray, 1987, A generic recurrence interval distribution for earthquake forecasting: *Seismological Society of America Bulletin*, v. 77, no. 4, p. 1382-1399.
- Oakeshott, G.B., ed., 1955, Earthquakes in Kern County, California during 1952: California Division of Mines Bulletin 171, 283 p.
- Plafker, George, and Galloway, J.P. eds., 1989, Lessons learned from the Loma Prieta, California, earthquake of October 17, 1989: U.S. Geological Survey Circular 1045, 48 p.
- Reasenber, P.A., and Ellsworth, W.L., 1982, Aftershocks of the Coyote Lake, California earthquake of August 6, 1979: A detailed study: *Journal of Geophysical Research*, v. 87, no. B13, p. 10637-10655.
- Reid, H.F., 1910, The mechanics of the earthquake, v. 2 of *The California earthquake of April 18, 1906: Report of the State Earthquake Investigation Commission*: Carnegie Institution of Washington Publication 87, 192 p.
- Richter, C.F., 1935, An instrumental earthquake scale: *Seismological Society of America Bulletin*, v. 25, no. 1, p. 1-32.
- 1958, *Elementary seismology*: San Francisco, W.H. Freeman and Co., 768 p.
- 1973, Historical seismicity of San Fernando earthquake area, in Benfer, N.A., Coffman, J.L., and Bernick, J.R., eds., *San Fernando, California, earthquake of February 9, 1971*: Washington, U.S. Department of Commerce, National Oceanic and Atmospheric Administration, Environmental Research Laboratories, v. 3, p. 5-11.
- Rymer, M.J., and Ellsworth, W.L., eds., 1990, *The Coalinga, California, earthquake of May 2, 1983*: U.S. Geological Survey Professional Paper 1487, 417 p.
- Sanders, C.O., and Slemmons, D.B., 1979, Recent crustal movements in the central Sierra Nevada-Walker Lane region of California-Nevada: Part III, The Olinghouse fault zone: *Tectonophysics*, v. 52, no. 1-4, p. 585-597.
- Savage, J.C., and Cockerham, R.S., 1987, Quasi-periodic occurrence of earthquakes in the 1978-1986 Bishop-Mammoth Lakes sequence, eastern California: *Seismological Society of America Bulletin*, v. 77, no. 4, p. 1347-1358.
- Segall, Paul, and Harris, R.A., 1987, Earthquake deformation cycle on the San Andreas fault near Parkfield, California: *Journal of Geophysical Research*, v. 92, no. B10, p. 10511-10525.
- Seismological Society of America Bulletin*, 1916, The earthquake at Volcano Lake, Mexico, November 20, 1915: v. 6, no. 2-3, p. 181-184.
- Sharp, R.V., 1982, Comparison of 1979 surface faulting with earlier displacements in the Imperial Valley, in *The Imperial Valley, California earthquake of October 15, 1979*: U.S. Geological Survey Professional Paper 1254, p. 213-221.
- Shawe, D.R., 1965, Strike-slip control of Basin-Range structure indicated by historical faults in western Nevada: *Geological Society of America Bulletin*, v. 76, no. 12, p. 1361-1378.
- Shor, G.G., Jr., and Roberts, Ellis, 1958, San Miguel, Baja California Norte, earthquakes of February, 1956: A field report: *Seismological Society of America Bulletin*, v. 48, no. 2, p. 101-116.



- Sieh, K.E., 1978a, Central California foreshocks of the great 1857 earthquake: *Seismological Society of America Bulletin*, v. 68, no. 6, p. 1731-1749.
- 1978b, Slip along the San Andreas fault associated with the great 1857 earthquake: *Seismological Society of America Bulletin*, v. 68, no. 5, p. 1421-1448.
- Sieh, K.E., Stuiver, Minze, and Brillinger, David, 1989, A more precise chronology of earthquakes produced by the San Andreas fault in southern California: *Journal of Geophysical Research*, v. 94, no. B1, p. 603-623.
- Singh, S.K., and Havskov, Jens, 1980, On moment-magnitude scale: *Seismological Society of America Bulletin*, v. 70, no. 1, p. 379-383.
- Slemmons, D.B., Steinbrugge, K.V., Tocher, Don, Oakeshott, G.B., and Gianella, V.P., 1959, Wonder, Nevada, earthquake of 1903: *Seismological Society of America Bulletin*, v. 49, no. 3, p. 251-265.
- Smith, S.W., and Knapp, J.S., 1980, The northern termination of the San Andreas fault, *in* Streitz, Robert, and Sherburne, R.W., eds., *Studies of the San Andreas fault zone in northern California*: California Division of Mines and Geology Special Report 140, p. 153-164.
- Stein, R.S., and King, G.C.P., 1984, Seismic potential revealed by surface folding: 1983 Coalinga, California, earthquake: *Science*, v. 224, no. 4651, p. 869-871.
- Strand, C.L., 1980, Pre-1900 earthquakes of Baja California and San Diego County: San Diego, Calif., San Diego State University, 320 p.
- Sykes, L.R., and Nishenko, S.P., 1984, Probabilities of occurrence of large plate rupturing earthquakes for the San Andreas, San Jacinto, and Imperial faults, California, 1983-2003: *Journal of Geophysical Research*, v. 89, no. B7, p. 5905-5927.
- Thatcher, Wayne, 1975, Strain accumulation and release mechanism of the 1906 San Francisco earthquake: *Journal of Geophysical Research*, v. 80, no. 35, p. 4862-4872.
- Thatcher, Wayne, and Lisowski, Michael, 1987, 1906 earthquake slip on the San Andreas fault in offshore northwestern California [abs.]: *Eos (American Geophysical Union Transactions)*, v. 68, no. 44, p. 1507.
- Tocher, Don, 1956, Movement on the Rainbow Mountain fault: *Seismological Society of America Bulletin*, v. 46, no. 1, p. 10-14.
- 1959, Seismic history of the San Francisco region, in *San Francisco earthquakes of March 1957*: California Division of Mines Special Report 57, p. 39-48.
- Topozada, T.R., 1975, Earthquake magnitude as a function of intensity data in California and western Nevada: *Seismological Society of America Bulletin*, v. 65, no. 5, p. 1223-1238.
- Topozada, T.R., and Parke, D.L., 1982, Areas damaged by California earthquakes, 1900-1949: California Division of Mines and Geology Open-File Report 82-17 SAC, 65 p.
- Topozada, T.R., Real, C.R., and Parke, D.L., 1981, Preparation of isoseismal maps and summaries of reported effects for pre-1900 California earthquakes: California Division of Mines and Geology Open-File Report 81-11 SAC, 182 p.
- 1988, Earthquake history of California, *in* Lee, W.H.K., Meyers, Herbert, and Shimazaki, Kunihiko, eds., *Historical seismograms and earthquakes of the world*: San Diego, Calif., Academic Press, p. 267-275.
- Townley, S.D., and Allen, M.W., 1939, Descriptive catalog of earthquakes of the Pacific coast of the United States 1769 to 1928: *Seismological Society of America Bulletin*, v. 29, no. 1, p. 1-297.
- Trifunac, M.D., and Brune, J.N., 1970, Complexity of energy release during the Imperial Valley, California, earthquake of 1940: *Seismological Society of America Bulletin*, v. 60, no. 1, p. 137-160.
- U.S. Geological Survey, 1971, The San Fernando, California, earthquake of February 9, 1971: Professional Paper 733, 254 p.
- 1972, The Borrego Mountain earthquake of April 9, 1968: Professional Paper 787, 207 p.
- 1982, The Imperial Valley, California, earthquake of October 15, 1979: Professional Paper 1254, 451 p.
- Wallace, R.E., 1984, Fault scarps formed during the earthquakes of October 2, 1915, in Pleasant Valley, Nevada, and some tectonic implications: U.S. Geological Survey Professional Paper 1274-A, p. A1-A33.
- Walter, S.R., 1986, Intermediate-focus earthquakes associated with Gorda plate subduction in northern California: *Seismological Society of America Bulletin*, v. 76, no. 2, p. 583-588.
- Wong, I.G., Ely, R.W., and Kollmann, A.C., 1988, Contemporary seismicity and tectonics of the northern and central Coast Ranges-Sierran block boundary zone, California: *Journal of Geophysical Research*, v. 93, no. B7, p. 7813-7833.
- Working Group on California Earthquake Probabilities, 1988, Probabilities of large earthquakes occurring in California on the San Andreas fault: U. S. Geological Survey Open File Report 88-398, 62 p.
- Ziony, J.I., ed., 1985, Evaluating earthquake hazards in the Los Angeles region—an earth-science perspective: U.S. Geological Survey Professional Paper 1360, 505 p.
- Zoback, M.D., Zoback, M.L., Mount, V.S., Suppe, John, Eaton, J.P., Healy, J.H., Oppenheimer, D.H., Reasenberg, P.A., Jones, L.M., Raleigh, C.B., Wong, I.G., Scotti, Oona, and Wentworth, C.M., 1987, New evidence on the state of stress of the San Andreas fault system: *Science*, v. 238, no. 4830, p. 1105-1111.
- Zoback, M.L., and Zoback, M.D., 1980, Faulting patterns in north-central Nevada and strength of the crust: *Journal of Geophysical Research*, v. 85, no. B1, p. 275-284.





---

---

## TABLE 6.1

Earthquake origin times, magnitudes, and locations before 1990 principally derived from interpretations of felt reports by Topozada and others (1981); after 1900, data principally derived from Gutenberg and Richter (1954) and bulletins of the California Institute of Technology, University of California, Berkeley, University of Nevada, Reno, and U.S. Geological Survey. See text for discussion of summary magnitude  $M$ . Other magnitude scales are  $M_L$ , local-magnitude scale of Richter (1935);  $M_{G-R}$ , magnitudes from Gutenberg and Richter (1954), generally based on 20-s surface waves;  $M_S$ , 20-s surface-wave magnitude;  $M_I$ , magnitude estimated from felt area at various intensity levels; and  $M$ , moment magnitude, defined as  $M = \frac{2}{3} \log_{10} M_0 - 10.7$ , where  $M_0$  is in dyne-centimeters—parentetical values based on seismogram envelope.  $M_S$  values before 1935 generally derived from undamped Milne seismographs, using the formula of Abe (1988)—parentetical values based on one or two amplitudes;  $M_S$  values since 1968 measured from vertical seismographs. Absence of reported amplitudes on Milne seismographs (\*) suggests  $M_S < 6$ .

---

---



TABLE 6.1.—Major California and Nevada earthquakes, 1769–1989

Date and origin time (GMT)	M	Lat N. and Long W.	Locality	$M_L$	$M_{G-R}$	$M_S$	$M_I$	M
1769/07/28	6?	34° 118°	Los Angeles Basin-----	—	—	—	6	—
1800/11/22 21:30	6½?	33° 117°18'	San Diego region-----	—	—	—	≥6½	—
1808/06/21	6?	37°48' 122°30'	San Francisco region-----	—	—	—	6	—
1812/12/08 15:00	7	34°22' 117°39'	Wrightwood-----	—	—	—	6.9	—
1812/12/21 19:00	7	34°12' 119°54'	Santa Barbara Channel-----	—	—	—	7.1	—
1827/09/24 04:00	5½?	34° 119°	Los Angeles region-----	—	—	—	5½ to 6	—
1836/06/10 15:30	6¼	37°48' 122°12'	Hayward fault-----	—	—	—	6.8	—
1838/06/7 p.m.	7	37°36' 122°24'	San Francisco Peninsula-----	—	—	—	≥7.0	—
1852/11/29 20:00	6½	32°30' 115°	Volcano Lake, B.C.-----	—	—	—	6 to 7	—
1855/07/11 04:15	6?	34° 6' 118° 6'	Los Angeles region-----	—	—	—	6	—
1856/02/15 13:25	5¾	37°30' 122°18'	San Francisco Peninsula-----	—	—	—	5.5	—
1857/01/09 16:00	8¼	35°42' 120°18'	Great Fort Tejon earthquake-----	—	—	—	7.6	7.8
1857/09/03 03:05	6¼	39°18' 120°	Western Nevada or eastern Sierra Nevada-----	—	—	—	6.0	—
1858/11/26 08:35	6¼	37°30' 121°54'	San Jose region-----	—	—	—	6.1	—
1858/12/16 10:00	6	34° 117°30'	San Bernardino region-----	—	—	—	6	—
1860/03/15 19:00	6½	39°30' 119°30'	Carson City, Nev. region-----	—	—	—	6.3	—
1861/07/04 00:11	5¼	37°48' 122° 0'	San Ramon Valley-----	—	—	—	5.6	—
1862/05/27 20:00	6	32°42' 117°12'	San Diego region-----	—	—	—	5.9	—
1864/02/26 13:47	6	37° 6' 121°42'	Southern Santa Cruz Mountains-----	—	—	—	5.9	—
1864/03/05 16:49	5¾	37°42' 122°	East of San Francisco Bay-----	—	—	—	5.7	—
1865/10/08 20:46	6½	37° 0' 122° 0'	Southern Santa Cruz Mountains-----	—	—	—	6.3	—
1866/07/15 06:30	6	37°30' 121°18'	Western San Joaquin Valley-----	—	—	—	5.8	—
1868/05/30 05:10	6	39°18' 119°42'	Virginia City, Nev.-----	—	—	—	5.8, 6	—
1868/10/21 15:53	7	37°42' 122° 6'	Hayward fault-----	—	—	—	6.8	—
1869/12/27 01:55	6¼	39°24' 119°42'	Olinghouse fault, Nev. (?)-----	—	—	—	6.1	—
1869/12/27 10:00	6	39° 6' 119°48'	Carson City, Nev. region-----	—	—	—	5.9	—
1870/02/17 20:12	6	37°12' 122° 6'	Los Gatos-----	—	—	—	5.8	—
1871/03/02 21:05	6	40°24' 124°12'	Cape Mendocino-----	—	—	—	5.9	—
1872/03/26 10:30	7.6	36°42' 118° 6'	Owens Valley-----	—	—	—	7.3	7.6
1872/03/26 14:06	6¾	36°54' 118°12'	Owens Valley-----	—	—	—	6.5	—
1872/04/03 12:15	6¼	37° 118°12'	Owens Valley-----	—	—	—	6.1	—
1872/04/11 19:00	6¼	37°30' 118°30'	Owens Valley-----	—	—	—	6.6	—
1872/05/03 01:00	5¾	33° 115°	Imperial Valley (?)-----	—	—	—	≥5.5	—
1872/11/12 00:00	6	39°? 117°?	Austin, Nev. region (?)-----	—	—	—	6	—
1873/11/23 05:00	6¼	42° 124°	Crescent City-----	—	—	—	6.7	—
1875/01/24 12:00	6	40°12' 120°30'	Honey Lake-----	—	—	—	5.8	—
1875/11/15 22:30	6¼	32°30' 115°30'	Imperial Valley to Colorado River delta (?)-----	—	—	—	6.2	—
1878/05/09 04:25	6	40° 6' 124°	Punta Gorda region-----	—	—	—	5.8	—
1881/02/02 00:11	5¾	36° 0' 120°30'	Parkfield-----	—	—	—	5.6	—
1881/04/10 10:00	6	37°24' 121°24'	Western San Joaquin Valley-----	—	—	—	5.9	—
1882/03/06 21:45	5¾	36°54' 121°12'	Hollister-----	—	—	—	5.7	—
1883/09/05 12:30	6¼	34°12' 119°54'	Santa Barbara Channel-----	—	—	—	6.0	—
1884/01/28 07:30	5¾	41°6' 123°36'	Klamath Mountains-----	—	—	—	5.7	—
1884/03/26 00:40	6	37°6' 122°12'	Santa Cruz Mountains-----	—	—	—	5.9	—
1885/01/31 05:45	5¾	40°24' 120°36'	Susanville-----	—	—	—	5.7	—
1885/04/12 04:05	6¼	36°24' 121°	Southern Diablo Range-----	—	—	—	6.2	—
1887/06/03 10:48	6¼	39°12' 119°48'	Carson City, Nev. region-----	—	—	—	6.3	—
1888/04/29 04:48	6	39°42' 120°42'	Mohawk Valley-----	—	—	—	5.9	—
1889/05/19 11:10	6¼	38° 0' 121°54'	Antioch-----	—	—	—	6.0	—
1889/06/20 06:00	6	40°30' 120°42'	Susanville-----	—	—	—	5.9	—
1889/09/30 05:20	5¾	37°12' 118°42'	Bishop region-----	—	—	—	5.6	—
1890/02/09 12:06	6¼	33°24' 116°18'	San Jacinto or Elsinore fault region (?)-----	—	—	—	6.3	—
1890/04/24 11:36	6¼	36°54' 121°36'	Pajaro Gap-----	—	—	—	6.0	—
1890/07/26 09:40	6¼	40°30' 124°12'	Cape Mendocino-----	—	—	—	6.0	—
1891/07/30 14:10	6	32° 115°	Colorado River delta region-----	—	—	—	6.0	—

TABLE 6.1.—Major California and Nevada earthquakes, 1979-1989—Continued

Date and origin time (GMT)	M	Lat N. and Long W.	Locality	$M_L$	$M_{G-R}$	$M_S$	$M_I$	M
1892/02/24 07:20	7	32°33' 115°38'	Laguna Salada, B.C.	—	—	—	6.7, 7.2	—
1892/04/19 10:50	6½	38°24' 122° 0'	Vacaville	—	—	—	6.4	—
1892/04/21 17:43	6¼	38°30' 121°54'	Winters	—	—	—	6.2	—
1892/05/28 11:15	6½	33°12' 116°12'	San Jacinto or Elsinore fault region (?)	—	—	—	6.3	—
1892/11/13 12:45	5¾	36°48' 121°30'	Hollister	—	—	—	5.6	—
1893/05/19 00:35	5¾	34° 6' 119°24'	Pico Canyon	—	—	—	5.5, 5.9	—
1894/07/30 05:12	6	34°18' 117°36'	Lytle Creek region	—	—	—	5.9, 6.0	—
1894/09/30 17:36	6	40°18' 123°42'	Cape Mendocino region	—	—	—	5.8	—
1894/10/23 23:03	5¾	32°48' 116°48'	East of San Diego	—	—	—	5.7	—
1896/08/17 11:30	6	36°42' 118°18'	Southeastern Sierra Nevada	—	—	—	5.9	—
1897/06/20 20:14	6¼	37° 0' 121°30'	Gilroy	—	—	—	6.2	—
1898/03/31 07:43	6½	38°12' 122°24'	Mare Island	—	—	(6.5)	6.2	—
1898/04/15 07:07	6½	39°12' 123°48'	Mendocino	—	—	(6.7)	6.4	—
1899/04/16 13:40	7	41°? 126°?	West of Eureka	—	—	7.0	5.7	—
1899/07/06 20:10	5¾	37°12' 121°30'	Morgan Hill	—	—	(4.7)	5.8	—
1899/07/22 20:32	5¾	34°18' 117°30'	Lytle Creek region	—	—	(5.6)	6.5, 6.4	—
1899/12/25 12:25	6.4	33°48' 117° 0'	San Jacinto and Hemet	—	—	6.4	6.6, 6.7	—
1901/03/03 07:45	6.4	36° 0' 120°30'	Parkfield	—	—	6.4	5.8	—
1903/01/24 05:27	6.6	31°30' 115°	Colorado River delta region	—	7+	6.6	—	—
1903/06/11 13:12	5½	37°24' 121°54'	San Jose	—	—	(5.4)	5.8	—
1903/08/03 06:49	5½	37°18' 121°48'	San Jose	—	—	(5.3)	5.8	—
1906/04/18 13:12	8¼	37°42' 122°30'	Great 1906 earthquake	6.9	8¼, 8.3	7.8, 8.3	7.8	7.7
1906/04/19 00:30	6.2	32°54' 115°30'	Imperial Valley	—	6+	6.2	5.8	—
1906/04/23 09:10	6.4	41° 124°	Arcata	—	—	6.4	—	—
1907/09/20 01:54	5.3	34°12'? 117° 6'?	San Bernardino region	—	6	*	5.3	—
1908/11/04 08:37	6?	36°? 117°?	Death Valley region	—	6½	*	—	—
1909/10/29 06:45	5.8	40°30' 124°12'	Cape Mendocino	—	6+	5.8, (5.1)	6.4	—
1910/03/11 06:52	5.8	36°54' 121°48'	Watsonville	—	—	5.8	5.5	—
1910/03/19 00:11	6.0	40°? 125°?	West of Cape Mendocino	—	—	6.0	6.2	—
1910/05/15 15:47	5½	33°42' 117°24'	Glen Ivy Hot Springs	—	—	(5.5)	6.0, 5.3	—
1910/08/05 01:31	6.6	42° 127°	West of Crescent City	—	6.8	6.6	—	—
1911/07/01 22:00	6.5	37°15' 121°45'	Calaveras fault	—	6.6	6.5	6.2	—
1914/02/18 18:17	5½?	39°30' 119°48'	Truckee region	—	—	*	6	—
1914/04/24 08:34	6	39°30' 119°48'	Truckee region	—	—	(5.5), (5.6)	6.4	—
1915/05/06 12:09	6.2	40° 126°	West of Cape Mendocino	—	6¼	6.2, (6.0)	—	—
1915/06/23 03:59	6.0	32°48' 115°30'	Imperial Valley	—	6¼	6.0, (5.6)	5.6, 5.5	—
1915/06/23 04:56	5.9	32°48' 115°30'	Imperial Valley	—	6¼	5.9	5.6, 5.5	—
1915/10/03 06:52	7.3	40°30' 117°30'	Pleasant Valley, Nev.	—	7¾	7.6, 7.4, 7.3	—	7.2
1915/11/21 00:13	7.1	32° 115°	Volcano Lake, B.C.	—	7.1	7.1, 6.8	—	—
1915/12/31 12:20	6.5	41° 126°	West of Eureka	—	6½	6.5, (6.4)	—	—
1916/02/03 05:03	5.9	41° 117°48'	North of Pleasant Valley, Nev.	—	—	(5.1)	5.9	—
1916/10/23 02:44	5.3	34°54' 118°54'	Tejon Pass region	—	5½±	6	5.2, 5.3	(5.3)
1916/11/10 09:11	6.1	35°30' 116° 0'	South of Death Valley	—	6.1	(5.7, 5.9)	—	—
1918/04/21 22:32	6.9	33°48' 117° 0'	San Jacinto	—	6.8	7.2, 6.9	6.6	(6.8)
1918/07/15 00:23	6.5	41° 125°	West of Eureka	—	6½	6.5	5.9	—
1922/01/26 09:31	6.0	41° 126°	West of Eureka	—	6	(6.1)	—	—
1922/01/31 13:17	7.3	41° 125°30'	West of Eureka	—	7.3	7.4	—	—
1922/03/10 11:21	6.3	36° 0' 120°30'	Parkfield	—	6½	6.3	6.3	6.1
1923/01/22 09:04	7.2	40°30' 124°30'	Cape Mendocino	—	7.2	7.3	6.5, 6.8	—
1923/07/23 07:30	6.0	34° 0' 117°18'	San Bernardino region	—	6¼	—	6.0	6.0
1925/06/04 12:02	6	41°30' 125°	West of Eureka	—	6	(5.8)	—	—
1925/06/29 14:42	6.3	34°18' 119°48'	Santa Barbara	—	6¼	—	6.3	(6.9)
1926/10/22 12:35	6.1	36°37' 122°21'	Monterey Bay	—	6.1	—	6.1	—
1926/10/22 13:35	6.1	36°33' 122°11'	Monterey Bay	—	6.1	—	—	—
1926/12/10 08:38	6.0	40°45' 126°	West of Cape Mendocino	—	6.0	(6.2)	—	—



TABLE 6.1.—Major California and Nevada earthquakes, 1979–1989—Continued

Date and origin time (GMT)	<i>M</i>	Lat N. and Long W.	Locality	<i>M<sub>L</sub></i>	<i>M<sub>G-R</sub></i>	<i>M<sub>S</sub></i>	<i>M<sub>I</sub></i>	<i>M</i>
1927/09/18 02:07	6	37°30' 118°45'	Bishop region-----	—	6	—	5.5	—
1927/11/04 13:50	7.3	34°42' 120°48'	Southwest of Lompoc-----	—	7.3, 7.5	(7.2)	6.2	(7.3)
1932/06/06 08:44	6.4	40°45' 124°30'	Eureka-----	—	6.4	(6.4)	5.9	—
1932/12/21 06:10	7.2	38°45' 118°	Cedar Mountain, Nev.-----	—	7.2	(7.4)	—	—
1933/01/05 06:51	5.9	38°46' 117°44'	Cedar Mountain, Nev.-----	5.7	5.9	—	—	—
1933/03/11 01:54	6.3	33°37' 117°58'	Long Beach-----	6.3	6¼	(6.5)	6.2	6.2
1933/06/25 20:45	6.1	39° 4' 119°20'	Yerington, Nev.-----	—	6.1	—	—	—
1934/01/30 20:16	6.3	38°18' 118°24'	Excelsior Mountain, Nev.-----	—	6.3, 6.3	(6.4)	—	—
1934/06/08 04:47	6.0	36° 0' 120°30'	Parkfield-----	5.2, 6.0, 6.1	6.0	—	5.6	6.1
1934/07/06 22:48	6.5	41°15' 125°45'	West of Eureka-----	—	6.5	—	—	—
1934/12/30 13:52	6.5	32°15' 115°30'	Laguna Salada, B.C.-----	6.5	6.5	—	—	(6.4)
1934/12/31 18:45	7.0	32° 114°45'	Colorado River delta-----	7.1	7.0	—	—	(7.1)
1935/02/24 01:45	5.3	31°59' 115°12'	Colorado River delta-----	6.0	5¼	—	—	(≤5.3)
1936/06/03 09:15	5.9	40° 125°30'	West of Cape Mendocino-----	—	5.9	—	—	—
1937/03/25 16:49	6.0	33°28' 116°25'	Buck Ridge-----	6.0, 5.9	6.0	—	5.9	—
1940/02/08 08:05	6	39°45' 121°15'	Chico-----	5.7	6	—	—	—
1940/05/19 04:36	7.1	32°44' 115°30'	Imperial Valley-----	6.2	6.7, 7.1	7.2	6.4, 6.6	6.9, 7.1
1940/12/07 22:16	5½	31°40' 115° 5'	Colorado River delta-----	6.0	5¼	—	—	(≤5.3)
1941/02/09 09:44	6.6	40°42' 125°24'	West of Cape Mendocino-----	6.4	6.6	—	—	—
1941/04/09 17:08	5.3	31° 114°	Gulf of California-----	6.0	5¼	—	—	—
1941/05/13 16:01	6.0	40°18' 126°24'	West of Cape Mendocino-----	6.0	6	—	—	—
1941/07/01 07:50	5.9	34°22' 119°35'	Carpenteria-----	5.9	5.9	—	5.5, 6.0	(6.0)
1941/09/14 16:43	5.8	37°34' 118°44'	Tom's Place-----	5.8, 6.0	5.8	—	5.6	—
1941/09/14 18:39	6.0	37°34' 118°44'	Tom's Place-----	6.0	6.0	—	5.6	(5.5)
1941/10/03 16:13	6.4	40°24' 124°48'	West of Cape Mendocino-----	6.4	6.4	—	—	—
1942/10/21 16:22	6.5	33° 3' 116° 5'	Fish Creek Mountains-----	6.5	6½	—	6.0, 6.3	6.6
1942/12/03 09:44	5.9	39°42' 119°18'	North of Wadsworth, Nev.-----	5.5	5.9	—	—	—
1945/05/19 15:07	6.2	40°24' 126°54'	West of Cape Mendocino-----	6.0	6.2	—	—	—
1945/09/28 22:24	6.0	41°54' 126°42'	West of Crescent City-----	6.0	6.0	—	—	—
1946/03/15 13:49	6.3	35°44' 118° 3'	Walker Pass-----	6.3	6¼	—	6.1	6.0
1947/04/10 15:58	6.4	34°59' 116°33'	Manix-----	6.2	6.4	—	6.3, 6.4	6.6
1948/12/04 23:43	6.5	33°56' 116°23'	Desert Hot Springs-----	6.5	6.5±	—	6.2, 6.5	6.0
1948/12/29 12:53	6.0	39°33' 120° 5'	Verdi, Nev.-----	6.0	6.0	—	5.7	—
1949/03/24 20:56	6.2	41°18' 126°	West of Eureka-----	5.9	6.2	—	—	—
1949/05/02 11:25	5.9	34° 1' 115°41'	Pinto Mountain-----	5.9	5.9	—	—	—
1951/10/08 04:10	6	40°15' 124°30'	West of Cape Mendocino-----	5.8	6	—	—	—
1951/12/26 00:46	5.9	32°48' 118°18'	San Clemente Island-----	5.9	5.9	—	—	—
1952/07/21 11:52	7.7	35° 0' 119° 1'	Kern County earthquake-----	7.2	7.7	7.8	7.0	7.5, 7.3
1952/07/21 12:05	6.4	35° 0' 119° 0'	Kern County-----	6.4	—	—	—	—
1952/07/23 00:38	6.1	35°22' 118°35'	Kern County-----	6.1	—	—	—	5.7
1952/07/29 07:03	6.1	35°23' 118°51'	Bakersfield-----	6.1	—	—	—	6.3
1952/11/22 07:46	6.0	35°44' 121°12'	Bryson-----	6.0	6±	—	—	—
1954/01/12 23:33	5.9	35° 0' 119° 1'	West of Wheeler Ridge-----	5.9	—	—	—	5.7
1954/03/19 09:54	6.2	33°17' 116°11'	Arroyo Salada-----	6.2, 6.2	—	—	6.2	6.4
1954/07/06 11:13	6.6	39°25' 118°32'	Rainbow Mountain, Nev.-----	6.8	6.6	6.3	—	6.2
1954/07/06 22:07	6.4	39°18' 118°30'	Rainbow Mountain, Nev.-----	6.0	6.4	—	—	6.1
1954/08/24 05:51	6.8	39°35' 118°27'	Stillwater, Nev.-----	6.8	6.8	6.9	—	6.6
1954/08/31 22:20	6.3	39°30' 118°30'	Stillwater, Nev.-----	5.8	6.3	—	—	5.8
1954/10/24 09:44	6.0	31°30' 116°	East of Santo Tomas, B.C.-----	6.0	—	—	—	6.0
1954/11/12 12:26	6.3	31°30' 116°	East of Santo Tomas, B.C.-----	6.3	—	—	—	6.3
1954/11/25 11:16	6.5	40°16' 125°38'	West of Cape Mendocino-----	6.1	6.5	7.2	—	—
1954/12/16 11:07	7.1	39°19' 118°12'	Fairview Peak, Nev.-----	7.2	7.1	—	—	7.2
1954/12/16 11:11	6.8	39°30' 118° 0'	Dixie Valley, Nev.-----	7.1	6.8	—	—	7.0
1954/12/21 19:56	6.6	40°56' 123°47'	East of Arcata-----	6.5	6.6	—	—	—
1956/02/09 14:32	6.8	31°45' 115°55'	San Miguel, B.C.-----	6.8	—	—	6.3	6.5

TABLE 6.1.—Major California and Nevada earthquakes, 1979–1989—Continued

Date and origin time (GMT)	<i>M</i>	Lat N. and Long W.	Locality	<i>M<sub>L</sub></i>	<i>M<sub>G-R</sub></i>	<i>M<sub>S</sub></i>	<i>M<sub>I</sub></i>	<i>M</i>
1956/02/09 15:24	6.1	31°45′ 115°55′	San Miguel, B.C.-----	6.1	—	—	—	6.0
1956/02/14 18:33	6.3	31°30′ 115°30′	San Miguel, B.C.-----	6.3	—	—	—	6.2
1956/02/15 01:20	6.4	31°30′ 115°30′	San Miguel, B.C.-----	6.4	—	—	—	6.2
1956/10/11 16:48	6.0	40°40′ 125°46′	West of Cape Mendocino-----	6.0	—	—	—	—
1956/12/13 13:15	6.0	31° 115°	Western shore, Gulf of California-----	6.0	—	—	—	—
1959/03/23 07:10	6.3	39°36′ 118° 1′	Dixie Valley, Nev.-----	6.3	—	—	—	—
1959/06/23 14:35	6.1	39° 5′ 118°49′	Schurz, Nev.-----	6.1	—	—	—	—
1960/08/09 07:39	6.2	40°19′ 127° 4′	West of Cape Mendocino-----	6.2	—	—	—	—
1966/06/28 04:26	6.0	36° 0′ 120°30′	Parkfield-----	5.5, 5.6, 5.7	—	6.0	5.7	6.1
1966/08/07 17:36	6.3	31°48′ 114°30′	Gulf of California-----	6.3	—	—	—	6.3
1966/09/12 16:41	6.0	39°25′ 120° 9′	Truckee-----	6.0	—	—	—	5.9
1968/04/09 02:28	6.5	33°11′ 116° 8′	Borrego Mountain-----	6.4, 6.3, 6.8	—	6.8	6.3	6.5
1968/06/26 01:42	5.4	40°14′ 124°16′	Punta Gorda-----	5.9	—	5.4	—	—
1971/02/09 14:00	6.5	34°25′ 118°24′	San Fernando-----	6.4, 5.8	—	6.5, 6.5	6.5	6.7
1973/02/21 14:45	5.2	34° 4′ 119° 2′	Point Mugu-----	5.9, 5.6	—	5.2	—	5.3
1979/08/06 17:05	5.7	37° 7′ 121°31′	Coyote Lake-----	5.8	—	5.7	5.6	5.7
1979/10/15 23:16	6.5	32°36′ 115°18′	Imperial Valley-----	6.6, 6.5, 6.4	—	6.9, 6.7	6.0	6.4 to 6.6
1980/01/24 19:00	5.8	37°50′ 121°47′	Livermore-----	5.8	—	5.9	—	5.8
1980/05/25 16:33	6.1	37°36′ 118°50′	Mammoth Lakes-----	6.1, 6.4, 6.2	—	6.1	—	6.2
1980/05/25 16:49	5.9	37°39′ 118°54′	Mammoth Lakes-----	6.0, 5.9	—	—	—	—
1980/05/25 19:44	5.8	37°33′ 118°49′	Mammoth Lakes-----	6.1, 6.6, 6.4	—	5.8	—	5.9
1980/05/27 14:50	6.0	37°29′ 118°48′	Mammoth Lakes-----	6.2, 6.4, 5.8	—	6.0	—	5.9
1980/06/09 03:28	6.4	32°12′ 115° 5′	Victoria, B.C.-----	6.1, 6.1	—	6.4	—	6.4
1980/11/08 10:27	7.2	41° 7′ 124°40′	West of Eureka-----	6.9	—	7.2	—	7.4
1981/04/26 12:09	6.0	33° 8′ 115°39′	Westmorland-----	5.6	—	6.0	—	5.9
1981/09/04 15:50	5.9	33°40′ 119° 7′	North of Santa Barbara Island-----	5.3	—	5.9	—	5.9
1981/09/30 11:53	5.8	37°35′ 118°52′	Mammoth Lakes-----	5.9, 6.0, 5.9	—	5.8	—	5.7
1983/05/02 23:42	6.5	36°14′ 120°19′	Coalinga-----	6.7, 6.1, 6.1	—	6.5	—	6.4, 6.5
1983/07/22 02:39	5.7	36°14′ 120°25′	Coalinga-----	6.0, 5.6	—	5.7	—	5.7, 6.0
1984/04/24 21:15	6.1	37°19′ 121°39′	Morgan Hill-----	6.2	—	6.1	—	6.2, 6.5
1984/09/10 03:14	6.7	40°23′ 127° 9′	Mendocino Fracture Zone-----	6.6	—	6.7	—	6.7
1984/11/23 18:08	5.7	37°27′ 118°36′	Round Valley-----	6.1, 6.2	—	5.7	—	5.8
1985/08/04 12:01	5.9	36° 8′ 120°10′	North Kettleman Hills-----	5.6	—	5.9	—	6.1, 6.1
1986/07/08 09:20	6.0	34° 0′ 116°36′	North Palm Springs-----	5.9	—	6.0	—	6.2
1986/07/20 14:29	5.6	37°34′ 118°26′	Chalfant Valley-----	5.9, 5.9	—	5.6	—	5.8
1986/07/21 14:42	6.2	37°32′ 118°26′	Chalfant Valley-----	6.5, 6.0	—	6.2	—	6.3, 6.4
1986/07/31 07:22	5.2	37°28′ 118°22′	Chalfant Valley-----	5.8, 5.9	—	5.2	—	5.5
1987/10/01 14:42	5.8	34° 3′ 118° 5′	Whittier Narrows-----	5.9	—	5.8	—	6.1
1987/11/24 01:53	6.2	33° 4′ 115°47′	Elmore Ranch fault-----	5.8	—	6.2	—	5.9
1987/11/24 13:16	6.6	33° 1′ 115°51′	Superstition Hills-----	6.0	—	6.6	—	6.5
1989/10/18 00:04	7.1	37° 2′ 121°53′	Loma Prieta-----	7.0	—	7.1	—	7.0







earthquakes have been documented, some on the same fault strand, and the entire zone of plate-boundary deformation is exceptionally broad. Major changes in fault strike also play a role in redistributing plate-boundary deformation and diffusing it over a wider zone. Compressional bends introduce uplift, crustal thickening, and subsidiary reverse faulting, such as in the Transverse Ranges of southern California. Extensional bends are characterized by subsidence, basin filling, and, possibly, volcanism, as occurs in the Imperial Valley. Extensional and compressional features are more localized at the smaller-scale discontinuities and changes in fault strike that occur throughout the San Andreas system.

Crustal movements observed at the surface reflect deformation processes occurring at depth in the lithosphere. Both laboratory rock-mechanics experiments and studies of exhumed fault zones define the nature of these processes, which, in turn, constrain the classes of large-scale faulting models consistent with surface measurements. In the cool and brittle seismically active parts of the crust, elastic processes are dominant, the frictional strength of active faults increases linearly with depth, and faulting is controlled by Coulomb failure. The transition from brittle seismic behavior to ductile aseismic deformation occurs in the midcrust. Although it is generally agreed that this transition occurs as a result of increasing temperature, its precise mechanism is uncertain. If deformation in the midcrust is concentrated within a narrow vertical shear zone lying beneath the seismically active fault plane, then the brittle/ductile transition may reflect either the increasing importance of ductile or cataclastic flow at depth (Sibson, 1982) or a thermally controlled transition from unstable to stable frictional sliding (Brace and Byerlee, 1966; Tse and Rice, 1986). However, if ductile deformation is broadly distributed in the midcrust, then the cyclic buildup and relief of stresses in the brittle seismogenic crust is controlled by the stress transfer between the elastic lithosphere and ductile "asthenosphere" and the flow properties of the latter.

Both the steady, aseismic movements within the San Andreas plate-boundary zone and the coseismic strain release in large earthquakes are well within the range of detectability of repeated geodetic-survey measurements. The purpose of this chapter is to summarize the salient features of these observations, demonstrating the constraints they place on the amount of present-day plate motion occurring across the San Andreas plate-boundary zone and showing how measurements shed light on the mechanics of the cycle of strain accumulation and release. The emphasis is necessarily on movements close to the main strands of the San Andreas fault system, where observations are most numerous, although some networks extend as far as 100 km from the major faults. The

measurements include triangulation, repeated observations of the angular separation of permanent survey markers, for which useful data date back to about 1850, when gold was first discovered in California; trilateration, repeated line-length measurements made by laser ranging since about 1970; and local measurements of aseismic fault slip made periodically or recorded continuously over apertures of about 10 to 100 m since about 1960.

## OBSERVATIONS OF CRUSTAL DEFORMATION

The focus here is on the spatial and temporal patterns of interearthquake horizontal crustal movements in California that owe their origins to relative motion between the Pacific and North American plates, movements that supply the strain energy which is stored in crustal rocks and ultimately released in large shallow-focus earthquakes. Observations of purely coseismic crustal deformation are not explicitly considered in this chapter; such movements are now well-understood consequences of slip on approximately the upper 10 to 15 km of vertical strike-slip faults. These models and their predicted deformation patterns are discussed within the context of the entire earthquake deformation cycle in the next section. Readers interested in the coseismic movements observed for specific San Andreas earthquakes are referred to the reports by Lawson (1908) and Thatcher (1975) (1906 San Francisco earthquake), Zhang and others (1988) (1940 El Centro earthquake), and Segall and Harris (1987) (1966 Parkfield earthquake).

Vertical crustal movements can locally be substantial, at least when averaged over recent geologic time (see Yeats, 1977; Lajoie, 1986). Deformation from reverse-faulting earthquakes has also been well documented in several events (for example, 1952 Kern County earthquake by Stein and Thatcher, 1981; 1971 San Fernando earthquake by Castle and others, 1975; 1983 Coalinga earthquake by Stein, 1983). Nonetheless, vertical movements are second-order features along most of the San Andreas fault system, and so they are not considered further in this chapter.

Furthermore, in this chapter there is no review of measurement techniques, methods of analyzing and reducing data, or the mathematical and computational tools used in modeling deformation processes. Interested readers are referred to the reports by Bomford (1980) and Savage and Prescott (1973) for descriptions of horizontal-deformation-surveying methods and their precision, to those by Prescott (1976, 1981), Thatcher (1979), and Segall and Harris (1987) for discussions of data-analysis methods, and to the references cited below in the section entitled "Mechanics of Deformation" for details of the mathematical techniques used in model formulation.



*Contemporary crustal movements in California are concentrated within a plate-boundary deformation zone that is typically 50 to 200 km wide, centered approximately on the San Andreas fault. Observations of coseismic, postseismic, and interseismic movements define the earthquake deformation cycle and constrain models of strain accumulation and release for strike-slip plate boundaries.*

## 7. PRESENT-DAY CRUSTAL MOVEMENTS AND THE MECHANICS OF CYCLIC DEFORMATION

By WAYNE THATCHER

### CONTENTS

	Page
Introduction-----	189
Observations of crustal deformation-----	190
Shear strain on the San Andreas fault system-----	191
Aseismic slip, integrated displacement rates, and Pacific-North American plate motion-----	191
Detailed displacement-rate patterns-----	193
Mechanics of deformation-----	195
Thick- and thin-lithosphere models-----	195
Stress-slip-constitutive-law fault models-----	201
Summary-----	202
Future directions for research-----	203
References cited-----	203

### INTRODUCTION

Crustal movements measured in California today sample deformation processes that have continued through at least the past 5 Ma of Pliocene, Pleistocene, and Holocene time. During this interval, several hundred kilometers of right-lateral offset has accumulated across the San Andreas fault system, and many thousands of great earthquakes similar to the historical events of 1857 and 1906 have undoubtedly occurred. The observed deformation results from relative right-lateral translation of the Pacific and North American plates far from the main

plate-boundary faults, which are either freely slipping and without major seismic activity, or are in locked frictional contact and slip episodically in repeated great earthquakes. Aseismic fault slip (creep), as occurs across the San Andreas fault in central California (fig. 7.1), causes no crustal deformation beyond a growing offset across the fault, although this offset may be distributed across a zone as broad as a few tens or hundreds of meters. Where the plate-boundary fault is alternately locked aseismically in its upper 10 km or so and abruptly slipping in great earthquakes, deformation extends several tens of kilometers into the plate interiors. Between large events, elastic strains build up in this zone and are episodically released every few hundred years. Subsequent postearthquake recovery processes redistribute the strains aseismically for years to decades after a major shock, and this deformation gradually merges into the steady accumulation of elastic-strain energy that persists until the frictional strength of the fault is again exceeded. This sequence of interearthquake strain accumulation, coseismic strain release, and postseismic readjustment is thus a recurring process, here referred to inclusively as the earthquake deformation cycle.

Several fault-zone features result in measurable deformation spread over an extremely broad plate-boundary zone. This deformation occurs where the San Andreas fault system comprises several subparallel splays, as in both the San Francisco Bay region and southern California. There, both aseismic slip and major strike-slip

◀ FIGURE 7.1.—A wall and sidewalk in Hollister, Calif., are bent and offset by creep on the Calaveras fault. A slip rate of 5 to 6 mm/yr characterizes much of the Calaveras fault. View eastward along north side of Sixth Street. Photograph by R.E. Wallace, U.S. Geological Survey.



Horizontal interearthquake deformation is summarized below in rates of both displacement and shear strain. For both of these parameters, the components parallel to major active faults are the most significant and best illustrate the dominant pattern of present-day tectonic movements, and so in this chapter these components are commonly shown exclusively. For example, although three independent tensor components are needed to completely characterize the horizontal-deformation field, in California the only significantly nonzero strain-rate component is commonly the shear strain parallel to the local trend of faults in the San Andreas system. Here, I consider only the component of maximum horizontal shear-strain rate, which, within observational uncertainty, almost invariably parallels the San Andreas fault or one of its major strands.

#### SHEAR STRAIN ON THE SAN ANDREAS FAULT SYSTEM

Rates of contemporary shear strain are displayed in several complementary ways in figures 7.2 through 7.4; details of each rate determination are summarized in table 7.1. Although only the magnitude of the maximum shear-strain rate is shown in each figure, the orientation of the maximum-horizontal-contraction axis is listed in table 7.1. Note that for each of the strain rates shown in figures 7.2 through 7.4, aseismic fault slip contributes only negligibly, if at all, to the measured deformation. Further details on each strain field determination can be found in the references cited in table 7.1.

Shear-strain rates peak at 0.4 to 0.6  $\mu\text{rad}/\text{yr}$  (fig. 7.2) across the currently locked northern and southern sections of the San Andreas fault. Significant but slightly lower strain rates of 0.3 to 0.4  $\mu\text{rad}/\text{yr}$  are observed across right-lateral strike-slip faults in the northern California Coast Ranges (north of lat  $38^\circ\text{N}$ .) east of the San Andreas fault, as well as across the San Jacinto fault in southern California. Shear-strain rates resolvably greater than zero are observed as far as about 80 km from the San Andreas fault itself.

In addition, significant deformation is occurring across active faults in east-central California. In the White Mountains, along the southern California-Nevada State line, small but resolvable strain rates ( $0.06 \pm 0.02 \mu\text{rad}/\text{yr}$ ) have been measured, and the orientation of the strain field indicates crustal extension perpendicular to north-south-striking normal faults in the area. Somewhat higher deformation rates are observed farther south, where right-lateral strain is occurring parallel to the Owens Valley fault, site of the  $M \approx 8$  earthquake of 1872 (see chap. 6).

Shear-strain rate is plotted as a function of perpendicular distance from the San Andreas fault in figure 7.3. Deformation rates peak at the fault and decrease to half

their maximums at a distance of about 30 km from the fault. Most of the deformation is encompassed within a zone about 100 km wide centered on the fault ("San Andreas boundary deformation zone"), as discussed below. However, the reader may confirm that this total lies in the range of about 30–40 mm/yr by drawing a smooth curve through the data plotted in figure 7.3 and integrating this curve (that is, measuring and summing the total area underneath the curve) from  $-60$  to  $+60$  km.

Maximum shear-strain rates at the San Andreas fault tend to be higher across the 1906 earthquake rupture in northern California (approx 0.6  $\mu\text{rad}/\text{yr}$ ) than in southern California (0.4  $\mu\text{rad}/\text{yr}$ ), although the Carrizo Plain data violate this generalization. Rather high deformation rates are also observed 20 to 60 km east of the San Andreas fault in the northern California Coast Ranges.

Shear-strain rates at various locations on the two currently locked sections of the San Andreas fault are plotted versus time since the most recent great earthquake at each locality in figure 7.4. Most of these data are derived from triangulation measurements, many of which were first made in the late 19th or early 20th century. Thus, these determinations are much less precise than those listed in table 7.1 and plotted in figures 7.2 and 7.3, most of which are from the post-1970 period. Nonetheless, it is clear from figure 7.4 that deformation rates on the fault are much higher in the years to tens of years immediately after a great earthquake than they are later. Although it may be questionable to lump values from northern and southern California together on a single plot, the temporal decline in shear-strain rate shown in figure 7.4 depends only on about the first 70 years of data plotted, all of which come from the 1906 rupture on the northern section of the San Andreas fault.

#### ASEISMIC SLIP, INTEGRATED DISPLACEMENT RATES, AND PACIFIC-NORTH AMERICAN PLATE MOTION

Rates of surface aseismic slip (fault creep) at representative points on the San Andreas fault system are listed in table 7.2 and plotted in figure 7.5. All fault segments displaying measurable aseismic slip are represented, but the detailed distribution along each segment is not shown; interested readers are referred to the references cited in table 7.2 for more details. Figure 7.5 also displays the rates of relative right-lateral displacement integrated across geodetic networks of 50- to 140-km aperture that span the San Andreas and related faults in seven areas of California, for several of which the detailed displacement-rate pattern is shown in figures 7.6 and 7.7.

With the notable exception of the central, creeping section of the San Andreas fault, aseismic slip at the surface represents only a very small proportion of the



total right-lateral displacement across the San Andreas fault system. On the 160-km-long central section of the San Andreas fault, maximum fault-creep rates average 30 mm/yr, close to the geodetically derived displacement rate of  $33 \pm 1$  mm/yr obtained over a 60-km aperture that spans the fault and the California Coast Ranges to the southwest. These data are the strongest evidence that no significant strain is accumulating in the crustal blocks

adjacent to the fault in this region, and so all the relative plate motion taken up by the San Andreas system is here being accommodated by rigid-block translation across the fault. Just north of this segment, on the southern section of the Calaveras fault, a significant amount of right-lateral slip at a rate of about 13 mm/yr, occurs as fault creep. Elsewhere in California, however, measured aseismic-slip rates range from 2 to 6 mm/yr, and creep

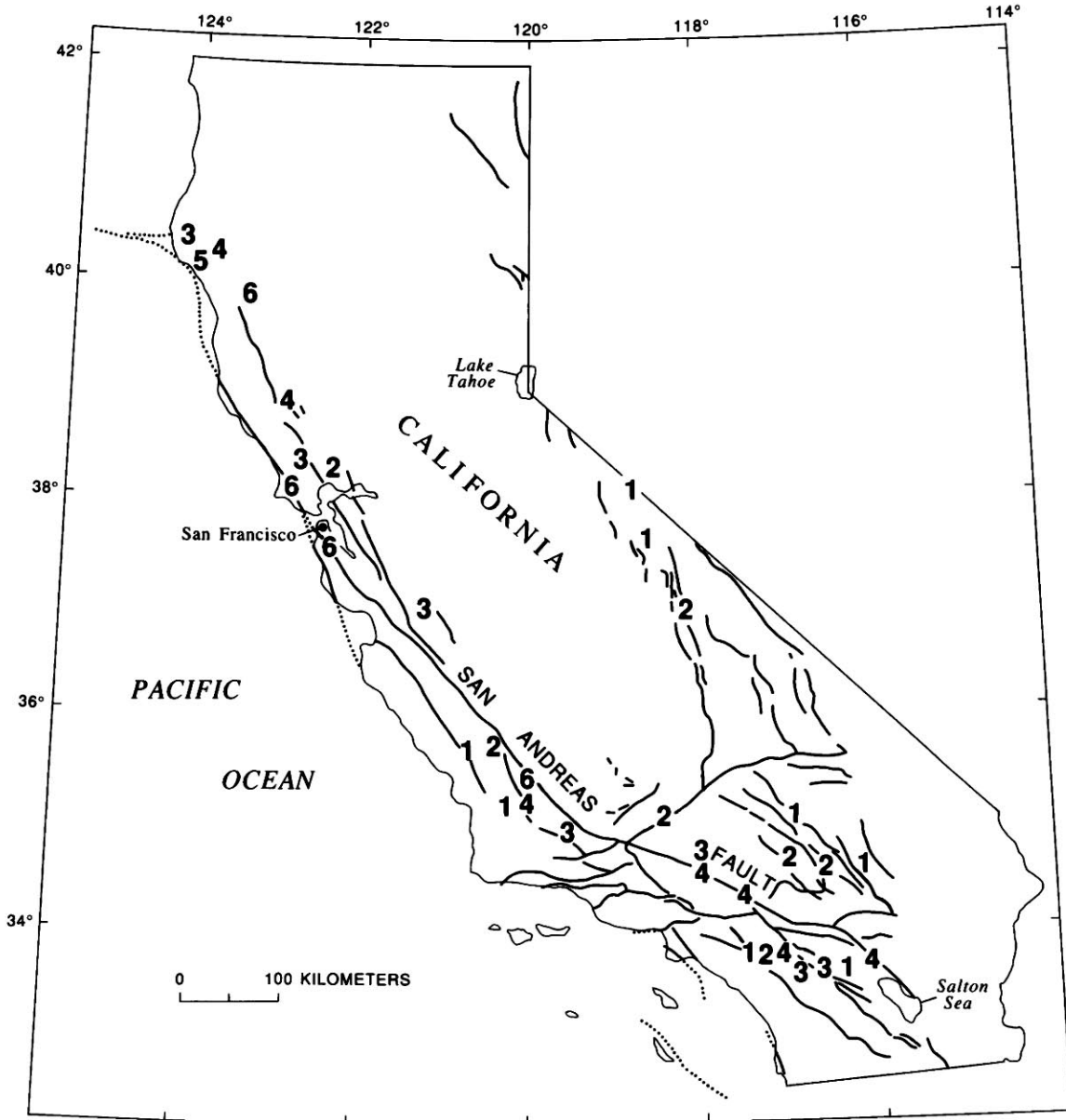


FIGURE 7.2.—Shear-strain rates (in  $10^{-7}$  rad/yr) and major active Quaternary faults of California; faults dotted where concealed. See table 7.1 for details.

commonly occurs only on restricted segments of otherwise-locked faults (for example, the Garlock and San Jacinto faults).

The integrated right-lateral displacement rates shown in figure 7.5 firmly constrain the proportion of Pacific-North American relative plate motion accommodated across the San Andreas fault system in California. In northern, central, and southern California, maximum rates range from 33 to 37 mm/yr. Global reconstructions of the motions of the major tectonic plates over the past 3 Ma, as well as analyses of magnetic-anomaly lineations at the mouth of the Gulf of California, point to a relative Pacific-North American plate-motion rate of  $49 \pm 3$  mm/yr (DeMets and others, 1987). The San Andreas fault system thus accounts for 70 to 80 percent of the relative plate motion, although the San Andreas fault itself does not everywhere take up all of this motion, and deformation is typically distributed across a boundary zone about 100 km wide.

Precisely how much additional relative plate motion is accommodated across other faults in California is uncertain, although the amount is probably very little. According to Minster and Jordan (1987), very long baseline interferometric (VLBI) surveying results indicate that oblique extension of the Basin and Range province, directly east of California, is occurring at a rate of  $10 \pm 2$  mm/yr with an orientation of  $N. 56^\circ \pm 10^\circ W$ . Depending

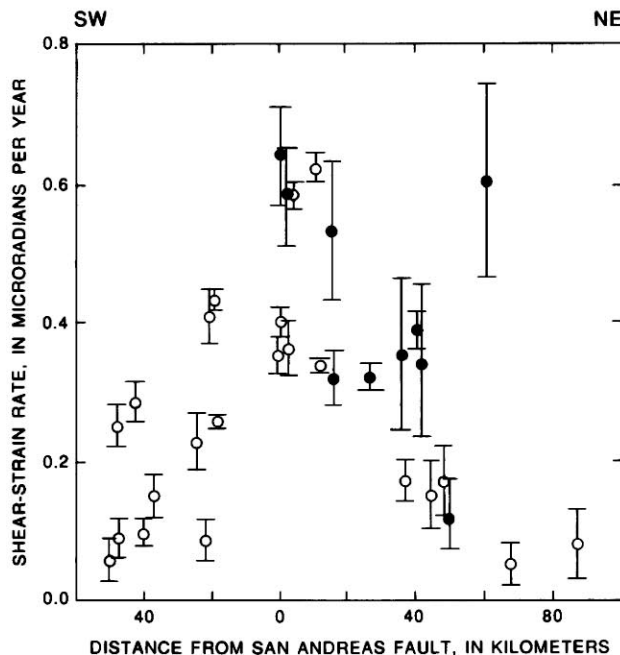


FIGURE 7.3.—Shear-strain rate versus perpendicular distance from the San Andreas fault. Dot, determination from northern California; circle, determination from southern California. 1- $\sigma$  error bars shown for reference.

on the exact rate and orientation of this extension, as well as on the precise direction of relative Pacific-North American plate motion, the residual “missing” plate motion being accommodated in California on faults other than those of the San Andreas system ranges from negligibly small to possibly as much as 10 mm/yr. Thus, although the geodetic coverage in California is far from complete (see figs. 7.2, 7.5), all or most of the zone of significant plate-boundary deformation apparently has been encompassed.

#### DETAILED DISPLACEMENT-RATE PATTERNS

Considerable detail on the distribution of deformation in the San Andreas boundary zone is provided by the rather complete geodetic coverage available in the San Francisco Bay region and southern California. In the method used to reduce these data, geodetic-line-length changes are used to determine station-displacement rates relative to a point at the center of gravity of the network. Fault-normal displacements are permitted by this method, but their values are minimized in the inversion

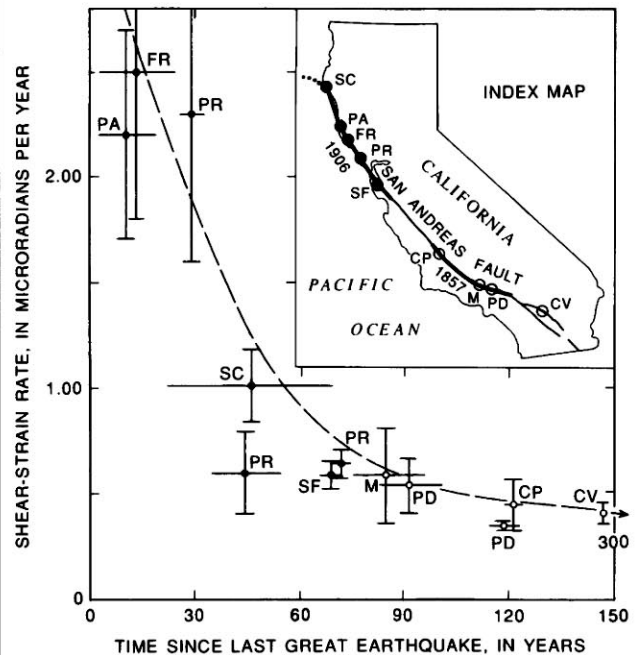


FIGURE 7.4.—Shear-strain rate versus time since last great earthquake (years 1906 and 1857 in inset; heavy line indicates extent of fault rupture) on the San Andreas fault. CP, Carrizo Plain; CV, Coachella Valley; FR, Fort Ross; M, Mojave; PA, Point Arena; PD, Palmdale; PR, Point Reyes; SC, Shelter Cove; SF, San Francisco. Locations of data points are keyed to index map. For each data point, vertical bar is 1  $\sigma$ , and horizontal line indicates time interval between surveys. Data points are plotted at middle of intervals. Dots, determinations from northern California; circles, determinations from southern California; dashed curve, approximate fit to data (Thatcher, 1983).



TABLE 7.1.—*Shear-strain rates in California*

[Maximum compression measured from north, with clockwise direction positive]

Area	Location		Rate (ppm/yr)	Maximum compression direction* (°)	Interval	Reference
	Lat N.	Long W.				
Mendocino .....	40.1°	124.0°	0.53±0.10	3±4	1981-84	Breen and others (1987).
	40.1°	123.7°	.35±0.11	11±6	--	
	40.2°	124.1°	.34±0.11	21±9	--	
Round Valley .....	39.9°	123.3°	.60±0.14	-11±5	1942-64	Prescott (1985).
Point Reyes .....	38.1°	122.8°	.64±0.07	2±2	1972-82	Prescott and Yu (1986).
Santa Rosa (Rodgers Creek fault).	38.4°	122.8°	.32±0.02	12±2	--	--
The Geysers (Maacama fault).	38.8°	122.9°	.39±0.03	11±3	--	--
Napa (West Napa fault) .....	38.8°	122.3°	.17±0.05	20±9	--	--
San Francisco peninsula .....	38.5°	122.4°	.58±0.07	-2±9	1970-80	Prescott and others (1981).
White Mountains .....	37.9°	118.6°	.06±0.02	-13±12	1972-79	Savage and Lisowski (1984).
	37.5°	118.5°	.06±0.02	-8±14	--	--
Owens Valley .....	36.9°	118.1°	.16±0.06	23±12	1974-79	Savage and Lisowski (1980).
Hollister (E. of Calaveras fault).	36.9°	121.3°	.32±0.04	-16±3	1971-78	Savage and others (1979).
San Luis network:						
Central .....	35.5°	120.4°	.23±0.04	-23±3	1977-83	N.E. King (unpub. data, 1988).
West .....	35.4°	120.7°	.09±0.03	-18±10	--	--
Carrizo network:						
A .....	35.4°	119.8°	.62±0.02	--	1977-83	N.E. King (unpub. data, 1983).
B .....	35.3°	119.8°	.58±0.02	--	--	--
C .....	35.1°	119.9°	.43±0.02	--	--	--
D .....	35.1°	120.2°	.10±0.02	--	--	--
Tehachapi network:						
Garlock fault .....	34.9°	118.5°	.17±.03	4±3	1973-83	King and Savage (1984).
San Andreas fault .....	34.6°	118.0°	.34±.01	-17±1	--	--
Cajon network .....	34.3°	117.5°	.36±.04	-16±2	1974-84	Savage and others (1986).
Los Padres network .....	34.8°	119.5°	.26±.01	-1±1	--	--
Barstow .....	35.0°	116.9°	.08±.05	24±17	1979-84	King (1985).
Palmdale .....	34.4°	118.2°	.35±.03	-19±4	1971-80	Savage and others (1981).
Mojave network:						
W1 .....	34.6°	117.0°	.17±.05	4±11	1934-82	Sauber and others (1986).
W3 .....	34.4°	116.6°	.15±.05	5±8	--	--
Eastern .....	34.5°	116.1°	.05±.03	--	--	--
Anza network:						
A .....	33.8°	117.4°	.06±.03	--	1973-81	King and Savage (1983).
B .....	33.8°	117.1°	.15±.03	30±13	--	--
C .....	33.8°	117.0°	.41±.04	21±5	--	--
D .....	33.5°	116.8°	.25±.03	30±8	--	--
E .....	33.5°	116.7°	.29±.03	1±5	--	--
F .....	33.6°	116.4°	.09±.03	--	--	--
G .....	33.7°	116.1°	.40±.02	8±2	--	--

process (see Prescott, 1981). Gross departures from this constraint would be revealed by notable disagreements between observed and predicted line-length changes, but no such discrepancies were found for the results presented here. Because the fault-normal displacement rates are small and show no consistent trends, they are not plotted on the profiles presented here.

Displacement rates in the San Francisco Bay region are plotted in figure 7.6. The distribution of deformation varies considerably across the San Andreas boundary zone from north to south of the San Francisco Bay. In the north bay, the integrated right-lateral-displacement rate across the network of  $27 \pm 3$  mm/yr (fig. 7.6B) indicates

that not all of the boundary zone has been captured within its 110-km aperture. Within about 5 km of the San Andreas fault, rapid change in the gradient of deformation rate indicates that interearthquake strain is concentrated close to the fault. Outside this near-fault region, deformation southwest of the fault appears to be negligible. Northeast of the fault, however, the persistence of significant movements right to the edge of the profile suggests that the 5- to 10-mm/yr deficit in boundary-zone deformation across this profile is being accommodated to the east of the Green Valley fault. Across the central and south bay (fig. 7.6C), movements are more evenly distributed through the network, and the integrated

TABLE 7.2.—Representative aseismic-slip rates on faults of the San Andreas system

Fault	Site	Lat N.	Long W.	Rate (mm/yr)	Reference
Hayward.....	Hayward network.....	37.6°	122.1°	6	Prescott and Lisowski (1983).
Northern section of the Calaveras.	Camp Parks.....	37.7°	121.9°	3	Do.
Southern section of the Calaveras.	San Felipe.....	37.0°	121.5°	13	Lisowski and Prescott (1981).
San Andreas.....	Cienega Winery.....	36.7°	121.5°	13	Schulz and others (1982).
Do.....	Eade Ranch.....	36.4°	121.0°	30	Buford and Harsh (1980).
Do.....	Parkfield (Durham Ranch).....	35.9°	120.4°	13	Do.
Garlock.....	Cameron.....	35.1°	118.3°	4	Louie and others (1985).
San Andreas.....	Indio Hills.....	33.7°	116.2°	2	Do.
San Jacinto (Coyote Creek strand).	Bailey's Well.....	33.0°	116.0°	5	Do.
Imperial.....	Interstate Highway 80.....	32.8°	115.5°	5	Do.

displacement rate of  $37 \pm 3$  mm/yr across the south bay suggests that the entire boundary zone has been spanned. Closer examination of the profile, however, reveals several zones of locally high deformation gradient, one across the San Andreas fault, where it resembles that observed near the fault in the north bay. In addition, rapid changes in the profile across the Hayward and Calaveras faults reflect aseismic slip at rates of 3 to 6 mm/yr on these faults (see fig. 7.5).

In southern California (fig. 7.7), deformation across the San Andreas boundary zone notably broadens from the Salton Sea, in the south, northwestward to the Big Bend region of the San Andreas fault north of Los Angeles (see fig. 7.5). At the south end of the Salton Sea, all of the boundary-zone deformation,  $35 \pm 1$  mm/yr, occurs within an area about 50 km wide (profile S, fig. 7.7C) that rapidly broadens to more than 100 km wide north and west of the Salton Sea (profile N, fig. 7.7C) and, possibly, broader still by about 50 km farther northwest (fig. 7.7B). North and west of Los Angeles, networks of 100-km aperture capture only  $18 \pm 2$  mm/yr of the total right-lateral-displacement rate (fig. 7.5). The profiles in figures 7.7B and 7.7C also show that in contrast with the northern section of the San Andreas fault, deformation gradients across the fault are smoother, and deformation is not so closely concentrated near the fault.

#### MECHANICS OF DEFORMATION

The observations described in the previous section point to a range of mechanical behavior for the faults comprised by the San Andreas system, from freely sliding with only minor accompanying seismicity, to completely locked from the surface to seismogenic depths except for abrupt slip during infrequent great earthquakes.

On the 160-km-long central section of the San Andreas fault, virtually all fault slip occurs aseismically. Slip rates measured at or near the fault are close to the average rate for the entire San Andreas boundary zone (fig. 7.5), no strain is detectable in the crustal blocks adjacent to the fault, and historical earthquakes of  $M \geq 5\frac{1}{2}$  have not occurred. Abundant minor seismicity (see fig. 4.10) contributes only negligibly to the slip budget, and except for a few small patches of fault surface that are in frictional contact between these small earthquakes, the first-order steady-state model for this segment involves rigid translation of adjacent fault blocks across the freely sliding plane of the San Andreas.

A transitional behavior applies to those fault segments where steady-state fault creep is observed at the surface but historical or prehistoric earthquakes of  $M \geq 6$  have been documented. Examples include the Parkfield and Coachella Valley segments of the San Andreas fault, the Hayward fault, and the Imperial fault. On these segments, during the interseismic phase of the earthquake cycle, the fault is inferred to be freely slipping in its upper few kilometers, in locked frictional contact at seismogenic depths (approx 3–10 km), and once again freely slipping at greater depths (fig. 7.8A). The result of this slip distribution is interseismic creep at the surface fault trace and elastic-strain accumulation in the adjacent blocks (figs. 7.8B, 7.8C).

#### THICK- AND THIN-LITHOSPHERE MODELS

The most extreme features of locked fault behavior are currently observed on the two San Andreas fault segments where great earthquakes have occurred in historical time, in 1857 and 1906 (see fig. 5.11 for locations and coseismic-slip distributions). On these segments, no aseismic slip is observed at the Earth's surface, the two faces of the fault are in locked frictional contact to depths



of 10 to 15 km, and interearthquake slip is either extremely small or absent. At greater depths, the mechanics of fault movement is uncertain, but two models bound the range of expected behavior (fig. 7.9). In the first, the thick-lithosphere model, the depth  $D$  of coseismic faulting is much less than the thickness  $H$  of elastically strong lithosphere. Interearthquake deforma-

tion then predominantly results from episodic or steady aseismic slip on the downward extension of the seismogenic fault zone, and any effects of the underlying weak asthenosphere can be safely neglected. In the second, the thin-lithosphere model (fig. 7.9), coseismic faulting depth is comparable to elastic-plate thickness. In this model, transient postseismic and steady interseismic flow in the

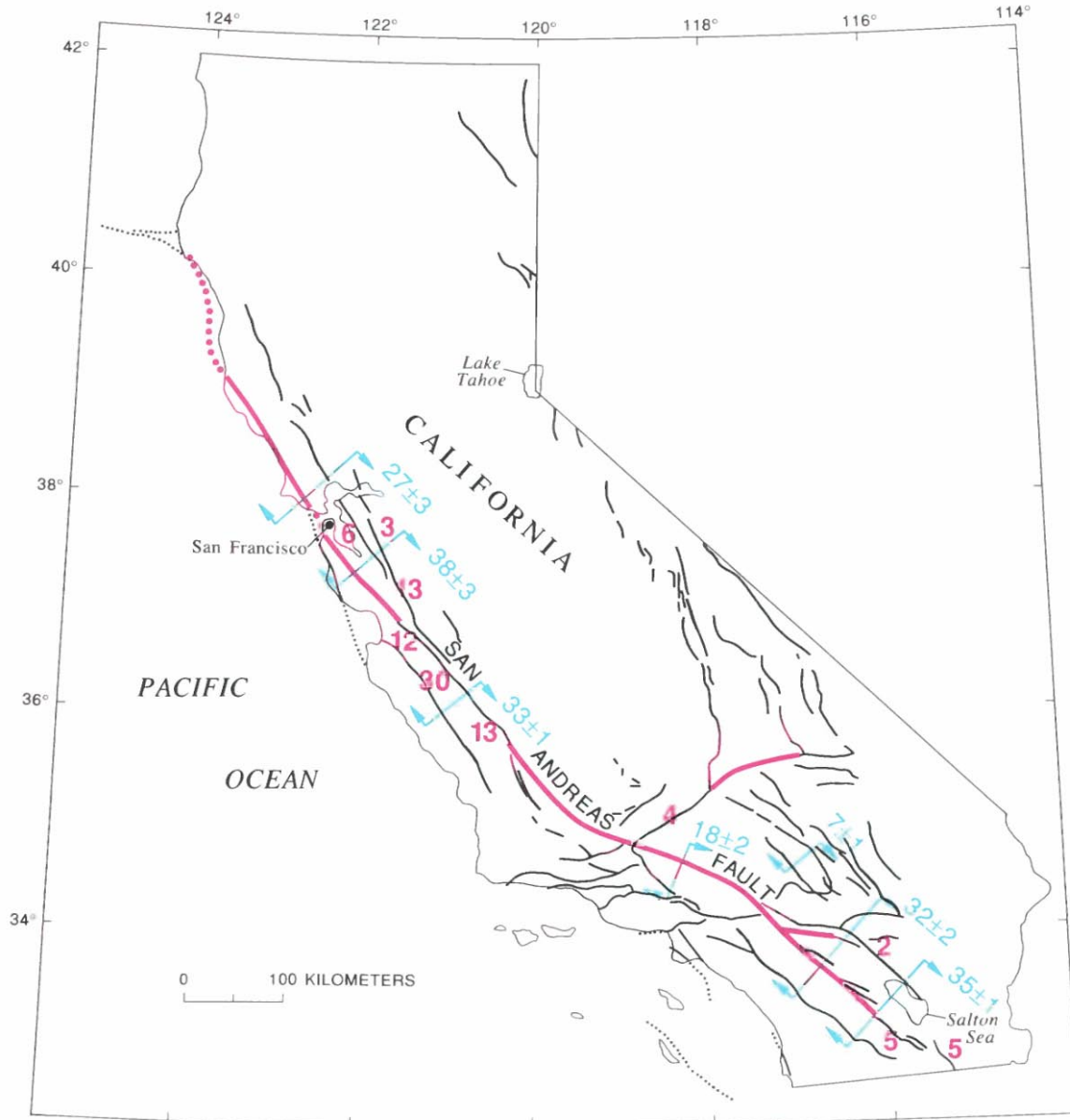


FIGURE 7.5.—Sketch map of California, showing rates (red numbers) of aseismic slip (fault creep) and relative right-lateral-displacement rates (blue numbers) near arrows, which indicate direction of relative movement along major active

strands of the San Andreas fault system. Values in millimeters per year. Locked (no surface slip) segment of major fault, red line; other Quaternary fault, black line; faults dotted where concealed. See table 7.2 for details.

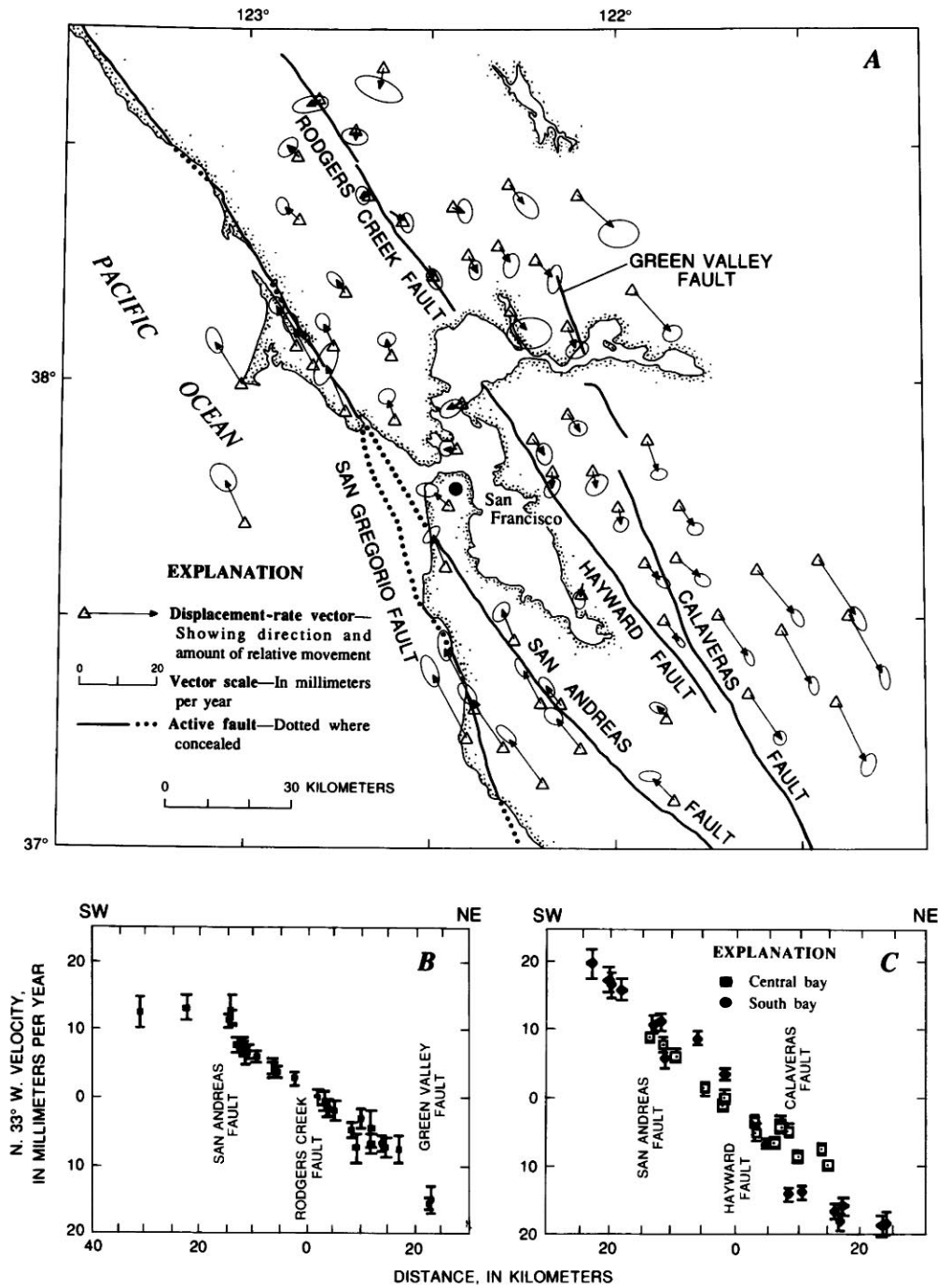


FIGURE 7.6. — Displacement rates across the San Francisco Bay region. A, Relative right-lateral displacement rates determined from repeated geodetic surveys made during 1971–87. Error ellipses show 95-percent-confidence limits for each determination (Prescott and others, 1987). B, Relative station velocities parallel to approximate trend of the San Andreas fault (N. 33° W.) plotted against distance perpendicular to this trend for north bay. 1- $\sigma$  bars are indicated. Perpendicular velocity component is negligible and omitted here. C, Same as figure 7.6B for central and south bay.



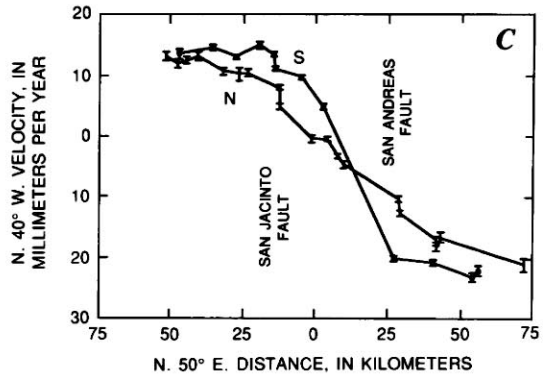
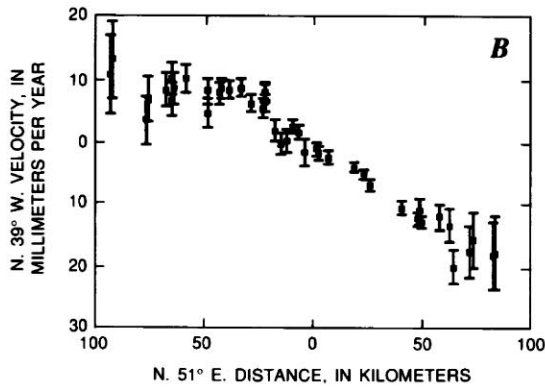
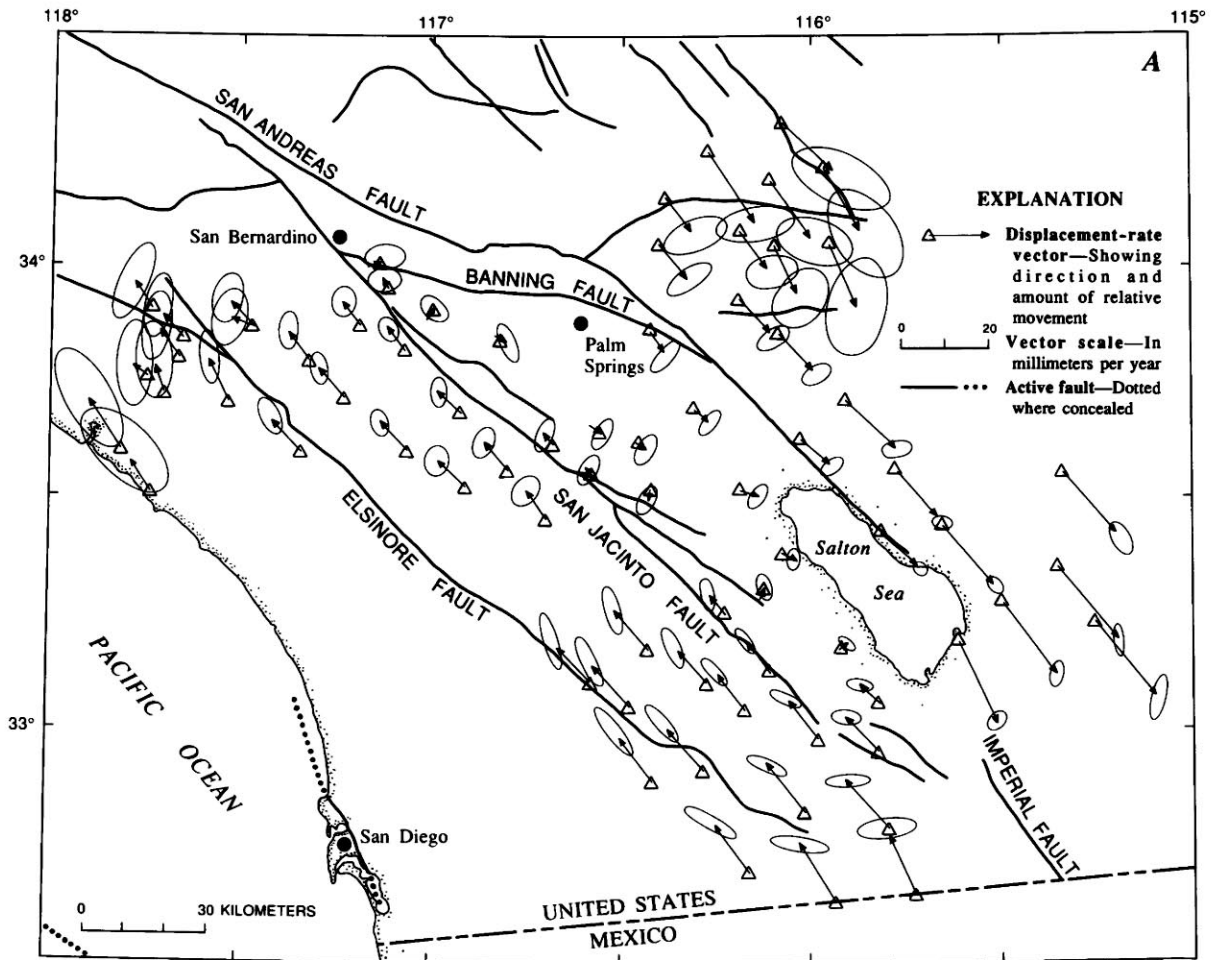


FIGURE 7.7.—Displacement rates in southern California. A, Relative right-lateral displacement rates determined from repeated geodetic-survey measurements during 1973–87. Error ellipses show 95-percent-confidence limits for each determination (Prescott and others, 1987). B, Relative station velocities parallel to approximate trend of the San Andreas fault (N. 39° W.) plotted

against distance perpendicular to this trend, for stations in northern part of map in figure 7.7A. 1- $\sigma$  error bars are indicated. Perpendicular velocity component is negligible and is not plotted here. C, Same as figure 7.7B for stations largely to north (N) and south (S) of the Salton Sea.

asthenosphere provide the dominant mechanism for interearthquake strain accumulation.

Note that in the context of these two models, the terms "lithosphere" and "asthenosphere" are linked to mechanical properties of the Earth's crust and upper mantle: The lithosphere is the strong elastic layer near the Earth's surface, and the asthenosphere is the region of ductile flow that lies beneath. Their boundary may thus lie well above the thermal boundary layer that separates the moving plates from the convecting mantle. If so, then at least the upper part of the "asthenosphere" forms part of the tectonic plate and moves with it.

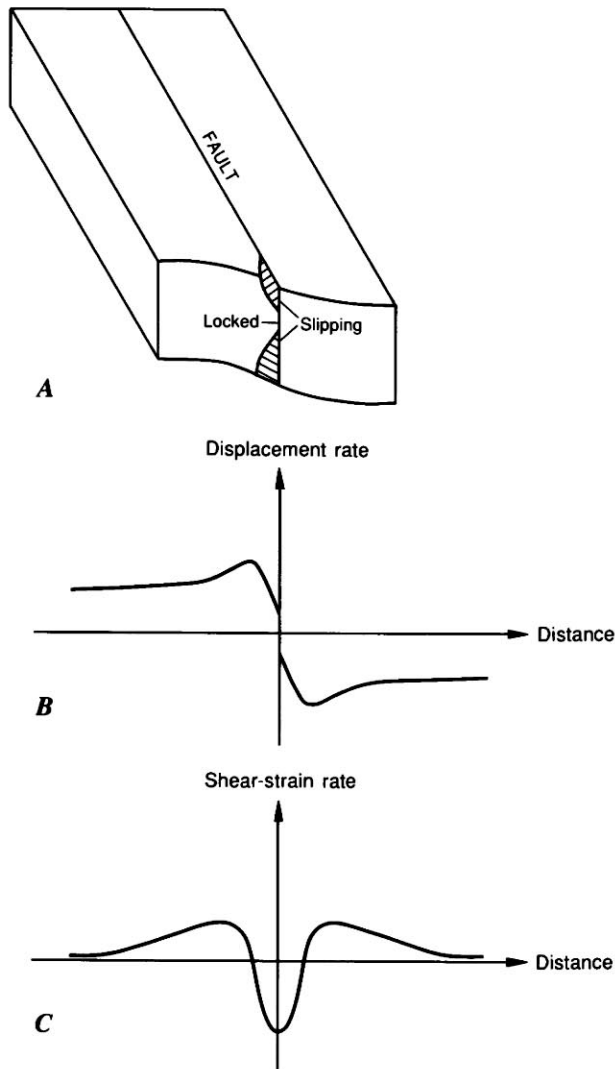


FIGURE 7.8.—Elastic-half-space model showing fault creep at surface, locked (nonslipping) fault at depth, and freely sliding zone at great depth (A). Displacement rate (B) and strain rate (C) are plotted against distance from fault.

Thus considered, the boundary between "lithosphere" and "asthenosphere" defines the zone of decoupling between surface tectonic processes and those that occur in the ductile region beneath. The location of this boundary is thus of central importance to the broad-scale tectonics of the San Andreas fault, the nature of the earthquake-generation process and its thermomechanical implications (see chap. 9), and the relation between shallow structural features and those inferred at depth (see chap. 8). I explore below the influence of this boundary location on cyclic earthquake-related deformation at the currently locked transform fault zones in the San Andreas, illustrating the contrasting mechanical behavior of the thick- and thin-lithosphere models.

All of the models considered here are two dimensional, and so neither slip nor mechanical properties vary along fault strike. Each model consists of only a single planar, vertical strike-slip fault. However, because the medium properties are linear elastic and (or) viscoelastic, the effects of multistranded fault zones can be obtained by simply superposing the deformation due to slip on individual fault segments. Furthermore, all of the two-dimensional models discussed here have also been considered in three dimensions, and so complexities arising from changes in fault strike, variations in slip along strike, and the finite extent of faulting can be incorporated straightforwardly as necessary. Similarly, except for the transition from elastic lithosphere to viscoelastic asthenosphere, depth variations in material properties are not considered, although, again, solutions have been obtained for faulting in plane-layered elastic

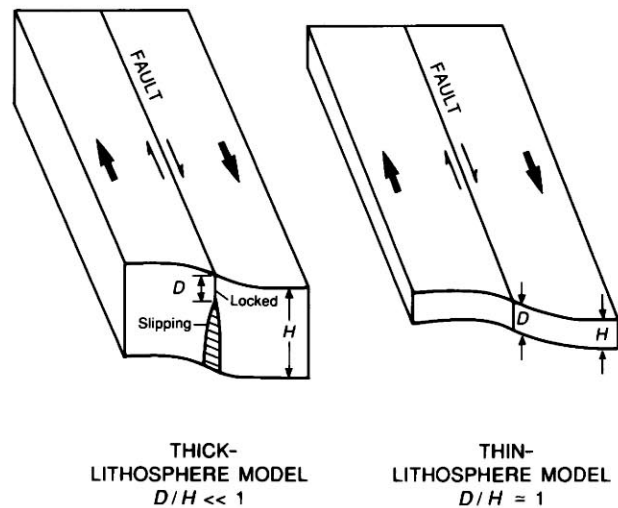


FIGURE 7.9.—Thick- and thin-lithosphere models.  $D$ , depth of coseismic faulting;  $H$ , thickness of elastically strong lithosphere. Small arrows along fault and larger arrows indicate direction of relative movement of fault and tectonic plates, respectively.



and viscoelastic media. Although fault end effects and changes in slip and geometry along fault strike can be locally important, these effects, as well as those due to depth-varying material properties, are generally second order relative to the deformation features described here. More important are the effects of the several subparallel strands that compose much of the San Andreas fault system along its two currently locked sections. In these sections, the interseismic deformation due to each major fault strand contributes significantly to the observed displacement pattern, and as a rule the effects of faults lying off the San Andreas proper cannot be safely ignored in matching models to data across the entire San Andreas boundary zone.

The simplest form of the thick lithosphere model, first proposed by Savage and Burford (1970), is illustrated in figure 7.10. In this idealized model, interearthquake strains accumulate uniformly throughout the deformation cycle and have precisely the same spatial pattern as coseismic strains, except that the sense of movement is reversed. The cycle consists of coseismic slip  $\Delta u$  extending from the surface to depth  $D$  and steady interearthquake aseismic slip at a constant rate  $\dot{u}$  ( $=\Delta u/T$ , where  $T$  is the earthquake recurrence interval) beginning at  $z=D$  and extending to great depth. For this model of interearthquake deformation, simple expressions relate

surface-displacement rates  $\dot{u}_x(y)$  and shear-strain rates  $\dot{\epsilon}_{xy}(y)$  to the fault parameters  $\dot{u}$  and  $D$  and the distance  $y$  from the fault trace:

$$\frac{du_x(y)}{dt} = \dot{u}_x(y) = \frac{\dot{u}}{\pi} \tan^{-1} \left( \frac{y}{D} \right)$$

$$\text{and} \quad \dot{\epsilon}_{xy}(y) = \frac{d}{dy} [\dot{u}_x(y)] = \frac{\dot{u}}{\pi D} \left[ \frac{1}{1 + \left( \frac{y}{D} \right)^2} \right]$$

A principal utility of this model is the ease with which approximate values of displacement and strain rate can be computed, commonly as a preliminary step to more detailed computations that employ complex models which nonetheless show many of the same general features. For example, using typical San Andreas values of  $\Delta u=4$  m,  $T=200$  yr, and  $D=15$  km, then  $\dot{u}=20$  mm/yr, and the engineering shear-strain rate (twice the tensor strain rate  $\dot{\epsilon}_{xy}$ ) at the fault trace ( $y=0$ ) is about  $0.8 \mu\text{rad/yr}$ , a value close to some of the peak strain rates plotted in figures 7.2 and 7.3. Furthermore, the bell-shaped distribution of secular strain across the model fault (middle right, fig. 7.10) generally accords with observations (fig. 7.3), and the width of the profile is a direct measure of the fault-locking depth  $D$ . (Note, however, that the observations summarized in figure 7.3 include strain rates determined from multistranded segments of the San Andreas fault system, and so they are not directly comparable to the model calculations for a single fault strand illustrated in fig. 7.10.) Recalling the observations discussed in the section above entitled "Observations of Crustal Deformation," the wider zone of secular strain across the southern section of the San Andreas can be rationalized if the depth of seismic slip and, thus, the locking depth of the fault are simply greater in southern than in northern California. As it stands, this model has no transient effects and so is too simple to explain the postearthquake strain changes plotted in figure 7.4. However, introducing a rather straightforward modification remedies this defect while accounting for the observed difference in strain-rate profiles between northern and southern California. Surprisingly, these same features are, for different reasons, natural consequences of the thin-lithosphere model.

The two models are illustrated in figure 7.11. In the thick-lithosphere model, postseismic effects are introduced by specifying transient postearthquake slip on a segment of the fault immediately beneath the coseismic rupture. Its time history is constrained by an exponentially decreasing slip rate (time constant  $\alpha$ ), and its magnitude by the requirement that the cumulative slip sum to the coseismic offset  $\Delta u$  by the end of the cycle. In the thin-lithosphere model, the transient deformation

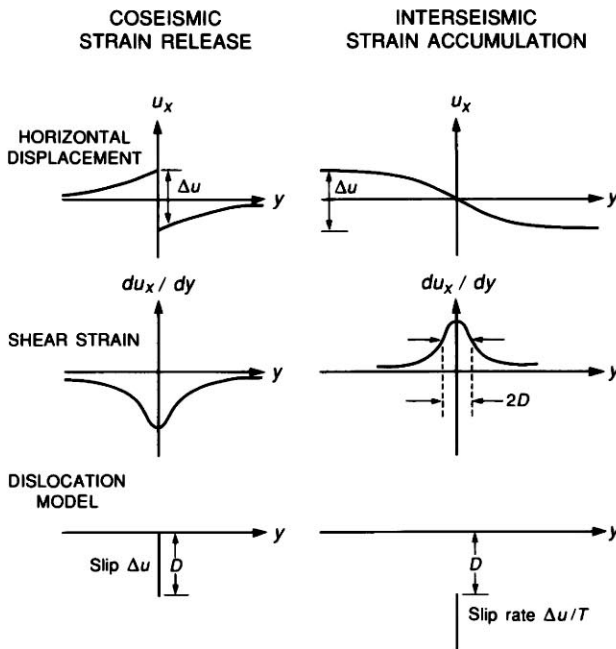


FIGURE 7.10.—Elastic-half-space model for earthquake cycle.  $\Delta u$ , coseismic slip;  $D$ , depth of coseismic slip;  $T$ , earthquake recurrence interval;  $u_x$ , horizontal displacement parallel to fault;  $du_x/dy$ , shear-strain component parallel to fault;  $y$ , distance from fault.



results from flow in the asthenosphere due to stress relaxation after seismic faulting in the lithosphere. Its time scale is controlled by the asthenosphere-relaxation time  $\tau=2\eta/\mu$ , when  $\eta$  is the effective viscosity of the asthenosphere and  $\mu$  is the average shear modulus of lithosphere and asthenosphere, here taken to be equal. In both models, the transient motions are superimposed on a steady component of deformation that is due to relative plate motion.

Detailed computations show that the two models produce surface deformations that with suitable choices of model parameters are observationally indistinguishable (see Thatcher, 1983). Here, the discussion is restricted to qualitative features, as summarized in figure 7.12. Near the fault, shear-strain rates monotonically decrease over time and gradually approach a constant (fig. 7.12B), while the deformation profile broadens and strains diffuse into the interiors of the adjacent plates as the cycle progresses (fig. 7.12A). It is easy to match the observed temporal decline in strain rate with either model; the particular parameter combinations are themselves not unique, and a range of choices can provide equally good agreement. All satisfactory thin-lithosphere models, however, require an elastic plate only 10 to 15 km thick, the maximum depth of coseismic slip in the 1906 earthquake (Thatcher, 1975). Both models predict a broadening of the zone of deformation that depends on the time interval since the latest great earthquake, and so the greater width of the strain-rate profile in southern California can be accounted for. For example, data from the northern, locked section of the San Andreas fault may correspond to times  $t_1$  to  $t_3$  in figure 7.12, whereas those from the southern section may correspond to times  $t_4$  and  $t_5$ .

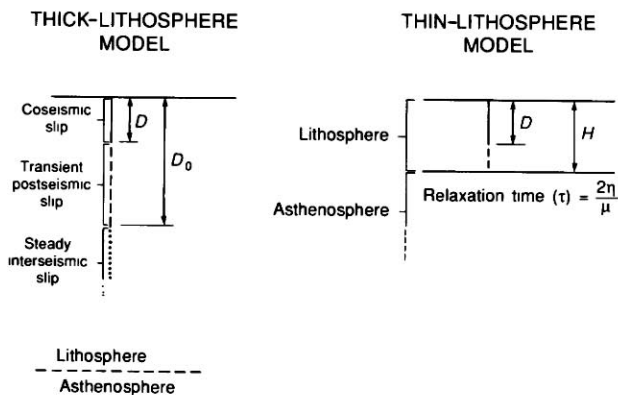


FIGURE 7.11.—Specific features of thick- and thin-lithosphere models.  $D$ , depth of coseismic slip;  $D_0$ , depth to bottom of zone of transient postseismic slip;  $H$ , thickness of elastically strong lithosphere;  $\eta$ , effective viscosity of asthenosphere;  $\mu$ , average shear modulus of lithosphere and asthenosphere.

More complex models that combine features of both the thick- and thin-lithosphere models are also consistent with available data (for example, Li and Rice, 1987). Furthermore, coseismic and interearthquake fault slip undoubtedly vary as a function of depth, rather than abruptly terminating at some specified fault depth. Although this gradationality of the slip distribution modifies the detailed patterns of surface strain and displacement from those illustrated in figure 7.10, for example, the same qualitative features are preserved, and it will be difficult to distinguish between differing slip-depth distributions on the basis of surface-deformation measurements alone.

In summary, at transform plate boundaries, available data are consistent with both thick- and thin-lithosphere models but do not strongly constrain either. The most geophysically interesting feature of both models is the predicted postearthquake diffusion-like spread of strain from the plate-bounding fault into the interiors of the adjacent plates. Postearthquake surveys, however, are sufficiently infrequent and areal coverage sufficiently limited that these effects, if they indeed occur, have not been directly observed. Details of the temporal decline in deformation rate near the fault are also absent.

#### STRESS-SLIP-CONSTITUTIVE-LAW FAULT MODELS

A completely different class of large-scale-faulting models are now being developed to more realistically incorporate the fault-failure process into the earthquake deformation cycle (for example, Stuart, 1979; Tse and Rice, 1986). Instead of specifying slip on the plate-bounding fault, these models extrapolate from laboratory

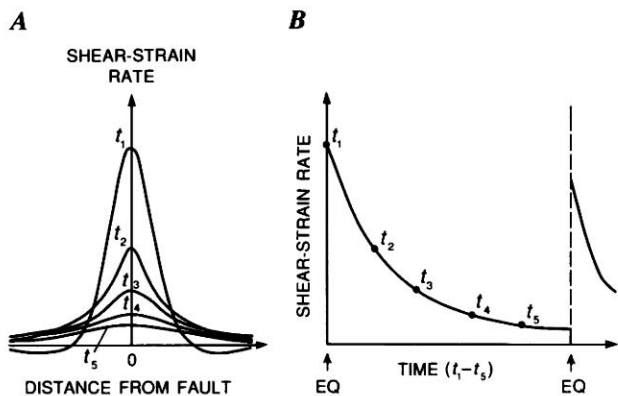


FIGURE 7.12.—Complete earthquake-cycle model predictions for thick- and thin-lithosphere models. A, Shear-strain rate versus distance from fault and its temporal evolution through deformation cycle. B, Shear-strain rate on fault versus time for one complete cycle. EQ, earthquake.



observations of the time-dependent frictional properties of rocks (for example, Dieterich, 1979; Tullis, 1988) to assign slip-stress-constitutive laws to the fault surface. As remotely applied stresses increase, each segment of the fault slips at a rate that depends on both the previous slip history and the current applied stress, and so the cycle of elastic-strain accumulation and release can be simulated. By specifying the depth dependence of fault frictional properties, a slip behavior nearly identical to that of the thick-lithosphere model (fig. 7.11A) follows naturally. A sample calculation of this type (Tse and Rice, 1986) illustrates the method and shows typical results (fig. 7.13). After a large coseismic slip event in approximately the upper 10 km of the model fault, transient postseismic slip occurs on both the coseismic fault plane and its downdip extension. As slip rates decline to near zero on the shallow segments of the fault, interseismic slip at greater depths approaches nearly steady-state values. Finally, near the end of the cycle, the constitutive model predicts an increase in slip rate on the shallow coseismic fault segment before the next large slip instability ("earthquake").

Although the appropriateness of this extrapolation of laboratory results to large-scale faulting is a matter of current debate and the scaling of laboratory parameters to the field is uncertain, Tse and Rice's calculations clearly demonstrate that the principal observed features

of the earthquake deformation cycle on the San Andreas fault can be reproduced by such models. Ongoing laboratory studies should refine and modify the stress-slip-constitutive laws, and geodetic and continuous strain-monitoring observations of preearthquake and postearthquake crustal deformation can test the applicability of these postulates to large-scale faulting processes.

### SUMMARY

Contemporary crustal movements in California are concentrated within a plate-boundary-deformation zone that is typically 50 to 200 km wide, approximately centered on the San Andreas fault. Integrated right-lateral displacement rates across this zone range from 33 to 37 mm/yr, representing about 75 percent of the Pacific-North American relative plate motion. Most or all of the rest may be taken up east of the San Andreas fault system in the Basin and Range province. Although aseismic fault slip (creep) is a locally important component of this relative plate motion, most of the geodetically measured deformation represents elastic strain on the crustal blocks adjacent to faults of the San Andreas system. Rates of secular (interseismic) shear strain are a maximum on the two currently locked segments of the San Andreas fault, sites of the great 1857 and 1906

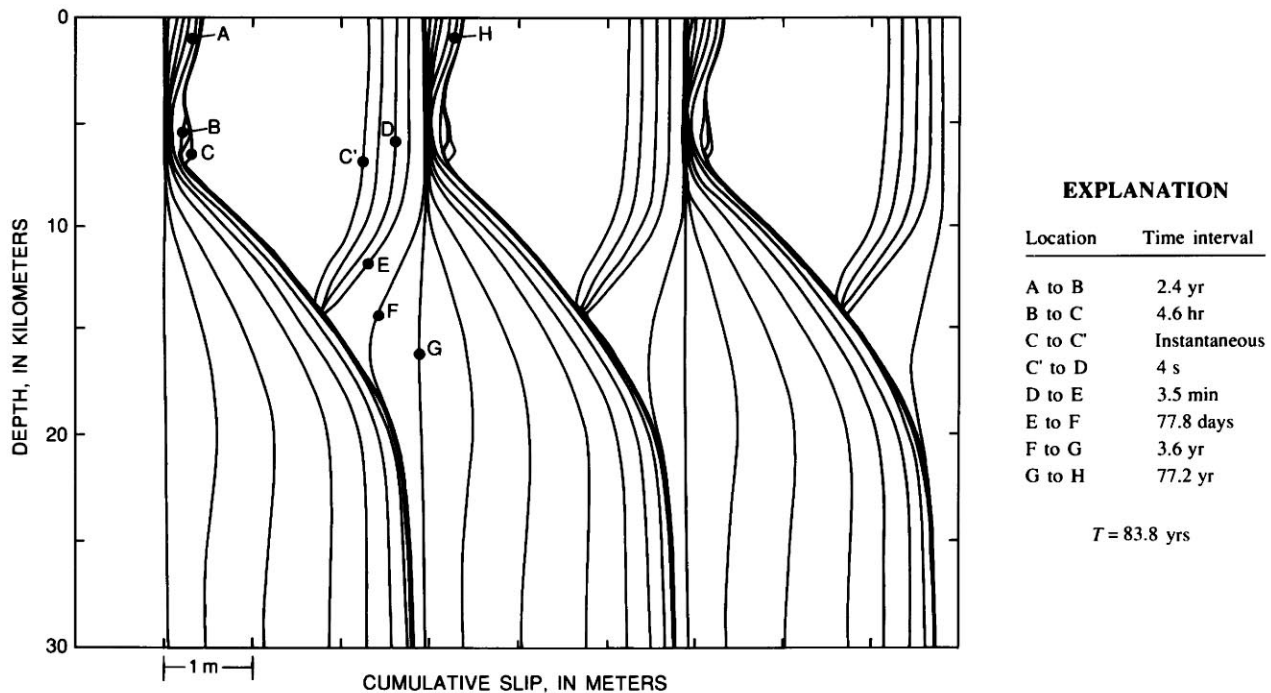


FIGURE 7.13.—Cumulative slip versus depth for selected time intervals through deformation cycle in quasi-static fault-instability model modified from Tse and Rice (1986).  $T$ , recurrence interval.



earthquakes. Values range from 0.4 to 0.6 parts per million per year (ppm/yr) at the fault to 0.1 ppm/yr 30 to 80 km from it. Deformation occurring at the times of large strike-slip earthquakes (coseismic strain) is concentrated within a few tens of kilometers of the surface fault rupture, indicating that earthquake fault slip is largely confined to the upper 10 to 15 km of the crust. After major events, postseismic shear strain occurs at transiently high rates (more than 2 ppm/yr) that decay to background interseismic rates over a time scale of years to tens of years.

Observations of coseismic, postseismic, and interseismic movements define the earthquake deformation cycle and constrain models of strain accumulation and release for strike-slip plate boundaries. Observations are fitted equally well by two contrasting models. In the first model, the depth of coseismic faulting is much less than the thickness of the elastically strong lithosphere, and postseismic and interseismic deformation result from transient and steady aseismic slip on the downward extension of the earthquake fault plane. At the other extreme, if earthquake slippage extends through most or all of the elastic lithosphere, interearthquake deformation is due to transient or steady flow in the underlying weak substrate ("asthenosphere").

#### FUTURE DIRECTIONS FOR RESEARCH

Although the broad outlines of current movement across the San Andreas boundary zone are now known and the main features of the cyclic deformation expected from great strike-slip earthquakes have been delineated, many issues still remain to be explored. Although all of the relative Pacific-North American plate motion occurring across California may have been measured geodetically, this determination is not yet definitive, and as much as 10 mm/yr of motion may be accommodated east or west of the approximately 100-km-wide zone defined by current measurements. Furthermore, the thickness of the elastically strong crust is uncertain by at least a factor of 3, and so major alternative models of the earthquake deformation cycle cannot be distinguished (fig. 7.9). Because surface-deformation observations cannot themselves resolve this ambiguity, other data, possibly gravity-field observations and lithospheric-deflection models (for example, McNutt, 1980), are needed.

Few details exist on the preseismic and postseismic movements related to large plate-boundary earthquakes. Whether detectably anomalous crustal movements precede large earthquakes is uncertain. Theoretical models and fragmentary observations suggest that precursory slip may occur on or beneath the eventual coseismic rupture plane. However, except for the observation that

premonitory deformations must be small relative to coseismic movements (for example, Johnston and others, 1987), precursory slip is otherwise unconstrained. Existing data are sufficient to demonstrate that postseismic movements, at least those from great earthquakes, are large—commonly, 10 to 30 percent of the coseismic deformation (Thatcher, 1984)—but the time scale and spatial distribution of these motions are not well determined at strike-slip plate boundaries. Laboratory experiments on lower-crustal rock types suggest that their ductile behavior is not approximated well by linear viscoelasticity, as assumed in the thin-lithosphere model, but postseismic observations are not yet sufficiently detailed to confirm this expectation.

Furthermore, vertical crustal movements in California are not well understood. Though not dominant in California's largely strike-slip-faulting environment, vertical movements can nonetheless be locally important in such regions as the Los Angeles and Ventura Basins, the Transverse Ranges of southern California, and the Cape Mendocino area of northern California. Current and future work that integrates geologic and geodetic information in these regions should begin to shed light on long-term, secular vertical-movement patterns and their origins.

Within complex, multistranded fault zones and, possibly, in simpler regions, permanent inelastic deformation of upper-crustal rocks may contribute significantly to the current movement pattern. For example, at subduction boundaries, geologic and geodetic observations indicate a substantial imbalance between cumulative interearthquake strain and coseismic strain release, commonly reflected in long-term uplift or subsidence of coastal and inland regions. However, at such predominantly transcurrent boundaries as the San Andreas, the observable effects of inelastic strain are more subtle. The thermal consequences of such deformation may be the most direct evidence for inelastic strain (see chap. 9). However, for California at least, the available data are either contradictory or ambiguous, and the extent to which measured interearthquake movements release elastically stored strain is currently unresolved.

#### REFERENCES CITED

- Bomford, Guy, 1980, *Geodesy* (4th ed.): London, Oxford University Press, 731 p.
- Brace, W.F., and Byerlee, J.D., 1966, Stick-slip as a mechanism for earthquakes: *Science*, v. 153, no. 3739, p. 990-992.
- Breen, N.A., Lisowski, Michael, and Prescott, W.H., 1987, Spatially varying patterns of crustal strain near the Mendocino triple junction, California [abs.]: *Eos* (American Geophysical Union Transactions), v. 68, no. 44, p. 1240.
- Burford, R.O., and Harsh, P.W., 1980, Slip on the San Andreas fault in central California from alignment array surveys: *Seismological*

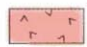








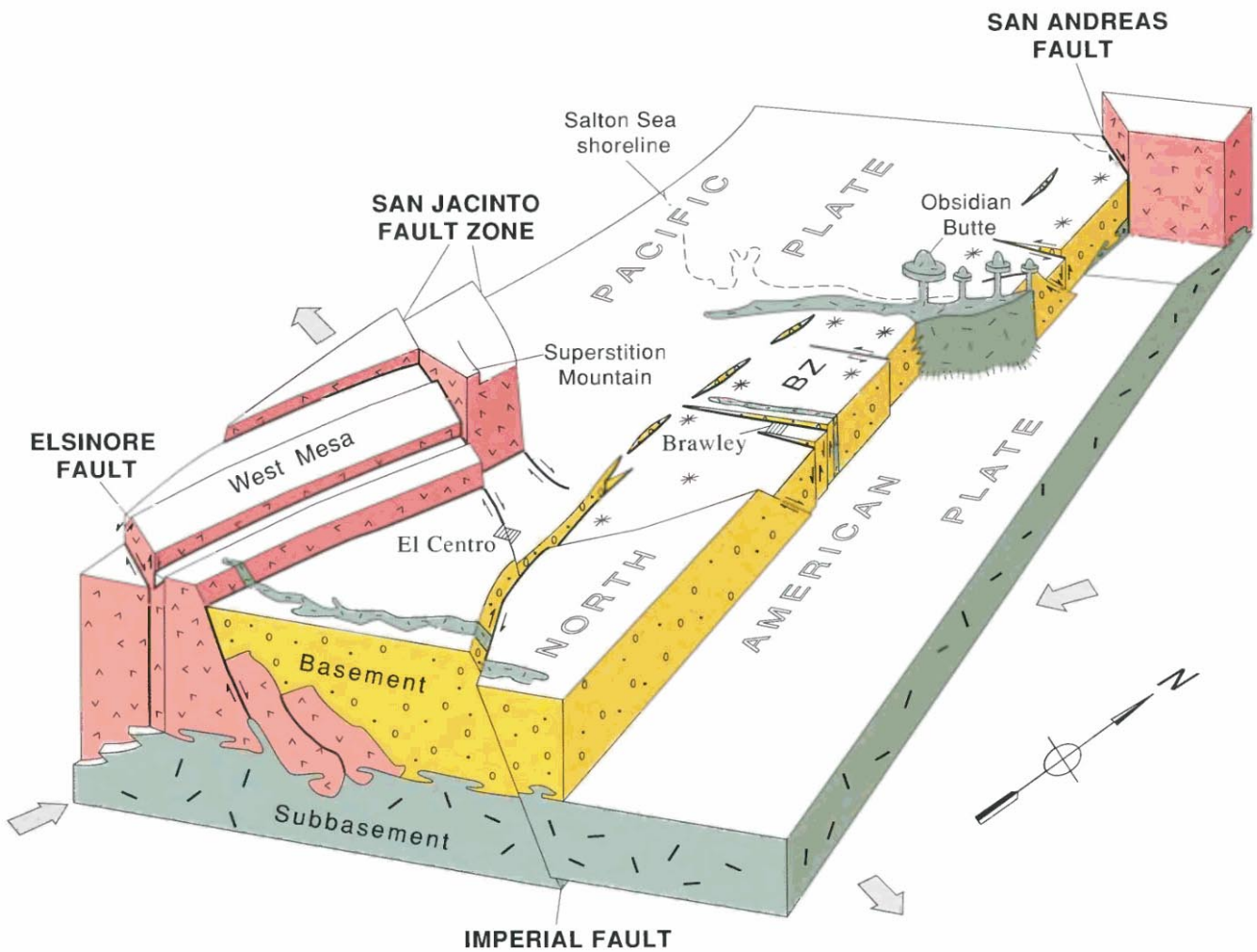
- Society of America Bulletin, v. 70, no. 4, p. 1223-1261.
- Castle, R.O., Church, J.P., Elliott, M.R., and Morrison, N.L., 1975, Vertical crustal movements preceding and accompanying the San Fernando earthquake of February 9, 1971: A summary: *Tectonophysics*, v. 29, p. 127-140.
- DeMets, Charles, Gordon, R.G., Stein, Seth, and Argus, D.F., 1987, A revised estimate of Pacific-North America motion and implications for western North America plate boundary zone tectonics: *Geophysical Research Letters*, v. 14, no. 9, p. 911-914.
- Dieterich, J.H., 1979, Modelling of rock friction, 1, Experimental results and constitutive equations: *Journal of Geophysical Research*, v. 84, no. B5, p. 2161-2168.
- Johnston, M.J.S., Linde, A.T., Gladwin, M.T., and Borcherdt, R.D., 1987, Fault failure with moderate earthquakes: *Tectonophysics*, v. 144, no. 1-3, p. 189-206.
- King, N.E., 1985, Horizontal deformation in the Mojave Desert near Barstow, California, 1979-1983: *Journal of Geophysical Research*, v. 90, no. B6, p. 4491-4494.
- King, N.E., and Savage, J.C., 1983, Strain-rate profile across the Elsinore, San Jacinto and the San Andreas faults near Palm Springs, California, 1973-81: *Geophysical Research Letters*, v. 10, no. 1, p. 55-57.
- 1984, Regional deformation near Palmdale, California, 1973-1983: *Journal of Geophysical Research*, v. 89, no. B4, p. 2471-2477.
- Lajoie, K.R., 1986, Coastal tectonics, in *Active tectonics*: Washington, National Academy Press, p. 95-124.
- Lawson, A.C., chairman, 1908, The California earthquake of April 18, 1906: Report of the State Earthquake Investigation Commission: Carnegie Institution of Washington Publication 87, 2 v.
- Li, V.C., and Rice, J.R., 1987, Crustal deformation in great California earthquake cycles: *Journal of Geophysical Research*, v. 92, no. B11, p. 11533-11551.
- Lisowski, Michael, and Prescott, W.H., 1981, Short-range distance measurements along the San Andreas fault system in central California, 1975 to 1979: *Seismological Society of America Bulletin*, v. 71, no. 5, p. 1607-1624.
- Louie, J.N., Allen, C.R., Johnson, D.C., Haase, P.C., and Cohn, S.N., 1985, Fault slip in southern California: *Seismological Society of America Bulletin*, v. 75, no. 3, p. 811-833.
- McNutt, Marcia, 1980, Implications of regional gravity for state of stress in the earth's crust and upper mantle: *Journal of Geophysical Research*, v. 85, no. B11, p. 6377-6396.
- Minster, J.B., and Jordan, T.H., 1987, Vector constraints on Western U.S. deformation from space geodesy, neotectonics, and plate motions: *Journal of Geophysical Research*, v. 92, no. B6, p. 4798-4804.
- Prescott, W.H., 1976, An extension of Frank's method for obtaining crustal shear strains from survey data: *Seismological Society of America Bulletin*, v. 66, no. 6, p. 1847-1853.
- 1981, The determination of displacement files from geodetic data along a strike slip fault: *Journal of Geophysical Research*, v. 86, no. B7, p. 6067-6072.
- 1985, An overview of the distribution of relative plate motion along the San Andreas fault system from Hollister, California, to the Mendocino triple junction, in Shearer, C.F., Minutes of the National Earthquake Prediction Evaluation Council, July 26-27, 1985, Menlo Park, California: U.S. Geological Survey Open-File Report 85-754, p. 232-246.
- Prescott, W.H., and Lisowski, Michael, 1983, Strain accumulation along the San Andreas fault system east of San Francisco Bay, California: *Tectonophysics*, v. 97, no. 1-4, p. 41-56.
- Prescott, W.H., Lisowski, Michael, and Savage, J.C., 1981, Geodetic measurement of crustal deformation on the San Andreas, Hayward, and Calaveras faults near San Francisco, California: *Journal of Geophysical Research*, v. 86, no. B11, p. 10853-10869.
- 1987, Velocity field along the San Andreas fault in southern California [abs.]: *Eos (American Geophysical Union Transactions)*, v. 68, no. 44, p. 1506.
- Prescott, W.H., and Yu, S.-B., 1986, Geodetic measurements of horizontal deformation in the northern San Francisco Bay region, California: *Journal of Geophysical Research*, v. 91, no. B7, p. 7475-7484.
- Sauber, Jeanne, Thatcher, Wayne, and Solomon, S.C., 1986, Geodetic measurement of deformation in the central Mojave Desert, California: *Journal of Geophysical Research*, v. 91, no. B12, p. 12683-12693.
- Savage, J.C., and Burford, R.O., 1970, Accumulation of tectonic strain in California: *Seismological Society of America Bulletin*, v. 60, no. 6, p. 1877-1896.
- Savage, J.C., and Lisowski, Michael, 1980, Deformation in Owens Valley, California: *Seismological Society of America Bulletin*, v. 70, no. 4, p. 1225-1232.
- 1984, Deformation in the White Mountain seismic gap, California-Nevada, 1972-1982: *Journal of Geophysical Research*, v. 89, no. B9, p. 7671-7687.
- Savage, J.C., and Prescott, W.H., 1973, Precision of geodolite distance measurements for determining fault movements: *Journal of Geophysical Research*, v. 78, p. 26, p. 6001-6008.
- Savage, J.C., Prescott, W.H., and Gu, Guohua, 1986, Strain accumulation in southern California 1973-1984: *Journal of Geophysical Research*, v. 91, no. B7, p. 7455-7473.
- Savage, J.C., Prescott, W.H., Lisowski, Michael, and King, N.E., 1979, Geodolite measurements of deformation near Hollister, California, 1971-1978: *Journal of Geophysical Research*, v. 84, no. B13, p. 7599-7615.
- 1981, Strain accumulation in southern California, 1973-1980: *Journal of Geophysical Research*, v. 86, no. B8, p. 6991-7001.
- Schulz, S.S., Mavko, G.M., Burford, R.O., and Stuart, W.D., 1982, Long-term fault creep observations in central California: *Journal of Geophysical Research*, v. 87, no. B8, p. 6977-6982.
- Segall, Paul, and Harris, R.A., 1987, Earthquake deformation cycle on the San Andreas fault near Parkfield, California: *Journal of Geophysical Research*, v. 92, no. B10, p. 10511-10525.
- Sibson, R.H., 1982, Fault zone models, heat flow, and the depth distribution of earthquakes in the continental crust of the United States: *Seismological Society of America Bulletin*, v. 72, no. 1, p. 151-163.
- Stein, R.S., 1983, Reverse slip on a buried fault during the 2 May 1983 Coalinga earthquake: Evidence from geodetic elevation changes, in Bennett, J.H., and Sherburne, R.W., eds., *The 1983 Coalinga, California earthquakes*: California Division of Mines and Geology Special Publication 66, p. 151-163.
- Stein, R.S., and Thatcher, Wayne, 1981, Seismic and aseismic deformation associated with the 1952 Kern County, California, earthquake and relationship to the Quaternary history of the White Wolf fault: *Journal of Geophysical Research*, v. 86, no. B6, p. 4913-4928.
- Stuart, W.D., 1979, Strain softening prior to two-dimensional strike slip earthquakes: *Journal of Geophysical Research*, v. 84, no. B3, p. 1063-1070.
- Thatcher, Wayne, 1975, Strain accumulation and release mechanism of the 1906 San Francisco earthquake: *Journal of Geophysical Research*, v. 80, no. 35, p. 4862-4872.
- 1979, Systematic inversion of geodetic data in central California: *Journal of Geophysical Research*, v. 84, no. B5, p. 2283-2295.
- 1983, Nonlinear strain buildup and the earthquake cycle on the San Andreas fault: *Journal of Geophysical Research*, v. 88, no. B7, p. 5893-5902.
- Tse, S.T., and Rice, J.R., 1986, Crustal earthquake instability in

- relation to the depth variation of frictional slip properties: *Journal of Geophysical Research*, v. 91, no. B9, p. 9452-9472.
- Tullis, T.E., 1988, Rock friction constitutive behavior from laboratory experiments and its implications for an earthquake prediction field monitoring program: *Pure and Applied Geophysics*, v. 126, no. 2-4, p. 555-588..
- Yeats, R.S., 1977, High rates of vertical crustal movement near Ventura, California: *Science*, v. 196, no. 4287, p. 295-298.
- Zhang, Y., Thatcher, Wayne, and Snay, R.A., 1988, Coseismic slip in the 1940 and 1979 Imperial Valley earthquakes and its implications [abs.]: *Eos (American Geophysical Union Transactions)*, v. 69, p. 1433.



**EXPLANATION**

-  Pre-late Miocene crystalline basement
-  Late Miocene and younger metasedimentary basement
-  Subbasement (basaltic intrusions)
-  Inferred intrusions or fractures underlying geothermal areas
-  Brawley seismic zone
-  Fault— Arrows indicate direction of relative movement
-  Principal stress direction



*The crust of much of California was formed at an Andean-type continental margin during the Mesozoic and early Cenozoic, and was modified by large strike-slip offsets along the San Andreas fault system during the late Cenozoic. Decoupling within the crust, as implied by present upper-crustal tectonic wedging in central California, and decoupling between the crust and mantle, as implied by "subduction" of lithospheric mantle in southern California, indicates that the San Andreas fault system must change with depth in its location and (or) style of deformation.*

## 8. LITHOSPHERIC STRUCTURE AND TECTONICS FROM SEISMIC-REFRACTION AND OTHER DATA

By GARY S. FUIS and WALTER D. MOONEY

### CONTENTS

	Page		Page
Introduction-----	207	Southern California-----	222
Crustal-thickness map of California-----	208	Transect C3-----	223
Central California-----	212	Borderland-----	223
Transect C2-----	212	Peninsular Ranges-----	223
Offshore region-----	212	Salton Trough-----	226
Salinian block-----	212	Chocolate Mountains-----	228
Santa Clara Valley—San Andreas to Calaveras faults—	216	Tectonics—the three-dimensional picture-----	228
Diablo Range-----	217	Structure of the upper mantle-----	229
Great Valley and Sierran foothills-----	218	Summary-----	230
Discussion—tectonic wedging-----	220	Acknowledgments-----	231
Geologic history-----	220	References cited-----	231
Past and present tectonic regimes-----	221		

### INTRODUCTION

Studies of the crustal and upper-mantle structure of California along the San Andreas fault system have been

underway for more than half a century, beginning with the early studies by Byerly and Wilson (1935) and Byerly (1946) in northern California and by Gutenberg (1943) in southern California. Crustal profiling along and

◀ **FIGURE 8.1.**—Schematic block diagram of Imperial Valley region of the Salton Trough, with unmetamorphosed sedimentary rocks removed and seismic basement cut away along line approximately parallel to the Brawley seismic zone (BZ; see fig. 8.7). Seismic basement consists of rocks with *P*-wave velocities of 5.5 to 6.5 km/s. In this region, there are two types of seismic basement: one type, on flanks of the Salton Trough, consists of pre-late Miocene igneous and metamorphic rocks; other type, in central part of trough, consists of late Miocene and younger metasedimentary rocks (similar in age and provenance to sedimentary rocks stripped off in this diagram). Pacific and North American plates are separating across the Brawley seismic zone,

an inferred onshore spreading center of the East Pacific Rise. North and south of the Brawley seismic zone, these two plates are separated from each other by transform faults, the San Andreas and Imperial faults, respectively. As the plates pull apart, subsidence occurs within the Brawley seismic zone, sediment is deposited to fill rift from above, and mafic intrusions (basalt, diabase, and gabbro) enter rift from below, metamorphosing sedimentary rocks below a certain depth (generally approx 5 km in central part of rift). This process is repeated until central part of rift consists entirely of young crust. Geographic locations projected downward onto seismic basement for reference.



near the San Andreas fault was first accomplished in the early 1960's by Eaton (1963), Healy (1963), and Roller and Healy (1963). Research accelerated after the 1966  $M=6.0$  Parkfield, Calif., earthquake to include both detailed crustal profiling and installation of dense seismic networks for the study of earthquakes (see chap. 5; Eaton and others, 1970). Since 1970, a wide variety of seismologic methods have been used to investigate crustal and upper-mantle structure in the vicinity of the San Andreas fault system. In this chapter, we summarize the main features of this structure and relate the structure to broad-scale tectonic processes.

Seismologic studies of crustal and upper-mantle structure in California make use of three primary data sources: (1) traveltimes of local earthquakes as measured by permanent and temporary seismic arrays, (2) seismic-refraction and reflection profiles, and (3) teleseismic delay times measured by seismic arrays. Traveltimes of local earthquakes, in addition to containing the information needed to locate earthquakes, contain a wealth of information regarding the seismic-velocity structure of the crust and upper mantle. Velocity structure can be determined from these traveltimes by iteratively adjusting an initial velocity model and associated hypocentral parameters, using inversion methods (for example, Crosson, 1976; Eberhart-Phillips and Oppenheimer, 1984). The resolution of velocity structure from local earthquake data is a function of the interstation spacing of the network and the abundance and distribution of seismicity.

Seismic refraction and reflection profiles together form a complementary set of seismic measurements. Seismic-refraction profiles provide the highest resolution of seismic  $P$ -wave velocities in the crust and upper mantle. The seismic-refraction method, however, generally does not provide the sharpest picture of lithologic interfaces, from which geologic structure is inferred; such a picture is better provided by seismic-reflection profiling.

Teleseismic delay-time studies offer the most effective means of determining the structure of the subcrustal lithosphere. The method is based on interpreting relative arrival times of compressional waves throughout a seismic array in terms of velocity variations at depth beneath the array. The Earth structure in the volume beneath the array generally is described by a series of blocks, and velocity deviations are derived for each block from the observed delay times (Aki and others, 1977; Thurber and Aki, 1987). The California seismic array is ideally suited for such investigations because of its large areal extent and the length of time it has been in operation (see chap. 5).

The primary product of the seismologic methods described above is a model of the seismic  $P$ -wave-velocity distribution in the crust and upper mantle. However, the

interpretation of seismic  $P$ -wave velocities in terms of rock type is highly nonunique because laboratory velocity data indicate that numerous rock types can have similar velocities (for example, Birch, 1960). This interpretation is further complicated by the fact that, in rocks at pressures of less than 2 kbars (depths above 8 km), seismic velocities are strongly affected by the presence of cracks (on all scales) and porosity. In addition, rock velocities are affected by temperature and the presence of water. Thus, the interpretation of  $P$ -wave velocities in terms of rock types must involve other data sets, including laboratory velocity measurements on rocks at different pressures, temperatures, and water saturations, surface geologic data, well data, and other geophysical data, including gravity and magnetic data. Fortunately, abundant laboratory velocity data (for example, Stewart and Peselnick, 1977; Lin and Wang, 1980), geologic data (see chaps. 1, 3), and geophysical data (see chap. 9) are available for California, making the lithosphere of this region one of the best studied in the world.

In this chapter, we summarize the lithospheric structure and tectonics along the San Andreas fault system of California (fig. 8.2) with maps of crustal thickness and upper-mantle seismic-velocity anomalies, and with crustal cross sections for central and southern California. Structure changes more rapidly parallel to the San Andreas fault in southern California than in central California, and so we supplement the cross section for southern California with a map showing crustal-block motions and a diagram illustrating the different motion of the lithospheric mantle below. Seismic and other data currently are still not dense enough to construct a cross section along the San Andreas fault system itself.

Construction of the crustal cross section for central California led us to a new interpretation of upper-crustal tectonic wedging, the mechanism whereby the Franciscan assemblage was emplaced in the Coast Ranges during the late Mesozoic(?) and Cenozoic. This interpretation extends that of Wentworth and others (1984) to include a two-part history whereby the observed structures atop the wedge, which include both extensional and compressional faults, were created. We further speculate that similar tectonic wedging occurred in southern California from the Mojave Desert to the Chocolate Mountains to emplace the Rand schist and the Pelona-Orocopia schist of Haxel and Dillon (1978) into rocks east of the San Andreas fault.

#### CRUSTAL-THICKNESS MAP OF CALIFORNIA

A contour map of crustal thicknesses in California (fig. 8.3A) provides an overview of the geophysical setting of the San Andreas fault system. The seismic and gravity

data used in compiling this map (fig. 8.3B) were discussed by Mooney and Weaver (1989).

Crustal thickness along the San Andreas fault increases from 16–24 km in northern California to 28–32 km in

southern California. Thus, the crust along the San Andreas fault system is everywhere thinner than the 36-km average for the conterminous United States (Braile and others, 1989), and in northern California it is

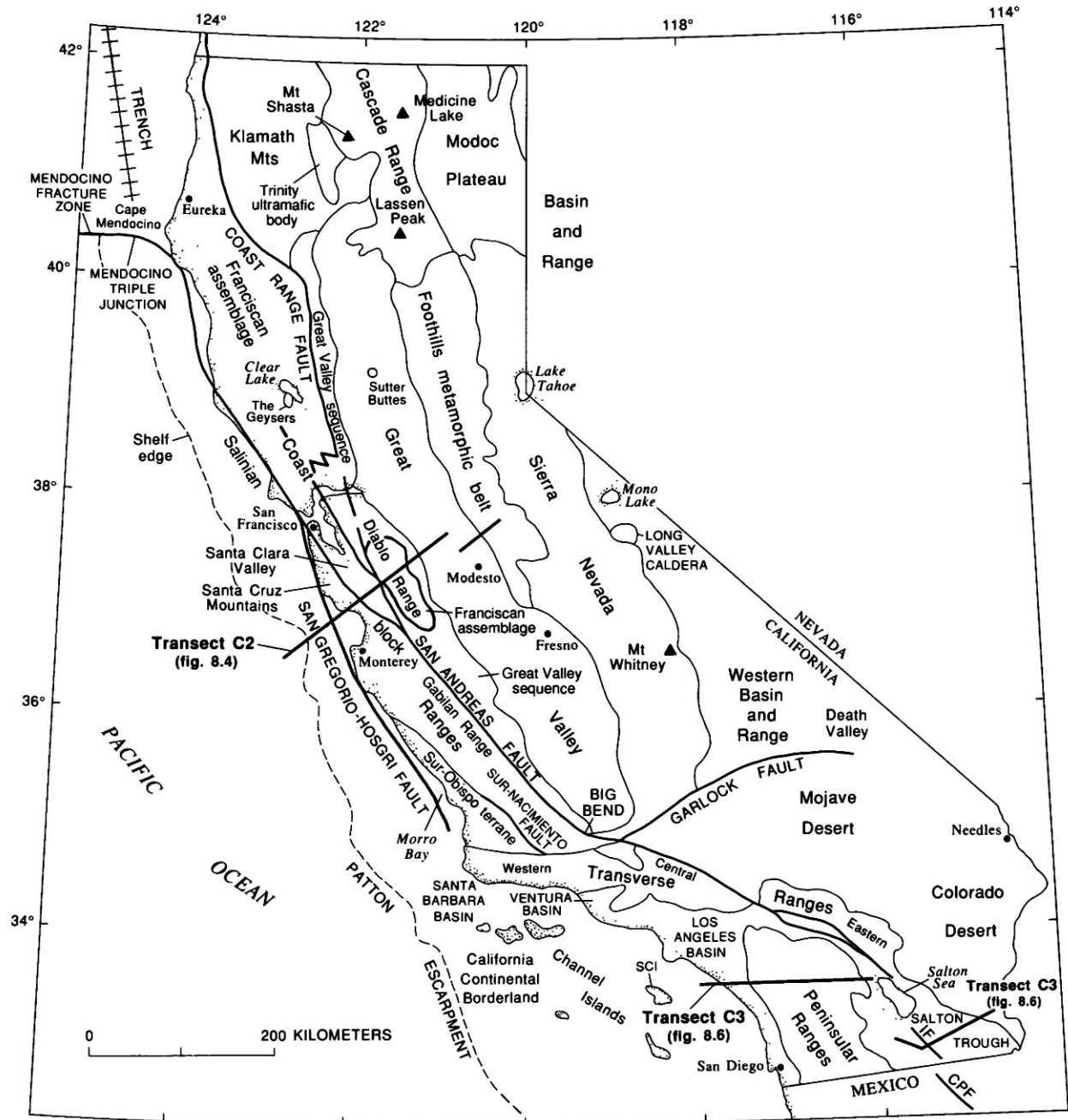


FIGURE 8.2.—California, showing place names, geologic provinces, selected geologic units, and locations of crustal transects shown in figures 8.4 and 8.6. The San Andreas fault extends from the Salton Trough to triple junction at Cape Mendocino. CPF, Cerro Prieto fault; IF, Imperial fault; SCI, Santa Catalina Island. Fault with crosslining is trench, offshore northern California.



substantially thinner than this average. To a first-order approximation, crustal thickness resembles the topography (see Jachens and Griscom, 1983, fig. 13).

Cape Mendocino in northern California marks the change from the strike-slip regime of the San Andreas fault to the subduction regime of the Cascade Range.

North of Cape Mendocino, the crust thickens eastward from about 16 km at the coast to about 38 km in the southern Cascade Range (fig. 8.3A). Near the coast, this thickness includes both the North American plate and the subducting Gorda plate. Estimates of crustal thickness in the northern Coast Ranges at Cape Mendocino lack

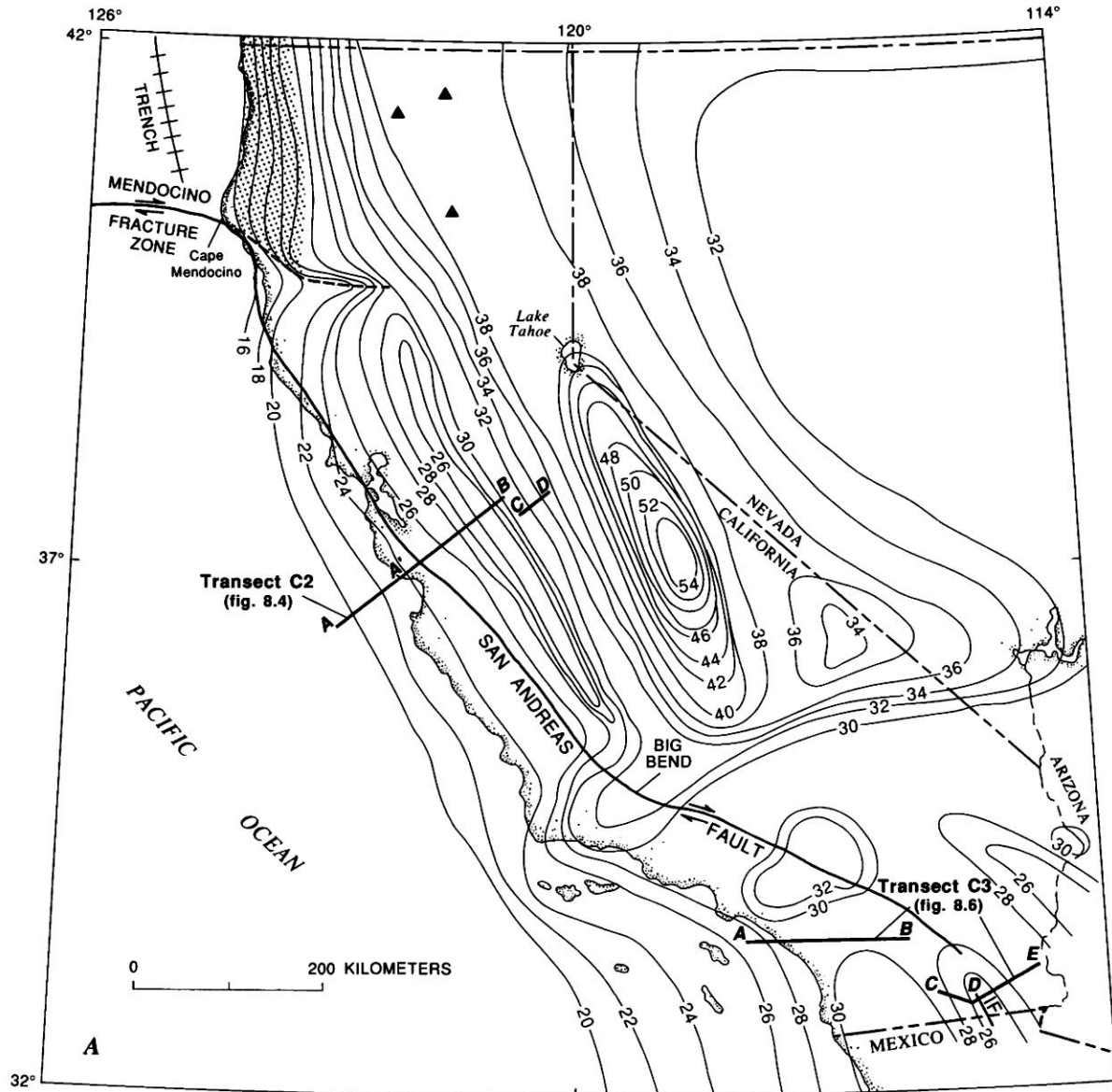


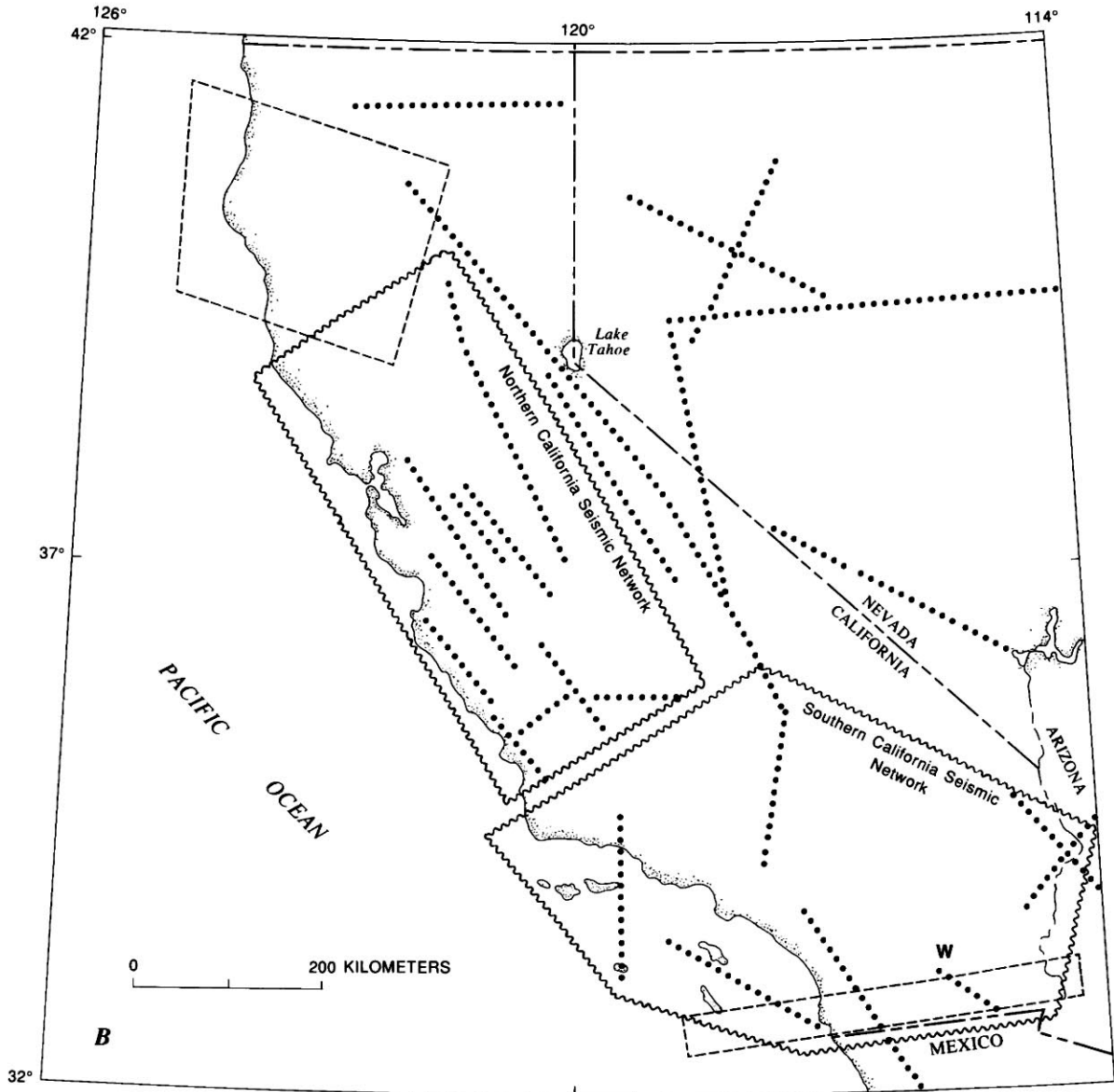
FIGURE 8.3.—Crustal thickness (A) for California and adjacent regions, modified from Mooney and Weaver (1989), with data sources (B). Contour interval, 2 km. Northeast of the San Andreas fault in central California, thin crust (within enclosed 28-km contour) corresponds to Mesozoic/early Cenozoic forearc basin (Great Valley; see fig. 8.2 for place names), and thick crust

(within enclosed 40-km contour) corresponds to magmatic arc of same age (Sierra Nevada). Southwest of the San Andreas fault in central California, this Andean-marginal sequence is repeated but shortened; crust is relatively thin there. In southern California, crustal thickness is relatively uniform (about 30 km), despite considerable tectonic activity throughout most of geologic time,

seismic refraction or reflection control, but detailed gravity models, heat-flow observations, and teleseismic data indicate an abrupt decrease in both crustal and lithospheric thickness southward of the landward projec-

tion of the Mendocino Fracture Zone (see chaps. 9, 10; Zandt and Furlong, 1982; Jachens and Griscorn, 1983).

In central California, the crust thickens eastward from about 25 km near the coast to as much as 55 km in the



including present subduction of lithospheric mantle (see below). Estimated error in figure 8.3A is 10 percent, or 1 to 1½ contour intervals. Heavy lines, faults—dashed where the Mendocino Fracture Zone extends onshore (and beneath North American plate); arrows indicate direction of relative movement; crosslined along trench, offshore northern California. Triangles, volcanoes of

Cascade Range continental arc. Dot pattern, area of contours on Gorda-plate Moho. IF, Imperial fault. Data sources in 8.3B include seismic-refraction profiles (dotted lines), earthquake networks (wavy outlines), and gravity (dashed outlines). "W" associated with seismic-refraction profile in the Salton Trough indicates that only wide-angle reflections are available to constrain Moho depth.



Sierra Nevada, but this general landward thickening is interrupted by thin crust (25 km) beneath the Great Valley (fig. 8.3A; compare Oppenheimer and Eaton, 1984). The crust of central California represents a Mesozoic and early Cenozoic Andean-type continental margin (see chap. 3; Hamilton, 1969) that has been modified by late Cenozoic strike-slip faulting along the San Andreas fault system and by uplift of the Sierra Nevada. Andean features include a subduction complex (eastern Coast Ranges), a forearc basin (Great Valley), and a magmatic arc (Sierra Nevada). Cenozoic strike-slip faulting along the San Andreas fault system has moved a shortened Andean-marginal sequence outboard of this sequence. Southwest of the San Andreas fault, the batholithic Salinian block (western Coast Ranges) is juxtaposed, across other right/oblique-slip faults of the San Andreas fault system, against an inactive accretionary prism, or subduction complex (western Coast Ranges and offshore California).

In southern California, the crust thickens eastward from about 20 km at the western margin of the California Continental Borderland to about 32 km in the eastern Transverse Ranges (fig. 8.3A). Over most of onshore southern California, crustal thickness is  $30 \pm 2$  km. Considering the complex tectonic history of this region, including the present subduction of lithospheric mantle (see below), this uniformity in crustal thickness is remarkable.

### CENTRAL CALIFORNIA

Crustal structure in central California is grossly two dimensional, as can be readily inferred from the crustal-thickness map (fig. 8.3A). There are five blocks or provinces with subparallel fault boundaries: an accretionary prism, which is partly off shore; the Salinian block, which underlies the western Coast Ranges, including the Santa Cruz Mountains and Gabilan Range; a complex block between the San Andreas and Calaveras faults, underlying the Santa Clara Valley; the Diablo block, beneath the Diablo Range; and the Great Valley/Sierran block (fig. 8.2). To illustrate the crustal structure of central California, we have modified and reinterpreted the part of Centennial Continent-Ocean Transect C2 (Saleeby, 1986) that extends from offshore California at Monterey Bay to the Sierran foothills near Modesto (figs. 8.2, 8.4). Seismic control, which is exceptionally good along this transect, has been augmented since Saleeby's (1986) study primarily by analysis of seismic-refraction profiles in the Great Valley (fig. 8.4A). The reader is referred to Hill (1978) for an earlier treatment of deep structure along approximately this same transect.

### TRANSECT C2

#### OFFSHORE REGION

The offshore region of transect C2 is underlain by an inactive, early Tertiary accretionary prism overlapped by uppermost Oligocene to Holocene sedimentary rocks (see Saleeby, 1986). The San Simeon terrane, consisting of Late Cretaceous Franciscan rocks (disrupted marine sedimentary rocks; see chap. 3), is imbricated in this prism along with poorly known, lower Tertiary sedimentary rocks. The prism is underlain by oceanic crust with an inferred age of about 26 to 20 Ma (Atwater and Menard, 1970; Atwater, 1989). The accretionary prism is juxtaposed against granitic rocks of the Salinian block across the (inactive) Nacimiento fault, which is overlapped by upper Tertiary sedimentary rocks. This fault, in turn, is offset by the (active) right/oblique-slip San Gregorio-Hosgri fault. The Moho is 10 km below sea level near the west end of the transect (Shor and others, 1971) and deepens to 24- to 26-km depth beneath the Gabilan Range and Santa Cruz Mountains (Walter and Mooney, 1982).

We follow D.S. McCulloch (in Saleeby, 1986) in showing steep northeastward dips on both the Nacimiento and San Gregorio-Hosgri faults (fig. 8.4A) that are based on marine reflection data. Focal mechanisms for earthquakes on the San Gregorio-Hosgri fault at this latitude indicate nearly pure strike slip on vertical planes; however, farther south, they indicate chiefly reverse faulting on northeast- or southwest-dipping planes (see chap. 5).

#### SALINIAN BLOCK

The area between the Nacimiento and San Andreas faults is underlain by a batholithic terrane that has been transported northwestward by the San Andreas (and other?) fault(s) by amounts estimated to range from 550 km (see Ross, 1978) to 2,500 km (Champion and others, 1984). Plutonic rocks include tonalite, granodiorite, and quartz monzonite of mostly Late Cretaceous age (Ross, 1978; Mattinson, 1982). Metamorphic pendants and screens include mostly quartz-rich clastic rocks of amphibolite facies. Ross and McCulloch (1979) postulated that these upper-crustal plutonic and metamorphic rocks are not rooted to the lower crust but are in fault contact with a buried terrane, possibly consisting of Franciscan rocks.

The velocity structure derived by Walter and Mooney (1982) from Stewart's (1968) seismic-refraction measurements in the Gabilan Range and Santa Cruz Mountains can be subdivided into four separate crustal layers with velocities of 2.1–4.6 km/s (layer 1), 5.3–5.6 km/s (layer 2),

**EXPLANATION FOR FIGURES 8.4A AND 8.6A**

- 3.6/4.6 **P-wave velocity in kilometers per second at top/base of layer**—Velocities in parentheses are projected
- P-wave velocity boundary**—Heavy tick where profile perpendicular to page; light line where profile in plane of page; short dashed where change in gradient only; long dashed in figure 8.4A for model of Dean Whitman and others (unpub. data, 1985). Boundaries are determined by refraction profiling except for offshore central California (fig. 8.4A) where they are determined by reflection profiling
- ? **Reflector from reflection profiling**—Queried where uncertain
- **Density and magnetic boundary**
- ? **Inferred region in which midcrustal and Moho discontinuities may exist**—Queried where uncertain
- LVZ, **Possible low-velocity zone**
- **Fault**

**EXPLANATION FOR FIGURES 8.4B AND 8.6B**  
LITHOLOGIC SYMBOLS FOR TECTONIC ENVIRONMENT

- Sedimentary rocks**
  - Oceanic Basin floor and trench turbidites**
  - Pelagic sedimentary rocks**
- Igneous and metamorphic rocks**
  - Seamounts**
  - Ophiolite, or top of ophiolite where undivided mafic crust is shown below**
  - Serpentine**
- Sedimentary rocks**
  - Magmatic arc Forearc rocks**
  - Intra-arc rocks**
- Volcanic rocks**
  - Rocks of mixed and (or) intermediate composition**
- Plutonic rocks**
  - Granite and quartz monzonite**
  - Granodiorite and tonalite**
  - Gabbro**

- Sedimentary rocks**
  - Continental and continental rift Nonmarine clastic rocks**—Circles, conglomerate; circles and dots, conglomerate and sandstone; darker color, metamorphosed
  - Marine clastic rocks**—Strike-and-dip symbol, carbonate bearing
- Volcanic rocks**
  - Rocks of mixed felsic to mafic composition**
- Metamorphic rocks**
  - Middle crust**—Inferred to be gneiss and schist developed at 10- to 20-km depth at greenschist to amphibolite facies
  - Lower crust**—Inferred to be gneiss developed below 20-km depth at amphibolite to granulite facies
- Mafic crust, undivided**—Denser pattern; higher velocity
- Mantle**—Closely spaced ticks, top of lithospheric mantle; widely spaced ticks, top of asthenospheric mantle or lithospheric mantle with partial melt

**OTHER SYMBOLS**

- Melange**—Symbols enclosed by zigzag lines indicate block type
- $\alpha \beta \gamma$  **Metamorphic facies**—Amphibolite, blueschist ( $\pm$  eclogite), greenschist
- Shear zone**
- Lithologic contact**
- Normal or strike-slip fault**—Sense of motion shown: arrows indicate direction of relative movement; A, away from observer; T, toward observer
- Mesozoic thrust fault**—Sawteeth on upper plate
- Mesozoic or Cenozoic thrust fault**—Teeth on upper plate; arrow indicates inferred motion of upper plate; dotted where inferred to have formerly existed
- Cenozoic thrust fault**—Teeth on upper plate; arrow indicates inferred motion of upper plate
- Mesozoic or Cenozoic detachment fault**—Ticks on upper plate
- Cenozoic detachment fault**—Ticks on upper plate
- In figure 8.6, Chocolate Mountains: Mesozoic or Cenozoic thrust or detachment fault ("Chocolate Mountains thrust fault"; see text)**

NOTE: Lithologic contacts and faults—Long dashed where not constrained by figures 8.4A and 8.6A or by earthquakes of chapter 5; short dashed where gradational (lithologic contact only) or projected above surface; queried where existence uncertain

? **Top of brittle-ductile transition zone inferred from earthquakes (see text)**—Queried where uncertain

Explanation for figures 8.4 and 8.6.



W

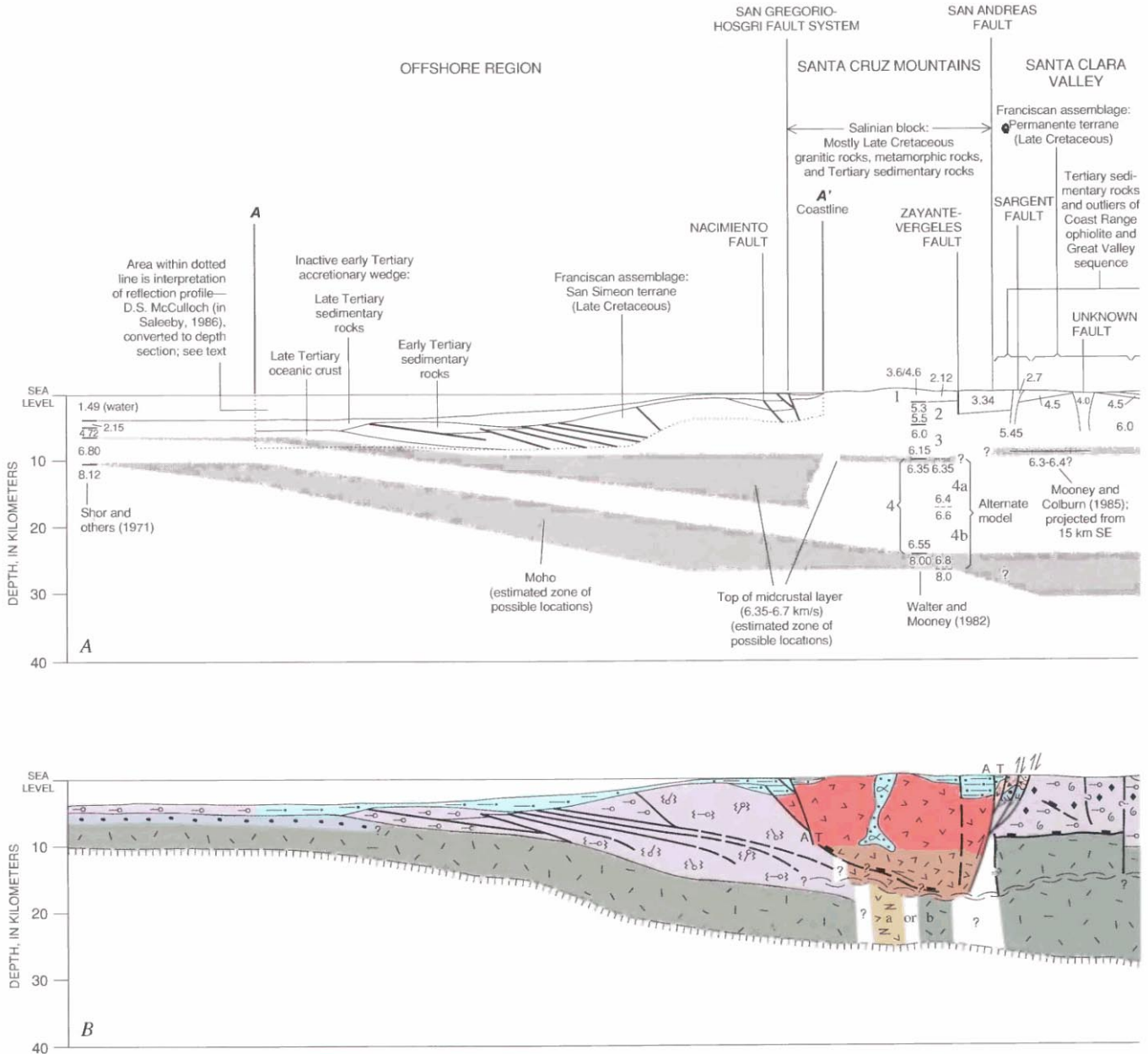
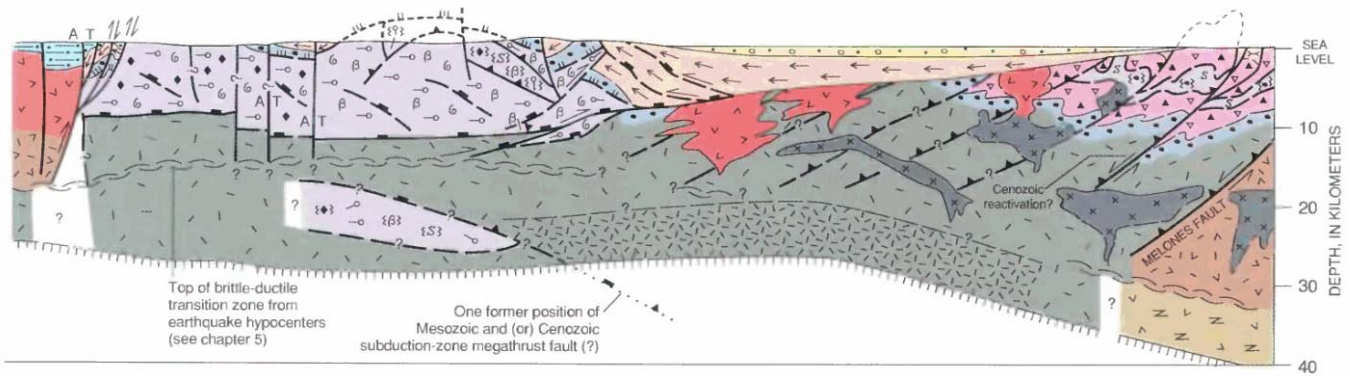
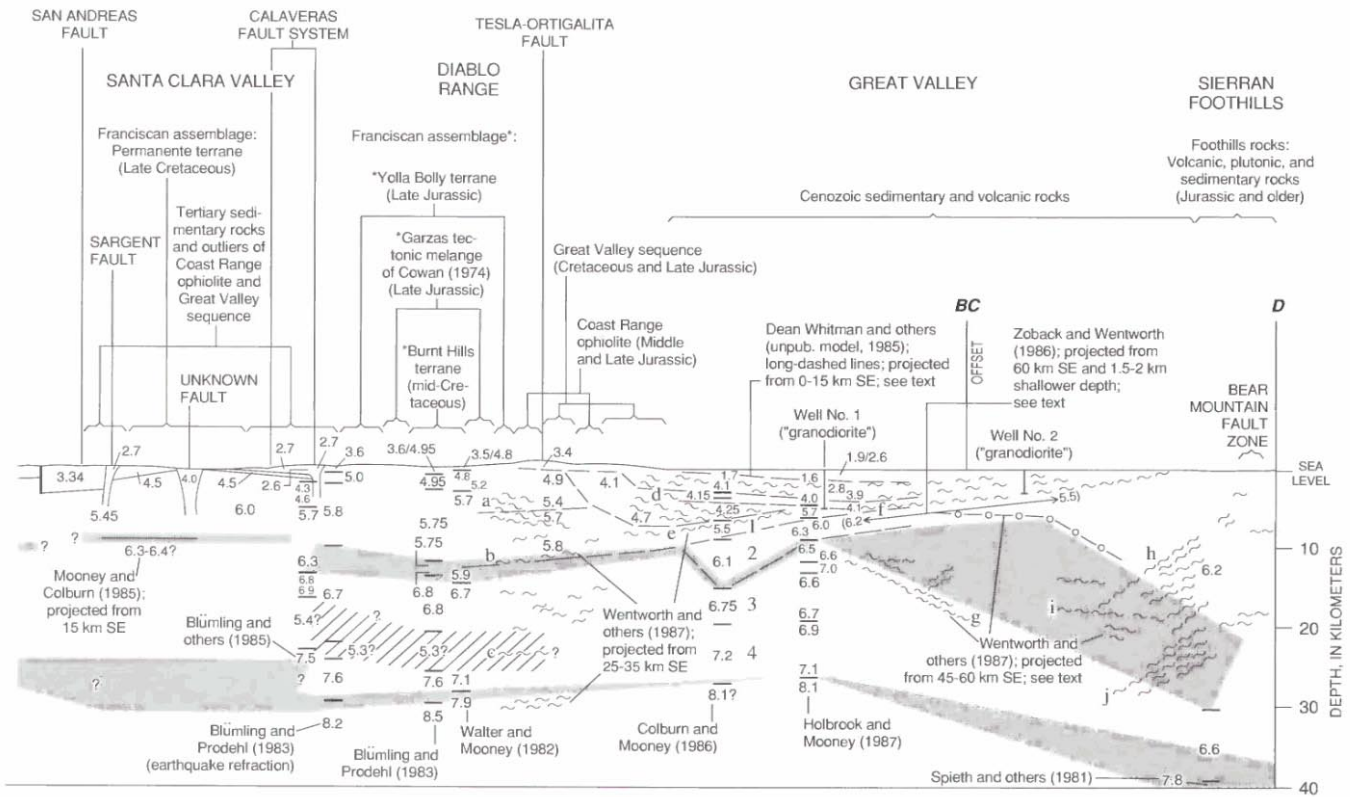


FIGURE 8.4.—Crustal structure of central California. *A*, Surface geology, depth-converted seismic-reflection data, and models of seismic-refraction, gravity, and magnetic data along western part of Centennial Continent-Ocean Transect C2 (see Saleeby, 1986). *B*, Reinterpretation of Transect C2. Major features in figure 8.4*B* include, from west to east, (1) offshore, inactive, early Tertiary accretionary wedge; (2) batholithic Salinian block of the Santa Cruz Mountains, positioned between the active oblique-slip San Gregorio-Hosgri and San Andreas faults; (3) Franciscan terranes of the Santa Clara Valley and Diablo Range, interpreted to compose a tectonic

wedge; (4) Mesozoic and Cenozoic sedimentary rocks of the Great Valley; and (5) rocks of the Sierran foothills, including Jurassic and older volcanic, plutonic, and related sedimentary rocks accumulated or emplaced in an island-arc setting and Cretaceous plutonic rocks. Tectonic wedge in feature 3 is interpreted to have moved during the late Mesozoic(?) and Cenozoic, possibly in several episodes, largely along contact between Mesozoic crystalline rocks and overlying Mesozoic sedimentary rocks. In the eastern Great Valley, these sedimentary rocks are still rooted to (or depositionally overlie) this basement. Movement of

E



wedge during present San Andreas transform-faulting regime may be along one or more thrust faults that merge with postulated decollement in brittle-ductile transition zone in the crust. This reinterpretation differs from Saleeby's (1986) in eliminating inferred east-dipping subduction zone or thrust fault beneath the western Great Valley. Off shore, interpretation of unmigrated reflection section by D.S. McCulloch (in Saleeby, 1986) has been converted to depth section, using assumed velocities for each inferred geologic unit. In the Santa Cruz Mountains, velocity model consisting of

layers 1 through 4 is shown (fig. 8.4A; see fig. 8.5A), along with alternative model in which layer 4 is subdivided into layers 4a and 4b. First model gives rise to interpretation a, and alternative model to interpretation b (fig. 8.4B). a-j, reflectors in the eastern Diablo Range, Great Valley, and Sierran foothills; 1-4, seismic-velocity layers in the Great Valley (fig. 8.4A) discussed in text. See figures 8.2 and 8.3 for location of Transect C2. No vertical exaggeration.



6.0–6.15 km/s (layer 3), and 6.35–6.55 km/s (layer 4). Layer 4, middle and lower crust, can alternatively be modeled as two layers of velocities 6.3 km/s (layer 4a) and 6.6–6.8 km/s (layer 4b). These layer velocities can be correlated to rock type using surface geologic data and laboratory velocity data. Layer 1 corresponds to outcrops of Cenozoic sedimentary rocks along the transect. Basement outcrops along or near the transect include abundant quartz monzonite (Ross, 1972). Lin and Wang (1980) studied the velocity behavior of a sample of quartz monzonite from this region as a function of pressure and temperature, and constructed a velocity-depth curve for this rock appropriate for the Coast Ranges. On their curve (fig. 8.5A), the rock is slightly faster than layers 2 and 3 and slower than layer 4. Walter and Mooney (1982) interpreted layers 2 and 3 as granitic rocks similar to this

quartz monzonite. The somewhat lower velocity of these two layers in comparison with the laboratory sample may be interpreted to result from (1) megascopic fractures in the Earth, not present in the laboratory sample; (2) a slightly lower content of mafic minerals (which have high seismic velocity) in the granitic rocks beneath the transect in comparison with the laboratory sample; or (3) both. Layer 4 is intermediate in velocity between the quartz monzonite sample and gabbro samples (hornblende gabbro and olivine gabbro) from the Coast Ranges. Walter and Mooney (1982) interpreted this layer to correspond to gneiss of intermediate composition, on the basis of a comparison of layer 4 with other laboratory data. In an alternative model, however, where middle and lower crust are separated as layers 4a and 4b, layer 4b may be reasonably interpreted as gabbro (fig. 8.5A).

Alternative interpretations of these several crustal layers are also possible, given the fact that different rock types may have similar velocities. Stewart and Peselnick (1977) and Lin and Wang (1980) studied the velocity behavior of Franciscan rocks, also common in the Coast Ranges (Jennings and Strand, 1958). Two lithologic components of the Franciscan assemblage, unmetamorphosed and metamorphosed graywacke, produce velocity-depth curves (fig. 8.5B) that bracket those for most other components of the Franciscan assemblage (including basalt). On the basis of velocity data alone, layers 2 and 3 might be interpreted as Franciscan rocks, but surface geologic data lead us to reject this interpretation. On the basis of velocity data alone, however, layer 4 is most likely not Franciscan rocks. Thus, if the middle and lower crust of the Salinian block represents a different terrane from the upper crust, as postulated by Ross and McCulloch (1979), that terrane is most likely not Franciscan assemblage.

In our cross section (fig. 8.4B), we show alternative interpretations of layer 4, given the alternative velocity models discussed above. In one interpretation (a, fig. 8.4B), layer 4 is entirely gneiss of intermediate composition. In a second interpretation (b, fig. 8.4B), layer 4a is intermediate gneiss, and layer 4b is gabbro. In interpretation a, no buried terranes are present; in interpretation b, the lower-crustal gabbro may be a buried terrane (oceanic crust) or magmatically underplated gabbro.

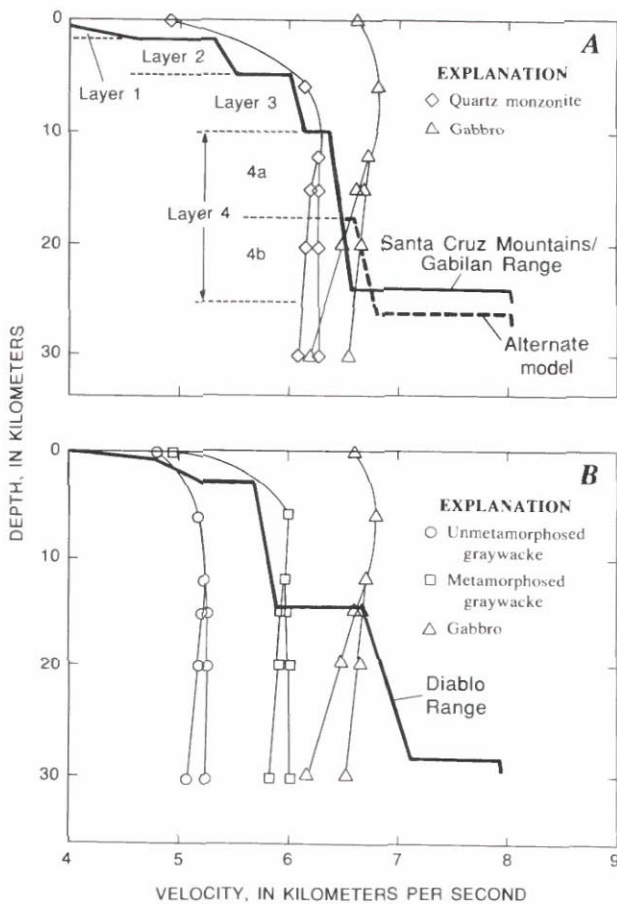


FIGURE 8.5.—Velocity-depth curves. A, Santa Cruz Mountains and Gabilan Range (Salinian block). B, Diablo Range. Heavy curves from seismic results (Walter and Mooney, 1982); light curves from laboratory velocity measurements and heat-flow modeling (two different geotherms assumed below about 10-km depth; Lin and Wang, 1980). See text for discussion of layers shown in figure 8.5A.

SANTA CLARA VALLEY—SAN ANDREAS  
TO CALAVERAS FAULTS

In the Santa Clara Valley, between the San Andreas and Calaveras faults, Franciscan assemblage (Permanente terrane; Blake and others, 1982) is overlain by outliers of Late Jurassic Coast Range ophiolite and Upper Cretaceous Great Valley sequence (McLaughlin



and others, 1988a). The Franciscan assemblage includes melange, volcanogenic sandstone, pillow basalt, serpentine, chert, and limestone. The Franciscan sedimentary rocks were deposited in equatorial waters and presumably transported thousands(?) of kilometers northward before accretion to the North American Continent (Blake and others, 1982).

Along transect C2, the San Andreas fault juxtaposes a thick section of Tertiary marine sedimentary rocks on the southwest against slivers of Coast Range ophiolite, Great Valley sequence, and other Tertiary marine rocks on the northeast that have been imbricated along the southwest-dipping Sargent fault and related thrust faults (McLaughlin and others, 1988a). Presumably, the granitic rocks of the Salinian block and Franciscan assemblage are juxtaposed at depth. In contrast, similar rocks are juxtaposed on either side of the Calaveras fault, including Coast Range ophiolite, Great Valley sequence, and, at depth, presumably the Franciscan assemblage.

Aftershocks of the  $M=7.1$  Loma Prieta earthquake of 1989 indicate a steep southwestward dip (approx  $70^\circ$ ) on the San Andreas/Sargent fault zone, and the main shock produced subequal components of strike- and reverse-slip motion (Plafker and Galloway, 1989). Relatively low elevations in this region, however, indicated that the motion along this fault zone in the past has been chiefly strike slip, and seismicity before the Loma Prieta earthquake (Olsen and Lindh, 1985; Olsen, 1986) indicates a complex fault zone that may include both vertical and southwest-dipping fault strands (see fig. 8.4B).

Although a steep ( $80^\circ$ – $85^\circ$ ) eastward dip on the Calaveras fault is indicated by earthquakes (see cross sec.  $D-D'$ , fig. 5.7B; Reasenber and Ellsworth, 1982; Oppenheimer and others, 1988), such an attitude is not resolvably different from a vertical dip (shown in fig. 8.4B), given errors in earthquake locations.

A seismic-refraction profile across the Santa Cruz Mountains and Santa Clara Valley reveals a heterogeneous upper crust (Mooney and Colburn, 1985). Layer offsets and velocity changes are visible in the model for this profile at the Zayante-Vergeles, Sargent, and Calaveras faults but, surprisingly, not at the San Andreas fault. An additional discontinuity is visible at an inferred buried fault in the central Santa Clara Valley (fig. 8.4A). Vertical zones of low velocity, 1 to 2 km wide, extending to a depth of as much as 3 to 5 km, are visible at a few of these faults (Mayer-Rosa, 1973; Blümling and others, 1985; Mooney and Colburn, 1985). The surficial layer (2.1–4.5 km/s) corresponds to different rocks in different places (fig. 8.4B). The "basement" layer has a velocity (5.4–6.0 km/s) appropriate for either granitic or Franciscan rocks at shallow crustal levels (Mooney and Colburn, 1985; see discussion above and fig. 8.5); presumably, it represents Franciscan rocks except west of

the San Andreas fault. The higher-velocity basement (6.0 km/s) in the eastern Santa Clara Valley may represent metamorphosed Franciscan rocks. A strong reflector is visible at 8- to 9-km depth beneath the Santa Clara Valley, but the seismic velocity below it is unknown. By analogy with the strong midcrustal reflector in the Diablo Range (see below), we infer this reflector to be the top of accreted island-arc and (or) oceanic crust.

Moho depth beneath the Santa Clara Valley is not known accurately enough to resolve whether the Moho steps downward to the east at the San Andreas and Calaveras faults or dips smoothly eastward between control points in the Santa Cruz Mountains/Gabilan Range (24- to 26-km depth) and the Diablo Range (29- to 30-km depth). McEvilly and Clymer (1975) conducted a seismic-reflection survey across the San Andreas fault south of its junction with the Calaveras and found a crustal thickness of 24 km with no change in thickness across the fault. Peake and Healy (1977), however, indicated a change in crustal thickness at the fault in this area.

#### DIABLO RANGE

The Diablo Range, the east-central Coast Ranges between the Calaveras fault and the Great Valley, is underlain chiefly by Franciscan assemblage. These rocks constitute at least three thrust sheets or nappes that are folded into an antiform (fig. 8.4; Blake, 1981; Saleeby, 1986). The youngest thrust sheet, the Burnt Hills terrane (Blake and others, 1982; Saleeby, 1986), consists of mid-Cretaceous blueschist-facies graywacke, arkose, conglomerate, argillite, and chert, approximately equivalent in age and provenance to mid-Cretaceous forearc sedimentary rocks of the Great Valley sequence. The Burnt Hills terrane is exposed in the core of the antiform. The oldest thrust sheets are the Upper Jurassic (informal) Garzas tectonic melange (Cowan, 1974) and the Yolla Bolly terrane (Blake and others, 1982). The Garzas tectonic melange consists of mafic blueschist-amphibolite, greenstone, serpentinized peridotite, and metagraywacke; it contains fragments of Upper Jurassic rocks (Coleman and Lanphere, 1971; Suppe and Armstrong, 1972) similar to those accreted in the Sierran foothills during the Nevadan orogeny (see below). The Yolla Bolly terrane lithologically resembles the Burnt Hills terrane, although there are some important differences. Both the Garzas tectonic melange and Yolla Bolly terrane crop out on the flanks of the antiform. The Coast Range ophiolite and Great Valley sequence lie above the Franciscan rocks on the low-angle Coast Range fault, which is complexly offset by the steeply dipping Cenozoic Tesla-Ortiguera fault on the northeast flank of the Diablo Range (fig. 8.4). (We follow Jayko and others, 1987, in referring to the



“Coast Range thrust fault” as simply the “Coast Range fault”—see below.)

The velocity structure of the Diablo Range derived by Walter and Mooney (1982) from seismic-refraction data collected by Stewart (1968) includes, beneath a 3.5- to 5.3-km/s near-surface layer, a 5.7- to 5.9-km/s layer beginning at 3-km depth, a 6.7- to 7.1-km/s layer beginning at 15-km depth, and the Moho at 29-km depth (fig. 8.4A). Importantly, a strong reflection is observed from the layer boundary at 15 km, indicating a strong velocity contrast between upper and lower crust. Blümling and Prodehl (1983) reanalyzed the same data and derived a similar velocity structure, except that they interpreted more phases in the data and added a lower-crustal low-velocity layer (5.3? km/s), with its base at about 26-km depth.

Seismic-reflection data have been collected in the eastern Diablo Range (Zoback and Wentworth, 1986) and compiled with other seismic data (Wentworth and others, 1987). These reflection data include a band of strong reflectors in the upper crust that dips shallowly east (reflectors a, fig. 8.4A), a weak reflector in the middle crust that dips shallowly west (reflector b), and a weak reflector at about 30-km depth (reflector c). The shallowly west-dipping reflector b, appears to link the top of the Great Valley basement with the top of the 6.7- to 7.1-km/s layer (Wentworth and Zoback, 1989).

Between 3- and 15-km depth, seismic velocities in the Diablo Range are well bracketed by velocity-depth curves predicted for end-member rocks of the Franciscan assemblage (fig. 8.5B; Steward and Peselnick, 1977; Lin and Wang, 1980). Within this depth range, the observed velocities also are slightly lower than those predicted for most granitic rocks (see fig. 8.5A). Between 15- and 20-km depth, the observed velocities agree well with those predicted for gabbro (fig. 8.5B; Lin and Wang, 1980) or, possibly, high-grade metamorphic rocks (Birch, 1960; Christensen and Fountain, 1975).

The 6.7- to 7.1-km/s layer in the Diablo Range may represent the middle and lower crust of an island arc or several imbricated island arcs. If so, this layer might include mixed intermediate and mafic plutonic rocks, including compositions from granodiorite to gabbro, as well as metamorphic rocks (see description of the Coast Range ophiolite by Evarts, 1977). Its relatively high velocity indicates that rocks of mafic composition must dominate or that the rocks are of amphibolite to granulite facies. This “island arc” interpretation is consistent with linking this layer to rocks beneath the Great Valley and thence to rocks of the Sierran foothills, which represent the middle and upper crust of island arc(s) (Saleeby, 1986). The 6.7- to 7.1-km/s layer, however, may also represent middle and lower oceanic crust, or diabase and gabbro, similar to the lowest layer of oceanic crust at the

west end of transect C2 (fig. 8.4A). The 6.7- to 7.1-km/s layer is too thick, however, to represent a single layer of oceanic crust. It consists of either several slices of tectonically underplated oceanic crust or of oceanic crust that has been augmented by mafic intrusions after underplating. If the low-velocity zone of Blümling and Prodehl (1983) is present, the 6.7- to 7.1-km/s layer may include oceanic sedimentary rocks tectonically underplated along with the oceanic crust.

We show a fault contact between the Franciscan assemblage and the 6.7- to 7.1- km/s layer in the Diablo Range to reflect the eastward transport of a wedge of Franciscan rocks (fig. 8.4B), similar to that discussed by Wentworth and others (1984). This interpretation departs from that of Saleeby (1986), who linked the shallowly east-dipping reflectors in the eastern Diablo Range (a, fig. 8.4A) with a hypothetical subduction zone or thrust fault beneath the Great Valley and Sierran foothills (see section below entitled “Discussion—Tectonic Wedging”).

#### GREAT VALLEY AND SIERRAN FOOTHILLS

Rocks of the Great Valley are known from exposures in an upturned section on the east side of the Diablo Range and from wells. The upturned section rests structurally above the Franciscan assemblage on the low-angle Coast Range fault, although in many places this relation is obscured by younger high-angle faults. This upturned section includes, from oldest to youngest, Middle and Late Jurassic Coast Range ophiolite and a related tuffaceous unit; Upper Jurassic and Cretaceous Great Valley sequence, which is chiefly forearc flysch; lower Cenozoic postarc marine and terrestrial sedimentary rocks; and upper Cenozoic continental-arc sedimentary rocks (Maddock, 1964; Evarts, 1977; Bartow and others, 1985).

At the latitude of transect C2, the Coast Range ophiolite is interpreted to be a (rifted) island-arc assemblage because it contains abundant silicic volcanic and intrusive rocks (Bailey and Blake, 1974; Evarts, 1977; Hopson and others, 1981; McLaughlin and others, 1988b). Its contact with the overlying sedimentary rocks, though faulted in most places, is believed to be fundamentally depositional (Bailey and others, 1970); on transect C2 it is demonstrably depositional (Evarts, 1977).

The Great Valley sequence and younger rocks exposed in the upturned section in the eastern Diablo Range appear to be nearly twice as thick as the section of sedimentary rocks penetrated in wells farther east in the Great Valley (fig. 8.4). Some of this apparent westward thickening results from the stratigraphic addition of older rocks to the basal part of the section in the west; some may be caused by imbrication along thrust faults (Wentworth and others, 1984). Similar apparent thickening



west of the synclinal axis of the Great Valley has been documented in other localities as well. In the southern Great Valley, Wentworth and others (1984) indicated an apparent doubling of thickness west of the axis, and in the northern Great Valley, an apparent trebling of thickness.

Most of the basement rocks that have been penetrated by wells in the Great Valley have been identified as granitic rocks (Saleeby, 1986). Rocks exposed in the Sierran foothills, east of the Great Valley, may be related to basement rocks beneath the Great Valley, but they are not so dense or magnetic (see below; fig. 8.4A).

Deep structure along transect C2 in the Great Valley has been elaborated in some detail by Colburn and Mooney (1986), Holbrook and Mooney (1987), and Dean Whitman and others (unpub. data, 1985) from seismic-refraction data, and by Wentworth and others (1987) primarily from seismic-reflection data. Seismic velocities in the sedimentary section range from 1.6 to 4.1 km/s where these velocities can be clearly ascribed to sedimentary rocks, such as near well No. 1 (fig. 8.4A). In the eastern Diablo Range, velocities as high as 4.7 km/s may also be due to sedimentary rocks (fig. 8.4A). East of the synclinal axis in the Great Valley, reflections within the sedimentary section are subparallel to the top of basement, which is marked by the disappearance of reflections (f, fig. 8.4A). West of the synclinal axis, these reflections (d, fig. 8.4A) diverge slightly from the inferred top of basement (e, fig. 8.4A).

Beneath the sedimentary rocks of the Great Valley are several layers of increasing seismic velocity: a 5.5- to 5.7-km/s layer, 1.5 to 2 km thick (layer 1), a 6.0- to 6.3-km/s layer, 2.5 to 6 km thick (layer 2); a 6.6- to 6.75-km/s layer, 4 to 7 km thick (layer 3); and a 6.9- to 7.2-km/s layer, about 7 km thick (layer 4) (fig. 8.4A). In addition, there is a thin, laterally discontinuous 7.0-km/s layer embedded in the top of layer 3. Well No. 1 indicates that layer 1 is granitic rocks. Farther west, however, this layer may be interpretable either as granitic rocks or as Franciscan assemblage, which have similar velocities at this depth (fig. 8.5). In the original data of Colburn and Mooney (1986) and Holbrook and Mooney (1987), there is no perceptible reflection from an interface between layers 1 and 2 (as there is, for example, between layer 1 and the overlying sedimentary rocks), and so these two layers may, in fact, grade into one another. Layer 2 could then also be granitic rocks, and layers 1 and 2 together would constitute a velocity-depth section similar, for example, to upper crust of the batholithic Salinian block (figs. 8.4A, 8.5). Layers 3 and 4 (6.6-7.2 km/s), which are analogous to the lower-crustal layer in the Diablo Range (6.7-7.1 km/s), may represent the middle and lower crust of accreted island arc(s) and (or) oceanic crust. The Moho is well documented at about 27-km depth. Deep reflection

data beneath the Great Valley (Wentworth and others, 1987) indicate a conspicuous east-dipping band of reflections (g, fig. 8.4A) and less conspicuous subhorizontal and west-dipping reflectors.

Rocks of the Sierran foothills consist of Lower to Upper Jurassic mafic to felsic volcanic and plutonic rocks and related sedimentary rocks (argillite, chert, and flysch) that were accumulated or emplaced in an island-arc setting (Clark, 1964; Schweickert and Cowan, 1975; Saleeby, 1982; Schweickert and Bogen, 1983). The basement and metamorphic wallrocks for the intrusive rocks are tectonically disrupted and polymetamorphosed Paleozoic ophiolitic rocks (approx 300 Ma; Saleeby, 1982).

The island arc(s) in which the Jurassic rocks of the Sierran foothills were formed collapsed against the margin of the North American Continent during the Late Jurassic Nevadan orogeny (Jones and others, 1976). How this collapse occurred is problematic. Steeply east-dipping faults and upright antiforms are seen in the Sierran foothills, but a study by Moores and Day (1984) of surface relations 300 km north of transect C2 indicates obduction of the arc(s) on west-dipping thrust faults. These rocks were intruded during the Early Cretaceous by mafic to intermediate plutons belonging to the western phase of Sierra Nevada plutonism (Evernden and Kistler, 1970).

The deep structure of the Sierran foothills is known from the reconnaissance seismic-refraction experiment of Spieth and others (1981), the reflection profiling of Zoback and Wentworth (1986), and the compilation of reflection, refraction, and potential-field results by Wentworth and others (1987). The refraction data can be modeled with a 6.2-km/s basement from near the surface to about 30-km depth, a 6.6-km/s lower crust, and a Moho at 39-km depth. Other models are possible, however, and the Moho may be as shallow as 30 km (Spieth and others, 1981). We have projected the seismic-reflection results and gravity/magnetic boundary of Wentworth and others (1987) from 45 to 60 km southward onto transect C2. Two conspicuous west-dipping sets of reflections are visible, as well as a few subhorizontal reflectors. The gravity/magnetic boundary, however, has a moderate eastward dip.

Our projection of the results of Wentworth and others (1987) is uncertain not only because of the distances involved but also because their profile terminates on the east in an area that is anomalous both geologically and geophysically. In this area, batholithic rocks (trondhjemite) engulf most accreted rocks of the Sierran foothills (Jennings, 1977) and are associated with a gravity low (Oliver and others, 1980). Our projection, however, may be defensible as follows. (1) The batholithic rocks responsible for the gravity low probably do not extend below 10-km depth (R.C. Jachens, oral commun., 1988); most of the reflectors that we have projected are largely below



that depth. (2) The modeled gravity/magnetic boundary is approximately similar in shape throughout the length of the Great Valley (Andrew Griscorn, oral commun., 1988); in our projection, we have attempted to correct for the difference in azimuth between transect C2 and the profile of Wentworth and others (1987) by assuming a strike parallel to the Great Valley.

Given the geologic and seismic constraints discussed above, we have interpreted the cross section through the Great Valley and Sierran foothills (fig. 8.4B), using some of the ideas of Wentworth and others (1984, 1987) for the configuration of an inferred tectonic wedge of Franciscan rocks, and some of the ideas of Saleeby (1986) for structure within crystalline rocks. The uppermost part of our cross section (to approx 2-km depth) on the east flank of the Diablo Range (fig. 8.4A) was supplied by R.C. Evarts (written commun., 1989). Below this area, we have added a hypothetical west-dipping thrust fault to bring the Great Valley sequence beneath the easternmost block of the Coast Range ophiolite and to grossly satisfy the velocity constraints of Dean Whitman and others (unpub. data, 1985; fig. 8.4A). East of the Coast Range ophiolite, we postulate thrust faults that largely follow bedding planes in the upturned section of the Great Valley sequence, similar to those postulated by Wentworth and others (1984) for the northern Great Valley. These "backthrust" faults are required for emplacement of the wedge and help explain the thickening of the Great Valley sequence in the western limb of the syncline (see section below entitled "Discussion—Tectonic Wedging"). From the easternmost backthrust fault in the Great Valley to the San Andreas fault, we have modeled the discontinuity between variably reflective rocks of lower velocity (Franciscan assemblage, Coast Range ophiolite, and Great Valley sequence; 1.7–5.8 km/s) and poorly reflective rocks of higher velocity (mafic rocks of the Diablo Range and crystalline basement of the Great Valley; 5.5–6.8 km/s) as the floor thrust fault of the wedge. Wentworth (1987) presented a similar interpretation.

The details of composition and structure in the crystalline rocks beneath the Great Valley and Sierran foothills are speculative. Saleeby (1986) interpreted these rocks to consist fundamentally of slabs or nappes of island-arc and oceanic rocks obducted along west-dipping Nevadan thrust faults intruded by chiefly Early Cretaceous Sierran granitic plutons. We have adopted this basic scheme and added some details, interpreting layers 1 and 2 in the basement beneath the Great Valley (5.5–6.3 km/s; see above) as post-Nevadan felsic plutonic rocks, although, as noted above, the western part of layer 1 (5.5 km/s) may be Franciscan assemblage. We interpret the east-dipping gravity/magnetic boundary of Wentworth and others (1987) as the average top of mafic crust

(pre-Nevadan gabbro, diabase, or basalt) in the inferred obducted sequence. Alternatively, this boundary may be the average top of mafic, magnetic intrusions in the crust (post-Nevadan gabbro) or the average base of felsic, nonmagnetic intrusions (post-Nevadan granitic rocks). At the location where this boundary was actually modeled, it may be the average base of a large trondhjemite intrusion. We associate the east-dipping reflections beneath the central Great Valley (g, fig. 8.4A) with the thin, discontinuous 7.0-km/s layer of Holbrook and Moonhey (1987), although the depth correspondence is imperfect, and we interpret this feature as a gabbroic dike. Alternatively, these east-dipping reflections may represent an east-dipping fault zone. Following Saleeby (1986), we correlate the upper and lower west-dipping bands of reflections in the eastern Great Valley and Sierran foothills (h, j, fig. 8.4A) with the Bear Mountain and Melones fault zones, which may represent Cenozoic reactivations of inferred west-dipping Nevadan thrust faults.

## DISCUSSION—TECTONIC WEDGING

### GEOLOGIC HISTORY

Wentworth and others (1984) interpreted the juxtaposition of Franciscan assemblage and a coeval section consisting of Coast Range ophiolite and Great Valley sequence as having occurred during landward movement of the Franciscan assemblage as a tectonic wedge. They reinterpreted the "Coast Range thrust fault" of Bailey and others (1970), a subduction megathrust between the Coast Range ophiolite and the Franciscan assemblage, as the roof thrust of the wedge. More recently, the thrust nature of the "Coast Range thrust fault" has been reevaluated. Jayko and others (1987), testing an hypothesis by Platt (1986), produced abundant evidence that the contact between Franciscan assemblage and Coast Range ophiolite is a detachment surface along which the upper plate was extended during uplift of the Franciscan assemblage. Their evidence is the consistent attenuation, as opposed to repetition, of geologic section across this discontinuity and associated faults above it. They proposed the term "Coast Range fault" for this discontinuity, which we adopt here. Evidence of attenuation is present even on transect C2, in that the two outcrops of the Coast Range ophiolite in the eastern Diablo Range (fig. 8.4A) represent an abridged section of ophiolite: The western outcrop is partially serpentized ultramafic rock of the basal part of an ophiolite, whereas the eastern outcrop is the sill complex and volcanic flows of the upper part of an ophiolite. These two parts of the ophiolite are now juxtaposed across the crooked, steeply dipping Tesla-Ortogonalita fault. Although this fault now offsets the



Coast Range fault, it may represent reactivation of a normal fault that originally soled into the Coast Range fault (compare Raymond, 1973).

The extensional nature of the Coast Range fault poses several problems for emplacement of the Franciscan assemblage as a tectonic wedge. Where is the roof thrust fault of the wedge? How did the Franciscan assemblage reach its current position with an extended overlying section of the Coast Range ophiolite and Great Valley sequence? Was the Franciscan assemblage uplifted from beneath the western Great Valley? The apparent continuity between the Great Valley basement and the 6.7- to 7.1-km/s layer in the Diablo Range indicates a negative answer to the last question.

These problems can be solved if the extensional event was separated in time and space from the compressional event, or tectonic wedging. Jayko and others (1987) reviewed the published evidence regarding the geologic history of extensional faulting. In one place, the Coast Range fault and associated faults are overlapped by sedimentary rocks of Oligocene and younger age, and in another place by sedimentary rocks of Paleocene and younger age. The occurrence of detritus derived from the Franciscan assemblage in Paleocene and Eocene strata of the Coast Ranges (Dickinson, 1966; Berkland, 1973) indicates that the lower plate was exposed by the early Tertiary. Jayko and others (1987) inferred that uplift of the Franciscan assemblage and associated extensional faulting in the upper plate occurred during the Late Cretaceous and (or) early Tertiary.

The history of compressional tectonics in the Coast Ranges is sparse and varies from place to place. In the northern Coast Ranges, thrust faulting and folding began during the early Tertiary (Blake and others, 1987; M. C. Blake, Jr., oral commun., 1989), and compressional deformation is continuing today in rocks of the northern Great Valley (Harwood and Helley, 1987). In the southern Coast Ranges, at least four Cenozoic deformations or uplifts, indicated by unconformities or eastward-migrating depocenters, have ages of late Paleocene, late Eocene to early Miocene, late Miocene, and late Pliocene (Namson and Davis, 1988; Namson and others, 1990; Rentschler and Bloch, 1988). Modern thrust faulting and folding still is occurring, as indicated by the 1983 Coalina earthquake (see chap. 5; Eaton, 1990).

Landward movement of the Franciscan assemblage as a wedge may have even begun in the Mesozoic. In the northern Coast Ranges, several northwest-striking faults (Paskenta, Elder Creek, and Cold Fork faults) offset rocks structurally above the Franciscan assemblage (but not the Franciscan assemblage itself) and represent major discontinuities in the depositional environment of the Great Valley sequence (Jones and Irwin, 1971). These faults, which have displacements of tens of

kilometers to as much as 100 km, are interpreted to have moved primarily during the Cretaceous (Jones and Irwin, 1971), although the latest limit on the time of movement is about 3.4 Ma (Hardwood and Helley, 1987; M. C. Blake, Jr., oral commun., 1989). Wentworth and others (1984) and Jayko and others (1987) interpreted these faults as tear faults in the plate structurally above a wedge of Franciscan assemblage.

In light of the above data and interpretations, we postulate (1) that uplift of the Franciscan assemblage and extension of the upper plate, consisting of Coast Range ophiolite and Great Valley sequence, occurred during the Cretaceous (or, at the latest, during the early Tertiary, if Cretaceous movement on the Paskenta-Cold Fork fault system is not linked to landward wedge transport) well west of the present Diablo Range; and (2) that a tectonic wedge of Franciscan assemblage was subsequently driven landward, with the extended upper plate riding passively atop it. This wedge is interpreted to have moved along a floor thrust fault aligned with the contact between the Great Valley sequence and its crystalline basement. To the west of the present Diablo Range, where movement initiated, the basement was an outboard part of the Coast Range ophiolite. Beneath the Great Valley, where the movement is presently occurring, the basement is similar to the Coast Range ophiolite but contains numerous younger plutons. A roof thrust fault apparently developed only near the east tip of the wedge (fig. 8.4B); presumably, erosion kept pace with uplift near the tip. Differential vertical or horizontal movements of the wedge may have produced tear faults, such as the Paskenta, Elder Creek, and Cold Fork faults, and may have reactivated extensional faults to produce complex faults, such as the Tesla-Ortogonalita fault.

#### PAST AND PRESENT TECTONIC REGIMES

The Mendocino triple junction has moved northward through offshore central California during approximately the past 20 Ma, and subduction of the Farallon plate (or its derivative) was replaced by transform motion of the Pacific plate past North America (see chap. 3; Atwater, 1970, 1989). If tectonic wedging occurred during the late Mesozoic and Cenozoic, in association with all of the episodes of tear faulting or compression outlined above, then clearly it was driven during both subduction and transform regimes. At present, it is being driven by a transform regime. At least two additional arguments can be made that wedge motion—indeed, probably a major fraction of wedge motion—occurred during the subduction regime. The first argument is simply based on geometry: The east boundary of the Coast Ranges, inferred to coincide approximately with the buried tip of the wedge, largely parallels Mesozoic structures in the



Sierran foothills and the Great Valley rather than the late Cenozoic San Andreas fault (Wentworth and Zoback, 1989; C.M. Wentworth, oral commun., 1990). The second argument, developed below, is based on the total apparent displacement of the wedge.

If the inferred tectonic wedge of Franciscan assemblage extends to the San Andreas fault, as we have shown (fig. 8.4B), then a minimum shortening of about 70 km has occurred along faults at the top and bottom of the wedge in the Diablo Range. Likewise, in the northern Coast Ranges, the inferred tear faults in the plate above the wedge have a total displacement—and, thus, shortening—of many tens of kilometers (Wentworth and others, 1984), possibly as much as 100 km (Jones and Irwin, 1971).

Although a transform regime has replaced a subduction regime in central California over approximately the past 20 Ma, plate-margin compression, necessary to drive the wedge, has persisted for only approximately the past 5 Ma (Page and Engebretson, 1984). At about 5.5–4.5 Ma, transform motion was also transferred from offshore faults to the modern San Andreas fault system (see chap. 3; Atwater, 1989; Humphreys and Weldon, in press). Present plate-margin compression is understandable from (1) the slight misalignment of the direction of relative plate motion (N. 35° W.; Minster and Jordan, 1978) and the strike of the San Andreas fault (N. 40° W.), and (2) the opening of the Basin and Range province. Crouch and others (1984) calculated from these two effects a rate of shortening across the Coast Ranges that, integrated over the past 5.5 Ma, predicted a total shortening of 28 to 72 km. Most of this shortening could be accounted for in small fault displacements and folds distributed throughout the Coast Ranges (Crouch and others, 1984). Thus, the minimum shortening of 70 to 100 km represented by the tectonic wedge, as discussed above, would appear to equal or exceed the maximum shortening calculated for the transform regime, a result suggesting that some, if not most, of the wedge motion occurred during the subduction regime.

Shear coupling between the subducting plate and overlying accretionary prism (Franciscan assemblage) could conceivably drive the wedge during the subduction regime. Such a mechanism has been postulated for southern Alaska by Fuis and Plafker (in press). To drive the wedge during a transform regime appears to require a less obvious mechanism, such as plate-margin compression combined with differing deformation in the upper and lower crust. Such a mechanism is developed below.

Sibson (1982) pointed out, on the basis of strength considerations, that ductile flow could be expected in the middle crust, below the maximum depth of earthquake hypocenters. Several workers (Crouch and others, 1984; Namson and Davis, 1988; Eaton and Rymer, in press)

have postulated a decollement near the base of the seismicity in the Coast Ranges (avg 15-km depth; see chap. 5; Wesson and others, 1973) into which thrust and oblique-slip faults on both sides of the Coast Ranges sole. They envision differential movement between upper and lower crust caused by differing alignment of the transform faults in these two layers, or by shortening of the lower crust by ductile thickening.

We have incorporated the idea of a Coast Range-wide detachment in our cross section (fig. 8.4B). In the Diablo Range, we show a young thrust fault at the base of the inferred tectonic wedge soling into the brittle-ductile transition zone, which in this area is, coincidentally, near the interface between Franciscan rocks and mafic crust. Although we also indicate soling of the San Gregorio-Hosgri fault into such a zone and underthrusting of the Salinian block by the early Tertiary accretionary prism, focal mechanisms in this region indicate pure strike slip on the San Gregorio-Hosgri fault (see chap. 5) and argue against this interpretation. Such an interpretation of a Coast Ranges-wide midcrustal detachment requires that the deformational style and (or) location of the San Andreas fault system change from the upper to the lower crust.

If we have correctly inferred the geologic history of wedge movement, it is remarkable that such movement has apparently occurred in two quite different tectonic regimes, a subduction regime and a transform regime.

## SOUTHERN CALIFORNIA

The crustal structure of southern California is complicated by the Big Bend in the San Andreas fault, situated between the Coast Ranges and Transverse Ranges, and by onshore spreading centers of the East Pacific Rise, situated in the Salton Trough (figs. 8.2, 8.3). The Big Bend is thought to result from westward movement of the Sierra Nevada relative to the Mojave Desert, along the Garlock fault (Hill and Dibblee, 1953). The San Andreas fault crosses the Transverse Ranges, between the Big Bend and Salton Trough, at an angle oblique to relative plate motion, while somehow remaining a largely vertical, strike-slip fault.

The onshore spreading centers in the Salton Trough are situated at echelon offsets between the San Andreas, Imperial, and Cerro Prieto faults (see fig. 3.8; Lomnitz and others, 1970). These three faults are interpreted as transform faults; the San Andreas links the northernmost spreading center in the Salton Trough with the Mendocino triple junction. A progressive decrease in spreading rate northward along the East Pacific Rise is inferred to give rise to movement on the San Jacinto, Elsinore, San Miguel/Newport-Inglewood, and other faults in southern



California and Mexico (Lomnitz and others, 1970; Elders and others, 1972).

First, we discuss a transect across southern California, Centennial Continental-Ocean Transect C3 (Howell and others, 1985). Second, because of the three-dimensionality of the geology and tectonics in southern California, we include a discussion of block motions, largely from Weldon and Humphreys (1986).

#### TRANSECT C3

We modify and reinterpret the section of Centennial Continent-Ocean Transect C3 (Howell and others, 1985) that extends from Santa Catalina Island to the Colorado Desert (fig. 8.2). This section of the transect crosses four blocks or provinces, the California Continental Borderland (hereafter referred to simply as the "borderland"), Peninsular Ranges, Salton Trough, and Chocolate Mountains (fig. 8.6). The transect crosses the Newport-Inglewood, Elsinore, San Jacinto, and Imperial strike-slip faults. Constraints for the transect include surface geology, isotopic studies, seismic-refraction profiling (which is sparse, except in the Salton Trough), tomographic studies, and potential-field studies.

#### BORDERLAND

The borderland is broken up by right-slip faults into several northwest-trending blocks. Our cross section (fig. 8.6) begins on the easternmost block, the "Catalina terrane" (Howell and others, 1985), bounded on the east by the Newport-Inglewood fault. The Catalina terrane is underlain, beneath patches of Tertiary volcanic rocks, by Franciscan assemblage, on the basis of outcrops on Santa Catalina Island (Platt, 1975, 1976; Jones and others, 1976) and submarine dredge and core samples (Vedder and others, 1974). The block west of the Catalina terrane, the "San Nicholas terrane" (Howell and others, 1985), is inferred to be underlain, beneath Cenozoic marine sedimentary rocks, by rocks similar to the Great Valley sequence and Coast Range ophiolite of central California, possibly in fault contact with Franciscan assemblage at depth (Vedder and others, 1974).

A reversed seismic-refraction profile just west of Santa Catalina Island indicates *P*-wave velocities of 5.8 km/s to 6-km depth and of 6.7 km/s to the Moho at about 24-km depth (fig. 8.6A, Shor and Raitt, 1958). This velocity-depth section is similar to that for the Diablo Range of central California (see above), where Franciscan rocks are equated with the 5.8-km/s interval, and middle and lower crust of island arc(s) and (or) oceanic crust are equated with the 6.7-km/s interval. In this region, there is no clear evidence of landward movement of the Franciscan assemblage as a tectonic wedge, although

such evidence may surface during future investigations. As in the Diablo Range, the lower crust must have been brought to its present 18-km thickness by (1) imbrication of slices of island-arc crust, (2) tectonic underplating of several thicknesses of oceanic crust, and (or) (3) magmatic underplating. Subduction continued beneath the borderland until sometime between 30 and 20 Ma (see Atwater, 1970), depending on the latitude to which the borderland is palinspastically restored.

#### PENINSULAR RANGES

The Peninsular Ranges are underlain in the west by supracrustal rocks, including, from top to bottom, Cenozoic marine sedimentary rocks, Cretaceous forearc sedimentary rocks, Lower(?) Cretaceous and Upper Jurassic andesite (Santiago Peak Volcanics), and Middle Jurassic flysch (Bedford Canyon Formation) that was disrupted and overturned before the Late Jurassic (Larsen, 1948; Jennings, 1977; Criscione and others, 1978). These rocks are intruded by Early Cretaceous plutons of the Peninsular Ranges batholith that include chiefly tonalite and gabbro and show no special age trends (static magmatic arc; Silver and others, 1979). About 80 km east of the coastline, both prebatholithic and batholithic rocks change (fig. 8.6A): To the east, the prebatholithic rocks are dominantly metamorphosed clastic rocks of amphibolite grade, and the batholithic rocks are chiefly tonalite and granodiorite whose ages decrease progressively eastward (from 105 to 80–90 Ma; migrating magmatic arc; Silver and others, 1979). Major-element chemistry and oxygen isotopes indicate that deep crustal rocks in the west half of the batholith are dominantly primitive and tholeiitic but, in the east, more aluminous and oxidized (fig. 8.6A). Older crust that was once at the Earth's surface is inferred at depth in the east (Silver and others, 1979).

Seismic constraints for the deep structure of the Peninsular Ranges are sparse. Using blasts at the Corona Quarry in the northernmost Peninsular Ranges, Gutenberg (1951) and Shor (1954) obtained an unreversed refraction profile, extending southward to the United States-Mexican border, along with a reflection record at the blast site. Interpretation of these data by Shor and Raitt (1958) indicated velocities of 5.9 km/s to 8-km depth, 6.8 km/s to 26-km depth (with a possible low-velocity zone in this interval), and 7.0 km/s to the Moho at 30- to 32-km depth (fig. 8.6A). In contrast, a study by Nava and Brune (1982) using a blast at the same quarry, reversed by an earthquake in Baja, Mexico, indicated a Moho depth of 42 km. Hearn and Clayton (1986a, b) used as many as 600,000 arrivals from local earthquakes in southern California to map the velocity of the crust and upper mantle, using tomography. Their map indicates



that the west half of the Peninsular Ranges has a higher average upper-crustal velocity and a lower average mantle velocity in comparison with the east half. Their map of  $P_n$  delays for the Peninsular Ranges suggests no crustal root and an average crustal thickness of nearly 30

km. Gravity modeling of the Peninsular Ranges (Fuis and others, 1984) and isostatic calculations also indicate a maximum crustal thickness of 30 to 33 km. In our cross section (fig. 8.6B), we adopt a maximum crustal thickness of 33 km.

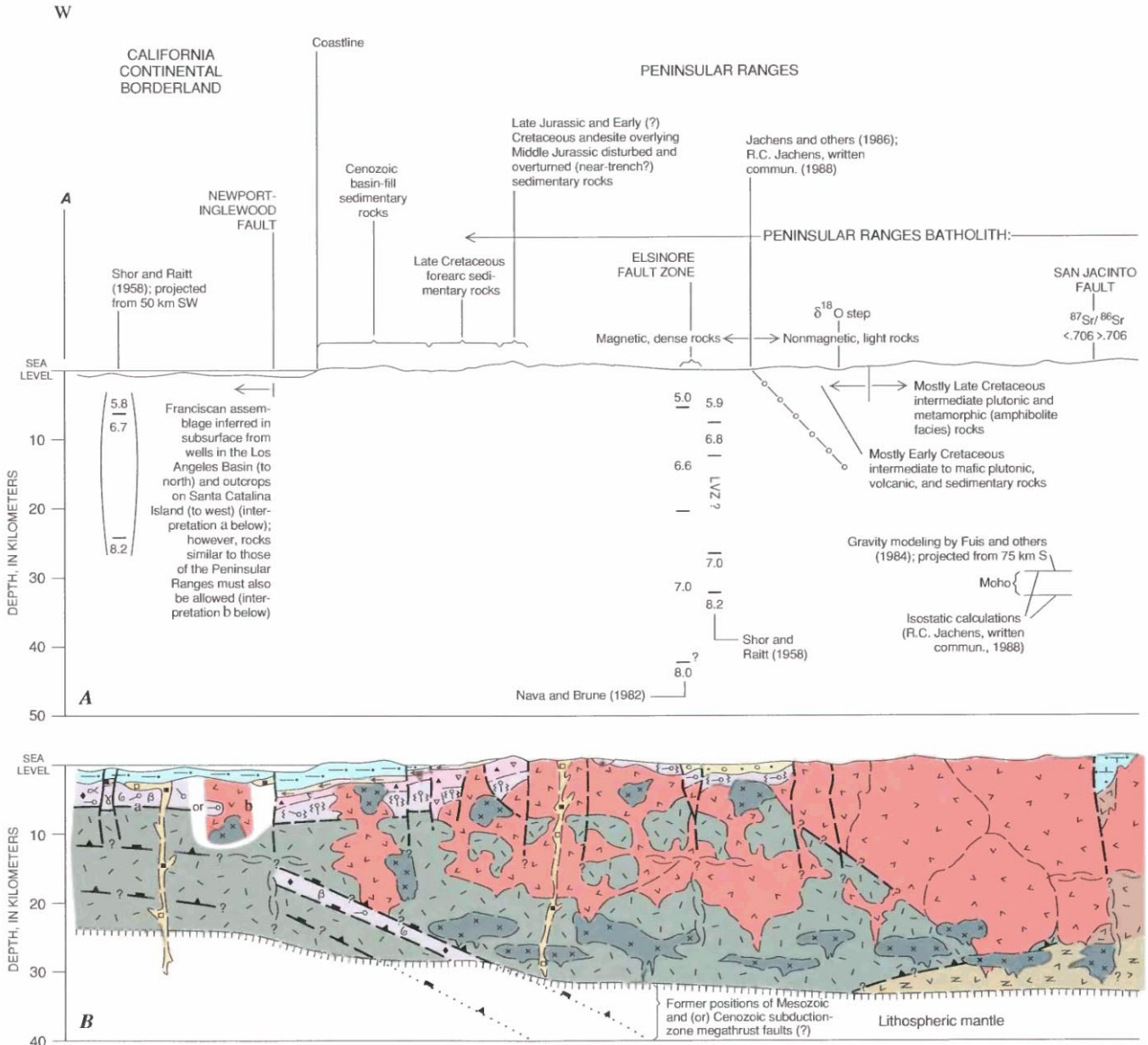
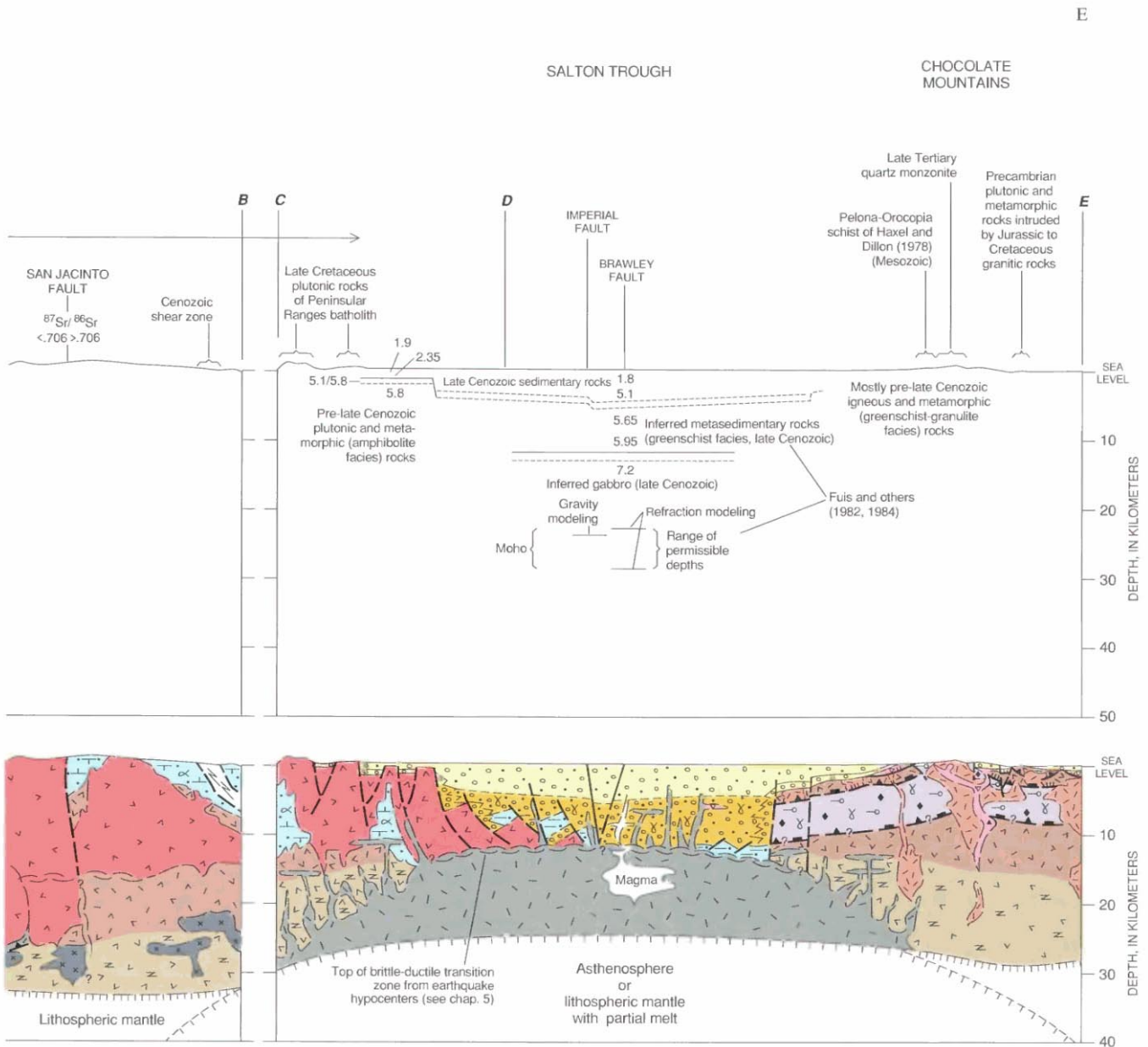


FIGURE 8.6.—Crustal structure of southern California. A, Surface geology, isotope data, and models of seismic-refraction, gravity, and magnetic data for part of Centennial Continent-Ocean Transect C3 (see Howell and others, 1985). B, Reinterpretation of Transect C3. Major features in figure 8.6B include, from west to east, (1) Franciscan assemblage overlying mafic crust in the borderland; (2) Peninsular Ranges batholithic block, consisting of

west half inferred to be underlain at depth by mafic (island arc or oceanic) crust and east half inferred to be underlain at depth by intermediate continental Precambrian(?) rocks; (3) late Cenozoic rift, the Salton Trough, whose central part is inferred to be underlain by entirely new crust that includes, from top to bottom, sedimentary rocks, thermally metamorphosed sedimentary rocks, and gabbro generated at onshore

An additional constraint on crustal structure is the modeling by Jachens and others (1986; R.C. Jachens, written commun., 1988) of strong magnetic and gravity steps (500 nT and 40 mGal, respectively) in the central Peninsular Ranges: A moderately east dipping boundary

is modeled between more magnetic, dense rocks on the west and less magnetic, lighter rocks on the east. This boundary is poorly defined at the latitude of our transect; it correlates approximately (within 15 km or so) with the boundary between the east and west halves of the



spreading center; and (4) Pelona-Orocopia schist of Haxel and Dillon (1978) (similar to the Franciscan assemblage), interpreted to compose tectonic wedge. Tectonic wedge in feature 4 is postulated to have been obducted onto continental crust (see text); its tip would lie well east of east end of cross section. This reinterpretation differs from Howell and others' (1985)

primarily in interpreting mafic crust at shallower depths beneath the borderland and western Peninsular Ranges (5–8 km versus 11–15 km) to better match seismic and potential-field results. See figures 8.2 and 8.3 for location of Transect C3; see figure 8.4 for explanation. No vertical exaggeration.



Peninsular Ranges batholith, as discussed above (fig. 8.6A). In the cross section (fig. 8.6B), we interpret an eastward deepening of mafic rocks, including prebatholithic and (or) batholithic mafic rocks (gabbro, diabase, and metamorphic rocks), along this magnetic/gravity boundary. R.C. Jachens (oral commun., 1989) indicated that, in some places, this boundary is so planar as to be interpretable as a fault. As beneath the borderland, the mafic rocks beneath the Peninsular Ranges may have reached their current thickness by thrust imbrication, tectonic underplating, or magmatic underplating. We speculatively show some tectonic underplating on the west side.

#### SALTON TROUGH

The Salton Trough is the landward extension of a ridge/transform-fault system, the East Pacific Rise, of the Gulf of California (see fig. 3.13). This system became well established during the late Cenozoic (approx 5 Ma) as the plate boundary jumped inland from offshore Baja California (Atwater, 1970, 1989; Humphreys and Weldon, in press).

The Salton Trough is underlain by upper Cenozoic sedimentary rocks and minor amounts of volcanic rocks, which are exposed chiefly around its edge and are penetrated in wells. Onset of rifting and major subsidence in the Salton Trough was followed by marine incursion during the latest Miocene to late(?) Pliocene, as indicated by the Imperial Formation (Dibblee, 1954; Powell, 1984). The thick Cenozoic sedimentary section is offset by Quaternary faults, both exposed and buried, and is intruded by Quaternary volcanic rocks, both silicic rocks that form volcanoes at the two inferred onshore spreading centers (fig. 8.7) and mafic rocks that are penetrated in geothermal wells (Elders and others, 1972; Robinson and others, 1976). Faulting in the Salton Trough occurs primarily on conjugate northwest- and northeast-striking faults and is largely strike slip (Johnson and Hadley, 1976; Johnson, 1979; Fuis and others, 1982). North-south-striking faults, however, such as the north end of the Imperial fault, the Brawley fault, and north-south-striking seismicity lineaments (that outline inferred spreading centers; figs. 8.1, 8.7), have normal components and lead to the subsidence that ultimately created the Salton Trough. Earthquake hypocentral depths indicate that brittle fault motion extends to about 12-km depth in the Imperial Valley but deeper in the adjacent Peninsular Ranges along the San Jacinto fault (Doser and Kanamori, 1986).

Detachment faulting on the east flank of the Salton Trough, in the Chocolate Mountains and other ranges, preceded the Pliocene and later basin-forming tectonics in the Salton Trough (Dillon, 1975; Berg and others, 1982;

Frost and others, 1982). Similar faulting on the west flank of the Salton Trough, however, may have both preceded and overlapped in time the tectonics in the Salton Trough (Wallace and English, 1982; Schultejaahn, 1984; Isaac and others, 1986).

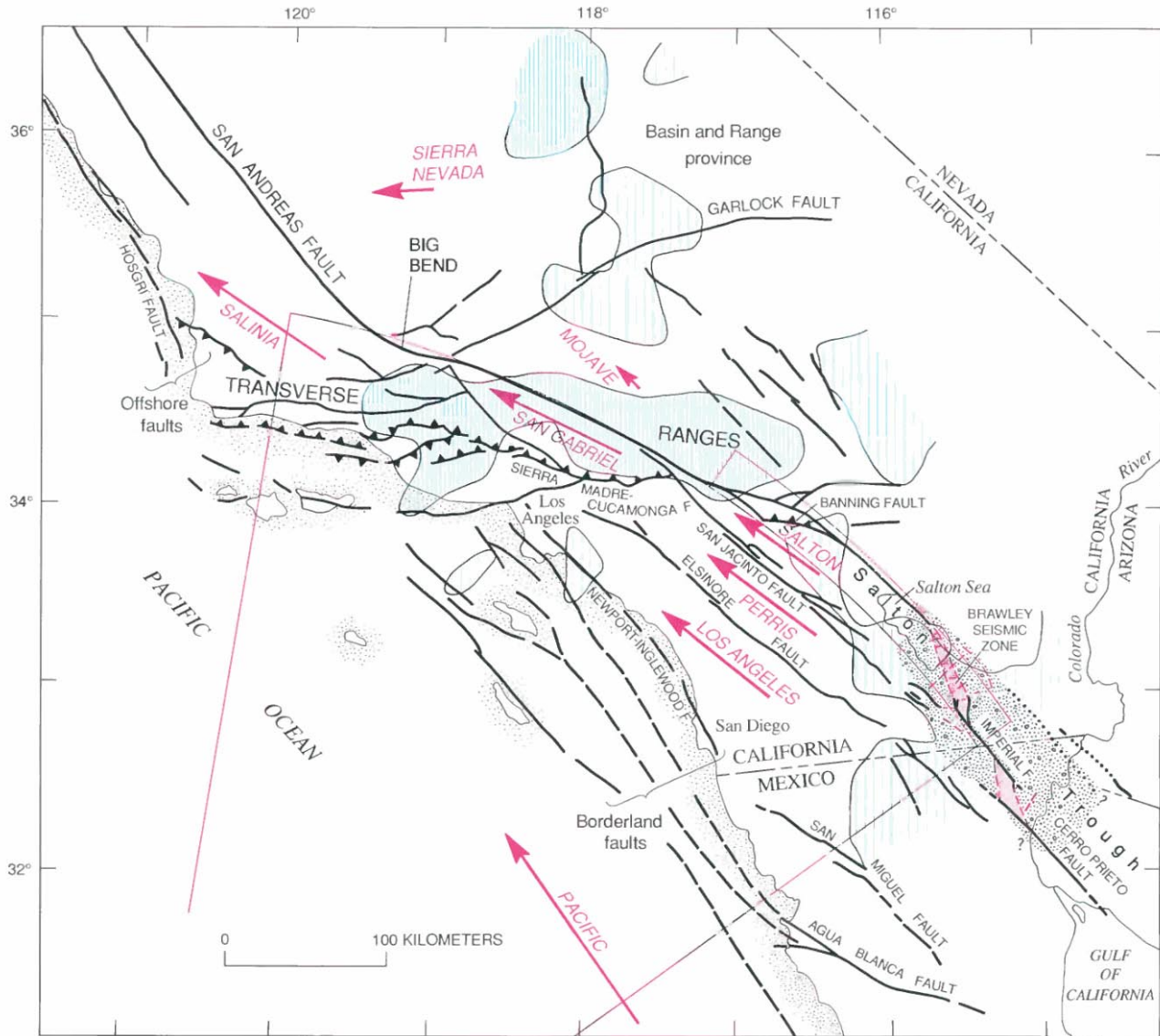
Biehler and others (1964) and Fuis and others (1982, 1984) demonstrated from seismic surveys that the sedimentary rocks (1.8–5.5 km/s) in the central Salton Trough are as much as 5 km thick (fig. 8.6A). Below 5-km depth, a low-velocity (5.6 km/s) “basement,” which is not separated from the overlying sedimentary rocks by a velocity discontinuity, is inferred to be metamorphosed (greenschist facies) sedimentary rocks (Fuis and others, 1982, 1984); this “basement” layer extends to 12-km depth. High heat flow in the Salton Trough (see Lachenbruch and others, 1985) is inferred to cause the metamorphism of the sedimentary rocks. Thus, the entire section of inferred upper Cenozoic sedimentary rocks, metamorphosed and unmetamorphosed, is as much as 12 km thick.

Below 12- to 14-km depth in the Salton Trough, a high-velocity (7.1–7.2 km/s) “subbasement” that is indicated by seismic-refraction data (fig. 8.6A) is inferred to be gabbro generated at one of the nearby spreading centers (Fuis and others, 1982, 1984). Modeling of seismic-refraction and gravity data indicate that the Moho in the central Salton Trough is 23 to 28 km deep (Fuis and others, 1982, 1984). The central Salton Trough is interpreted to be underlain entirely by late Cenozoic crust (fig. 8.6B).

Buried scarps separating old crust (plutonic and metamorphic rocks; 5.9–6.0 km/s) from new crust (sedimentary and basaltic rocks; 1.8–7.2 km/s) are visible by seismic methods on both sides of the Salton Trough (Fuis and others, 1982; Fuis and Kohler, 1984). On the west side of the rift, where the new-crust/old-crust boundary is ragged in outline (fig. 8.7), we interpret normal faults

►  
 FIGURE 8.7.—Tectonic block motion in southern California (modified from Weldon and Humphreys, 1986, and Humphreys and Weldon, in press). Various blocks (italicized names near motion vectors) move through region where the San Andreas fault trends obliquely to plate motion, between the Big Bend and the Salton Trough, without major convergence with each other. Through this region they move counterclockwise, following nearly concentric arcs (arcs and radii, thin red lines). New crust, which is forming in wake of the Salton and Perris blocks in the Salton Trough, is created by sedimentary-basin fill and gabbroic intrusions at onshore spreading centers, outlined by seismicity lineaments. High-velocity mantle beneath the Transverse Ranges is interpreted as cold, sinking lithospheric mantle, and low-velocity mantle beneath the Salton Trough as hot upwelling asthenosphere or lithospheric mantle containing partial melt (Humphreys and others, 1984; Humphreys and Clayton, in press). Motion vectors for the Mojave Desert and Sierra Nevada modified to incorporate results of Sauber and others (1986).

(fig. 8.6B); on the east side, where this boundary is linear, we interpret a strike-slip fault. In our cross section, faults on the west side of the Salton Trough are inferred to have originated by pullaway from the Cerro Prieto spreading center to the southeast; the fault on the east side is inferred to be a largely passive suture (figs.



EXPLANATION

- Motion vector of tectonic block—  
Relative to North America  
Vector scale 20 mm/yr
- New crust (late Cenozoic)
- Onshore spreading center
- High-velocity mantle
- Low-velocity mantle
- Seismicity lineament
- Fault—Dashed where approximately located; dotted where buried
- Thrust fault—Dashed where approximately located. Sawteeth on upper plate



8.6B, 8.7; Fuis and others, 1982). A similar rift configuration is seen, for example, in the Gulf of Elat (Gulf of Aqaba, Red Sea; Ben-Avraham, 1985).

#### CHOCOLATE MOUNTAINS

Rocks on the east flank of the Salton Trough are igneous and metamorphic rocks that compose two or more fault-bounded packages, or tectonostratigraphic terranes (see Howell and others, 1985). A complex of metasedimentary and mafic metaigneous rocks described by Dillon (1975) may include two Precambrian terranes, the Joshua Tree and San Gabriel terranes, described farther north by Powell (1981). This complex is intruded by intermediate to felsic Mesozoic plutons and rests on the low-angle Chocolate Mountains thrust fault above the (informal) Pelona-Orocopia schist of Haxel and Dillon (1978; see also Haxel, 1977). The Pelona-Orocopia schist consists chiefly of metagraywacke and lesser metapelite, metabasite, metachert, marble, and serpentinite (albite-epidote-amphibolite facies) of uncertain but probable late Mesozoic or early Tertiary age (Conrad and Davis, 1977; Miller and Morton 1977, 1980). It resembled the Franciscan assemblage but lacks melange.

Many workers have speculated on the depositional environment and origin of the Pelona-Orocopia schist. Haxel and Dillon (1978) postulated formation in an ensimatic rift basin with continent on both sides—not unlike the current Salton Trough. Powell (1981) favored an origin as a parautochthonous continental-marginal deposit. In any case, from its quartz content, the Pelona-Orocopia schist clearly originated near a continent and incorporated continental detritus. It was thrust beneath the continental metasedimentary-metigneous complex some time after Mesozoic plutonism (80 Ma; Powell, 1981) and before Oligocene volcanism (35 Ma; Crowe 1978; Crowe and others, 1979). The thrust fault may have been reactivated one or more times as a low-angle normal, or detachment, fault (Frost and others, 1982).

Evidence from refraction profiling in the western Mojave Desert across the Rand schist, which has been correlated with the Pelona-Orocopia schist (Ehlig, 1968), indicates relatively low-velocity crust beneath this body (max 6.4 km/s; Fuis and others, 1986) that we infer to be continental crust. We speculate that the Pelona-Orocopia schist also rests on continental crust and that the Rand and Pelona-Orocopia schists were emplaced as a tectonic wedge into continental crust in a manner similar to the Franciscan assemblage of central and northern California. We hypothesize that the metasedimentary-metigneous complex structurally above the schist is analogous to either (1) rocks of the Coast Range ophiolite/Great Valley sequence which rode passively atop the wedge in

central and northern California after being extended during uplift of the Franciscan assemblage, or (2) rocks of the Great Valley sequence which were peeled up along backthrust faults during landward movement of the wedge. In southern California, tectonic wedging clearly occurred before the present transform regime, presumably during subduction of the Farallon plate (or its derivative). The geologic data discussed above indicate that the Salton Trough has undergone extension, rather than compression, for approximately the past 5 Ma (probably even longer; see Humphreys and Weldon, in press).

Crustal thickness is unknown in the Chocolate Mountains; however, the Colorado Desert, to the east and north, has a generally thin (26–28 km) crust (fig. 8.3) and a local root (32 km deep) under the Whipple Mountains metamorphic-core complex (Fuis, 1981; Jill McCarthy, written commun., 1988).

#### TECTONICS—THE THREE-DIMENSIONAL PICTURE

The geology and, presumably, the deep structure of southern California illustrated along transect C3 (fig. 8.6) is grossly two dimensional as far north as the Transverse Ranges. In the Transverse Ranges, the rocks on the southwest side of the San Andreas fault are similar to those in the Chocolate Mountains. These rocks are bounded on the south and west by older, deformed strands of the San Andreas fault system (fig. 8.7; Powell, 1981). The tectonics also changes in the Transverse Ranges: Crustal-block motion swings to the west to follow the trend of the San Andreas fault, as discussed below.

Using Quaternary geologic and geodetic evidence, Weldon and Humphreys (1986) documented complex motion of crustal blocks in southern California that is not simply predictable from the motion vectors of the Pacific and North American plates. These motion vectors predict a large component of convergence across the San Andreas fault in the Transverse Ranges between the Big Bend and the Salton Trough (fig. 8.7). For a total offset on the San Andreas fault system of about 300 km (Hill and Dibblee, 1953; Crowell, 1962, 1981; Powell, 1981), a maximum of 45 km of uplift in the Transverse Ranges would be expected (Weldon and Humphreys, 1986). However, the preservation in the Transverse Ranges of upper Cenozoic sedimentary rocks and of offset bedrock features on either side of the San Andreas fault argues against such major uplift and associated consumption of crust, as does the relatively minor crustal root in the Transverse Ranges (fig. 8.3). Weldon and Humphreys (1986) constructed a kinematic model in which crustal blocks between the San Andreas fault and a system of borderland and other offshore faults rotate counterclock-



wise, parallel to the San Andreas fault, between the Salton Trough and the Big Bend (fig. 8.7). Approximately two-thirds of the relative northwestward motion of the Pacific plate past the North American plate is taken up by the San Andreas fault system, including the San Jacinto fault; approximately one-third of it is taken up by the Elsinore fault, a system of borderland faults, and offshore faults in central California, including the San Gregorio-Hosgri fault (fig. 8.7); and only a minor fraction of it is taken up within the blocks (see Humphreys and Weldon, in press).

A marked advance in the *P*-wave traveltimes of teleseismic arrivals in southern California is associated with the Transverse Ranges and extends across the San Andreas fault (Hadley and Kanamori, 1977; Raikes, 1980). Tomographic analysis of this anomaly indicates that it results from a vertical slablike region of relatively high velocity in the mantle which extends downward as far as 250 km (Humphreys and others, 1984; Humphreys, 1985; Humphreys and Clayton, in press). The amount of velocity increase, a maximum of 3 percent, is most reasonably explained by a thermal difference in the mantle. This velocity increase, coupled with a velocity decrease in the upper 90 km or so of mantle beneath the Salton Trough, led Humphreys and Hager (1984 and in press) to infer small-scale mantle convection between the Salton Trough and the Transverse Ranges. This convection involves passive rising of asthenosphere beneath the Salton Trough and cooling and sinking of lithosphere beneath the Transverse Ranges. The vertical extent of the inferred lithospheric slab beneath the Transverse Ranges, 250 km, is similar to the 300-km estimate of total offset along the San Andreas fault system. However, because the cooled mantle slab extends across the San Andreas fault, most of the mantle seems to be moving independently of the crust (fig. 8.8; Hadley and Kanamori, 1977; Humphreys and others, 1984; Humphreys, 1985; Humphreys and Hager, in press). The horizon of decoupling is apparently at or below the Moho because crustal material is not entrained in the slablike feature. Additional decoupling may be occurring in the crust, similar to that postulated for central California (Yeats, 1981; Webb and Kanamori, 1985). Decoupling at the Moho requires that the deformational style and (or) location of the San Andreas fault system change from the crust to the mantle (fig. 8.8). We note that mantle drag on the crust is required to maintain the Big Bend in the San Andreas fault because plate-edge forces alone would tend to "short-circuit" the San Andreas fault south of the Big Bend and cause most plate motion to be taken up on the San Jacinto, Elsinore, or more westerly faults (Kosloff, 1978; Humphreys, 1985).

To summarize, block motions in the region between the Big Bend and the Salton Trough result in only minor

interblock convergence in the crust. In contrast, major convergence in the lithospheric mantle is indicated by the presence of an inferred, sinking lithospheric slab.

### STRUCTURE OF THE UPPER MANTLE

In addition to the Transverse Ranges and Salton Trough, other regions in California show mantle velocity anomalies that imply structure within the lithospheric mantle and even the asthenosphere. The seismic networks in California (see chap. 5) provide an abundant source of regional earthquake and teleseismic arrivals that have been used to determine this upper-mantle structure.

A detailed study of the compressional-wave velocity of the uppermost mantle in central California reveals a normal velocity of about 8.0 km/s and no evidence for

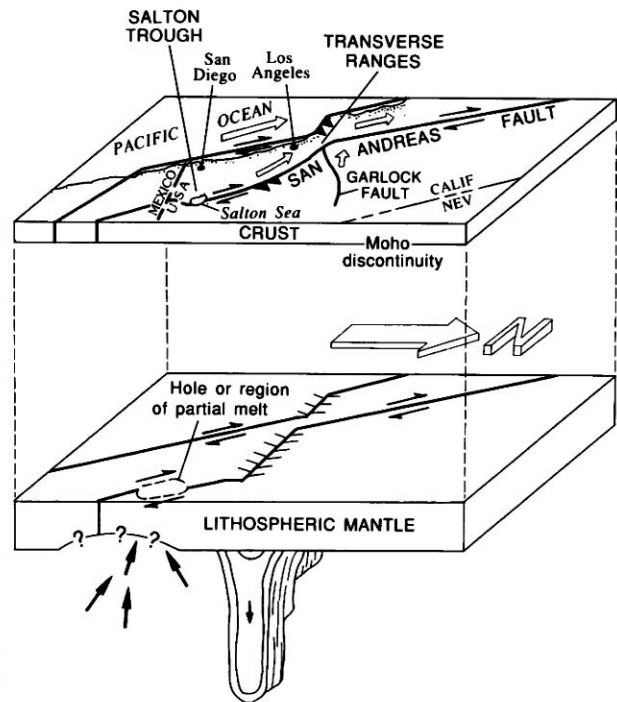


FIGURE 8.8.—Motion of crustal blocks in southern California (open arrows; see fig. 8.7) and somewhat different motion of lithospheric mantle below (solid arrows) (modified from Humphreys, 1985, and Humphreys and Hager, in press). Mantle convection cell is envisioned between the Salton Trough and the Transverse Ranges. Crust and lithospheric mantle appear to be moving independently of one another, as the San Andreas fault trends obliquely across region of inferred, sinking lithospheric mantle beneath the Transverse Ranges (see fig. 8.7). Small arrows, relative fault motion; sawteeth, upper plates of crustal thrust faults; crosslines, subduction zones in lithospheric mantle.